JOURNAL OF GEOPHYSICAL RESEARCH, VOL. 88, NO. C11, PAGES 6611–6621, AUGUST 20, 1983

APPENDIX IV

A Dynamic Model for the Production of H^+, NO_3^-, and SO_4^{2-} in Urban Fog

DANIEL J. JACOB AND MICHAEL R. HOFFMANN

Environmental Engineering Science, W. M. Keck Laboratories, California Institute of Technology, Pasadena, California 91125

The chemical composition of nighttime urban fog has been investigated using a hybrid kinetic and equilibrium model. Extremely high acidity may be imparted to the droplets by condensation and growth on acidic condensation nuclei or by in situ S(IV) oxidation. Important oxidants of S(IV) were found to be O_2 as catalyzed by Fe(III) and Mn(II), H_2O_2, and O_3. Formation of hydroxymethanesulfonate ion (HMSA) via the nucleophilic addition of HSO_3^- to $CH_2O(l)$ significantly increased the droplet capacity for S(IV) but did not slow down the net S(IV) oxidation rate leading to fog acidification. Gas phase nitric acid, ammonia, and hydrogen peroxide were scavenged efficiently, although aqueous phase hydrogen peroxide was depleted rapidly by reduction with S(IV). Nitrate production in the aqueous phase was found to be dominated by HNO_3 gas phase scavenging. Major aqueous phase species concentrations were controlled primarily by condensation, evaporation, and pH.

A. Introduction

Concentrations of major ions in nonprecipitating clouds [*Hegg and Hobbs*, 1981] and fogs [*Waldman et al.*, 1982; *Munger et al.*, 1983] have been reported to be significantly higher than those commonly observed in acidic precipitation. In Los Angeles, fogwater [*Waldman et al.*, 1982; *Munger et al.*, 1983] was reported to have acidities 100 times higher than those observed previously in rainwater by *Liljestrand and Morgan* [1981]. Lower dilutions and higher scavenging efficiencies due to reduced mass transfer limitations of gas absorption and longer residence times may explain, in part, the higher concentrations found in fog (1–100 μm) than in rain (0.1–3.0 mm).

A number of rainwater and cloudwater chemistry models have been proposed recently. *Adamowicz* [1979] simulated the chemistry of raindrops falling through a well-mixed polluted layer with uniform and constant concentrations of SO_2, CO_2, and NH_3. Gas and aqueous phase equilibria were established at all times, and aqueous phase transformation of S(IV) to S(VI) was allowed to proceed through the iron-catalyzed oxidation by O_2 according to the kinetic expression of *Brimblecombe and Spedding* [1974]. Mass transfer at the surface of the drop was modeled by two-film theory, but *Baboolal et al.* [1981] have since shown this simple model to be unsatisfactory since it ignores forced convection inside and outside of the falling drop. *Durham et al.* [1981] added NO_x to the gas phase and allowed some NO_x gas phase chemistry, considered kinetic expressions for all reactions instead of equilibrium relationships, and assumed O_3 to be the only liquid phase oxidant of S(IV) using the rate law of *Erickson et al.* [1977]. *Easter and Hobbs* [1974] modeled cloudwater chemistry by using a wave cloud model, an open atmosphere with trace concentrations of CO_2, SO_2, and NH_3, and a rudimentary S(IV) oxidation rate consisting of a simple first-order dependence on sulfite. More recent models have been proposed by *Middleton et al.* [1980], *Chameides and Davis* [1982], and *Carmichael et al.* [1983].

With this work in mind, a dynamic model for fogwater chemistry has been developed. The model has a hybrid kinetic and equilibrium structure: reactions which rapidly come to equilibrium are considered separately from reactions that are kinetically controlled. Gas phase chemistry, particle scavenging by droplets, evolution of the droplet microphysics, and deposition were not included explicitly.

Copyright 1983 by the American Geophysical Union.

Paper number 3C0722.
0148-0227/83/003C-0722$05.00

B. Structure of the Model

1 *Aqueous Phase Reactions*

The chemical composition of a fog droplet is assumed to be determined by the following factors: (1) the composition of the activated cloud condensation nuclei (CCN) on which the droplet condenses, (2) the absorption of atmospheric gases at the droplet surface, and (3) the subsequent aqueous phase reactions of homogeneous and heterogeneous species. Proton transfer and most ligand substitution reactions proceed extremely fast compared to the time scales of interest in this study [*Hoffmann*, 1981]; therefore they are treated as dynamic equilibria. The same assumption is applied to gas absorption in accordance with Henry's law, although mass transfer may be retarded by the formation of an organic film at the droplet surface [*Graedel et al.*, 1983]. Equilibrium constants K_T have been adjusted for temperature T with the van't Hoff relationship:

$$\int_{K_{298}}^{K_T} d \ln K = \frac{\Delta H^\circ_{298}}{R} \int_{298}^{T} \frac{dT}{T^2} \qquad (1)$$

ΔH° values at 298°K were obtained from literature sources (see Table 1). The equilibrium composition was determined using a MINEQL subroutine [*Morel and Morgan*, 1972; *Westall et al.*, 1976]. In MINEQL the equilibrium constant approach is used to solve the chemical equilibrium problem, which is defined by a system of mass action equations. The computed concentrations of constituents are constrained to remain positive and to satisfy mole balance relationships provided by the analytical information. Given a set of chemical constituents which have been defined operationally as metals and ligands, along with the corresponding stoichiometric and thermodynamic data, all the possible chemical species in a model system can be defined. The concentrations of these chemical species are written as functions of the free con-

TABLE 1. Henry's Law and Aqueous-Phase Equilibria Relevant to the Droplet Chemistry

Reaction No.	Reaction	pK*	$\Delta H°_{298.15°}$, kcal mole^{-1}	Reference†
(R1)	$H_2O(l) \rightleftharpoons H^+ + OH^-$	14.00	13.35	SM
(R2)	$SO_2(g) + H_2O \rightleftharpoons SO_2 \cdot H_2O$	−0.095	−6.25	SM
(R3)	$SO_2 \cdot H_2O \rightleftharpoons H^+ + HSO_3^-$	1.89	−4.16	SM
(R4)	$HSO_3^- \rightleftharpoons H^+ + SO_3^{2-}$	7.22	−2.23	SM
(R5)	$HNO_3(g) \rightleftharpoons H^+ + NO_3^-$	−6.51	−17.3	SW
(R6)	$HNO_2(g) \rightleftharpoons HNO_2(l)$	−1.7	−9.5	SW
(R7)	$HNO_2(l) \rightleftharpoons H^+ + NO_2^-$	3.29	2.5	SW
(R8)	$CO_2(g) + H_2O \rightleftharpoons CO_2 \cdot H_2O$	1.47	−4.85	SM
(R9)	$CO_2 \cdot H_2O \rightleftharpoons H^+ + HCO_3^-$	6.37	1.83	SM
(R10)	$HCO_3^- \rightleftharpoons H^+ + CO_3^{2-}$	10.33	3.55	SM
(R11)	$CH_2O(g) + H_2O \rightleftharpoons CH_2O \cdot H_2O$	−3.85	−12.85	LB
(R12)	$HOCH_2SO_3H \rightleftharpoons H^+ + HOCH_2SO_3^-$	<0‡	U§	R
(R13)	$HOCH_2SO_3^- \rightleftharpoons H^+ + {}^-OCH_2SO_3^-$	11.7	U	SA
(R14)	$NH_3(g) + H_2O \rightleftharpoons NH_3 \cdot H_2O$	−1.77	−8.17	SM
(R15)	$NH_3 \cdot H_2O \rightleftharpoons NH_4^+ + OH^-$	4.77	0.9	SM
(R16)	$O_2(g) \rightleftharpoons O_2(l)$	2.90	−3.58	P
(R17)	$H_2O_2(g) \rightleftharpoons H_2O_2(l)$	−4.85	−14.5	MD
(R18)	$O_3(g) \rightleftharpoons O_3(l)$	2.03	−5.04	L-B
(R19)	$CaHCO_3^+ \rightleftharpoons Ca^{2+} + HCO_3^-$	11.6	−2.78	SM
(R20)	$CaSO_4(l) \rightleftharpoons Ca^{2+} + SO_4^{2-}$	2.30	−1.65	SM
(R21)	$NaSO_4^- \rightleftharpoons Na^+ + SO_4^{2-}$	0.70	−2.23	SM
(R22)	$FeSO_4^+ \rightleftharpoons Fe^{3+} + SO_4^{2-}$	4.20	5.4	SM
(R23)	$Fe(SO_4)_2^- \rightleftharpoons Fe^{3+} + 2SO_4^{2-}$	5.60	U	SM
(R24)	$FeCl^{2+} \rightleftharpoons Fe^{3+} + Cl^-$	1.40	−7.91	SM
(R25)	$FeOH^{2+} \rightleftharpoons Fe^{3+} + OH^-$	12.30	0.04	SM
(R26)	$Fe(OH)_2^+ \rightleftharpoons Fe^{3+} + 2OH^-$	23.3	U	SM
(R27)	$Fe(OH)_3\downarrow \rightleftharpoons Fe^{3+} + 3OH^-$	39.0	20.7	SM
(R28)	$Fe_2(OH)_2^{4+} \rightleftharpoons 2Fe^{3+} + 2OH^-$	25.7	16.2	SM
(R29)	$FeSO_3^+ \rightleftharpoons Fe^{3+} + SO_3^{2-}$	10.0	U	this laboratory
(R30)	$MnSO_4(l) \rightleftharpoons Mn^{2+} + SO_4^{2-}$	2.30	−3.39	SM
(R31)	$MnCl^+ \rightleftharpoons Mn^{2+} + Cl^-$	1.10	−8.01	SM
(R32)	$HSO_4^- \rightleftharpoons H^+ + SO_4^{2-}$	2.20	−4.91	SM

*K is in M atm^{-1} or M. Temperature is 298°K.

†Reference code: SM = *Sillén and Martell* [1964]; SW = *Schwartz and White* [1981]; LB = *Ledbury and Blair* [1925]; SA = *Sørensen and Andersen* [1970]; MD = *Martin and Damschen* [1981]; L-B = *Landolt-Börnstein* [1976]; R = *Roberts et al.* [1971]; P = *Perry* [1963].

‡The pK for this reaction is very low.

§Unknown, $\Delta H = 0$ is assumed in the calculation.

centrations of the constituents by mass action equations. These functions are substituted into the mole balance equations with elimination of solids. The problem is reduced to a system of nonlinear equations in which the unknowns are the concentrations of the metals and ligands. This system of equations is solved by the Newton-Raphson method. The initial solution is tested against the solubility products of the solids and a new set of solids, which includes those solids with the most exceeded solubility products, is selected for the next computation. A final solution is achieved when the difference between the imposed analytical concentrations for a constituent and the sum of all individual species containing that constituent is less than or equal to a set value which is very small. Corrections for ionic strength were made using the Davies equation [*Stumm and Morgan*, 1981]. The thermodynamic data base consisted of 1300 equilibria; those found to influence the droplet composition are listed in Table 1.

For slower reactions, empirical rate laws were used. Specific rate laws for oxidation reactions involving N(III) and S(IV) have been incorporated in the model; they are listed in Table 2. Hydrogen peroxide, N(III), and O_3 are potentially important oxidants, and O_2 may also be important if catalyzed by active sites on soot or by transition metals, such as Fe(III) and Mn(II). Iron(III) and manganese(II) are effective catalysts when dissolved as free ions or complexes [*Hoffmann and Jacob*, 1983] but their catalytic properties are altered if they are present as solid phases. Surface catalysis may occur but in the absence of reliable data it has been neglected. In the kinetic formulation of (R35), [Fe(III)] and [Mn(II)] represent the summation of concentrations of all dissolved iron and manganese species. It should be noted that the kinetic data for this reaction is not satisfactory around pH 4 because of the influence of $Fe(OH)_3(s)$ which starts dissolving near pH 4. Rate expressions given by *Martin* [1983] at high pH and low pH fail to extrapolate to the same value at intermediate pH. To minimize this problem, an average of the two expressions was used near pH 4.

The reactions of absorption and aqueous phase disproportionation of NO_x to form nitrous and nitric acid have been reviewed by *Schwartz and White* [1981]. These reactions could be major contributors to nitrate formation in fog droplets if allowed to reach equilibrium; however, because of second-order kinetics they are too slow to be important on the time scales of concern in fog. Alternative aqueous phase nitrate formation pathways involve the oxidation of N(III) by H_2O_2 and O_3 [*Damschen and Martin*, 1982].

Overall, the rate laws shown in Table 2 indicate that oxidation reactions proceed on time scales of minutes to hours under urban atmospheric conditions. These rate laws are integrated with a simple finite difference scheme using adjustable

p. 6613, reactions (R38) and (R39):
"d[S(VI)]/dt" should read "d[N(V)]/dt"

TABLE 2a. Kinetic Expressions for the Aqueous Phase Oxidation Reactions of S(IV) to S(VI) and N(III) to N(V)

Reaction No.	Reaction	Conditions	Rate, $M\ s^{-1}$ at 25°C*	Activation Energy, kcal $mole^{-1}$	Reference†
(R33)	$S(IV) + H_2O_2$		$\frac{d[S(VI)]}{dt} = \frac{8 \times 10^4[H_2O_2(l)][SO_2(l)]}{0.1 + [H^+]}$	7.3	M
(R34)	$S(IV) + O_3$	$pH < 3$	$\frac{d[S(VI)]}{dt} = \frac{1.9 \times 10^4[SO_2(aq)][O_3(l)]}{[H^+]^{1/2}}$	6	M
		$pH > 3$	$\frac{d[S(VI)]}{dt} = 4.19 \times 10^5\left(1 + \frac{2.39 \times 10^{-6}}{[H^+]}\right)[O_3(l)][SO_2(aq)]$	6	Ma
(R35)	$S(IV) + O_2$ (with Fe (III) and Mn(II))	$[SO_2(aq)] > 10^{-5}$, $pH < 4$	$\frac{d[S(VI)]}{dt} = \frac{4.7[Mn(II)]^2}{[H^+]} + \left(\frac{0.82[Fe(III)][SO_2(aq)]}{[H^+]} \cdot \left(1 + \frac{1.7 \times 10^3[Mn(II)]^{1.5}}{6.3 \times 10^{-6} + [Fe(III)]}\right)\right)$	21.8	M
		$[SO_2(aq)] < 10^{-5}$, $pH < 4$	$\frac{d[S(VI)]}{dt} = 3\left(5000[Mn(II)][HSO_3^-] + \frac{0.82[Fe(III)][SO_2(aq)]}{[H^+]}\right)$	21.8	M
		$[SO_2(aq)] > 10^{-5}$, $pH > 4$	$\frac{d[S(VI)]}{dt} = \frac{4.7[Mn(II)]^2}{[H^+]} + 1 \times 10^7[Fe(III)][SO_2(aq)]^2$	27.3	M
		$[SO_2(aq)] < 10^{-5}$, $pH > 4$	$\frac{d[S(VI)]}{dt} = 5000\ [Mn(II)][HSO_3^-]$	27.3	M
(R36)	$S(IV) + O_2$ (with soot)‡		$\frac{d[S(VI)]}{dt} = 2.54 \times 10^7[O_2(l)]^{0.69} \cdot C_x \frac{[SO_2(aq)]^2}{1 + 3.06 \times 10^6[SO_2(aq)] + 1.5 \times 10^{12}[SO_2(aq)]^2}$	11.7	B
(R37)	$S(IV) + N(III)$	$pH < 3$	$\frac{d[S(VI)]}{dt} = 142[H^+][HNO_2(aq)][SO_2(aq)]$	12§	M
		$pH > 3$	$\frac{d[S(VI)]}{dt} = 2.2[HNO_2(l)][HSO_3^-]$	12§	O
(R38)	$N(III) + H_2O_2$		$\frac{d[S(VI)]}{dt} = 4.6 \times 10^3[H^+][H_2O_2(l)][HNO_2(l)]$	13.2	DM
(R39)	$N(III) + O_3$		$\frac{d[S(VI)]}{dt} = 5 \times 10^5[O_3(l)][NO_2^-]$	13.8	DM

*$[SO_2(aq)] = [SO_2(l)] + [HSO_3^-] + [SO_3^{2-}]$; $[HNO_2(aq)] = [HNO_2(l)] + [NO_2^-]$.
†Reference code: M = *Martin* [1982]; Ma = *Maahs* [1982]; B = *Brodzinsky et al.* [1980]; O = *Oblath et al.* [1981]; DM = *Damschen and Martin* [1982].
‡C_x is the concentration of active carbon in g l^{-1}.
§Assumed.

time steps ranging from 10 s to 200 s:

$$[R_i]_{t+\Delta t} = [R_i]_t + \left(\sum_{ox}\left(\frac{d[R_i]}{dt}\right)_{ox}\right)\Delta t \qquad (2)$$

where $[R_i]$ represents the concentration of the reduced component R_i (i.e. N(III) or S(IV)).

Of special interest in urban fog is the reaction of HSO_3^- with CH_2O and with other aldehydes, RCHO, to form hydroxymethanesulfonate ion (HMSA) and the corresponding sulfonates, $HOCHRSO_3^-$ [*Munger et al.*, 1983]:

$$CH_2O + HSO_3^- \underset{k_r}{\overset{k_f}{\rightleftharpoons}} HOCH_2SO_3^- \qquad (3)$$

Dasgupta et al. [1980] determined a conditional equilibrium constant for HMSA to be $K_{298} = k_f/k_r = 7.5 \times 10^4\ M^{-1}$, while S. D. Boyce and M. R. Hoffmann (unpublished manuscript, 1983) have determined that $k_f = 3\ M^{-1}\ s^{-1}$. Production of HMSA will contribute to the droplet acidity indirectly by producing a droplet that is supersaturated with respect to $SO_2(g)$, and because of the slow reversibility of (3), HMSA formation may inhibit the production of S(VI). Reaction (3) is integrated at each time step by using the integrated form of the rate law:

$$\ln\left|\frac{[HSO_3^-]_{t+\Delta t} - p}{[HSO_3^-]_{t+\Delta t} - q}\right| = k_f(q - p)\,\Delta t + \ln\left|\frac{[HSO_3^-]_t - p}{[HSO_3^-]_t - q}\right| \qquad (4)$$

TABLE 2b. Reaction Stoichiometries for Reactions in Table 2a

Reaction No.	Reaction Stoichiometries
(R33)	$HSO_3^- + H_2O_2(l) \rightarrow HSO_4^- + H_2O$
(R34)	$HSO_3^- + O_3(l) \rightarrow HSO_4^- + O_2$
(R35)	$HSO_3^- + 1/2O_2(l) \rightarrow HSO_4^-$
(R37)	$2HNO_2(l) + H_2O \cdot SO_2 \rightarrow 2NO + H^+ + HSO_4^- + H_2O$
(R38)	$2HNO_2(l) + 2H_2O \cdot SO_2 \rightarrow 2SO_4^{2-} + N_2O + H_2O + 4H^+$
(R39)	$HNO_2(l) + H_2O_2(l) \rightarrow NO_3^- + H_2O + H^+$
	$NO_2^- + O_3(l) \rightarrow NO_3^- + O_2$

$$[HMSA]_{t+\Delta t} = [HMSA]_t - ([HSO_3^-]_{t+\Delta t} - [HSO_3^-]_t) \quad (5)$$

where p and q are the solutions to the second-degree equation

$$KX^2 + (K([CH_2O(l)]_t - [HSO_3^-]_t) + 1)X - ([HSO_3^-]_t + [HMSA]_t = 0 \quad (6)$$

2. *Gas Phase and Aerosol*

At night the oxidation of nitrogeneous compounds and alkenes by ozone is important. The kinetics of these reactions are dependent on the downward diffusion of ozone to the boundary layer [*McRae*, 1981]. In the boundary layer, nitric acid may be produced [*Graham and Johnston*, 1978; *McRae and Russell*, 1983] by a variety of pathways. No attempt has been made to model gas phase chemistry. Instead, concentrations of gases and gas phase production rates (from emissions and homogeneous reactions) have been estimated from local field data and predictions from the Caltech air quality model for the Los Angeles basin [*McRae*, 1981].

The integrated mass and composition of the activated cloud condensation nuclei on which the fog droplets condense were estimated from field data. No subsequent scavenging of the interstitial aerosol by diffusion or impaction was considered.

3. *Physical Description*

A parcel of air is followed in which droplets form and grow by accretion of water vapor. The droplets are assumed to remain constantly within the air parcel (i.e., sedimentation and diffusion of the droplets are ignored).

The limitation of S(IV) oxidation rates by mass transfer has been discussed by *Schwartz and Freiberg* [1981] and *Baboolal et al.* [1981]. Schwartz and Freiberg have shown that for stationary droplets smaller than 50 μm the net rate of oxidation was limited strictly by oxidation. Baboolal et al. extended this analysis to droplets larger than 50 μm. These large droplets have a significant sedimentation velocity, which drives convection both inside and outside of the droplet. This mixing effect enhances the rate of mass transfer as calculated for stationary droplets. Therefore the chemical changes in fog droplets are most likely limited by the specific reaction rates.

Because fogs are localized events and occur on time scales of a few hours, advection of condensing and evaporating droplets can be ignored as a first approximation. Also, evolution of the droplet spectrum through coagulation can be neglected since mass transfer does not limit overall reaction rates. In this context the liquid water content of the air parcel and its time dependency are sufficient parameters for characterizing fog microphysics.

At $t = 0$, droplets are assumed to condense, receive an initial chemical loading from the water-soluble fraction of the activated nuclei, and immediately react with the gaseous environment. The growth and evaporation of the droplets is simulated by the external input of an evolving liquid water content. At each time step the equilibrium composition of the droplet is calculated along with the HMSA formation rate and the changes in component concentrations due to oxidation reactions.

C. Results and Discussion

1 *Sulfate and Nitrate Oxidation Pathways*

In this section the relative contributions of the various S(IV) and N(III) oxidation mechanisms to the droplet chemistry are discussed. For this specific purpose a closed parcel of air with a constant liquid water content has been assumed (i.e., droplets condense on the activated condensation nuclei at $t = 0$ with no droplet growth or evaporation). A nighttime air mass typical of the industralized coastline of the Los Angeles basin has been chosen. Concentrations of gases and preexisting nuclei were estimated from local field data and transport models (Table 3). Gases are depleted by absorption except for CO_2 and O_2, which are held constant at a fixed partial pressure. The liquid water content is $L = 0.1$ g m^{-3} and the temperature is $T = 283$ K.

Kinetic results shown in Figure 1 clearly show that H_2O_2 and O_2 (catalyzed by Fe and Mn) are the principal oxidants for S(VI) production in situ. Hydrogen peroxide is highly soluble in water and rapidly oxidizes S(IV) at low pH; however, if not replenished, it is quickly depleted from the parcel of air by reduction to water. In this case, in the absence of gas phase or aqueous phase H_2O_2 formation, no H_2O_2 remains in the system after 10 minutes.

The catalytic effectiveness of both Fe(III) and Mn(II) is dependent on their speciation in the droplet (Figure 2). The principal manganese species are $Mn(H_2O)_6^{2+}$ and $MnSO_4$(aq). Both of these species are assumed to be equally effective as catalysts for S(IV) autoxidation. On the other hand, Fe(III) above pH 4 is found primarily as an iron(III) hydroxide solid, which has been assumed to be catalytically inactive. As the pH decreases below 4, the solid phase dissolves and soluble Fe(III), the active catalyst, is released. The rate law indicates a decrease of the oxidation rate with pH but the dissolution of Fe(III) at low pH offsets this effect and the calculated rate actually increases between pH 4 and 3.5.

Oxidation by ozone contributes ~4% of the total S(VI)

TABLE 3. Composition of the Air Mass (Trace Gases and Condensation Nuclei) Prior to Fog Formation at a Polluted Site

Atmospheric Trace Gases		
	Concentration, ppb	Reference
SO_2	20	SCAQMD data*
HNO_2	1	*Hanst et al.* [1982]
HNO_3	3	id.
NH_3	5	id.
CH_2O	30	*Grosjean* [1982]
O_3	10	SCAQMD data
H_2O_2	1	*Graedel et al.* [1976]

Condensation Nuclei†			
	Concentration μg m^{-3}		Concentration, μg m^{-3}
SO_4^{2-}	10	NH_4^+	6.65
NO_3^-	10	Na^+	.61
Cl^-	1.1	Fe(III)	.5
CO_3^{2-}	1.83	Mn(II)	.02
C_x(soot)	30	Ca^{2+}	1.22

The air mass is typical of the industrial coastline of the Los Angeles basin for an inversion height of about 50 m. $P_{O_2} = 0.21$ atm, $P_{CO_2} = 330$ ppm.

*Data from the permanent records of the South Coast Air Quality Management District.

†$(NH_4)_2SO_4$, NH_4NO_3, NaCl, $CaCO_3$, metal oxides, and soot. References: *Gartrell et al.* [1980]; *Appel et al.* [1980].

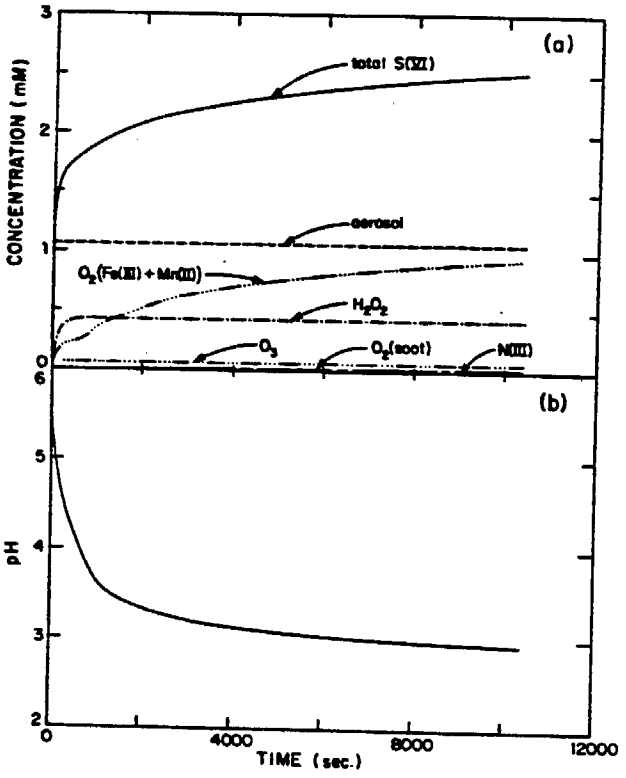

Fig. 1. (*a*) Profile versus time of total sulfate in the fogwater and of the individual contributions to the total sulfate of sulfate aerosol and different S(IV) oxidants. (*b*) Profile of *p*H versus time. The fog formed under the conditions of Table 3, with liquid water content = 0.1 g m^{-3}, temperature = 10°C.

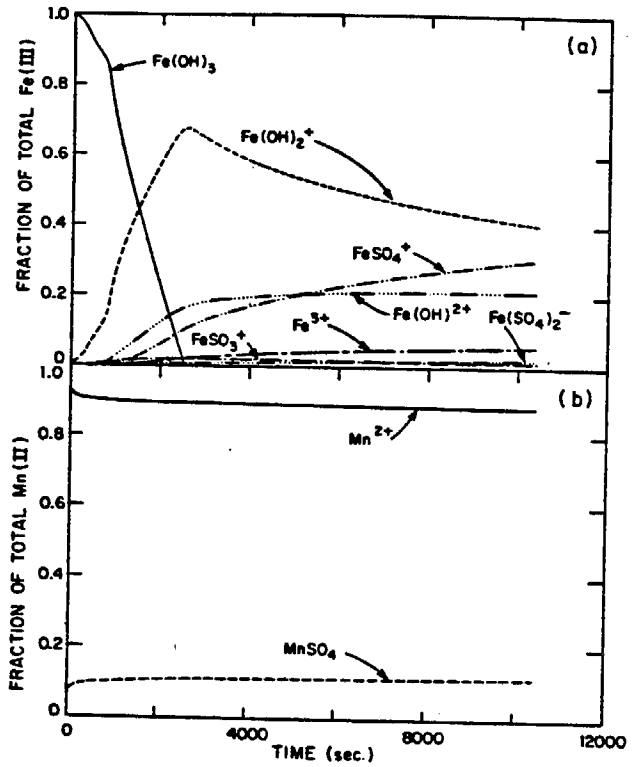

Fig. 2. Speciation of (*a*) Fe(III) and (*b*) Mn(II) in the fogwater as a function of time under conditions of Table 3, with liquid water content = 0.1 g m^{-3} and temperature = 10°C.

produced after 3 hours of fog. This is due to the low water solubility of ozone and the reciprocal hydrogen ion dependency of its reaction rate. Therefore little oxidation by ozone occurs below *p*H 4. Catalytic carbon sites in soot contribute <5% of the total S(VI) produced, even at the high carbon levels of urban environments. Oxidation by N(III) appears to be insignificant due to the low solubility of HNO_2(g) at *p*H < 4.

Oxidation of N(III) does not contribute appreciably to nitrate production. At $t = 180$ minutes, reaction with O_3 had generated less than 10^{-7} *M* NO_3^- and reaction with H_2O_2 less than 10^{-10} *M* NO_3^-.

The aqueous phase oxidation of S(IV) has an important consequence on the droplet acidity. Between *p*H 2 and 6 the principal reactive species of S(IV) is HSO_3^- [*Hoffmann and Jacob*, 1983]. The oxidation product, HSO_4^-, is completely dissociated above *p*H 3. Therefore the oxidation directly produces one free proton. Depletion of HSO_3^- leads to further dissolution of SO_2(g) which then dissociates to give HSO_3^- and H^+ in the droplet. Because the solubility of SO_2 decreases with *p*H, each depleted HSO_3^- molecule is not replaced in the droplet. Depending on the overall droplet chemistry, oxidation of one molar unit of S(IV) thus leads to the production of one- to two-fold that molar unit of free acidity. The impact on the droplet *p*H is dramatic, as shown in Figure 1*b*. In the first half hour of the fog, S(VI) production is the fastest and causes a *p*H drop of over two units. Field observations are consistent with these predictions [*Munger et al.*, 1983].

Components in the gas phase are scavenged by the droplets with efficiencies dependent on their Henry's law constants and aqueous phase chemistry. Table 4 shows the fraction of each gas scavenged at $t = 0$, $t = 30$ min, and $t = 180$ min. It must be kept in mind that these numbers vary with the liquid water content of the fog [*Schwartz*, 1983]. Nitric acid is totally dissolved and dissociated, while NH_3 dissolves totally at *p*H < 5. These two components essentially titrate each other in the aqueous phase. Formation of HMSA over the course of a fog event was found not to significantly increase the fraction of CH_2O scavenged; therefore the CH_2O partial pressure remains approximately constant throughout the simulation. Likewise, hydroxymethanesulfonate formation cannot be a significant sink for gas phase SO_2. The solubility of SO_2 is limited, but because $SO_2 \cdot H_2O$ is a weak acid, ~5% dissolves with the formation of the fog. S(IV) oxidation reactions further increase the fraction scavenged over the lifetime of the fog. Three hours after fog formation, over 80% of the initial SO_2 still remains in the gas phase, indicating that fog has little impact on the gaseous SO_2 concentration. Hydrogen peroxide

TABLE 4. Scavenging of Gases by Fog Droplets Under Conditions of Table 3

Gas	Fraction Scavenged From Gas Phase, %		
	$t = 0$	$t = 30$ min	$t = 180$ min
HNO_3	100	100	100
NH_3	43.9	99.5	100
CH_2O	5.0	5.3	5.3
SO_2	2.7	11.8	17.5
H_2O_2	32.1	100	100
O_3	0.0	1.5	1.5
HNO_2	3.8	0.0	0.0

Liquid water content = 0.1 g m^{-3}, temperature = 283 K.

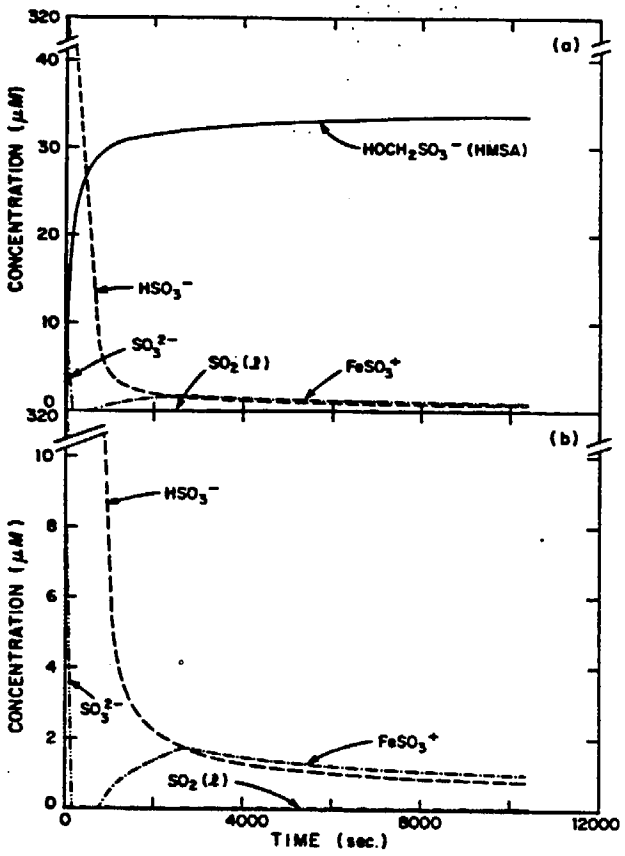

Fig. 3. (*a*) Concentrations of S(IV) species in the fogwater as a function of time under conditions of Table 3, with liquid water content = 0.1 g m^{-3} and temperature = 10°C. (*b*) Same as (*a*) but with no formaldehyde in the atmosphere.

is highly soluble in water. As was discussed above, reduction of H_2O_2 in the droplet is an efficient sink which depletes H_2O_2 from the system. Ozone, on the other hand, is poorly scavenged, as is HNO_2. Both react slowly in the droplet below *p*H 4.

The impact of HMSA formation on the droplet chemistry is worth discussing in some detail, as it has been the subject of recent interest [*Munger et al.*, 1983; *Boyce and Hoffmann*, 1983; *Richards et al.*, 1983]. Figure 3*a* shows the concentration profiles versus time for HSO_3^- and HMSA. The formation of HMSA is rapid but still slower than S(IV) oxidation. Consequently, the amount of HMSA produced is smaller than that of sulfate. Hydroxymethanesulfonate is the most important S(IV) species in solution; if formaldehyde was not present, the S(IV) concentration in the droplet would be much lower (Figure 3*b*).

It has been suggested that HMSA may inhibit S(IV) oxidation in atmospheric droplets by limiting the availability of reactive S(IV) species. This does not appear to be the case, since oxidation proceeds faster than adduct formation; furthermore, since the partial pressure of SO_2 remains approximately constant throughout the fog, the limiting concentrations of reactive S(IV) species are independent of the HMSA formation rate. However, the direct effect of HMSA on the fogwater acidity is of interest. Hydroxymethanesulfonate is the conjugate base of hydroxymethanesulfonic acid, which is a strong acid [*Roberts et al.*, 1971]. Hydroxymethanesulfonate is a weak acid (see Table 1). Between *p*H 2 and 10 and in a system open to SO_2, HMSA is stable and complexation of HSO_3^- leads to further dissolution of SO_2, which then dissociates and releases free acidity in the droplet. Because of the small amounts of HMSA produced with respect to the droplet $[H^+]$ concentration, this contribution is small.

In the first simulation, S(VI) formation buffered the droplet acidity at about *p*H 3, whereas in some extremely polluted atmospheres, higher acidity can be imparted to the droplet at $t = 0$ by simple dissolution of the activated nuclei. *Cass* [1975] reports some cases for Los Angeles, mostly under high humidity conditions, where the aerosol sulfate concentration was as high as 75 $\mu g\ m^{-3}$. A second simulation was run (Figures 4 and 5) under the same conditions as the first but with 75 $\mu g\ m^{-3}$ SO_4^{2-} in the air mass as NH_4HSO_4 nuclei instead of 10 $\mu g\ m^{-3}$ SO_4^{2-} as $(NH_4)_2SO_4$.

The *p*H of 2.4 at $t = 0$ (Figure 4) indicates the impact of the acid nuclei. At this low *p*H there is very little S(IV) in the droplet (Figure 5) and the only S(IV) oxidation reaction to proceed at a significant rate is that with H_2O_2. Therefore less sulfate and hydrogen ion are produced in situ. In the case of acidic condensation nuclei the *p*H of the fog may be controlled strictly by the nuclei composition instead of by S(VI) aqueous phase production. It should be mentioned that fogwater *p*H in the range of 2 to 2.5 has been observed in the Los Angeles basin following heavy 'smog' days. The lowest *p*H recorded was 1.69 in a dissipating fog along the coastline; in that case the dilution was probably less than the $L = 0.1$ g m^{-3} considered in the simulation.

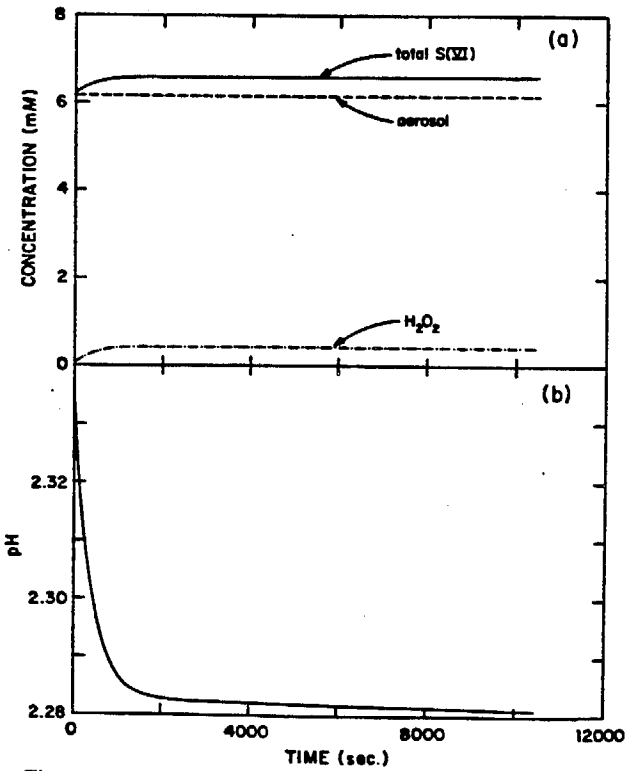

Fig. 4. (*a*) Profile versus time of total sulfate and of the individual contributions to the total sulfate of sulfate aerosol and different S(IV) oxidants. (*b*) Profile of *p*H versus time. The fog formed by condensation on highly acidic nuclei (75 $\mu g\ m^{-3}$ NH_4HSO_4), other conditions as in Table 3, with liquid water content = 0.1 g m^{-3} and temperature = 10°C.

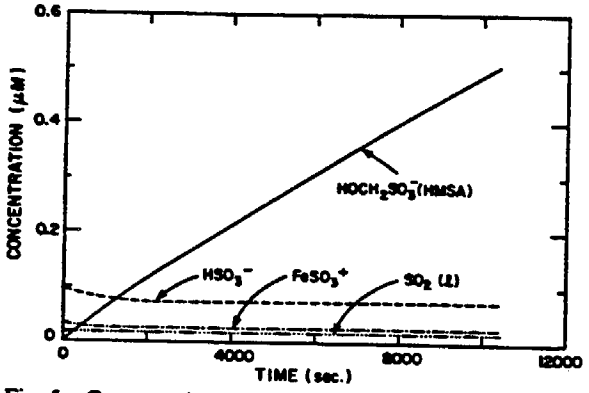

Fig. 5. Concentration of S(IV) species in the fogwater as a function of time. The fog formed by condensation on highly acidic nuclei (75 $\mu g\ m^{-3}$ NH_4HSO_4), other conditions as in Table 3, with liquid water content = 0.1 $g\ m^{-3}$ and temperature = 10°C.

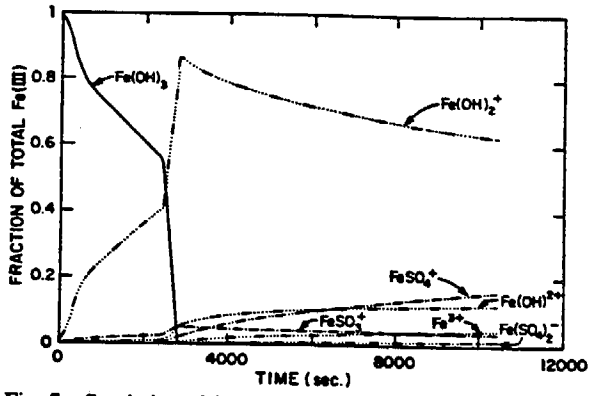

Fig. 7. Speciation of Fe(III) in the fogwater as a function of time under conditions of Table 3, with liquid water content = 0.1 $g\ m^{-3}$ and temperature = 1°C.

Fog frequently forms at temperatures lower than 10°C. Radiation fogs, in particular, often form near freezing. To check the chemical sensitivity of the system to temperature, a simulation was run at 1°C with $L = 0.1\ g\ m^{-3}$ and conditions given in Table 3. Reaction rates are slower at 1°C, but gas solubility increases. Solution equilibria are shifted in either direction depending on the sign of $\Delta H°$. The combination of these effects has an interesting impact on the sulfate production rates and the *p*H profile (Figure 6). The rate of S(IV) oxidation by H_2O_2 is relatively unaffected because of its low activation energy E_a, but metal-catalyzed oxidation by O_2, which has a high E_a, is much slower at 1°C than at 10°C. Oxidation by ozone becomes appreciable at the beginning of the fog because of its low E_a and the increased ozone solubility. However, between *p*H 4.5 and *p*H 4, H_2O_2 is totally depleted and oxidation by ozone becomes insignificant; the S(IV) autoxidation reaction is also very slow. The sulfate concentration and *p*H profiles are almost at a plateau in this *p*H range. Then, as the *p*H drops below 4, $Fe(III)(OH)_3$ starts dissolving and the rate of oxidation by O_2 increases, such that sulfate and acidity are again produced at an appreciable rate. After 3 hours of fog the values for *p*H and sulfate concentration are close to what they were at 10°C. The speciation profile of Fe(III) (Figure 7) is similar to that at 10°C, but dissolution of $Fe(OH)_3$ is retarded because of the slow drop in *p*H from 4.5 to 4. The speciation of Mn(II) is essentially the same as at 10°C.

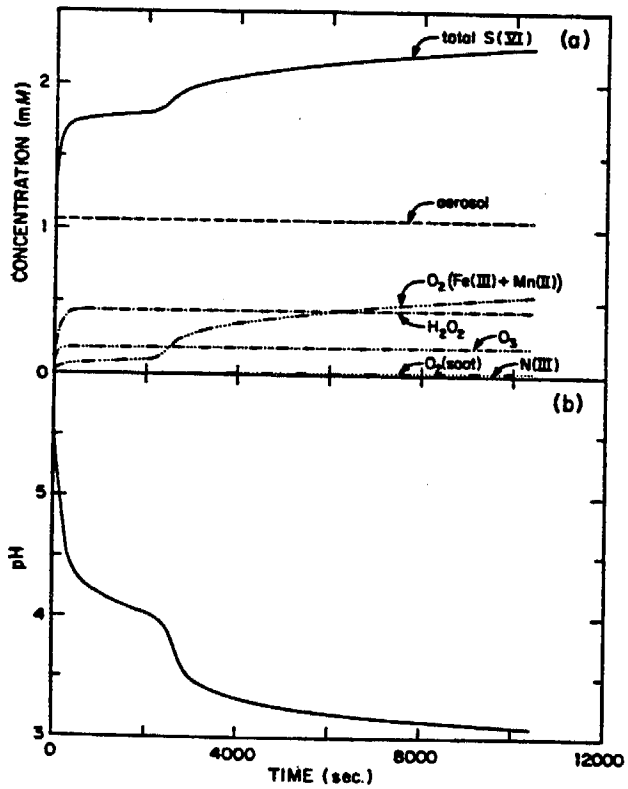

Fig. 6. (*a*) Profile versus time of total sulfate and of the individual contributions to the total sulfate of sulfate aerosol and different S(IV) oxidants. (*b*) Profile of *p*H versus time. The fog formed under the conditions of Table 3, with liquid water content = 0.1 $g\ m^{-3}$ and temperature = 1°C.

The scavenging efficiency of gases (Table 5) reflects their increased solubility; however, because the aqueous phase reactions are slower, little increase is seen between $t = 0$ and $t = 30$ min. After 3 hours the scavenging efficiency for SO_2 is similar to that at 10°C.

An interesting feature of the chemistry at 1°C is the high concentration of HMSA (Figure 8), which is due to the increased solubility of SO_2 and CH_2O. The reaction proceeds via a nucleophilic substitution of methylene glycol (S. D. Boyce and M. R. Hoffmann, unpublished manuscript, 1983) with an activation energy near 12 kcal $mole^{-1}$. Consequently, the reaction still proceeds rapidly at 1°C.

TABLE 5. Scavenging of Gases by Fog Droplets Under Conditions of Table 3

Gas	Fraction Scavenged From Gas Phase, %		
	$t = 0$	$t = 30$ min	$t = 180$ min
HNO_3	100	100	100
NH_3	76.0	97.0	100
CH_2O	9.8	10.3	10.5
SO_2	10.7	13.0	18.2
H_2O_2	58.0	100	100
O_3	0.0	4.2	4.2
HNO_2	10.2	3.4	0.0

Liquid water content = 0.1 $g\ m^{-3}$; temperature = 274 K.

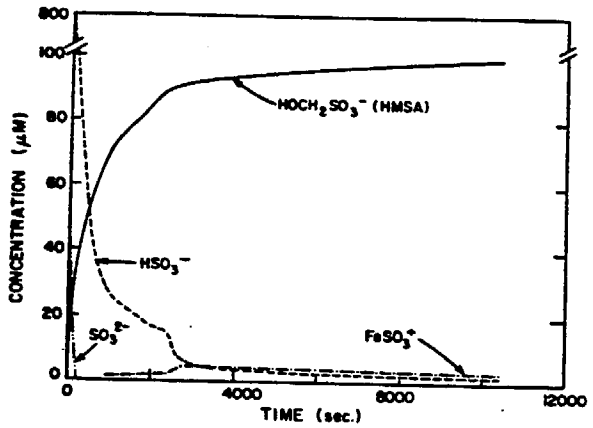

Fig. 8. Concentrations of S(IV) species in the fogwater as a function of time under conditions of Table 3, with liquid water content = 0.1 g m^{-3} and temperature = 1°C.

2. *Simulation of a Fog Event*

The simulation with the present model of an actual fog event necessitates the knowledge of input variables such as the condensation nuclei composition, the evolution of liquid water content with time, and the gas phase concentrations. Unfortunately, our field investigations [*Waldman et al.*, 1982; *Munger et al.*, 1983] so far have been limited to the determination of fogwater composition. Field data for the above parameters is incomplete; therefore a direct comparison of calculated and observed values is not possible at this time. In addition the current model neglects gas phase chemistry, transport mechanisms, and aerosol scavenging by droplets.

Fogwater composition and its variation with time for fog events at Lennox, a site in an industrial area near the Los Angeles coastline, have been documented thoroughly [*Waldman et al.*, 1982; *Munger et al.*, 1983]. In this section, a fog occurring under conditions typical of this highly impacted site has been simulated.

A plausible scenario for the evolution of liquid water content in fogs can be obtained from existing data [*Jiusto and Lala*, 1983]. The liquid water content often rises linearly following fog formation (neglecting small time scale oscillations), reaches a stable value after about an hour, and decreases linearly when the fog evaporates. Liquid water contents range from 0.01 g m^{-3} in very light fogs to 0.5 g m^{-3} in dense fogs. The profile chosen here is shown in Figure 9.

Concentrations of condensation nuclei and atmospheric gases prior to fog formation are given in Table 3. From the discussion of the previous section, it appears that some gas-phase emissions should be included. Hydrogen peroxide is not produced in the gas phase at night and thus actually disappears when the fog forms. Ammonia and HNO_3, which are scavenged efficiently by the droplets, are, on the other hand, continuously emitted into the atmosphere from a variety of sources. Because fog droplets are a sink for these two gases, fresh inputs into the parcel of air must be considered. At Lennox, plausible values associated with an inversion height of 50 m are 0.01 ppb min^{-1} for HNO_3 [*McRae and Russell*, 1983] and 0.01 ppb min^{-1} for NH_3 [*Russell et al.*, 1983]. Other gases included in the simulation are not depleted by fog, and a reasonable assumption is that their concentrations remain constant throughout the event. A constant temperature of 10°C has been chosen. Temperature changes during the course of fog events [*Jiusto and Lala*, 1983] are minimal.

The concentrations predicted for the major ions (Figure 10) are in the range of those reported by *Waldman et al.* [1982] and *Munger et al.* [1983], but no precise comparison should be made because of the reasons stated at the beginning of this section. The concave profiles observed (except for $[H^+]$) confirm the important role of dilution and evaporation that was suggested initially by Waldman et al. Aqueous phase oxidation of N(III) to N(V) is negligible and the only nitrate source is the slow gas phase production of HNO_3 followed by dissolution and dissociation. As a result, the nitrate concentration is controlled primarily by droplet growth. Similar behavior is predicted for ammonium ion, although in the initial stage of the fog the *p*H drop from a high value increases the NH_4^+ concentration. From equilibria described by (14) and (15), it is seen that scavenging of gaseous ammonia is highly *p*H-dependent over the range of 5 to 8, which is typical of fog forming in rural environments (D. J. Jacob, unpublished data, 1983) or influenced by alkaline atmospheric components [*Munger et al.*, 1983]. In such fogs, the NH_4^+ levels are expected to be controlled by acidity as well as dilution.

Oxidation of S(IV) contributes substantially to the sulfate level and the acidity in the early stages of the fog, and in the fully developed fog, 50% of the total sulfate present has been produced in the aqueous phase. During the first few minutes of the fog, S(IV) oxidation is in fact rapid enough to compensate for dilution; after H_2O_2 is depleted and the *p*H has dropped, the oxidation rate slows down and the role of dilution becomes predominant. Even with dilution the *p*H of the droplets does not rise because metal-catalyzed S(IV) oxidation by O_2 produces significant acidity in the droplet; instead, *p*H stabilizes at about 3.5. As the fog evaporates, concentration leads to a further *p*H decrease. The speciation of Fe(III) (Figure 11) correlates with *p*H in the manner discussed in the previous section. $FeSO_4^+$ becomes an important species as the fog evaporates because the sulfate concentration is so high. Speciation of Mn(II) (not shown) is similar to that in Figure 2.

An important question is, 'Is the sulfate formation predicted theoretically actually seen in the field?' The data of *Waldman et al.* [1982] and *Munger et al.* [1983] do not show obvious evidence for this. However, the bulk of the aqueous phase sulfate production is predicted to occur in the first hour of the fog, so that it could not be detected given the time resolution of the field study. A way to obtain experimental confirmation of this process would be to compare the amount of sulfate present in the atmosphere just before fog formation to that right after fog formation.

The HMSA concentration profile (Figure 12) shows the dominant effect of droplet growth and evaporation, except in

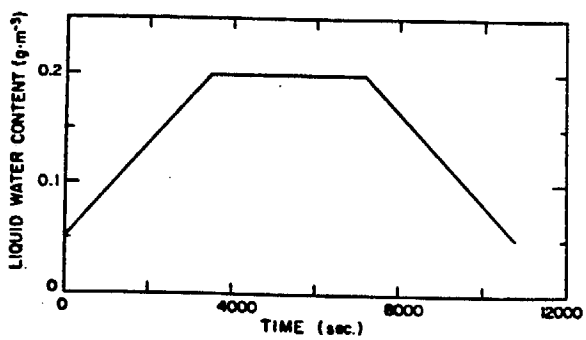

Fig. 9. Liquid water content profile versus time chosen for the simulation of a fog event in the Los Angeles basin.

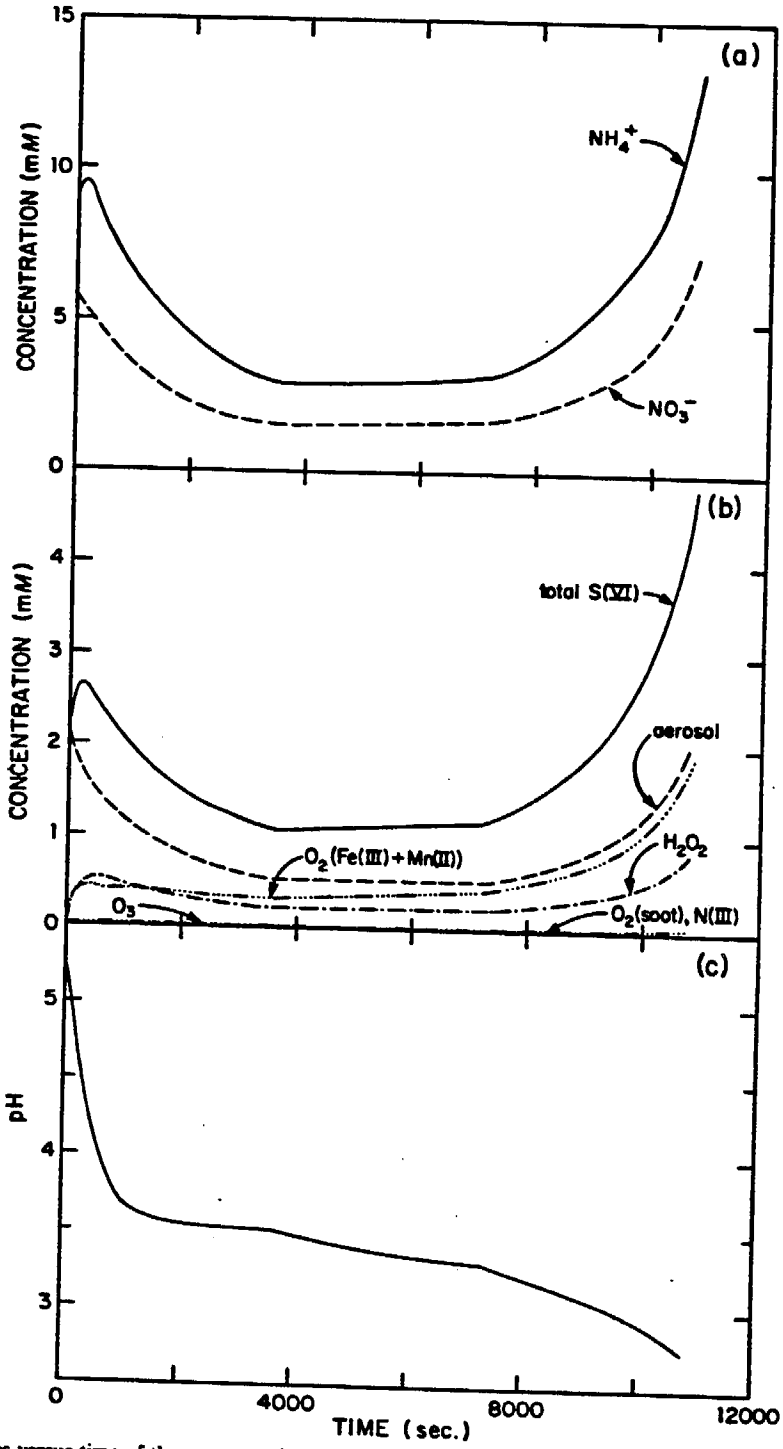

Fig. 10. Profiles versus time of the concentrations of the major ions in the fogwater under conditions of Table 3, with liquid water content as given in Figure 9 and temperature = 10°C. (*a*) Nitrate and ammonium ions. (*b*) Total sulfate and individual contributions of the different sulfate production mechanisms. (*c*) *p*H.

the first few minutes of the fog. Hydroxymethanesulfonate is the major S(IV) species, and its formation may explain the high S(IV) levels found in fogwater [*Munger et al.*, 1983]. It should be noted that in addition to formaldehyde, sulfite is known to readily form sulfonates with other aldehydes, some of which have been found in fog at concentrations comparable to formaldehyde [*Grosjean and Wright*, 1983]. These reactions would further explain the high S(IV) concentrations observed.

D. Conclusion

The chemistry of fogs forming in an urban environment has been investigated using a hybrid kinetic and equilibrium model. The most important conclusions are as follows.

1. Aqueous phase oxidation of S(IV) is an important source of sulfate in the droplet. The principal oxidants are H_2O_2 and O_2 (catalyzed by Fe(III) and Mn(II)), although ozone can also be an important oxidant above *p*H 5. Oxida-

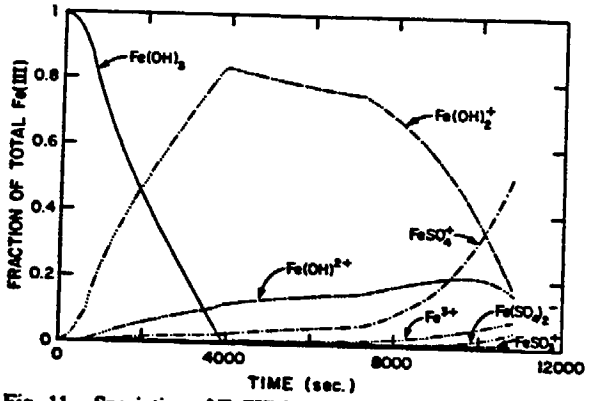

Fig. 11. Speciation of Fe(III) in the fogwater as a function of time under conditions of Table 3, with liquid water content as given in Figure 9 and temperature = 10°C.

tion by H_2O_2 is very fast but limited by its availability in the atmosphere. Most of the sulfate production occurs within the first hour following fog formation.

2. When fog condenses on alkaline to slightly acid nuclei, important acidification occurs as a result of S(IV) oxidation. In the first case simulated, the *p*H dropped two units from its initial value of 5.5 during the first half hour of the fog; it then stabilized around *p*H 3. When the fog formed on highly acidic condensation nuclei, however, the *p*H drop due to S(IV) oxidation was very small because of the high acidity initially present in the droplet.

3. Oxidation of N(III) in the droplet does not lead to significant production of nitrate. Production of nitrate proceeds through gas phase formation of HNO_3 followed by dissolution and dissociation in the droplet. Nitric acid is scavenged efficiently by the droplets as it is formed in the gas phase.

4. NH_4^+ concentration is dependent both on the liquid water content of the fog and the solubility of NH_3. Below *p*H 5 the droplets are essentially a total sink for NH_3, but above *p*H 5 the gas is partitioned between the two phases in a highly *p*H-dependent manner.

5. Over 90% of the S(IV) present in the droplet is complexed as HMSA, and this may explain the high S(IV) concentrations observed by *Munger et al.* [1983]. Formation of HMSA releases free acidity, but its effect on the droplet *p*H is negligible.

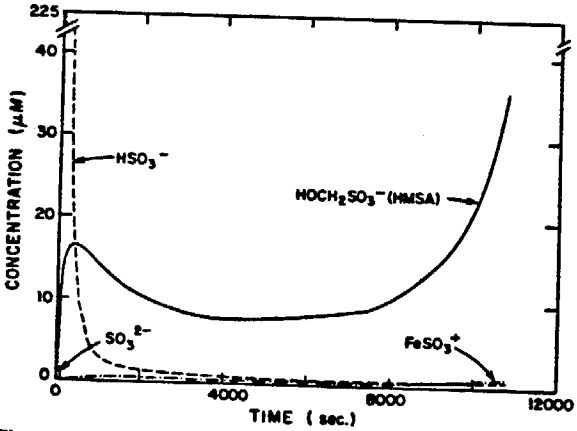

Fig. 12. Concentrations of S(IV) species in the fogwater as a function of time under conditions of Table 3, with liquid water content as given in Figure 9 and temperature = 10°C.

6. Fog does not affect the SO_2 gas phase concentrations greatly; as a result the supply of reactive S(IV) species for S(VI) and HMSA formation is determined primarily by the droplet *p*H. S(VI) formation proceeds faster than HMSA formation at all times and limits HMSA formation by causing the *p*H to drop and thus reducing the S(IV) supply.

7. At lower temperatures (1°C versus 10°C), metal-catalyzed oxidation by O_2 is slower and the importance of ozone as an S(IV) oxidant increases. Overall, sulfate and acidity are not produced as fast in the early stages of the fog but catch up later and become comparable in the later stage of the fog. Much more HMSA is produced at the lower temperature.

The model has thus revealed some important features of the chemistry and production of acidity in urban fogs. Gas phase and aerosol chemistry, droplet microphysics, and wind fields will have to be incorporated in future versions to give the simulations a predictive capability. These theoretical advances will have to be accompanied by concomitant sets of field measurements.

E. References

Adamowicz, R. F., A model for the reversible washout of sulfur dioxide, ammonia and carbon dioxide from a polluted atmosphere and the production of sulfates in raindrops, *Atmos. Environ., 13*, 105–121, 1979.

Appel, B. R., E. L. Kothny, E. M. Hoffer, and J. J. Wesolowski, Sulfate and nitrate data from the California Aerosol Characterization Experiment (ACHEX), *Adv. Environ. Sci. Technol., 9*, 315–335, 1980.

Baboolal, L. B., H. R. Pruppacher, and J. H. Topalian, A sensitivity study of a theoretical model of SO_2 scavenging by water drops in air, *J. Atmos. Sci., 38*, 856–870, 1981.

Brimblecombe, P., and D. J. Spedding, The catalytic oxidation of micromolar aqueous sulphur dioxide, *Atmos. Environ., 8*, 937–945, 1974.

Brodzinsky, R., S. G. Chang, S. S. Markowitz, and T. Novakov, Kinetics and mechanism for the catalytic oxidation of sulfur dioxide on carbon in aqueous suspensions, *J. Phys. Chem., 84*, 3354–3358, 1980.

Carmichael, G. R., T. Kitada, and L. K. Peters, The effects of in-cloud and below-cloud scavenging on the transport and gas phase reactions of SO_x, NO_y, HC_x, H_xO_y, and O_3 compounds, in *4th International Conference on Precipitation Scavenging, Dry Deposition, and Resuspension*, Santa Monica, December 1982, Elsevier, New York, in press, 1983.

Cass, G. R., Dimensions of the Los Angeles SO_2/sulfate problem, *Environ. Qual. Lab. Memo. 15*, Calif. Inst. of Technol., Pasadena, 1975.

Chameides, W. L., and D. D. Davis, The free radical chemistry of cloud droplets and its impact upon the composition of rain, *J. Geophys. Res., 87*, 4863–4877, 1982.

Damschen, D. E., and L. R. Martin, Aqueous aerosol oxidation of nitrous acid by O_2, O_3, and H_2O_2, *Atmos. Environ.*, in press, 1983.

Dasgupta, P. K., K. De Cesare, and J. C. Ullrey, Determination of atmospheric sulfur dioxide without tetrachloromerurate(II) and the mechanism of the Schiff reaction, *Anal. Chem., 52*, 1912–1922, 1980.

Durham, J. L., J. M. Overton, and V. P. Aneja, Influence of gaseous nitric acid on sulfate production and acidity in rain, *Atmos. Environ., 15*, 1059–1068, 1981.

Easter, R. C., and P. V. Hobbs, The formation of sulfate and the enhancement of cloud condensation nuclei in clouds, *J. Atmos. Sci., 31*, 1586–1594, 1974.

Erickson, R. E., L. M. Yates, R. L. Clark, and D. McEwen, The reaction of sulfur dioxide with ozone in water and its possible atmospheric significance, *Atmos. Environ., 11*, 813–817, 1977.

Gartrell, G., Jr., S. L. Heisler, and S. K. Friedlander, Relating particulate properties to sources: The results of the California Aerosol Characterization Experiment, *Adv. Environ. Sci. Technol., 9*, 665–713, 1980.

Graedel, T. E., L. A. Farrow, and T. A. Weber, Kinetic studies of the photochemistry of the urban atmosphere, *Atmos. Environ., 10*, 1095–1116, 1976.

Graedel, T. E., P. S. Gill, and C. J. Wechsler, Effects of organic surface films on the scavenging of atmospheric gases by raindrops and aerosol particles, in *4th International Conference on Precipitation Scavenging, Dry Deposition, and Resuspension, Santa Monica, December 1982*, Elsevier, New York, in press, 1983.

Graham, R. A., and H. S. Johnston, The photochemistry of NO_3 and the kinetics of the N_2O_5–O_3 system, *J. Phys. Chem., 82*, 254–268, 1978.

Grosjean, D., Formaldehyde and other carbonyls in Los Angeles ambient air, *Environ. Sci. Technol., 16*, 254–262, 1982.

Grosjean, D., and B. Wright, Carbonyls in urban fog, ice fog, cloudwater and rain water, *Atmos. Environ.*, in press, 1983.

Hanst, P. L., N. W. Wong, and J. Bragin, A long-path infra-red study of Los Angeles smog, *Atmos. Environ., 16*, 969–981, 1982.

Hegg, D. A., and P. V. Hobbs, Cloudwater chemistry and the production of sulfates and clouds, *Atmos. Environ., 15*, 1597–1604, 1981.

Hoffmann, M. R., Thermodynamic, kinetic and extrathermodynamic considerations in the development of equilibrium models for aquatic systems, *Environ. Sci. Technol., 15*, 345–353, 1981.

Hoffmann, M. R., and D. J. Jacob, Kinetics and mechanisms of the catalytic oxidation of dissolved sulfur dioxide in aqueous solution: An application to nighttime fogwater chemistry, in *Acid Precipitation*, edited by J. G. Calvert, Ann Arbor Science, Ann Arbor, Mich., in press, 1983.

Jiusto, J. E., and G. G. Lala, Radiation fog field programs—Recent studies, *ASRC-SUNY Publ. 869*, State Univ. of N. Y., Albany, 1983.

Landolt-Börnstein, *Zahlenwerte und Funktionen. Gleichgewicht der Absorption von Gasen in Flüssigkeiten von niedrigem Dampfdruck*, 6th ed., vol. 4, part 4, sect. C, Springer Verlag, Heidelberg, Federal Republic of Germany, 1976.

Ledbury, W., and E. W. Blair, The partial formaldehyde vapour pressure of aqueous solutions of formaldehyde, 2, *J. Chem. Soc., 127*, 2832–2839, 1925.

Liljestrand, H. M., and J. J. Morgan, Spatial variations of acid precipitation in Southern California, *Environ. Sci. Technol., 15*, 333–339, 1981.

Maahs, H. G., The importance of ozone in the oxidation of sulfur dioxide in nonurban tropospheric clouds, paper presented at the 2nd Symposium on the Composition of the Nonurban Troposphere, Am. Meteorol. Soc., Williamsburg, Va., 1982.

Martin, L. R., Kinetic studies of sulfite oxidation in aqueous solution, in *Acid Precipitation*, edited by J. G. Calvert, Ann Arbor Science, Ann Arbor, Mich., in press, 1983.

McRae, G. J., Mathematical modeling of photochemical air pollution, Ph.D. thesis, Calif. Inst. of Technol., Pasadena, 1981.

McRae, G. J., and A. G. Russell, Dry deposition of nitrogen containing species, in *Acid Deposition: Wet and Dry*, vol. 6, edited by B. B. Hicks, Ann Arbor Science, Ann Arbor, in press, 1983.

Middleton, P., C. S. Kiang, and V. A. Mohnen, Theoretical estimates of the relative importance of various urban sulfate aerosol production mechanisms, *Atmos. Environ., 14*, 463–472, 1980.

Morel, F., and J. J. Morgan, A numerical method for computing equilibria in aqueous chemical systems, *Environ. Sci. Technol., 6*, 58–67, 1972.

Munger, J. W., D. J. Jacob, J. M. Waldman, and M. R. Hoffmann, Fogwater chemistry in an urban atmosphere, *J. Geophys. Res., 88*, 5109–5121, 1983.

Oblath, S. B., S. S. Markowitz, T. Novakov and S. C. Chang, Kinetics of the formation of hydrozylamine disulfonate by reaction of nitrite with sulfites, *J. Phys. Chem., 85*, 1017–1021, 1981.

Perry, J. M., *Chemical Engineer's Handbook*, 4th ed., McGraw-Hill, New York, 1963.

Richards, L. W., J. A. Anderson, D. L. Blumenthal, J. A. McDonald, G. L. Kok, and A. L. Lazrus, Hydrogen peroxide and sulfur (IV) in Los Angeles cloud water, *Atmos. Environ.*, 17, 911–914, 1983.

Roberts, J. D., R. Stewart, and M. C. Caserio, *Organic Chemistry*, W. A. Benjamin, Menlo Park, Calif., 1971.

Russell, A. G., G. J. McRae, and G. R. Cass, Mathematical modeling of the formation and transport of ammonium nitrate aerosol, *Atmos. Environ.*, in press, 1983.

Schwartz, S. E., Gas-aqueous reactions of sulfur and nitrogen oxides in liquid-water clouds, in *Acid Precipitation*, edited by J. G. Calvert, Ann Arbor Science, Ann Arbor, Mich., in press, 1983.

Schwartz, S. E., and J. E. Freiberg, Mass-transport limitation to the rate of reaction of gases in liquid droplets: Application to oxidation of SO_2 in aqueous solutions, *Atmos. Environ., 15*, 1129–1144, 1981.

Schwartz, S. E., and W. H. White, Solubility equilibria of the nitrogen oxides and oxyacids in dilute aqueous solution, *Adv. Environ. Sci. Eng., 4*, 1–45, 1981.

Sillén, G. L. and A. E. Martell, Stability constants of metal-ion complexes, *Spec. Publ. 17*, Chem. Soc., London, 1964.

Sørensen, P. E., and V. S. Andersen,, The formaldehyde-hydrogen sulphite system in alkaline aqueous solution: Kinetics, mechanisms, and equilibria, *Acta Chem. Scand., 24*, 1301–1306, 1970.

Stumm, W., and J. J. Morgan, *Aquatic Chemistry*, 2nd ed., Wiley-Interscience, New York, 1981.

Waldman, J. M., J. W. Munger, D. J. Jacob, R. C. Flagan, J. J. Morgan, and M. R. Hoffmann, Chemical composition of acid fog, *Science, 218*, 677–680, 1982.

Westall, J. C., J. L. Zachary, and F. M. Morel, MINEQL, a computer program for the calculation of chemical equilibrium composition of aqueous solutions, *Tech. Note 18*, Dep. of Civ. Eng., Mass. Inst. of Technol., Cambridge, Mass., 1976.

(Received October 4, 1982;
revised April 14, 1983;
accepted April 14, 1983.)

APPENDIX V

Reprinted from ENVIRONMENTAL SCIENCE & TECHNOLOGY, Vol. *18*, Page 61, January 1984
Copyright © 1983 by the American Chemical Society and reprinted by permission of the copyright owner

SIR: Mr. W. B. Innes has stated that "low pH levels sound very damaging, but no damage to materials or health has been established. This lack of effect might be expected...". I strongly disagree with Mr. Innes' suggestion that fogs with pH of 2 and lower will have no impact on plants, materials, or humans. With respect to potential effects, the aqueous concentrations of fog droplets, the acidity per volume of air, and the acid deposition rate are all important factors to consider. The pH of urban fogs does not tell the whole story; however, it is sufficient information to prompt us to examine the severity of the situation and review past findings on the subject.

Fog water collected by a rotating (impaction) collector in the Los Angeles basin (*1*) has been found to routinely have pH values between 1.7 and 3.0. These values can be compared to Los Angeles rainfall for 1978–1979 with a volume-weighted mean pH of 4.5 (*2*). On a volumetric basis, maximum fog water values observed were 82 $\mu g/m^3$ of NO_3^-, 27 $\mu g/m^3$ of SO_4^{2-}, and 1.7 $\mu g/m^3$ of H^+. Mader et al. (*3*) measured total acidity in downtown Los Angeles fogs using a filtration technique; they reported a value of 144 $\mu g/m^3$ or 0.033 ppm as H_2SO_4 on Nov 22, 1949. This concentration corresponds to a pH of approximately 1.8, assuming a liquid water content (LWC) of 0.2 g/m^3. Even greater values have been reported for London fogs, which are discussed later. Thomas et al. (*4*) reported that Swiss chard and table-beet leaves exposed to fog on the same day (Nov 22, 1949) were extensively pockmarked and developed spot lesions. Similar damage was reported for alfalfa and spinach. Scherbatskoy and Klein (*5*) have shown that seedlings of yellow birch misted with sulfuric acid at pH of 2.8 developed necrotic spots after one or more exposures. They also showed an increase in the leaching of Ca^{2+}, K^+, and amino acids at pH 2.8 compared to pH 4.3 and 5.6. Taylor and co-workers (*6*) have presented evidence that a wide variety of plant species are injured significantly when misted with droplets in the pH range 1.7–2.5 (values commonly found in our field work).

The deposition of fog, mist, and cloud droplets by inertial impaction to vegetation can be a significant source of water and solute. In an extensive study in Japan, Yosida and Kuroiwa (*7*) reported an average fog water deposition rate of 0.5 mm/h in a coastal forest. Schlesinger and Reiners (*8*) found that artificial foliar collectors captured 4.5 times more water than open buckets, while Lovett et al. (*9*) have shown that direct cloud droplet deposition due to inertial impaction contributes about 46% of the total water in subalpine balsam fir forests. They also found chemical inputs via occult precipitation to range from 150–430% of bulk precipitation. In our own research, we (*10*) have found stratus clouds intercepting on the slope below Mount Wilson to have a median pH of 2.86 (38 samples in June 1982) with nitrate as the major anion (median $[NO_3^-] = 1435$ μeqiv/L). For a LWC = 0.2 g/m^3, this converts to approximately 18 μg of NO_3^-/m^3 of air. Assuming a water deposition rate of 0.2 mm/h and the median pH given above, the acid deposition could be greater than 200 $\mu equiv/(m^2 \cdot h)$. Thus, 8 h of fog precipitation at this rate can exceed the acid deposition accompanying 2 in. of average Los Angeles rainfall. Mr. Innes states that the buffering capacity of most biological systems is much greater than the amount of acid in "acid fog". The combination of occult precipitation with accumulated dry deposition may lead to a severe and damaging microenvironment for exposed plant tissue, beyond their buffering capacity. Fog water dripping from trees exposed to Los Angeles stratus (*10*) had a pH virtually the same as that in the fog, but with much higher solute concentrations—in one case $[NO_3^-] = 19.9$ mequiv/L, $[SO_4^{2-}] = 5.9$ mequiv/L, and pH = 3.1. It appears that wetting by fog interception can dissolve accumulated solutes from dry deposition and fog water evaporate. The effect is more dramatic for fog than rain because rainfall can rinse off and dilute the accumulated material. At this sampling site severely damaged needles of the *Pinus radiata* × *P attenuata* hybrid pine tree were found (*11*). Principal symptoms included necrosis and early abscission of second year and advanced yellow tip diback of first year needle growth. Ozone damage cannot be excluded, but symptoms were evident following a particularly foggy spring, before summer ozone levels became significant. In general, plant injury for sensitive tissues will be a function of aqueous concentration and exposure time. Acidity per volume of air will be less important, since plant surfaces often become fully coated by a fog water film. Los Angeles coastal fogs persist on the average for 4–12 h and occur on a significant number of days each spring and early winter. In the agriculturally rich San Joaquin Valley, "tule fogs" may persist 3–7 days on several occasions each winter. This year fog was observed in Bakersfield almost continually from Dec 28, 1982, to Jan 17, 1983.

In the case of material damage, Mr. Innes is again mistaken that exposure of material surfaces to low pH water derived from the atmosphere does not result in damage. Nriagu (*12*) has reviewed the literature on the subject of the deteriorative effects of sulfur pollution on materials. These effects have been well established. Sulfur dioxide and sulfuric acid at high relative humidities have been shown to damage extensively iron, steel, copper, zinc, aluminum, magnesium, limestone, building materials, paint, textiles, dyes, paper, wood, and leather. Fuzzi et al. (*13*) have reported pH values below 3 in Po Valley (northern Italy) fog. During the winter months fog frequently can be as high as 30%. Impaction of acid fog on the famous bronze Horeses of San Marco in Venice has been thought to be the primary contribution to their visible degradation due to bronze disease [i.e., corrosion] (*14*, *15*). The four horses stood for more than 700 years on the loggia high on the facade of the Basilica of San Marco with no visible sign of deterioriation. However, since World War II extensive damage has occurred. In 1974, restoration was initiated in an attempt to preserve these famous statues that had survived in remarkable condition from antiquity. Locally, Mr. Eric Holtz, a California Science Fair winner, has established that metal plates painted with conventional car paints lose measureable spectral reflectivity after exposure to mists of the composition and pH reported by Waldman et al. (*16*) and Munger et al (*1*). Significant losses of reflectivity were recorded for all paints except those with added hardners. Painted plates covered with automobile wax were also found to susceptibile to dulling.

Finally, Mr. Innes claimed that human health effects due to "acid fog" are not to be expected. Again, I believe that he is mistaken. On an historical basis (*17*) it is well-known that virtually all of the worlds's air pollution disasters occurred during fog events as indicated in Table I. To date the exact agent or combination of agents that caused death is unknown. Larsen (*18*) has speculated that the synergistic effect of SO_2 and particulate matter was the primary factor in the recorded excess deaths. Others have speculated that sulfuric acid in the range of 10^{-2} M concentration was the principal agent (*19*). In addition to the human deaths, the fogs of the Meuse Valley (*20*) and London (*21*) resulted in numerous animal deaths. At the Smithfield cattle show held on Dec 5–12, 1952, a fog period during which 4000 excess human deaths were reported, 12 young cattle in prime condition died while 160 exhibited acute respiratory symptoms which required veterinary treatment (*22*). Goodeve (*19*) reported $[H_2SO_4]$ ranging from 39 to 149 $\mu g/m^3$ in a 1934 London fog. These numbers can be compared directly to the range reported by Mader et al. (*3*) for L.A. fog in 1949 (25–157 $\mu g/m^3$). A maximum 24-h average concentration of H_2SO_4 of 347 $\mu g/m^3$ was reported for the London fog of 1962 in which 700 excess deaths were recorded.

Mr. Innes points out NH_3 in the human mouth may neutralize incoming sulfuric or nitric acid and that "acidity per volume of air is the important factor". I agree that this factor is important; however, the situation has been greatly oversimplified by Mr. Innes. With respect to human

Table I. Fog/Smog Episodes

meteorology	London	$[SO_2]$, ppm	$[H_2SO_4]_{max}$, 24 h, $\mu g/m^3$	excess deaths[a]	ref
fog	Dec 9–11, 1873			650	17
fog	Jan 26–29, 1880			1176	17
fog	Dec 28–30, 1892			779	17
fog	Nov 26–Dec 1, 1948	0.09–0.75		800	17
fog	Dec 5–9, 1952	0.09–1.34		4000	17
fog	Jan 3–6, 1956	0.19–0.55		1000	17
fog	Dec 2–5, 1957	0–0.4	144	250	27
fog	Dec 5–10, 1962	0–1.98	347	700	27
fog	Jan 7–22, 1963		88	700	27
	Meuse Valley, Belgium				
fog	Dec 1–5, 1930				20
	Dec 4–5, 1930			63	
	Donora, PA				
fog	Oct 27–31, 1948 (pop. 12 300)			20, 42.7% sick	28
	New York, NY				
haze	Jan 29–Feb 12, 1963	0.2–0.5 ppm		200–400	17

[a] Symptoms: bronchitis, emphysema, fever, wheezy chests, heart failure, cardiovascular problems, cough, sore throat, chest constriction, eye irritation, vomiting, nausea, vascular lesions, hypotension, asthma, and mucous membrane irritation.

health effects, other factors of importance will be the size of inhaled or respired droplet, the concentration of acid within the droplet, and the actual concentration of NH_3 in the oral cavity. Larson et al. (*23*) measured ammonia concentrations in expired human air in the range of 7–520 $\mu g/m^3$ and calculated that H_2SO_4 droplets at a concentration of 20 $\mu g/m^3$ with a $d_p = 0.3$ μm at RH = 30% would be completely neutralized after 0.5 s in the nose ($[NH_3] = 28$ $\mu g/m^3$) and 0.1 s ($[NH_3] = 140$ $\mu g/m^3$) in the mouth. The residence time of air in the upper airway is about 0.1 s before reaching the trachea. Since the neutralization time per unit aerosol mass is proportional to r^2, larger fog water droplets would require much longer times for neutralization (*23*). Inhaled fog water droplets with $d_p = 10$ μm with an effective concentration of 20 $\mu g/m^3$ H_2SO_4 would require approximately 20 s for complete neutralization in the nose and 4 s in the mouth. Clearly, with a residence time of 0.1 s very little of the acidity in fog water droplets would be neutralized before deposition in the trachea. This extrapolation assumes that no additional resistances to mass transfer are effective. Furthermore, the calculated neutralization times would be increased by depletion of gaseous NH_3, by incomplete internal mixing in the droplet, and by increased ventilatory flow rates (e.g., during physical exercise). Recently, McMurry et al. (*24*) found slower reaction times for neutralization of submicron sulfuric acid aerosols than predicted above. For ammonia concentrations of 13–63 ppb (9–44 $\mu g/m^3$) and particle size with $d_p = 0.03$–0.2 μm, the characteristic reaction time in a laminar flow reactor was determined to be 5.0 ± 0.5 s at 24 °C and 6% RH. Extrapolation to fog water droplets of 10-μm diameter gives reaction times on the order of 3.5 h for complete neutralization. They also determined for particles of $d_p = 0.1$ μm that only 18% of the NH_3–H_2SO_4 collisions resulted in neutralization. This fraction was shown to decrease with an increase in particle size. Clearly, NH_3 in human lungs may not provide significant protection against highly acidic fog water droplets. In addition, NH_3 concentrations are a function of dental plaque levels in the human mouth. Consequently good oral hygiene will lower NH_3 production.

In this laboratory, we feel that health effects of acid fog may be related to the formation of sulfonic acids in the droplet phase. As described by Munger et al. (*1*), bisulfite addition complexes such as hydroxymethanesulfonate are found in high levels in L.A. and Bakersfield fog water. Hydroxymethanesulfonic acid is a strong acid with a $pK_a \sim -3.0$ (i.e., same pK_a as nitric acid). In many cases, as much as 20% of the acidity in the fog may be due to the in situ formation of sulfonic acids. Eatough and Hansen (*25*) have suggested that organic sulfur(IV) species found in aerosol may be both mutagenic and carcinogenic, while Amdur (*26*) reports that inorganic S(IV) salts are more irritating to animals than the corresponding S(VI) salts.

As illustrated in the above arguments, Mr. Innes' claim that "pH data on fog is meaningless" is unfounded. Given a knowledge of the liquid water content during a fog event, pH as a measured parameter is a direct indicator of the potential severity of a fog in terms of effects on materials plants, or health.

Appendix

J. Firket, Professor at the University of Liêge, wrote the following (*20*):

"From the 1st to 5th of December, 1930, a thick fog covered a large part of Belguim along the Meuse Valley. A large number of people were injured, several hundred were severely attacked with respiratory troubles, and 63 died on the 4th and 5th of December. On the 6th of December, the fog disappeared; respiratory troubles improved. Wherever fogs of several days duration are frequent, public authorities were anxious to know the causes of this catastrophe. This apprehension was quite justified when, proportionally, the public services of London might be faced with the responsibility of *3,200* sudden deaths if such a phenomenon occurred there."

Literature Cited

(1) Munger, J. W.; Jacob, D. J.; Waldman, J. M.; Hoffman, M. R. *J. Geophys. Res.* **1983**, *88*, 5109–5119.
(2) Liljestrand, H. M.; Morgan, J. J. *Environ. Sci. Technol.* **1981**, *15*, 333–338.
(3) Mader, P. P.; Hamming, W. J.; Bellin, A. *Anal. Chem.* **1949**, *22*, 1181–1183.
(4) Thomas, M. D.; Hendricks, R. H.; Hill, G. R. In "Air Pollution"; McCabe, L., Ed.; McGraw-Hill: New York, 1952; pp 41–47.
(5) Scherbatskoy, T.; Klein, R. M. *J Environ. Qual.* **1983**, *12*, 189–195.
(6) Taylor, O. C., paper presented at a League of Women Voters symposium, "Hazards in the Air: Acid Rain and Acid Fog", Garden Grove, CA, June 15, 1983.

(7) Yosida, Z.; Kuroiwa, D. In "Studies on Fogs"; Hori, T., Ed.; Tanne Trading Co., Ltd.: Sapporo, Japan, 1953; pp 261–278.
(8) Schlesinger, W. H.; Reiners, W. A. *Ecology* **1974**, *55*, 378–386.
(9) Lovett, G. M.; Reiners, W. A.; Olson, R. K. *Science (Washington, D.C.)* **1982**, *218*, 1303–1304.
(10) Waldman, J. M.; Munger, J. W.; Jacob, D. J.; Hoffmann, M. R. submitted for publication in *Atmos. Chem.*
(11) Miller, P. R., U.S. Forest Service, Pacific Southwest Forest and Range Experiment Station, personal communication, July 14, 1982.
(12) Nriagu, J. O. In "Sulfur in the Environment. Part II: Ecological Impacts"; Wiley: New York, 1978; pp 1–59.
(13) Fuzzi, S.; Orsi, G.; Mariotti, J. *J. Aerosol Sci.*, **1983**, *14*, 298–301.
(14) Pearce, A. *Smithsonian*, 1982, *13*, 100–107.
(15) Metropolitan Museum of Art "The Horses of San Marco, Venice"; Wilton-Ely: Venice, 1979.
(16) Waldman, J. M.; Munger, J. W.; Jacob, D. J.; Flagan, R. C.; Morgan, J. J.; Hoffmann, M. R. *Science (Washington, D.C.)* **1982**, *218*, 1303–1304.
(17) U.S. EPA "Guide for Air Pollution Avoidance, Appendix B: History of Episodes"; U.S. EPA: Washington, DC, 1971; PH-22-78-32, pp 123–135.
(18) Larsen, R. I. *J. Air Pollut. Control Assoc.* **1970**, *20*, 214–225.
(19) Goodeve, C. F. *Trans. Faraday Soc.* **1936**, *32*, 1201–1202.
(20) Firket, J. *Trans. Faraday Soc.* **1936**, *32*, 1192–1197.
(21) Ministry of Health "Morality and Morbidity during the London Fog of December, 1952"; Her Majesty's Stationery Office London, 1954, Reports on Public Health and Medical Subjects No. 95, pp 1–63.
(22) Hudson, J. R. In "Mortality and Morbidity during the London Fog of December, 1952"; Appendix A "The Effect of the Fog on the Cattle at the Smithfield Show"; Her Majesty's Stationery Office: London, 1954; Ministry of Health, Reports on Public Health and Medical Subjects No. 95, p 45.
(23) (a) Larson, T. V.; Covert, D. S.; Frank, R.; Charlson, R. J. *Science (Washington, D.C.)* **1977**, *197*, 161–163; (b) Larson, T. V.; Frank, R.; Covert, D. S.; Morgan, M. S. *Am. Rev. Respir. Dis.* **1982**, *125*, 502–506.
(24) McMurry, P. H.; Takano, H.; Anderson, G. R. *Environ. Sci. Technol.* **1983**, *17*, 347–352.
(25) Eatough, D. J.; Hansen, L. D. *Adv. Environ. Sci. Technol.* **1983**, *12*, 221–268.
(26) Amdur, M. O. *Arch. Environ. Health* **1971**, *23*, 459–468.
(27) Commins, B. T.; Waller, R. E. *Atmos. Environ.* **1967**, *1*, 49–68.
(28) Schrenk, H. H.; Heiman, H.; Clayton, G. D.; Gafefer, W. M.; Wexler, H. "Air Pollution in Donora, PA: Epidemiology of the Unusual Smog Episode of October 1948, Preliminary Report"; Public Health Science: Washington, DC, 1949; Public Health Bulletin 306, pp 1–173.

Michael R. Hoffmann

Environmental Engineering Science
California Institute of Technology
Pasadena, California 91125

Acid fog

New findings widen the range of acid deposition phenomena

Recent measurements of fog in Southern California have generated strong scientific interest. At a number of sites, the acidity of the fog, determined by environmental engineer Michael R. Hoffmann and students at the California Institute of Technology, was far higher than that of previously reported samples of fog, cloud, and rainwater. Frequently, the Southern California fog was 100 times more acidic than the average rain in the region.

Volker A. Mohnen, director of the Atmospheric Sciences Research Center of the State University of New York at Albany, has shed further light on this phenomenon. He has been measuring fog and cloud water on Whiteface Mountain in the Adirondacks since 1978 and has found that the fog there is often 10 times more acidic than the rain in the same region.

Before Hoffmann began his research, most fog measurements had been taken in rural areas with no major pollution sources. These showed acidities comparable to those of clouds and rainwater. Hoffmann has been measuring fog primarily at four sites in areas subject to heavy industrial or urban pollution (see map). A first site at Lennox in the Los Angeles basin is adjacent to a freeway and near two power plants and an oil refinery. A second site is located in Oildale in the San Joaquin Valley. It is surrounded by secondary oil recovery operations. A third site at Upland is located in a residential area 60 km northeast of downtown Los Angeles. A steel plant and several other heavy industries are within 30 km of this site. A fourth site is in Pasadena, 25 km north of downtown Los Angeles, in a predominantly residential neighborhood with no heavy industry in the immediate vicinity.

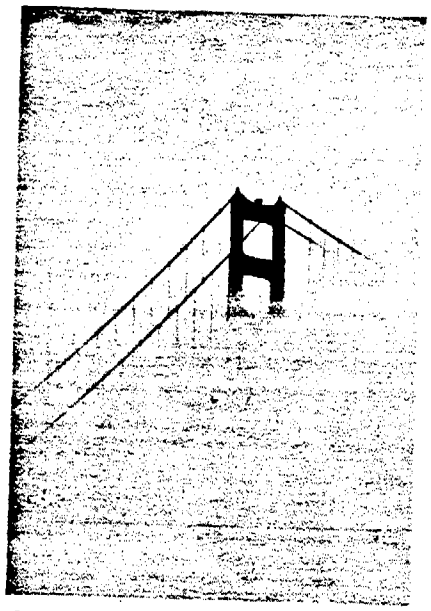

***Golden Gate Bridge.** In San Francisco, the fog is more acidic than rain.*

Hoffmann collects fog with a rotating device that consists of an arm with slits along each end to gather fog water. Like a propeller, it rotates at 1700 rpm, making its collection efficiency independent of wind speed. The fog water is pushed by centrifugal force into collection bottles near each end of the arm. It picks up most of the fog water, efficiently gathering droplets larger than 8 μm in diameter.

Nearly all the samples had to be diluted before analysis because the ion concentrations were so high. In addition to pH, the concentrations of 17 constituents were measured. NO_3^-, SO_4^{2-}, NH_4^+, and H^+ showed the highest concentrations (see table).

The most acidic sample collected thus far in Southern California was taken last December by Hoffmann at still another site—Corona del Mar, close to the ocean. Previously, this area was considered relatively clean because of its proximity to the ocean. The sample showed a pH of 1.69, an acidity equivalent to that of toilet bowl cleaner. During the two days preceding this pH reading, the Los Angeles basin's temperature inversion was close to ground level, preventing the pollutants from dispersing.

Hoffmann's investigations have shattered the general belief that fog in Southern California is relatively clean. Previously, foggy overcast days were thought to provide a respite from smog and pollution. This idea was furthered by the instruments used to measure air pollution. On foggy days, they register less pollution because they detect only ambient gases, not the constituents contained in liquid fog water droplets.

Hoffmann gives several reasons why fog water may be more acidic than cloud water and rainwater. Fog forms near the ground where pollution sources are located and pollution is the heaviest. The fog water droplets coalesce around preexisting aerosol, which is most highly concentrated near the ground. And because fog water droplets contain much less water than raindrops, they do not dilute the acidity nearly as much as rain.

The acid concentrations in the fog water usually follow a concave time profile. When the fog first forms, it consists of small droplets that are often highly acidic. As the drops grow in size and the fog becomes more dense, the acidity drops. As the fog evaporates and becomes thin again, the acidity rises once again. In some instances, the fog simply becomes more acidic as it apparently scavenges additional acid particles and gases from the air.

Smog–Fog–Smog

The fog in Southern California has been found to be most acidic after smoggy days, suggesting that it forms

on the aerosol associated with the previously existing smog. This observation has led to Hoffmann's hypothesis termed the "smog–fog–smog cycle." During the evening when the air is moist and stagnant, fog forms on the haze aerosol that made up part of the smog that day. When the fog evaporates the next morning, it leaves aerosol that helps to produce smog once again.

Photochemical processes used to be considered the major chemical pathways for the creation of smog. The smog–fog–smog hypothesis has led Hoffmann to believe that fog processes may play an important role in smog formation under some conditions. Further, he thinks that fog, clouds, and atmospheric water droplets in general also provide the major route for the conversion of SO_2 to sulfuric acid. Sunlight-activated reactions used to be considered the major pathway for the oxidation of both NO_x and SO_2.

Surprisingly, for some sites Hoffmann has found the ratio of NO_3^- to SO_4^{2-} in fog water to be quite different from the ratio in rainwater. In Pasadena and Lennox, this ratio on an equivalence basis in fog water was about 2.5:1, mirroring the emissions ratio of NO_x to SO_2, which is also 2.5:1. However, this same ratio of NO_3^- to SO_4^{2-} was less than 1 in the rainwater there. This further suggests that fog water forms around the secondary aerosol from recent emissions.

The pH of fog in Southern California is often lower than the pH of fog in any other region where it has been measured*

Location	Number of samples	Date	pH range	Concentration (μeq/L) H^+	NH_4^+	NO_3^-	SO_4^{2-}
Pasadena	4	11/15/81	5.25–4.74	5.6–55	370	130–830	82–390
Pasadena	4	11/23/81	4.85–2.92	14–1200	1290–2380	1220–3520	481–944
Lennox	3	12/7/81	5.78–2.55	2–2820	1120–4060	820–4560	540–2090
Lennox	3	12/17/81	2.81–2.52	1550–3020	960–1570	2070–3690	816–1978
Bakersfield	3	1/14/82	3.07–2.90	850–1200	5370–10 520	3140–5140	2250–6000
Pasadena	1	1/17/82	2.25	5623	7870	12 000	5060
Los Angeles rain (volume-weighted means at nine sites)		1976–79	5.4–4.4	4–38	1–39	11–43	7–56
Coastal California fogs		9/10/76			1–678	29–234	52–490
Whiteface Mountain		7–8/80	4.2–3.2	65–630	4–310	7–198	40–606
Fog and clouds, U.S.S.R.		1961–64	5.3–4.7	5–20	35–106	2–13	13–185

* The concentrations of NH_4^+, NO_3^-, and SO_4^{2-} were also far higher in Southern California fog than in samples of fog measured previously.

Source: Adapted from Waldman, J. M.; Munger, J. W.; Jacob, D. J.; Flagan, R. C.; Morgan, J. J.; Hoffmann, M. R. "Chemical Composition of Acid Fog." *Science* **1982**, *218*, 677–79.

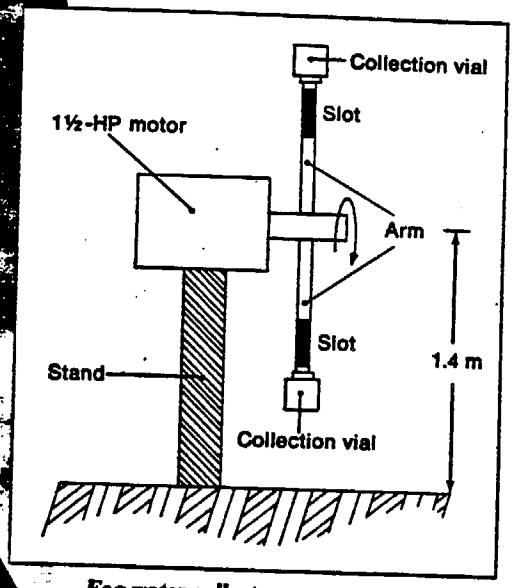

Fog water collector. *Hoffmann employs this rotating device to gather fog water in California.*

Hoffmann also has studied the pH of fog in areas not usually subject to pollution. At two remote sites, San Luis Obispo and Morro Bay, he found that the fog pH ranged from 5.6 to 7. Another remote site, San Nicholas Island 60 miles west of Los Angeles, showed a great deal of variation in pH. The pH of the fog there was usually 5.6 but moved downward sharply when the air mass from Los Angeles blew toward the island.

Eastern measurements

From his studies on Whiteface Mountain in the Adirondacks, Volker Mohnen also has concluded that acid fog is an important part of the acid deposition phenomenon. Because fog water there is often 10 times as acidic as rainwater, he believes that when scientists study only ordinary precipitation such as rain and snow, they are overlooking a major aspect of acid deposition. He finds that the transformation of SO_2 to SO_4^{2-} is very rapid in cloud and fog droplets. The passive device Mohnen uses to collect fog water depends on wind speed, but since wind blows most of the time on Whiteface, this is not an important factor.

Research results are not available on the effects of highly acidic fog on the physiology of vegetation. Nor is it known how much acid is deposited by the fog in any area. Mohnen believes that fog contributes an important portion of the acid deposited on the high peaks (>4000 ft) in the Adirondacks because the fog is mostly highly acidic, and these peaks experience cloud and fog nearly half of the time. Very recent measurements show that the gaseous SO_2 concentrations in the Adirondacks are less than 2 ppb on an annual basis. Therefore, dry acid deposition on these peaks is expected to be very low.

Another factor to consider is that spruce will grow on a mountain only at those elevations that receive frequent fog and, in northern climates, heavy rime (condensed fog frozen onto surfaces) in the winter. If this fog is more acidic than rainfall, that may be important in understanding the cause of the well-documented decline of the red spruce in the Northeast. The two main theories about this decline are that it is caused by drought or by a combination of drought and acid deposition (see *ES&T*, Vol. 17, No. 1, 1982, p. 15A).

Damage to vegetation

In order to assess possible damage to trees in the Northeast from acid fog, a research project, now scheduled to begin sometime this year, will measure the total amount of acid received from fog, for a given area, and compare it to the amount received from ordinary precipitation and dry deposition. The National Weather Service makes no estimates for any region of the quantity of moisture contributed by fog, rime, and other special events such as dew and frost. In this experiment, it will be necessary to measure stem flow and throughfall during and after fog events. Such measurements are difficult, but crucial to determining how much water and thus how much acid the trees and soil collect from fog and rime.

Laboratory research has revealed that acid rain with a pH of about 3 can damage the cuticles of leaves. Because of the large number of fog pH measurements showing a pH below 3 in Southern California, Hoffmann has concluded that fog causes some damage to the vegetation there, particularly in those areas where there are heavy emissions of SO_2 or NO_x. The extent of the damage would depend on the pH, duration, and frequency of the fog and also on how much fog water is gathered by the vegetation. In addition, the dry acid deposition that is dissolved by the collected fog water would also contribute to the damage.

Health effects

The extent of damage to human health from acid fog would be extremely difficult to evaluate. Unless an

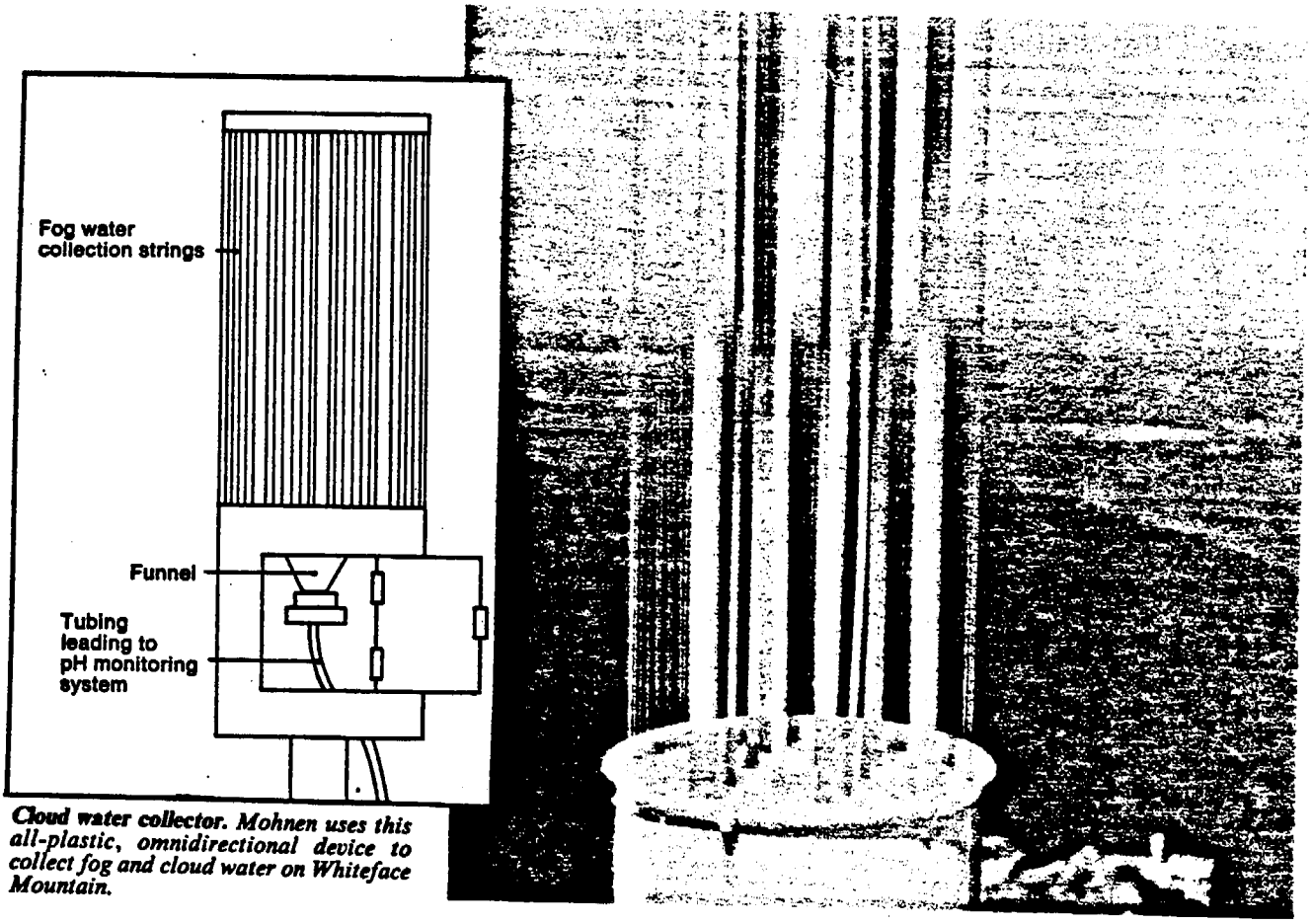

***Cloud water collector.** Mohnen uses this all-plastic, omnidirectional device to collect fog and cloud water on Whiteface Mountain.*

area were to have a killer fog with many excess deaths, as London experienced in 1952 and in 1957, health effects from acid fog could not be distinguished statistically from those produced by other causes.

From his measurements, Hoffmann has come to believe that there is a potential for a killer fog in Southern California. No pH measurements were made of the London fogs in 1952 and 1957. However, the sulfuric acid content of the 1957 fog, which lasted two to three days and caused about 1000 excess deaths, was measured at 680 $\mu g/m^3$. Hoffmann calculates that this would be equivalent to a pH of 1.5 if the fog had a low liquid water content and 1.8 with a high water content.

A California fog with a pH of 1.5–1.8 that lasted two to three days would not necessarily have the same health effects as the London fog, however. The emissions contained in the London fog were quite different from those in California fog. They resulted from the burning of large amounts of coal and contained heavy concentrations of particulate matter as well as SO_2.

Studying the chemical constituents of fog is important, not only for assessing possible damage from fog, but also for understanding cloud chemistry. Chemical reactions that take place in fog are likely to be quite similar to those in clouds, and in the field, fog processes are easier and cheaper to study. Elucidating cloud chemistry is thought to be important for formulating and testing acid rain models.

For some of the same reasons that acid fog is often highly acidic, dew and frost could also be highly acidic, according to Joe Wisniewski of General Research Corporation in McLean, Va. Dew and frost involve small amounts of water condensing or freezing over sometimes relatively large amounts of dry acid deposition. After formation, dew, as well as fog, can scavenge more acid particles and acid-forming gases from the air. Very few studies have been made of the acidity of dew and frost, however.

A lack of funding

In the federal interagency research program called the National Acid Precipitation Assessment Program (NAPAP), very little money is provided for the study of acid fog. Hoffmann's studies were financed by the California Air Resources Board and Mohnen's were funded only partially by NAPAP. This year, NAPAP is providing no funds for acid fog measurements, except, perhaps, for the analysis of measurements that have already been made. The NAPAP program does include extensive studies of cloud chemistry, but the aim of this research is to understand the chemical reactions that take place in the clouds, not the damage that might result from acid fog.

California initiatives

Hoffmann's studies of acid fog have aroused a great deal of concern in California and are partly responsible for California's decision to spend $4 million on acid deposition research next year. This is a large amount for a state to give for such research when compared to the federal government's expenditure of $22 million. Concern about acid fog has also led to the introduction of a bill in the California legislature that would require each air pollution control district to take concrete measures to combat the acid fog problem. —Bette Hileman

Additional Reading

(1) Waldman, J. M.; Munger, J. W.; Jacob, D. J.; Flagan, R. C.; Morgan, J. J.; Hoffmann, M. R. "Chemical Composition of Acid Fog," *Science* **1982**, *218*, 677–80.
(2) Wisniewski, J. "The Potential Acidity Associated with Dews, Frosts, and Fogs," *Water Air Soil Pollut.* **1982**, *17*, 361–77.
(3) "Cloud Chemistry and Meteorological Research at Whiteface Mountain: Summer 1980"; prepared by The Atmospheric Sciences Research Center, State University of New York; April 1981, Publication 806.

A field investigation of physical and chemical mechanisms affecting pollutant concentrations in fog droplets

By DANIEL J. JACOB, JED M. WALDMAN, J. WILLIAM MUNGER and MICHAEL R. HOFFMANN, *Environmental Engineering Science, W. M. Keck Laboratories, California Institute of Technology, Pasadena, CA 91125, USA*

(Manuscript received November 8, 1983; in final form February 15, 1984)

ABSTRACT

High ionic loadings were found in fogwater collected at Bakersfield, California during an extended stagnation episode. The major ions were NH_4^+, NO_3^-, and SO_4^{2-}, with concentrations usually in the millimolar range. Droplet growth played an important rôle in determining fogwater concentrations. The amount of solute decreased substantially over the course of each fog event; this was attributed, at least in part, to deposition of fog droplets on surfaces. The occurrence of dense fogs thus seemed to limit particle build-up during stagnation episodes. The sulfate fraction in the aerosol increased appreciably over several days of stagnation, but no statistical evidence for in situ S(IV) aqueous-phase oxidation was found. The high ammonia concentrations present were sufficient to neutralize a large fraction of the ambient acidity. As a result, fogwater pH values rarely attained the extremely low values found in other polluted environments.

1. Introduction

Concern about acidic precipitation has stimulated research efforts to understand the chemistry of non-precipitating clouds (Petrenchuk and Drozdova, 1966; Lazrus et al., 1970; Hegg and Hobbs, 1982; Hegg, 1983). Ionic concentrations higher than those found in rain have been observed in clouds and fogs (Munger et al., 1983). In fog, the condensation of water vapor on pre-existent particles in the boundary layer shifts the aerosol size distribution towards larger sizes and produces a dilute aqueous aerosol. These physical and chemical changes in the aerosol may significantly affect its characteristics with regard to air pollution potential and deposition.

Even though fogs have been linked in the past to health-threatening pollution episodes (Commins and Waller, 1967), few field studies of fogwater chemistry have been made. Houghton (1955) sampled fog at several sites in New England and observed high concentrations of components that he attributed to the dissolution of activated nuclei. He found relatively high acidities and suggested that they were due to the scavenging of free sulfuric acid nuclei. Mrose (1966) and Okita (1968) also found elevated ionic concentrations and acidities in East Germany and Japan, respectively. Mader et al. (1949) reported sulfuric acid aerosol concentrations as high as 150 $\mu g\ m^{-3}$ during fog events in Los Angeles. These values were comparable to those observed during some London fogs (Goodeve, 1936). Waldman et al. (1982) and Munger et al. (1983) found extremely high ionic concentrations in Los Angeles area fogwater; solute concentrations were in the millimolar range for the major components, and pH values were usually in the range of 2 to 4.

Fog droplets appear to be efficient scavengers of boundary layer pollutants, and could provide a favorable environment for aqueous-phase reactions leading to the production of strong acids (Jacob and Hoffmann, 1983). The oxidation of absorbed S(IV) to form S(VI), with the concomitant production of acidity, is suspected as being an important reaction in the aqueous phase. Cass (1979) has observed that the worst sulfate pollution episodes in Los Angeles occur during periods of high

humidities and coastal fog, and Hegg and Hobbs (1982) have reported SO_2 conversion rates of up to 1900% h^{-1} in clouds. Laboratory studies (Martin, 1984) indicate that the oxidation of S(IV) can proceed rapidly at atmospheric concentrations in the presence of strong oxidants.

This paper presents results of a field investigation of fogwater composition in the southern San Joaquin Valley of California. The San Joaquin Valley is a site of both agricultural activity and oil recovery operations, which lead to high atmospheric loadings of particulate matter and trace gases. Fogs are common in the Valley during the winter months and can form every night under near-stagnant conditions caused by mesoscale subsidence. Because of the unusual stability in the local weather pattern and air masses, as well as the identification of emission sources (California Air Resources Board (CARB), 1982), it was possible to study the physical and chemical parameters influencing the fogwater composition, and to evaluate the cumulative effect of repeated fog occurrences on the chemical loading of an air mass.

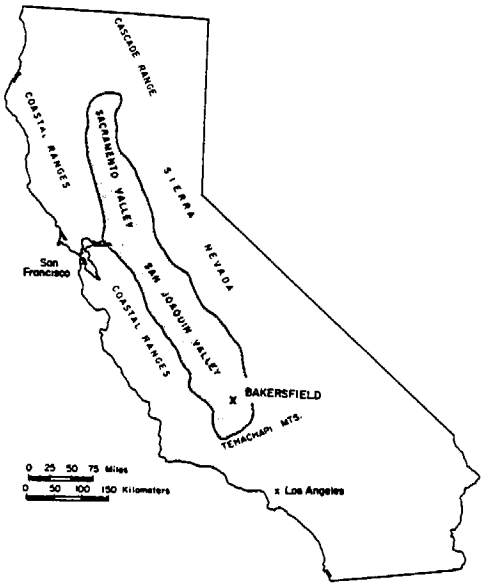

Fig. 1. The Central Valley of California.

2. Site description and measurement techniques

2.1. Site description

All measurements were made at Bakersfield (Kern county) from 30 December 1982 to 15 January 1983. Kern county is located at the southern tip of the Central Valley of California, which extends north about 700 km. The Valley is approximately 80 km wide over its entire length and is encompassed by mountain ranges (Fig. 1). Apart from a narrow gap at the Sacramento river delta, egress from the Valley is possible only through mountain passes. The lowest passes to the east and south are above 1000 m elevation. The Valley is subdivided into the San Joaquin and Sacramento Valleys, south and north of the Sacramento gap respectively. In the southern part of the San Joaquin Valley the lowest pass to the west is at 600 m elevation.

The wintertime meteorology of the Central Valley is dominated by the Basin High, which creates a very strong subsidence inversion (Holets and Swanson, 1981). The base of the inversion is typically 200 m to 500 m above ground level (AGL), although it occasionally comes down to the ground. This stable synoptic pattern is interrupted periodically by a frontal passage which often leads to precipitation on the Valley floor. As the subsidence resumes, the moist air is trapped inside the Valley. Loss of heat by radiation eventually leads to the formation of a widespread fog layer. Under these conditions, fog (locally called "Tule" fog) can form nightly and last into the late morning, with a persistent haze lasting through the afternoon.

Because the mixing height is usually lower than the natural boundaries of the Valley, the transport of air masses in and out of the Valley during these episodes is very limited. A weak net flow north out of the San Joaquin Valley leads to a residence time of 8 to 12 days for an air mass in the San Joaquin Valley (Reible et al., 1984). The daytime up-slope flow and the night-time drainage flow associated with the heating and cooling of the mountain slopes dominate the wind patterns in the Valley itself. Flow divergence from the Valley floor in the day, and convergence at night, has been observed by Smith et al. (1981). In the winter, because of the reduced insolation, this flow is probably too weak to ventilate the Valley by transport over the mountain ridges (Reible et al., 1983). As a result, between frontal passages and the ensuing at-

mospheric cleansing, the air in the Valley is near-stagnant.

Major oil fields are located in Kern county, and large amounts of SO_2 and NO_x are released in the steam-injection oil recovery operations (CARB, 1982). In addition, most of the Valley floor is occupied by farming and ranching activities, which are important sources of primary particulate matter (CARB, 1982) and ammonia. At the high humidities prevalent in the winter months, primary and secondary H_2SO_4 and HNO_3 react with NH_3 and H_2O to form ammonium sulfate and nitrate droplets (Stelson, 1982). Because of the production of this secondary aerosol, Kern county experiences severe sulfate pollution episodes in the winter months (Duckworth and Crowe, 1979).

2.2. *Measurement techniques*

Fog and aerosol samples were collected from the roof of a three-story building in downtown Bakersfield, above a CARB air monitoring station. The surroundings are residential and commercial, with no major point pollutant sources. There are no nearby structures taller than the site. An east–west highway, with usually moderate traffic, is located 500 m south of the site.

Fogwater was sampled with a rotating arm collector, which has been characterized in detail elsewhere (Jacob et al., 1984). This instrument samples air at a rate of 5 m^3 min^{-1}, performs well in preserving the chemical integrity of the sample at all stages of collection, and has a lower size cut of 20 μm diameter (determined by experimental calibration). Jacob et al. (1984) have estimated that on the average, 60% of the total liquid water is collected with this device. Fogwater samples were collected over periods ranging from 30 min to 3 h, and were analyzed for major ions, trace metals, S(IV), formaldehyde, and total organic carbon. Sample handling and analytical procedures were identical to those described previously (Munger et al., 1983).

Aerosol between fog events was collected on a set of two Gelman Zefluor Teflon filters. One filter, which was surmounted by a cap to prevent preferential sampling of large particles by sedimentation, was open-faced and collected total particulate matter; the other was set downstream of a cyclone separator which removed particles larger than 2 μm. After 11 January, only the open-faced filter was used. Filter samples were taken over time intervals ranging from 2.5 to 8 h. The filters were extracted in 10 ml of water on a reciprocating shaker for 60 min, and analyzed for major ions using the same analytical methods as for the fogwater.

Gaseous ammonia was collected by absorption on an oxalic acid impregnated Gelman glass fiber filter set downstream of the open-faced Teflon filter. Ammonium ion was determined by the phenol-hypochlorite method on a water extract using a modification described by Russell (1983).

Liquid water content was measured by drawing air at a rate of 1 m^3 min^{-1} through open-faced paper filters. The filters were exposed to the fog prior to use to equilibrate them with the ambient humidity. The liquid water content was determined by weight. This method has been found (Calspan Corp., Buffalo, NY, private communication) to yield results comparable to those obtained with more sophisticated optical methods (Chylek, 1978). It must be stressed that no fully reliable method for measuring absolute liquid water content exists to date, and that variations in results of up to 50% commonly occur from one method to another; therefore measurements must be interpreted with caution.

The CARB air monitoring station located at the site provided hourly averages of gas-phase NO, NO_x, SO_2, O_3, and CO concentrations. Hourly mixing height measurements (from 30 m up to 1000 m) were obtained at Bakersfield by acoustic sounding (Western Oil and Gas Association, Los Angeles, private communication). Hourly weather observations were recorded 8 km north of our site by the Bakersfield National Weather Service office (National Oceanic and Atmospheric Administration, 1983).

2.3. *Weather pattern*

On 22–23 December, a frontal passage over the Valley deposited 7.6 mm of rain on Bakersfield. A strong subsidence associated with the Basin High followed, and a stratus deck started forming on 26 December. Temperatures dropped and were 3 to 7 °C lower than normal during the period 30 December–15 January. Daily highs ranged from 4 to 8 °C and daily lows from −2 to 3 °C. Fog was reported at the Bakersfield site on 29 and 30 December, but was patchy in the surrounding area. In the text, the date of the fog will be given as that of the morning on which it occurred, even though it

may have already been formed the previous evening. On 31 December and 1 January, dense widespread fogs persisted through the night and well into the morning. The following three days, 2–4 January, thin radiation fogs formed at the site for a brief period in the early morning as the temperature dropped sharply. Dense widespread fog through the night again occurred on 5 January (not sampled) and on 6–8 January. On 9–10 January, a weak front passed through the Valley, resulting in some clear sunshine, high cloudiness, and drizzle in the morning of 9 January which deposited a trace amount of rain. On the morning of 10 January, a drop in temperature down to −2 °C at the site caused the formation of a thin, shallow fog which lasted for 3 h. After 1600 on 10 January, the subsidence inversion again limited the mixing heights to less than 500 m AGL and dense, all-night fogs formed every night from 11 January to 15 January. Sampling was discontinued after 15 January. All fogs were sampled from beginning to end, except the 31 December and 11 January fogs, for which sampling did not start until a few hours after fog formation.

3. Results and discussion

3.1. Fogwater concentrations

Table 1 gives the range and median value of fogwater concentrations for the entire data set ($n = 108$). Close ionic balances for most fogwater samples (±10% in over 80% of the cases) indicate that no important ions were missed in analysis. Ammonium, nitrate, and sulfate ions, by far the most important components present, had concentrations usually in the millimolar range. These high concentrations indicate the dominant impact of agriculture (NH_4^+) and fuel combustion (NO_3^-, SO_4^{2-}) on the fogwater composition. Occasionally, H^+, Ca^{2+}, and Cl^- contributed significantly to the total equivalent loading of the droplets. Ratios of concentrations of Na^+ to other ions indicated that sea salt was not a major source. Iron and lead were the most prominent trace metals.

Fig. 2 shows the evolution of fogwater concentrations with time during the 7 January fog. Winds were light and variable throughout the night, and temperatures ranged from 1 to 3 °C. As droplets grew at the beginning of the fog, they

Table 1. *Fogwater concentrations at Bakersfield, California**

Component	H^+	Na^+	K^+	NH_4^+	Ca^{2+}	Mg^{2+}	Cl^-
Range of concentrations (μeq l^{-1})	0.1–2750	1.4–325	1.6–368	490–13,300	7–3500	1.1–430	1–980
Median concentration (μeq l^{-1})	60	19.5	9.3	1440	47	6.3	47

Component	NO_3^-	SO_4^{2-}	S(IV)	CH_2O	TOC†
Range of concentrations (μeq l^{-1})	200–6800	194–9400	45–3000‡	53–710‡	710–23,000‡
Median concentration (μeq l^{-1})	850	1160	515‡	165‡	4000‡

Component	Fe	Mn	Pb	Cu	Ni	V
Range of concentrations (μg l^{-1})	81–10,700	3–525	48–3340	6–717	22–1232	7–850
Median concentration (μg l^{-1})	400	14	330	34	61	55

(a) Hydroxymethanesufonate ion coelutes with nitrate in the ion chromatographic column, so that nitrate concentrations could be overestimated.

* 108 samples over the period 30 December 1982–15 January 1983.

† Total organic carbon.

‡ For S(IV), CH_2O, and total organic carbon, concentrations are in μ moles l^{-1}.

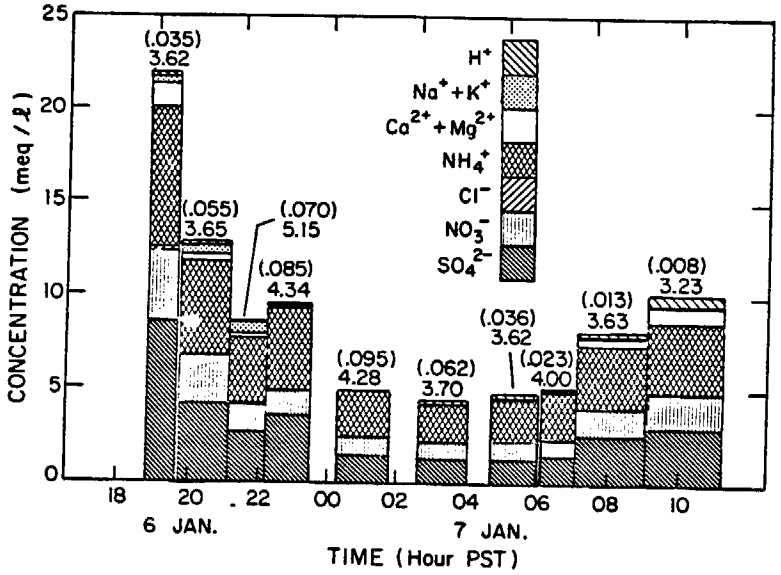

Fig. 2. Evolution of fogwater concentrations over the course of the 7 January 1983 fog event at Bakersfield. Fogwater pH and average liquid water contents (g m^{-3}, in parentheses) are indicated on top of each data bar.

became more dilute, and conversely as the fog dissipated, evaporation concentrated the droplets. The resulting concave profile for fogwater concentrations was evident in all the events sampled over the course of this investigation, and has been found to be a characteristic of fogs in other locations as well (Waldman et al., 1982). Droplet growth is therefore a dominant process in controlling fogwater concentrations. Accordingly, acidities were usually the highest at the beginning and end of fog events. The ratio of concentrations of one component to another was not subject to large variations from sample to sample within one event, which implies that the air masses were generally homogeneous. A trend of decreasing concentrations, superimposed on the concave profile, was noted. We will see that this can be attributed, at least in part, to deposition of fog droplets on surfaces.

3.2. Atmospheric particulate loadings in relation to fog occurrences

The major components of the daytime aerosol were NO_3^-, SO_4^{2-}, and NH_4^+. No significant differences were observed between the total aerosol and fine aerosol filters for NH_4^+, NO_3^-, SO_4^{2-}, and Cl^- concentrations. On the other hand, concentrations of Na^+, Ca^{2+}, and Mg^{2+} were higher in the total aerosol than in the fine aerosol; coarse soil dust is probably a major source of these components. Fig. 3 summarizes the evolution of atmospheric loadings over the 17-day sampling period. Mixing height data and concentrations of trace gases are given as hourly averages. Ozone concentrations were at or below the detection limit of 10 ppb in 96% of the hourly measurements. Time-averaged fogwater loadings/m^3 of air (calculated from liquid water content measurements) are given for each fog event, along with the aerosol loadings and gaseous ammonia concentrations between fog events. Prior to 6 January, the liquid water content was not directly measured; we estimated it by measuring the amount of water collected and assuming a 60% collection efficiency. In our calculations of the fogwater loadings, we assume that the collected samples are representative of the ambient fogwater in spite of the high lower size-cut of the sampler. The individual contributions of droplets of different sizes to the overall fogwater loading have not yet been rigorously investigated; they are difficult to predict from droplet growth theory (Pruppacher and Klett,

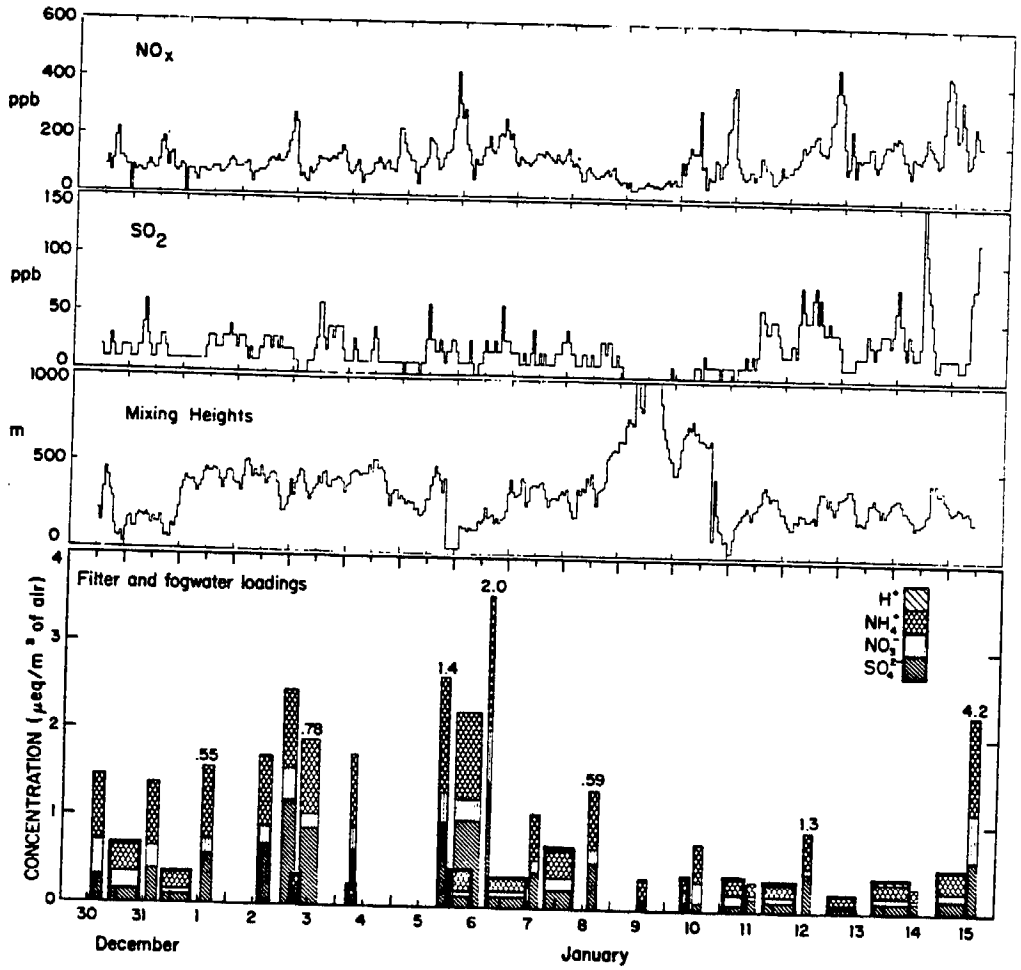

Fig. 3. Fogwater (in bold) and aerosol loadings of NH_4^+, NO_3^-, SO_4^{2-} and H^+ (fogwater) measured at Bakersfield during the period 30 December 1982–15 January 1983. When measured, gaseous ammonia concentrations (p.p.b.: 1 p.p.b. = 0.044 μmoles m^{-3} at 1 °C) are indicated on top of the aerosol data bars. Mixing heights are given in (m) above ground level.

1978) because supersaturations in fogs fluctuate rapidly in a poorly understood manner (Roach, 1976; Gerber, 1981). The large droplets in the fog are likely to have condensed on large nuclei, and therefore are not necessarily more dilute than the smaller droplets. A recent field intercomparison study of fogwater sampling devices (Hering and Blumenthal, 1983) seems to indicate that variations in the composition of the fogwater collected by instruments with different droplet size-cuts are insignificant.

The mixing height data show that two distinct air masses were involved during the 17-day period. The base of the inversion layer usually oscillated between 100 m and 500 m AGL. However, on 9 January, the inversion layer rose to above 1000 m and possibly vanished (no measurements were available above 1000 m). This allowed mixing with air from outside the Valley, and, with the added contribution of the 9 January morning drizzle, effectively renewed the air mass in the Valley. After the afternoon of 10 January, stagnation conditions resumed and no mixing heights above 500 m were recorded until after 15 January.

Aerosol and trace gas loadings reflected the apparent change in air masses. Since emission sources are located close to the ground, the majority of pollutants were released below the base of the inversion layer. Due to the lack of ventilation, accumulation of pollutants proceeded. During the period of 30 December to 9 January, the stagnant air mass was well-aged; high particulate and SO_2 levels were observed. After the effective cleansing of the atmosphere on 9–10 January, aerosol and SO_2 loadings dropped sharply.

On several occasions, aerosol samples were taken a few hours before a fog formation. The fraction of the afternoon aerosol found in the first fogwater sample collected the following night ranged from 0.1 to 0.8 and from 0.2 to 2.0 for sulfate and nitrate, respectively. These numbers varied considerably from fog to fog, and this can be attributed to variations in nucleation scavenging efficiencies and differences in the air masses advected over the site in the afternoon and at night. It is therefore not possible to make quantitative conclusions with regard to aerosol scavenging efficiencies, but it appears that a substantial fraction of the aerosol is incorporated into the fog droplets.

Scavenging of trace gases is an additional source of chemical input to the fogwater. The solubility of several gases in fog droplets has been discussed by Jacob and Hoffmann (1983). Nitric acid is 100% scavenged, and so is ammonia below pH 5. From the gas phase data, it appears that the occurrence of fog does not by itself affect partial pressures of SO_2; thermodynamic considerations indicate that, in spite of the dissociation of $SO_2 \cdot H_2O$ in solution and the formation of S(IV) adducts, absorption of $SO_2(g)$ by fog droplets is limited to a few % because of the small amount of water present. No correlation appears either between NO_x levels and fog occurrences. This agrees with the results of Schwartz and White (1981), who show that the dissolution of NO_x at atmospheric concentrations is too slow to be of relevance over the lifetime of the fog.

All the extended fog events sampled over the 17-day period showed a substantial decrease in the fogwater loadings over the course of the fog (Fig. 4). Loadings of major ions at the end of the fog ranged from 4% to 36% (median 17%) of those at the beginning of the fog, depending on the event. However, the steady decreasing pattern was not established until a few hours after fog formation; in the initial stage of the fog, the evolution of fogwater loadings was irregular. Changes in the fogwater loadings over the course of the fog could be

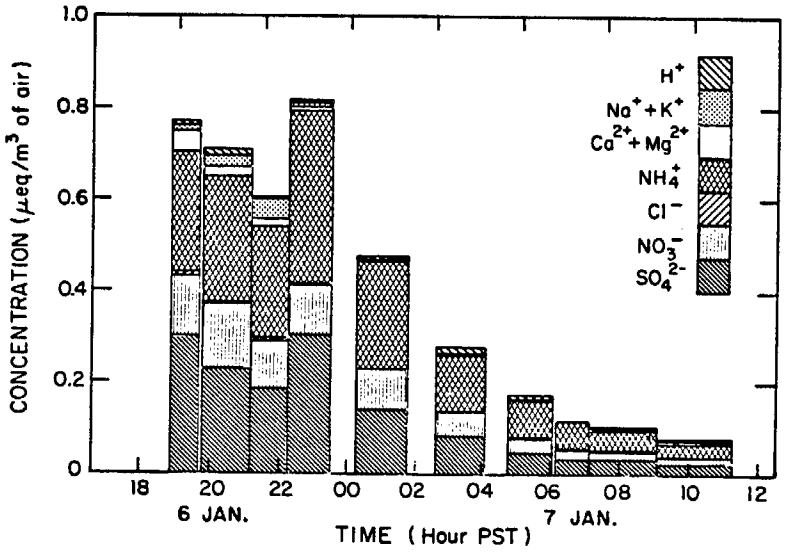

Fig. 4. Evolution of fogwater ionic loadings over the course of the 7 January fog event.

attributed to deposition of the coarse fog droplets, short-range transport, or displacement of the inversion base. Comparison of daytime aerosol or nighttime fog loadings to the mixing heights over the same time period did not show any strong correlation for mixing heights below 600 m. In addition, oscillations of the mixing height over the course of the fogs did not show a consistent trend which could be associated with a decrease in fogwater loadings. Therefore, this factor is probably not critical. Characterization of short-range transport at night is made difficult by the complex drainage flows converging to the center of the Valley. Because Bakersfield is located in the convergence zone, local winds oscillate considerably from hour to hour in both direction and speed (National Oceanic and Atmospheric Administration, 1983). Concentrations of CO, NO_x, and SO_2 during fog events did not show the strong decreases that would be associated with the advection of much cleaner air masses over the site. Therefore, it is unlikely that short-range transport could fully account for the considerable decrease of fogwater loadings with time.

Deposition of fog droplets on surfaces, on the other hand, could lead to the observed decreases in fogwater loading. Fog formation results in an important shift of the aerosol distribution towards larger particle sizes; because the residence time in the atmosphere of particles above 10 μm is of the order of hours, and rapidly decreases with increasing size (Muller, 1982), the deposition rate of the aerosol must be enhanced. During the early stage of the fog, the droplets presumably do not grow to a size large enough to be effectively deposited; factors other than deposition influence the fogwater loading, and hence the irregular behaviour of the profile of fogwater loadings with time. As a population of large droplets is later established, deposition becomes more rapid and overcomes other factors. Turbulent diffusion to the ground, impaction and sedimentation are probably all important in contributing to the removal of fog droplets. The numerical study of Brown and Roach (1976) has shown that important droplet settling must occur to explain the low liquid water content observed in fogs; Brown (1980) finds that the settling process does not become important until a few hours after fog formation, which is consistent with our observations. If scavenging of gases and particles by the droplets is followed by deposition, pollutants will effectively be removed from the atmosphere.

Particle concentrations in the Valley are determined by sources (fresh input of primary and secondary aerosol), sinks (transport aloft and out of the Valley, deposition), and intra-Valley transport. Under stagnant conditions, one would expect a pollutant build-up until a steady state is reached due to an eventual balance of sources and sinks. The characteristic time for deposition of haze particles (0.05–2 μm) is 3–6 days (Muller, 1982), but under fog conditions, particles scavenged by the fog droplets will deposit much more quickly. Dense fogs can therefore limit particle accumulation. The overall higher loadings during the 26 December–8 January stagnation episode (where dense fog did not form every night) compared to those during the 10 January–15 January episode (where dense fog formed every night) could then be explained by a pollutant build-up due to the predominance of haze but limited fog. This accumulation is obvious for ammonium nitrate and sulfate salts, which are the main constituents of the haze aerosol; on the other hand, concentrations of Ca^{2+} in the aerosol did not increase during the stagnation episodes. Calcium mostly originates from coarse dust particles with a residence time shorter than one day, and will settle out regardless of fog formation.

3.3. *Heterogeneous S(IV) oxidation*

Because of the high SO_2(g) concentrations in Bakersfield and the presence of an aquated aerosol, there is a potential for aqueous-phase oxidation of S(IV) to S(VI) by the strong oxidants H_2O_2, O_3, and O_2 (Jacob and Hoffmann, 1983; Martin, 1984). Evolution of sulfate concentrations in the fogwater between times t_1 and t_2 can be expressed by:

$$[\mathrm{S(VI)}]_{t_2}L(t_2) = \{[\mathrm{S(VI)}]_{t_1}L(t_1) + \int_{t_1}^{t_2} \frac{\mathrm{d[S(VI)]}}{\mathrm{d}t} L(t)\,\mathrm{d}t\}(1-r), \quad (1)$$

where $L(t)$ is the liquid water content of the fog, and r characterizes changes in [S(VI)] (assumed first-order) due to physical mechanisms such as deposition. We assume as a first approximation that $L(t)$ and r control the evolution of the chemically conservative quantity [T], defined as the sum of the equivalent concentrations of all

components A_i in solution minus sulfate and its counter-ion:

$$[T] = \sum_{i=1}^{n} [A_i]. - 2[\mathrm{S(VI)}] \quad (2)$$

With this assumption, we can write for a homogeneous air mass:

$$[T]_{t_2} L(t_2) = [T]_{t_1} L(t_1)\,(1 - r), \quad (3)$$

and substitute (3) into (1):

$$\int_{t_1}^{t_2} \frac{\mathrm{d[S(VI)]}}{\mathrm{d}t} L(t)\mathrm{d}t = L(t_1)\left([\mathrm{S(VI)}]_{t_2} \times \frac{[T]_{t_1}}{[T]_{t_2}} - [\mathrm{S(VI)}]_{t_1}\right). \quad (4)$$

A major difficulty in solving (4) for $\mathrm{d[S(VI)]}/\mathrm{d}t$ and using statistical analysis to verify or derive a rate law is that the variables on which $\mathrm{d[S(VI)]}/\mathrm{d}t$ depends are not satisfactorily quantified. Reactions of S(IV) with H_2O_2 and O_3 are expected to be first-order in oxidant concentrations (Martin, 1984), but H_2O_2 and O_3 concentrations were not measured at Bakersfield (ozone below the detection limit of 10 ppb, as observed, still cannot be neglected as an oxidant in droplets with high pH). Oxygen has been predicted to be an effective oxidant in solution when catalyzed by trace metals (Jacob and Hoffmann, 1983), but the form of the rate law has not been satisfactorily established at the pH and free S(IV) concentration ranges typical of the Bakersfield fogwater (Martin, 1984); furthermore, it may be complicated because of aqueous-phase speciation of metals and S(IV) (Hoffmann and Jacob, 1984).

Rates of sulfate production in the atmosphere have previously been derived from field data by Cass (1981) and Hegg and Hobbs (1981, 1982). These investigators expressed this rate in terms of a pseudo first-order rate constant k (% h^{-1}) referenced to gas-phase SO_2:

$$\frac{\mathrm{d[S(VI)]_{air}}}{\mathrm{d}t} = \frac{k}{100}[\mathrm{SO_2(g)}], \quad (5)$$

where $[\mathrm{S(VI)}]_{air}$ and $[\mathrm{SO_2(g)}]$ are concentrations per unit volume of air. Eq. (5) is obviously unjustified from a chemical standpoint, because it ignores the rate dependence on droplet pH, concentrations of oxidants and catalysts, temperature, and photochemical activity. Still, it provides a convenient parameterization of sulfate production and will be adopted here in the absence of a more reliable expression. Substituting (5) into (4):

$$\int_{t_1}^{t_2} \frac{k}{100}[\mathrm{SO_2(g)}]\mathrm{d}t = L(t_1)\left([\mathrm{S(VI)}]_{t_2} \frac{[T]_{t_1}}{[T]_{t_2}} - [\mathrm{S(VI)}]_{t_1}\right). \quad (6)$$

Assuming that $[\mathrm{SO_2(g)}]$ varies linearly with time over the interval considered:

$$k = \frac{200}{t_2 - t_1} \frac{L(t_1)}{[\mathrm{SO_2(g)}]_{t_2} + [\mathrm{SO_2(g)}]_{t_1}} \times \left([\mathrm{S(VI)}]_{t_2} \frac{[T]_{t_1}}{[T]_{t_2}} - [\mathrm{S(VI)}]_{t_1}\right). \quad (7)$$

Table 2 shows that the k values calculated from our data set with eq. (7) are lower than those obtained by Hegg and Hobbs (1981, 1982) for clouds over western Washington State, and are of the order of those observed in the Los Angeles aerosol by Cass (1981). However, both ozone concentrations and pH were higher in the clouds sampled by Hegg and Hobbs (1981, 1982) than in the Bakersfield fogs sampled in this study; in the same way, temperature, solar irradiation, and oxidant concentrations are all lower in Bakersfield (in the wintertime) than in Los Angeles. Therefore, comparison of the data sets in terms of k is difficult.

Cass (1981) noted that gas phase oxidation could not be sufficiently rapid to explain the S(IV) conversion rates in Los Angeles, and suggested aqueous-phase oxidation as an alternate mechanism. Hegg and Hobbs (1982) pointed to S(VI) in-cloud production from some basic statistical analysis of their data, a conclusion which has been disputed by Schwartz and Newman (Schwartz et al., 1983). Our data set does not allow us to conclude that k is significantly different from zero. Fig. 5 shows the frequency distribution we observed for k; the near symmetrical deviations about $k = 0\%\ \mathrm{h^{-1}}$ can be simply attributed to the non-Lagrangian nature of the sampling procedure. The presence of a few outliers on the positive side of the distribution could suggest that S(IV) in-fog oxidation proceeds under certain conditions, but these points are associated with SO_2

Table 2. *SO_2 oxidation rates in the atmosphere*

Location	k (% h^{-1})*	Reference
Western Washington (wave clouds)	0–300	Hegg and Hobbs (1981)
Western Washington (clouds)	−600 ± 1000–1900 ± 1900	Hegg and Hobbs (1982)
Los Angeles (aerosol, summer)	6.0†	Cass (1981)
Los Angeles (aerosol, winter)	2.0†	Cass (1981)
Bakersfield (fogs)	0.9 ± 5.5‡	This study

* k is a pseudo first-order rate constant expressing sulfate production as a % of $[SO_2(g)]$.
† Hourly production rates averaged over 3 years.
‡ Calculated from one fog sample to the next using equation (7). Data for $n = 80$ samples. Samples were excluded from the data set when: (i) SO_2 partial pressure was below the detection limit of 10 ppb; (ii) ionic balances were off by over 30%; or (iii) only one sample was collected during the event (2 January).

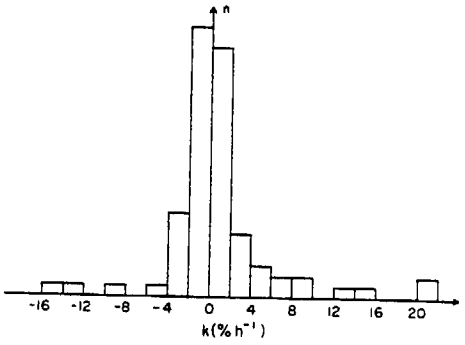

Fig. 5. Frequency distribution of the pseudo first-order rate constant for S(VI) in-fog production, k (% h^{-1}). Data from $n = 80$ fogwater samples collected at Bakersfield during the period 30 December 1982–15 January 1983.

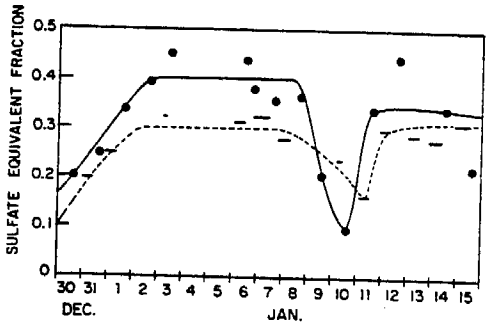

Fig. 6. Evolution of the sulfate equivalent fraction in the fogwater (–) and in the aerosol (●) at Bakersfield during the period 30 December 1982–15 January 1983. Lines have been added to show trends.

concentrations at, or close to, the detection limit of 10 ppb. The uncertainty on $[SO_2(g)]$ can then be as great as 50%, so that these outliers cannot be considered significantly different from the population as a whole.

Sulfate production was also analyzed in terms of k/L, which characterizes sulfate production referenced to the aqueous phase, and in terms of a zero-order dependence on $[SO_2(g)]$ (oxidation limited by mass transfer). Neither of these analyses showed evidence of S(VI) in-fog production.

In spite of this, the sulfate fraction of the aerosol increased over the course of the stagnation episodes (Fig. 6). After the two widespread fogs and persistent thick haze of 31 December and 1 January, the sulfate equivalent fraction (SEF) of the aerosol (defined as SEF = $[S(VI)]/[T]$) rose and stabilized at 0.40 ± 0.05. In comparison, the two-month aerosol averages reported by Heisler and Baskett (1981) for November–December 1978 at Bakersfield show an SEF of 0.22. The highest sulfate concentration we observed, 76 $\mu g\ m^{-3}$ on 6 January, is close to the highest 24-h value recorded in the area, 80 $\mu g\ m^{-3}$ (Duckworth and Crowe, 1979). On 9–10 January, along with the removal of the stagnant air mass from the Valley, the SEF dropped sharply, down to 0.10 on the afternoon of 10 January. After the inversion trapped the renewed air mass in the Valley, the SEF rose again to values similar to those before 10 January. The SEF values for the fogwater were lower than those

for the afternoon haze, but behaved qualitatively in the same way.

Preferential deposition of components other than sulfate would result in an increase in the sulfate content at the beginning of the stagnation episode. Because nitrate does not show the increase observed for sulfate, even though both components are mostly present in the same type of particles, it seems unlikely that preferential deposition alone could result in such a rise of the SEF. It therefore appears that S(VI) production reactions proceed in the stagnant air mass, and that the stabilization of the sulfate content then indicates the attainment of a steady-state between sulfate production and the sinks discussed previously. In-fog oxidation at an average rate of 0.9% h^{-1} (Table 2) with $P_{SO_2} = 20$ ppb would produce 16 neq m^{-3} S(VI)/h of fog. This is not sufficient to explain the increases in the SEF of the daytime aerosol, especially since a large fraction of the sulfate that could be produced in fog is expected to be lost by deposition. Gas-phase oxidation of SO_2 by radicals is expected to be unimportant because of the limited photochemical activity (reflected by the low O_3 levels). Instead, the higher SEF values in the daytime aerosol than in the fog suggest that sulfate production mostly occurs in the haze droplets forming at high humidities. This could be expected because of the higher catalyst concentrations in haze droplets, and because both temperatures and SO_2(g) concentrations usually peak in the afternoon. Oxidation of S(IV) in haze droplets should proceed along similar pathways as for fog droplets, and has been observed to proceed rapidly under controlled conditions (Matteson et al., 1969; Crump et al., 1983).

3.4. Fogwater acidity

Extreme acidity in fogwater, as has been documented in the Los Angeles area, may pose specific environmental problems because of the potential for injury to materials, vegetation (Scherbatskoy and Klein, 1983), and human health (Hoffmann, 1984). Sulfuric acid and nitric acid (which are the main strong acids present) can be emitted into the atmosphere as primary pollutants, or alternatively be produced in situ (Calvert, 1984). Alkaline components in the atmosphere will titrate free acidity. Gaseous ammonia, which is the most important alkaline component in the Valley, reacts with H_2SO_4 and HNO_3 at high humidities to form concentrated ammonium salt droplets (Stelson, 1982). Dissolution of SO_2(g) in the aquated aerosol leads to S(IV), which can then be oxidized to S(VI) as discussed in the previous section. Alternatively, S(IV) can be stabilized in the lower oxidation state by complexation with carbonyl compounds (Munger et al., 1984). The production of one molar unit of S(VI) releases one to two molar units of H^+; formation of S(IV) adducts also produces H^+ (Jacob and Hoffmann, 1983). The resulting input of acidity can be subsequently titrated by absorption of NH_3(g) in the droplet. Therefore, the acidity of liquid water in an air mass under high sulfate and nitrate conditions is limited by the availability of NH_3(g) (and other alkaline components) to neutralize the strong acids present. This has previously been observed for rainwater in the north-central United States (Munger, 1982).

In Los Angeles, where NH_3 emissions are relatively low (Russell et al., 1983), extremely high acidities are frequently found in the fogwater. In the Bakersfield fogwater, nitrate and sulfate concentrations are comparable to those in Los Angeles, but high acidities are much less common (Fig. 7). This is because ammonium concentrations are

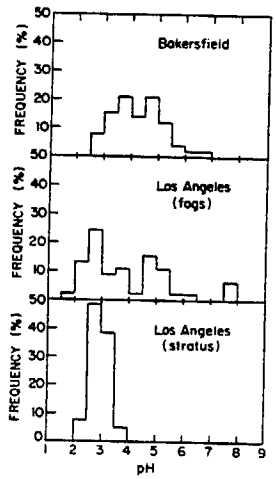

Fig. 7. pH frequency distribution for $n = 108$ fogwater samples collected at Bakersfield during the period 30 December 1982–15 January 1983. Results are compared with those obtained in the Los Angeles basin for fogs ($n = 45$) and stratus clouds ($n = 156$) (this laboratory, unpublished results, 1981–1983).

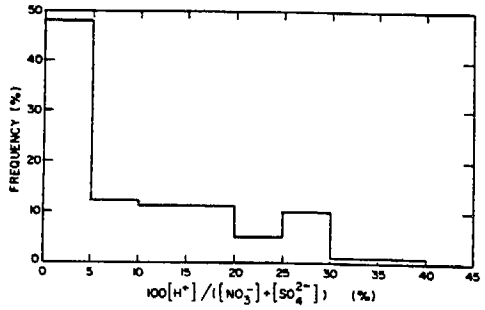

Fig. 8. Frequency distribution of the non-neutralized fraction of the acidity, as expressed by $[H^+]/([NO_3^-] + [SO_4^{2-}])$, for $n = 108$ fogwater samples collected at Bakersfield during the period 30 December 1982–15 January 1983.

considerably higher than in Los Angeles. A few samples at Bakersfield also had high concentrations of Ca^{2+}, indicating an alternative neutralization pathway by scavenging of alkaline dust.

Fig. 8 shows the fraction of non-neutralized acidic anions in our fog samples. In almost half of the samples, over 95% of the acidity was neutralized. At the same time, very low concentrations of gaseous ammonia were observed throughout the 17 days (Fig. 3). Most of the fogwater samples had pH values below 5, which suggests an absence of ammonia in the atmosphere from chemical equilibrium considerations. Ostensibly, the acidities present were sufficient to totally exhaust ammonia from the gas phase, and production of additional acidity resulted in a pH drop.

4. Conclusion

High ionic concentrations in the fogwater were observed at Bakersfield, California over the course of two stagnation episodes. The main contributors to the ionic loading of the fogwater were NH_4^+, NO_3^-, and SO_4^{2-}; this can be attributed to agricultural activity and oil recovery processes. Droplet growth was found to strongly influence the observed concentrations. Comparison of ionic loadings in the fogwater with those in the aerosol of the previous afternoon indicated that a sizable fraction of the aerosol was scavenged by the fog droplets. Fogwater ionic loadings decreased considerably over the course of the fog, and this was attributed to deposition of the large droplets on surfaces. In this manner, it was observed that a large fraction of the pollutants scavenged in the fog could be removed from the atmosphere. Deposition of fog droplets proceeds much more rapidly than deposition of the haze particles present at the high humidities between fog events, so that the occurrence of fog could slow down or limit the accumulation of particulate matter in a stagnant air mass.

Evolution of the sulfate content over the 17-day sampling period indicated an important increase of the sulfate fraction in the aerosol during stagnation episodes, but no statistical evidence for S(IV) oxidation in the fogwater was found. Most of the sulfate appeared to be produced in the daytime haze droplets. Preferential deposition of components other than sulfate could also partly explain the increase in the sulfate fraction.

High concentrations of acidic anions were present in the fogwater, but most of the acidity was neutralized by ammonia. In most cases, the neutralization of acidic components totally depleted NH_3 from the atmosphere; although the excess of acidity was usually not enough to lead to highly acidic conditions, 8% of the samples had pH values below 3.

5. Acknowledgements

This research was funded by the California Air Resources Board (CARB). We thank the staff of the CARB for their help and cooperation relating to our use of their facility at Bakersfield. We also acknowledge gratefully the CARB and the Western Oil and Gas Association for letting us use their data in this paper. Discussions with A. G. Russell were most helpful in the interpretation of some of the data.

REFERENCES

Brown, R. and Roach, W. T. 1976. The physics of radiation fog (II). A numerical study. *Q. J. R. Meteorol. Soc. 102*, 335–354.

Brown, R. 1980. A numerical study of radiation fog with an explicit formulation of the microphysics. *Q. J. R. Meteorol. Soc. 106*, 781–802.

California Air Resources Board 1982. Emission Inventory 1979, Stationary Source Control Division, Emission Inventory Branch, Sacramento, California.

Calvert, J. G. (ed.) 1984. *Acid precipitation*. Butterworth Publications, Boston.

Cass, G. R. 1979. On the relationship between sulfate air quality and visibility with examples in Los Angeles. *Atmos. Environ. 13*, 1069–1084.

Cass, G. R. 1981. Sulfate air quality control strategy design. *Atmos. Environ. 15*, 1227–1249.

Chylek, K. P. 1978. Extinction and liquid water content of fogs and clouds. *J. Atmos. Sci. 35*, 296–300.

Commins, B. T. and Waller, R. E. 1967. Observations from a ten-year study of pollution at a site in the city of London. *Atmos. Environ. 1*, 49–68.

Crump, J. G., Flagan, R. C. and Seinfeld, J. H. 1983. An experimental study of the oxidation of sulfur dioxide in aqueous manganese sulfate aerosols. *Atmos. Environ. 17*, 1277–1289.

Duckworth, S. and Crowe, D. 1979. Sulfur dioxide and sulfate trends, Bakersfield, 1977–1978. Technical Services Division, California Air Resources Board, Sacramento, California.

Gerber, H. E. 1981. Microstructure of a radiation fog. *J. Atmos. Sci. 38*, 454–458.

Goodeve, C. F. 1936. Discussion in "Sulphuric acid as a disperse phase in town air". *Trans. Faraday Soc. 32*, 1201–1202.

Hegg, D. A. and Hobbs, P. V. 1981. Cloud water chemistry and the production of sulfates in clouds. *Atmos. Environ. 15*, 1597–1604.

Hegg, D. A. and Hobbs, P. V. 1982. Measurements of sulfate production in natural clouds. *Atmos. Environ. 16*, 2663–2668.

Hegg, D. A. 1983. The sources of sulfate in precipitation (I). Parameterization scheme and physical sensitivities. *J. Geophys. Res. 88*, 1369–1374.

Heisler, S. and Baskett, R. 1981. Particle sampling and analysis in the California San Joaquin Valley. Research report CARB-RR-81-14, December 1981, available from Environmental Research and Technology, Westlake Village, California.

Hering, S. V. and Blumenthal, D. L. 1983. Field comparison of fog/cloud water collectors: preliminary results. Proceedings, Air Pollution Control Association Specialty Conference on the Meteorology of Acid Deposition, Hartford, Connecticut, 17 October 1983. Published by the Air Pollution Control Association, Pittsburgh.

Hoffmann, M. R. and Jacob, D. J. 1984. Kinetics and mechanisms of the catalytic autoxidation of dissolved sulfur dioxide in aqueous solution: an application to night-time fogwater chemistry. In *Acid precipitation* (ed. J. G. Calvert). Boston: Butterworth Publications, 101–172.

Hoffmann, M. R. 1984. Comment on acid fog. *Environ. Sci. Technol. 18*, 61–64.

Holets, S. and Swanson, R. N. 1981. High-inversion fog episodes in central California. *J. Appl. Meteorol. 20*, 890–899.

Houghton, H. G. 1955. On the chemical composition of fog and cloud water. *J. Meteorol. 12*, 355–357.

Jacob, D. J. and Hoffmann, M. R. 1983. A dynamic model for the production of H^+, NO_3^-, and SO_4^{2-} in urban fog. *J. Geophys. Res. 88*, 6611–6621.

Jacob, D. J., Wang, R.-F. T. and Flagan, R. C. 1984. Fogwater collector design and characterization. *Environ. Sci. Technol. 18*, (in press).

Lazrus, A. L., Baynton, H. W. and Lodge, J. P. 1970. Trace constituents in oceanic cloud water and their origin. *Tellus 22*, 106–114.

Mader, P. P., Hamming, W. J. and Bellin, A. 1949. Determination of small amounts of sulfuric acid in the atmosphere. *Anal. Chem. 22*, 1181–1183.

Martin, L. R. 1984. Kinetic studies of sulfite oxidation in aqueous solution. In *Acid precipitation* (ed. J. G. Calvert), Boston: Butterworth Publications, 63–100.

Matteson, M. J., Stober, W. and Luther, H. 1969. Kinetics of the oxidation of sulfur dioxide by aerosols of manganese sulfate. *I. & E. C. Fund. 8*, 677–686.

Mrose, H. 1966. Measurements of pH, and chemical analyses of rain-, snow-, and fog-water. *Tellus 18*, 266–270.

Muller, J. 1982. Rules in atmospheric behaviour of particulate substances. GAF-conference, Bologna, 14–17 September 1982, Fraunhofer Ges., Grafschaft/Schmallenberg, F. R. Germany.

Munger, J. W. 1982. Chemistry of atmospheric precipitation in the north central United States: influence of sulfate, nitrate, ammonia, and calcareous soil particulates. *Atmos. Environ. 16*, 1633–1645.

Munger, J. W., Jacob, D. J., Waldman, J. M. and Hoffmann, M. R. 1983. Fogwater chemistry in an urban atmosphere. *J. Geophys. Res. 88*, 5109–5123.

Munger, J. W., Jacob, D. J. and Hoffmann, M. R. 1984. The occurrence of bisulfite aldehyde addition products in fog- and cloudwater. *J. Atmos. Chem.* (in press).

National Oceanic and Atmospheric Administration 1983. Local climatological data (monthly summary) for Bakersfield, CA, Kern County air terminal, December 1982 and January 1983, Published by US Dept. of Commerce, National Climatic Data Center, Asheville, North Carolina, USA.

Okita, T. 1968. Concentration of sulfate and other inorganic materials in fog and cloud water and in aerosol. *J. Meteorol. Soc. Japan 46*, 120–126.

Petrenchuk, O. P. and Drozdova, V. M. 1966. On the chemical composition of cloudwater. *Tellus 18*, 260–286.

Pruppacher, H. R. and Klett, J. D. 1978. *Microphysics of clouds and precipitation*. Amsterdam: Reidel. 418–421.

Reible, D. D., Shair, F. H., Smith, T. B. and Lehrman, D. E. 1984. The origin and fate of air pollutants in California's San Joaquin Valley (I). Winter. *Atmos. Environ.* (in press).

Roach, W. T. 1976. On some quasi-periodic oscillations observed during a field investigation of radiation fog. *Q. J. R. Meteorol. Soc. 102*, 355–359.

Russell, A. G. 1983. Analysis of oxalic acid impregnated

filters for ammonia determination, Environmental Quality Lab open file report 83–1, California Institute of Technology, Pasadena, California.

Russell, A. G., McRae, G. J. and Cass, G. R. 1983. Mathematical modeling of the formation and transport of ammonium nitrate aerosol. *Atmos. Environ. 17*, 949–964.

Scherbatskoy, T. and Klein, R. M. 1983. Response of spruce and birch foliage to leaching by acidic mists. *J. Environ. Qual. 12*, 189–195.

Schwartz, S. E. and White, W. H. 1981. Solubility equilibria of the nitrogen oxides and oxyacids in dilute aqueous solution. *Adv. Environ. Sci. Eng. 4*, 1–45.

Schwartz, S. E., Newman, L., Hegg, D. A. and Hobbs, P. V. 1983. Measurements of sulfate production in natural clouds (discussion). *Atmos. Environ. 17*, 2629–2633.

Smith, T. B., Lehrman, D. E., Reible, D. D. and Shair, F. H. 1981. The origin and fate of airborne pollutants within the San Joaquin Valley. Final report to the California Air Resources Board, Sacramento, California.

Stelson, A. W. 1982. Thermodynamics of aqueous atmospheric aerosols. Ph.D. thesis, California Institute of Technology, Pasadena, California.

Waldman, J. M., Munger, J. W., Jacob, D. J., Flagan, R. C., Morgan, J. J. and Hoffmann, M. R. 1982. Chemical composition of acid fog. *Science 218*, 677–680.

APPENDIX VII

AEROSOL COMPOSITION IN A STAGNANT AIR MASS IMPACTED BY DENSE FOGS: PRELIMINARY RESULTS.

by D .J. Jacob, J. W. Munger, J. M. Waldman, and M. R. Hoffmann*
Environmental Engineering Science
W. M. Keck Engineering Laboratories
California Institute of Technology
Pasadena, CA 91125

submitted to the 77th Annual Meeting of the Air Pollution Control Association, San Francisco, CA, June 24-29, 1984 (paper 24.5).

February 1984

Dr M. R. Hoffmann is an Associate Professor at Caltech. Messrs. D. J. Jacob and J. M. Waldman are Graduate Research Assistants at Caltech. Mr. J. W. Munger is an Associate Research Engineer at Caltech.

* to whom correspondence should be addressed.

1. INTRODUCTION.

The effect of humidity on the physical and chemical behavior of atmospheric aerosols has been the topic of much attention. High relative humidities facilitate the formation of concentrated aqueous ammonium salt particles from the gaseous precursors HNO_3, H_2SO_4, NH_3, and H_2O [1]. These particles are major contributors to urban haze. Under supersaturated conditions, haze particles nucleate to form a dilute aqueous aerosol of supermicron fog droplets. Unusually high ionic concentrations and acidities have been reported in Los Angeles area fogwater[2,3]. Solute concentrations were in the millimolar range for H^+, NH_4^+, SO_4^{2-}, and NO_3^-. These high acidities have raised concern regarding potential damage to materials, vegetation[4], and public health[5].

Aqueous aerosols may be the site of redox reactions that lead to the production of strong acids. Aqueous-phase production of sulfate from reduced sulfur species has been observed to proceed rapidly in the laboratory in the presence of strong oxidants[6], and could be effective at the concentrations typically found in urban fogs and dense haze[7].

Over the last two winters, our research group has been investigating the chemical composition of fogwater and haze aerosol during wintertime stagnation episodes in the San Joaquin Valley of California. The valley is encompassed by mountain ranges. During the winter a strong subsidence inversion based below the natural boundaries of the Valley[8] restricts the ventilation of the air masses below the inversion. The residence time of an air parcel in the Valley under these stagnation conditions is on the order of 8 days[9]. Because the trapped air is very humid, stagnation episodes are associated with a persistent thick haze and frequent widespread nighttime fogs.

During the winter 1982-1983 we sampled fog and haze at one site (Bakersfield); results from this preliminary study have been discussed in detail in a previous report[10]. In the winter 1983-1984 the scale of the program was expanded in order to test hypotheses formulated as a result of first year data. In the present paper we first report briefly on the 1982-1983 results and outline the essential conclusions. We then describe the large-scale experiment conducted during the winter of 1983-1984, and discuss some preliminary fogwater data.

2. WINTER 1982-1983: SUMMARY OF RESULTS.

Fog and haze were sampled at Bakersfield for a period of 17 days, which included two extended stagnation episodes and numerous fog events. Fogwater was collected with a rotating arm collector[11]. Haze was collected on an open-faced Teflon filter, and

gaseous ammonia was collected on an oxalic acid-impregnated glass fiber filter[12] set downstream of the Teflon filter. Teflon filters were extracted in 10 ml of water with a reciprocating shaker for 60 minutes. Further aspects of the analytical protocol have been described previously[3]. Liquid water content in the fog was determined by weight after drawing a known amount of air through an open-faced, paper filter. The major components in the fogwater and in the water-soluble fraction of the haze aerosol were NH_4^+, NO_3^-, and SO_4^{2-} ; these were attributed to the important agricultural and oil recovery activities in the area. Figure 1 shows the aerosol and fogwater loadings observed throughout the investigation. Fogwater loadings are defined as the amount of solute in the fogwater per cubic meter of air, and are calculated from fogwater concentrations and liquid water content.

The mixing height profile shown in Figure 1 indicates that two distinct stagnation episodes occurred. From December 25 to January 9 the inversion base was lower than 600 m above ground level. Then on 9 - 10 January a front passed through the Valley, breaking down the inversion and ventilating the Valley. After 10 January subsidence conditions resumed, leading to a second stagnation episode. From 30 December to 9 January the air mass was well-aged, and high aerosol loadings were observed. After the ventilation on 9-10 January aerosol loadings dropped considerably, and a slow build-up was initiated again.

Figure 2 shows a typical example of the evolution of fogwater loadings over the course of a fog event. We observe a considerable decrease in pollutant levels in the fogwater, which does not correlate with a lifting of the inversion base or with the advection of much cleaner air masses over the site (as would be documented by a decrease in SO_2 and NO_x concentrations). A plausible explanation is that the supermicron fog droplets deposit rapidly on surfaces. If scavenging of pollutants by fog droplets is followed by deposition, pollutants will effectively be removed from the atmosphere. It should be noted that aerosol loadings were significantly higher during the first stagnation episode (where relatively little fog occurred) than during the second episode (where widespread dense fogs occurred every night). Deposition during fogs may therefore limit pollutant build-up during stagnation episodes.

The question of sulfate production in aerosol and clouds has been addressed in some recent field studies (Table 1). A parameterized expression has been used to express the production rate:

$$d[S(VI)]/dt = (k/100)[SO_2(g)] \qquad (1)$$

In our study, fogwater samples were collected over intervals ranging from one-half to three hours. Sulfate production was calculated in terms of k for each sampling interval within the same event. Corrections for changes in liquid water content and for deposition were introduced[10]. We obtained k values much lower than those obtained by Hegg and Hobbs in clouds, and also lower than those calculated by Cass for the Los Angeles aerosol. Our results show no statistical evidence of S(VI) production in fogwater; the deviations about $k = 0\ \%\ h^{-1}$ can be simply explained by the non-Lagrangian sampling procedure.

However, the sulfate equivalent fraction in the aerosol (SEF) increased appreciably at the beginning of the stagnation episodes, reaching a steady-state value of 0.40 ± 0.05 (Figure 3). Because the photochemical activity was low, as indicated by the low O_3 concentrations recorded at the site by the California Air Resources Board, it is unlikely that gas-phase oxidation of SO_2 could have caused this increase. Two more plausible explanations are: a) preferential deposition of components other than sulfate, or b) S(VI) production in the haze aerosol. The second explanation is favored because nitrate does not exhibit the increase observed for sulfate, even though both components are present in the same type of particles.

The oxidation of S(IV) to form S(VI) simultaneously releases free acidity in the droplet[15]. The acidity produced can be titrated by alkaline components in the atmosphere, such as ammonia. In Los Angeles, NH_3 emissions are low[16], leading to extremely high acidities in the fogwater. In the San Joaquin Valley, NH_3 emissions are much higher due to intensive agricultural activity. Even though the concentrations of acidic anions in the Bakersfield fogwater are comparable to those observed in Los Angeles[3], ammonium concentrations are much higher in Bakersfield. As a result, pH values are not as low[3,10]. The low gaseous ammonia concentrations observed in Bakersfield suggest that ammonia is scavenged efficiently from the gas phase; this agrees with thermodynamic predictions[15] that indicate NH_3 should be totally scavenged in a fog with $pH < 5$.

The 1982-1983 study allowed us to postulate hypotheses regarding the behavior of wet aerosol in the atmosphere. Sampling was limited to one location, and uncertainties due to short-range transport prevented us from making definitive, quantitative conclusions. This led to the design of a larger-scale field experiment for the following winter, which is described below.

3. WINTER 1983-1984: DESIGN OF FIELD EXPERIMENT.

Six sampling sites were operated in the southern San Joaquin Valley (Figure 4).

The sites were chosen so as to cover an area where strong internal mixing (time scale 1 - 2 days) has been observed during stagnation episodes[9]. Oil recovery operations are located in the area south of Wasco and Lost Hills, with the largest oil fields near Bakersfield (Oildale). Oil fields around Bakersfield emit a combined total of 1.0×10^5 tons SO_2 yr^{-1} and 3.5×10^4 tons NO_2 yr^{-1} [17], while oil fields on the western side of the Valley emit 8.5×10^3 tons SO_2 yr^{-1} and 2×10^4 tons NO_2 yr^{-1} [17]. Almost all the land in the area is used for agriculture and ranching. The population majority is in the eastern half of the Valley.

All Valley sites, except McKittrick, are in low-lying areas where radiation fogs form frequently. McKittrick is more likely to intercept low stratus clouds, and is often above the inversion in the wintertime. Two mountain sites (Tehachapi and Lake Isabella) were operated to evaluate the outflow of aerosol from the Valley by possible diurnal upslope flow through the inversion. This flow is important in the summertime[18], but it is substantially weakened in the winter months because of reduced solar insolation. The dominant geostrophic wind blows from the northwest, and the mountain sites were selected in the region of most probable outflow.

Aerosol and some trace gases were sampled at all eight sites. The filter set-up is illustrated in Figure 5. Filters were run twice a day (0000 to 0400 PST and 1200 to 1600 PST) in the Valley, and once a day (1000 to 1600 PST) at mountain sites. Also, deposition buckets were set out at each site and rinsed once a day with distilled water. The extract was analyzed for major ions.

Rotating arm fogwater collectors were operated at four sites. At the Bakersfield site, liquid water content was measured with a CO_2 laser transmissometer[19]. Also at Bakersfield, fog droplet size distributions were monitored with a CSASP-100-HV optical probe (Particle Measurements Systems,Inc.).

WINTER 1983-1984: PRELIMINARY RESULTS

Field data was collected over the period 15 December,1983 - 15 January,1984. At the time of this writing only preliminary fogwater data is available, and the discussion presented here should not be regarded as a definitive interpretation. Chemical analysis for fogwater samples followed the protocol described previously[3]. We have noted in the past year that the ion chromatographic method used to separate anions (Dionex AS-3 column, [3 m$\underline{M}$ HCO_3^- + 2.4 m$\underline{M}$ CO_3^{2-}] eluent, 3 ml min^{-1} flow rate) does not separate adequately S(IV) and NO_3^-. Better separation is achieved with a weaker eluent or with the Dionex AS-4 column, but quantification of the S(IV) still is unsatisfactory. To solve

this problem we make the solution 0.09 M H_2O_2 prior to injection in the ion chromatograph. This quantitatively converts SO_3^{2-} and hydroxymethanesulfonate to sulfate. Sulfur(IV) concentration is determined by colorimetry and sulfate calculated by difference.

The winter 1983 - 1984 was marked by extended stagnation episodes, but few dense fogs. Instead, a persistent stratus layer 100 - 200 m thick capped the Valley, preventing release of moisture from the ground in the day and radiational cooling at night. Most of the fog on the Valley floor occurred when the stratus cloud occasionally came down to the ground.

On 7 January, such conditions led to widespread fog throughout the southern part of the Valley. On that day fog was sampled at all four sites. Figure 6 shows the evolution of SO_4^{2-}, S(IV), NO_3^-, NH_4^+, and H^+ fogwater concentrations. Other ions analyzed contributed less than 10% to the total fogwater ionic loading. Alkalinity was not measured, although bicarbonate can contribute substantially to the ionic balances in samples with high pH.The liquid water content was estimated from the collection rate of the fogwater sampler, assuming a 60% collection efficiency[11]. At Bakersfield, fog was sampled from the onset; at other sites, fog had formed a few hours before sampling was initiated.

Average fogwater loadings calculated for each site over the sampling period are shown in Figure 7. The highest loadings were found at Bakersfield; that site is the major center of the area for population and industry, and is surrounded by oil fields. The 2.5:1 sulfate/nitrate equivalent ratio is typical of an area mostly affected by stationary fossil fuel sources, as opposed to the much lower ratios observed when mobile sources predominate[3]. The high variations in loadings observed from site to site show that, in spite of any intra-Valley mixing that may occur, the presence of local pollutant sources significantly influences the air quality. Visalia, which is some distance north of the oil fields, had low loadings of acidic anions.

High ammonium levels reflect the widespread agricultural and ranching activity. The high fogwater pH values at Bakersfield, Buttonwillow, and Visalia indicate that an excess of gaseous ammonia was available to entirely neutralize acidic anions at these sites[15]. Samples with pH above 6, such as those collected at Visalia on that day, routinely showed an excess of cations over anions in analysis. Titrations conducted on a few of these samples indicate alkalinities of over 200 $\mu eq\ l^{-1}$, which explain the deviations from the ionic balance.

McKittrick fog had much higher acidities than the other sites (Figure 6, Table 2), even though loadings of acidic anions were lower than at Bakersfield or Buttonwillow.

The land around McKittrick is arid and mostly uncultivated, as opposed to the other sites. Ostensibly, there was not enough ammonia to neutralize the sulfate and nitrate present.

Liquid water-weighted average concentrations of sulfur(IV) for the 7 January fog were 617 μM at Bakersfield, 75 μM at Buttonwillow, 45 μM at McKittrick, and 12 μM at Visalia. Because of the high fogwater pH, acid-base dissociation of $SO_2.H_2O$ in solution leads to high concentrations of HSO_3^-)[16,20]. Low partial pressures of SO_2 (<10 ppb) would be sufficient to explain the S(IV) levels observed at Buttonwillow and Visalia. At Bakersfield and McKittrick, on the other hand, equilibrium at the fogwater pH would require about 80 ppb of SO_2 if $SO_2 \cdot H_2O$, HSO_3^-, and SO_3^{2-} were the only species present. These would be unusually high SO_2 concentrations. Formation of hydroxyalkanesulfonic acids has been suggested to explain the high S(IV) concentrations in urban fogwater[20].

Because of its high elevation, McKittrick frequently intercepted the stratus layer during the month of January. and was the site most heavily impacted by fogs. Table 2 lists the liquid water-weighted average concentrations observed. On 2 January and on the following night, the eatern side of the Valley was overcast, but the west side (McKittrick, Lost Hills) remained clear. Fog formed at McKittrick on the morning of 3 January; a steady drainage flow from the west was observed during the fog. After 1000 PST the cloud base rose above McKittrick and from then on until 11 January the entire Valley was capped by the stratus deck. McKittrick periodically intercepted the cloud as the cloud moved up and down; except for 7 January, lower locations were always below the cloud base. Winds at McKittrick were highly variable throughout that period, which is characteristic of a site within the boundary mixing layer. On 11 January unstable air moved through the Valley, breaking up the stratus cover and resulting in clear skies and high cloudiness. Fog was observed again at Bakersfield and McKittrick on 13 January.

Figure 8 shows the evolution of the SEF at McKittrick. As the cloud ages the SEF increases and reaches a steady-state value after a few days. This profile is very similar to that observed in Bakersfield the preceding winter (Figure 3) and supports the importance of sulfate production in the stagnant air mass. A steady state was reached rapidly due to a balance of sources and sinks. After the Valley was ventilated on 12 January, the SEF dropped; the SEF was down at 0.19 in the 13 January fog.

SUMMARY.

A network of aerosol and fogwater sampling sites was operated in the southern San Joaquin Valley during the winter 1983 - 1984. The object of the program was to

characterize the effect of stagnation conditions on a wet aerosol. Fogwater data supports some of the conclusions reached in the previous year of study at Bakersfield : a)important production of sulfate occurs in the stagnant air mass, b)fogwater acidity is controlled by the availability of ammonia to neutralize the strong acids present. Major questions raised by the first year of study, such as the rate of aerosol removal by deposition and the rate of sulfate production in both the haze and the fog, will be addressed after the remainder of the data is processed. These will be the object of a future report.

ACKNOWLEDGEMENTS.

We gratefully thank the California Air Resources Board, the Getty Oil Co., and the Buttonwillow Parks and Recreation. This research was funded by the California Air Resources Board.

REFERENCES.

1. A.W. Stelson and J.H. Seinfeld, "Relative humidity and temperature dependence of the ammonium nitratedissociation constant." Atmos. Environ. 16: 983 (1982).
2. J.M. Waldman, J.W. Munger, D.J. Jacob, R.C. Flagan, J.J. Morgan and M.R. Hoffmann, "Chemical composition of acid fog." Science 218: 677 (1982).
3. J.W. Munger, D.J. Jacob, J.M. Waldman and M.R. Hoffmann, "Fogwater chemistry in an urban atmosphere." J.Geophys.Res. 88: 5109 (1983).
4. T. Scherbatskoy and R.M. Klein, "Response of spruce and birch foliage to leaching by acidic mists." J.Environ.Quality 12: 189 (1983).
5. M.R. Hoffmann, "Comment on acid fog." Environ.Sci.Technol. 18: 61 (1984)
6. L.R. Martin, "Kinetic studies of sulfite oxidation in aqueous solution." Acid Precipitation, Butterworth, Boston, 1984, pp 63-100.
7. R.J. Anderson, R.J. Pilie, E.J. Mack and W.C. Kockmond, "Laboratory investigation of the photooxidation and catalytic oxidation of SO_2." EPA-600/3-79-006 (Jan. 1979).
8. S. Holets and R.N. Swanson, "High-inversion fog episodes in central California." J.Appl.Met. 20: 890 (1981).
9. D.D. Reible, F.H. Shair, T.B. Smith and D.E.Lehrman, "The origin and fate of air pollutants in California's San Joaquin Valley. I.Winter." Atmos.Environ. (in press).
10 D.J. Jacob, J.M.Waldman, J.W.Munger and M.R.Hoffmann, "A field investigation of physical and chemical mechanisms affecting pollutant concentrations in fog droplets."

Tellus (in press).
11. D.J.Jacob, R.-F.T.Wang and R.C.Flagan, "Fogwater collector design and characterization." Environ.Sci.Technol. (in press).
12. A.G.Russell, "Analysis of oxalic acid impregnated filters for ammonia determination.", EQL open file rpt. 83-1, California Institute of Technology, Pasadena, CA.
13. D.A. Hegg and P.V. Hobbs, "Measurements of sulfate production in natural clouds." Atmos.Environ. 16: 2663 (1982).
14. G.R. Cass, "Sulfate air quality control strategy design.", Atmos.Environ. 15:1227 (1981).
15. D.J. Jacob and M.R. Hoffmann, "A dynamic model for the production of H^+, NO_3^-, and SO_4^{2-} in urban fog." J.Geophys.Res. 88: 6611 (1983).
16. A.G. Russell, G.J. McRae and G.R. Cass, "Mathematical modeling of the formation and transport of ammonium nitrate aerosol." Atmos.Environ. 17: 949 (1983).
17. California Air Resources Board Emissions Inventory, Sacramento, CA (1978).
18. D.D. Reible, J.R. Ouimette and F.H. Shair, "Atmospheric transport of visibility degrading pollutants into the California Mojave desert." Atmos.Environ. 16: 599 (1982).
19. J.E. Jiusto and G.G. Lala, ASRC-SUNY publ.869, State University of New York at Albany, Albany, NY,1983.
20. J.W. Munger, D.J. Jacob and M.R. Hoffmann, "The occurrence of bisulfite aldehyde addition products in fog- and cloudwater." Atmos.Chem. (in press).

FIGURE CAPTIONS.

Figure 1. Fogwater (in bold) and aerosol loadings of NH_4^+, NO_3^-, SO_4^{2-}, and H^+ (fogwater) measured at Bakersfield during December 1982 - January 1983. When measured, gaseous ammonia concentrations (ppb) are indicated on top of the aerosol data bars. Mixing heights are given in m above ground level.
Figure 2. Evolution of fogwater loadings over the course of the 7 January 1983 fog event.
Figure 3. Evolution of the sulfate equivalent fraction in the fogwater (—) and in the aerosol (●) at Bakersfield during December 1982 - January 1983. Lines have been added to show trends.
Figure 4. Fog and aerosol sampling network (winter 1983-1984).
Figure 5. Aerosol sampling set-up. Teflon filters 1,2,3 are used for determination of major ions, acidity, and formaldehyde, respectively. The nylon filter is used for determination of $HNO_3(g)$. The "Ox" filter[12] is used for determination of $NH_3(g)$. The "GA"

filter is a S(IV) impregnated paper filter used for determination of gaseous formaldehyde. The "S" filter is a formaldehyde-impregnated glass fiber filter used for determination of S(IV) in the aerosol.

Figure 6. Fogwater concentrations and liquid water contents at four sites during the 7 January 1984 fog. pH of the sample is indicated on top of each data bar. Concentrations of S(IV) were not determined in the last two samples at Bakersfield.

Figure 7. Average fogwater loadings at four sites for the 7 January 1984 fog.

Figure 8. Evolution of the sulfate equivalent fraction in the McKittrick fogwater during December 1983 - January 1984.

Table 1. SO_2 oxidation rates in the atmosphere.

location	k (% h^{-1})[a]	reference
western Washington (clouds)	-600±1000 - 1900±1900	Hegg and Hobbs(1982)
Los Angeles (aerosol,summer)	6.0[b]	Cass(1981)
Los Angeles (aerosol,winter)	2.0[b]	Cass(1981)
Bakersfield (fogs)	0.4 ± 1.8[c]	this study

(a) k is a pseudo first-order rate constant expressing sulfate production as a percentage of $[SO_2(g)]$.
(b) hourly production rates averaged over 3 years.
(c) calculated from one fog sample to the next using equation (7). Data for n=80 samples. Samples were excluded from the data set when (1) SO_2 partial pressure was below the detection limit of 10 ppb, (2) ionic balances were off by over 30 %, or (3) only one sample was collected during the event (2 January).

Table 2. Fogwater Concentrations at McKittrick, California

Date	Time (PST)	Concentration ($\mu eq\ \ell^{-1}$)[a]						$\bar{L}$ ($g\ m^{-3}$)[b]
		H^+	SO_4^{2-}	S(IV)	NO_3^-	NH_4^+	Ca^{2+}	
3 Jan.	0800-1000	2990	2110	85	5600	6010	NA	0.04
4 Jan.	0800-1000	371	721	31[c]	783	1010	55[c]	0.04
5 Jan.	0100-0630	70	183	35	191	337	10	0.21
	0750-1240	72	467	41	283	514	25[c]	0.08
6 Jan.	0030-0730	73	263	40[c]	135	346	11[c]	0.13
6-7 Jan.	2100-0700	52	156	45	42	181	2	0.16
7 Jan.	0700-1700	57	519	44	198	589	67	0.10
7-8 Jan.	1700-0400	104	427	52[c]	193	534	16	0.08
8 Jan.	0815-1220	102	732	45[c]	239	781	46[c]	0.03
	1815-1945	170	519	28	239	519	20	0.03
9 Jan.	0900-1100	282	767[d]	NA	379	686	73	0.02
10 Jan.	0010-0930	109	599	72	234	784	37	0.08
13 Jan.	0645-0945	70	359	29	581	809	79	0.15

NA: not analyzed.

(a) liquid water-weighted average concentrations over the time interval.

(b) average liquid water content (calculated from collection rate of sampler).

(c) calculated from incomplete data set.

(d) sulfate concentration not corrected for S(IV).

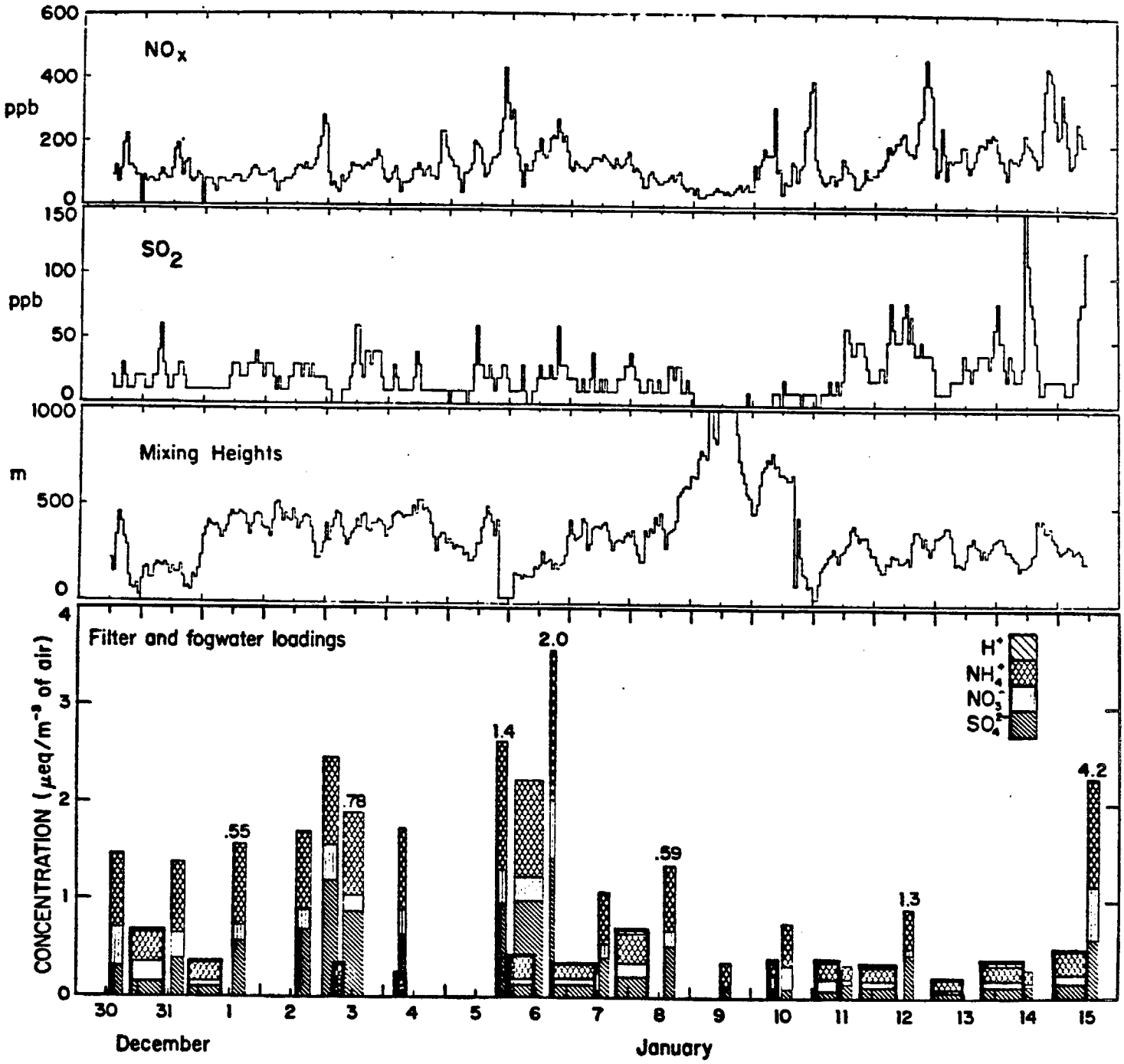
NOx
ppb
600
400
200
0
SO2
ppb
150
100
50
0
Mixing Heights
m
1000
500
0
Filter and fogwater loadings
CONCENTRATION (μeq/m⁻³ of air)
4
3
2
1
0
H+
NH4+
NO3-
SO4=
2.0
1.4
.78
.55
.59
1.3
4.2
30
31
1
2
3
4
5
6
7
8
9
10
11
12
13
14
15
December
January

Figure 1.

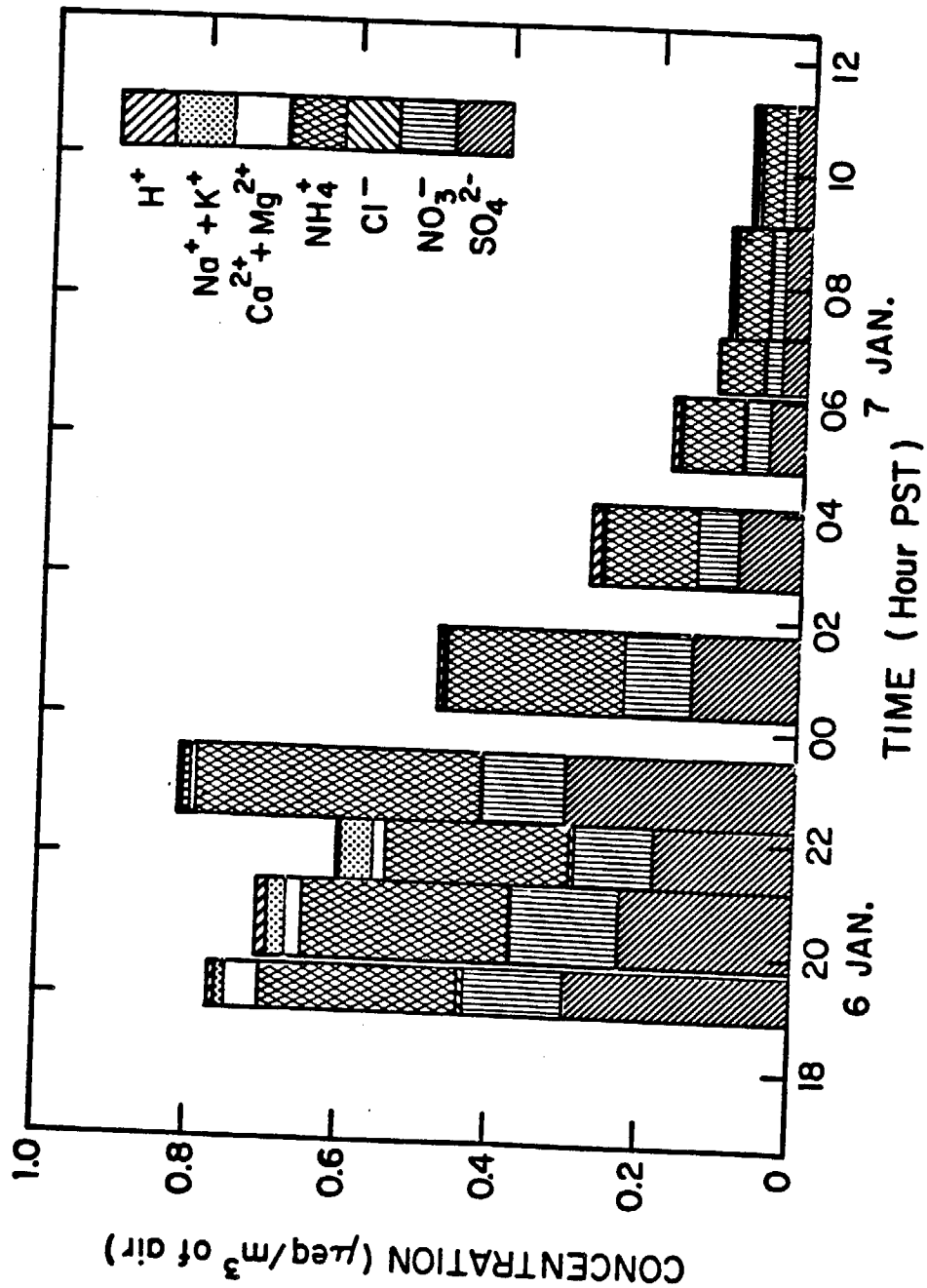
CONCENTRATION (μeq/m³ of air)
1.0
0.8
0.6
0.4
0.2
0
18
20
22
00
02
04
06
08
10
12
6 JAN.
7 JAN.
TIME (Hour PST)
H+
Na+ + K+
Ca2+ + Mg2+
NH4+
Cl−
NO3−
SO4 2-

Figure 2.

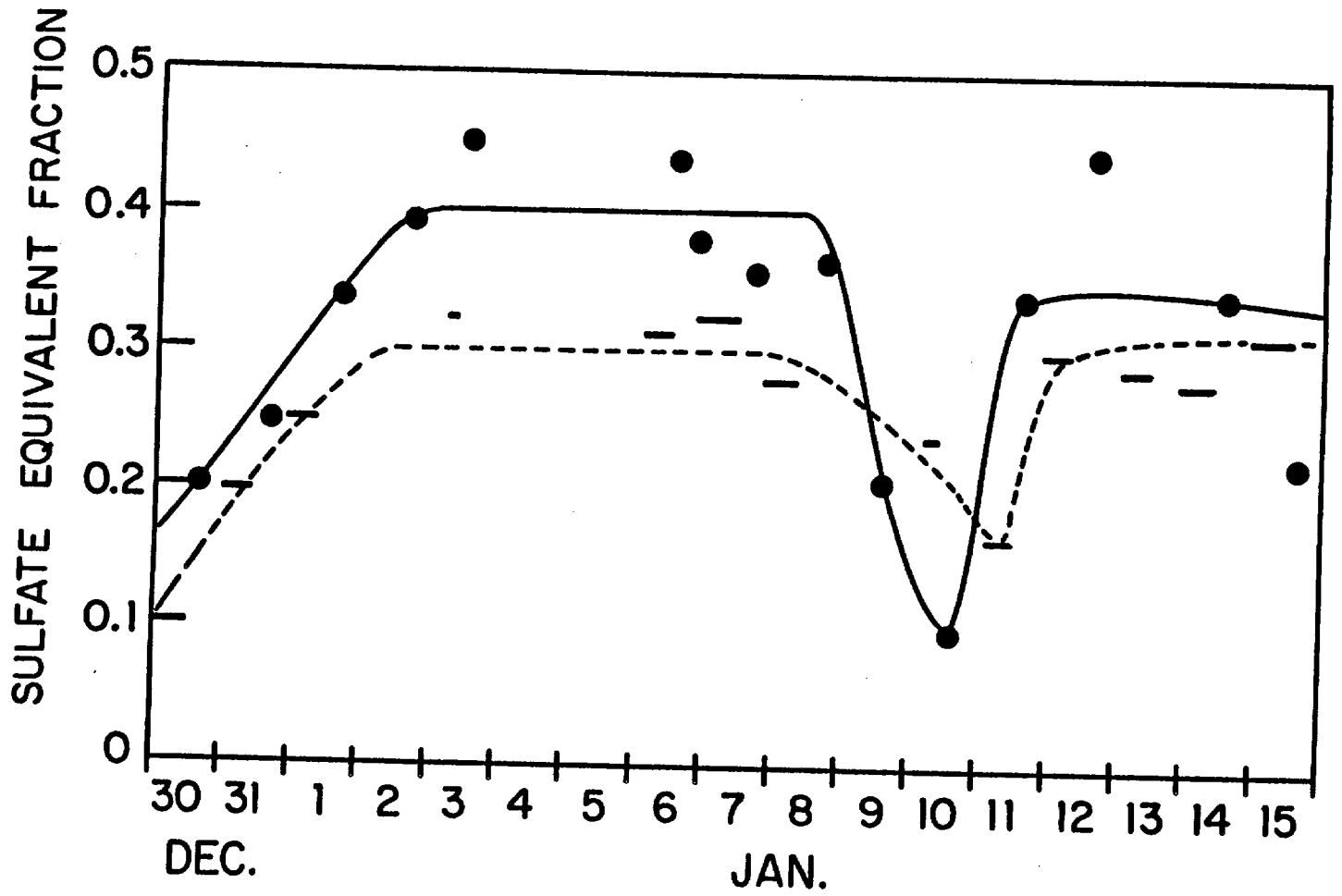
SULFATE EQUIVALENT FRACTION
0.5
0.4
0.3
0.2
0.1
0
30 31 1 2 3 4 5 6 7 8 9 10 11 12 13 14 15
DEC.
JAN.

Figure 3.

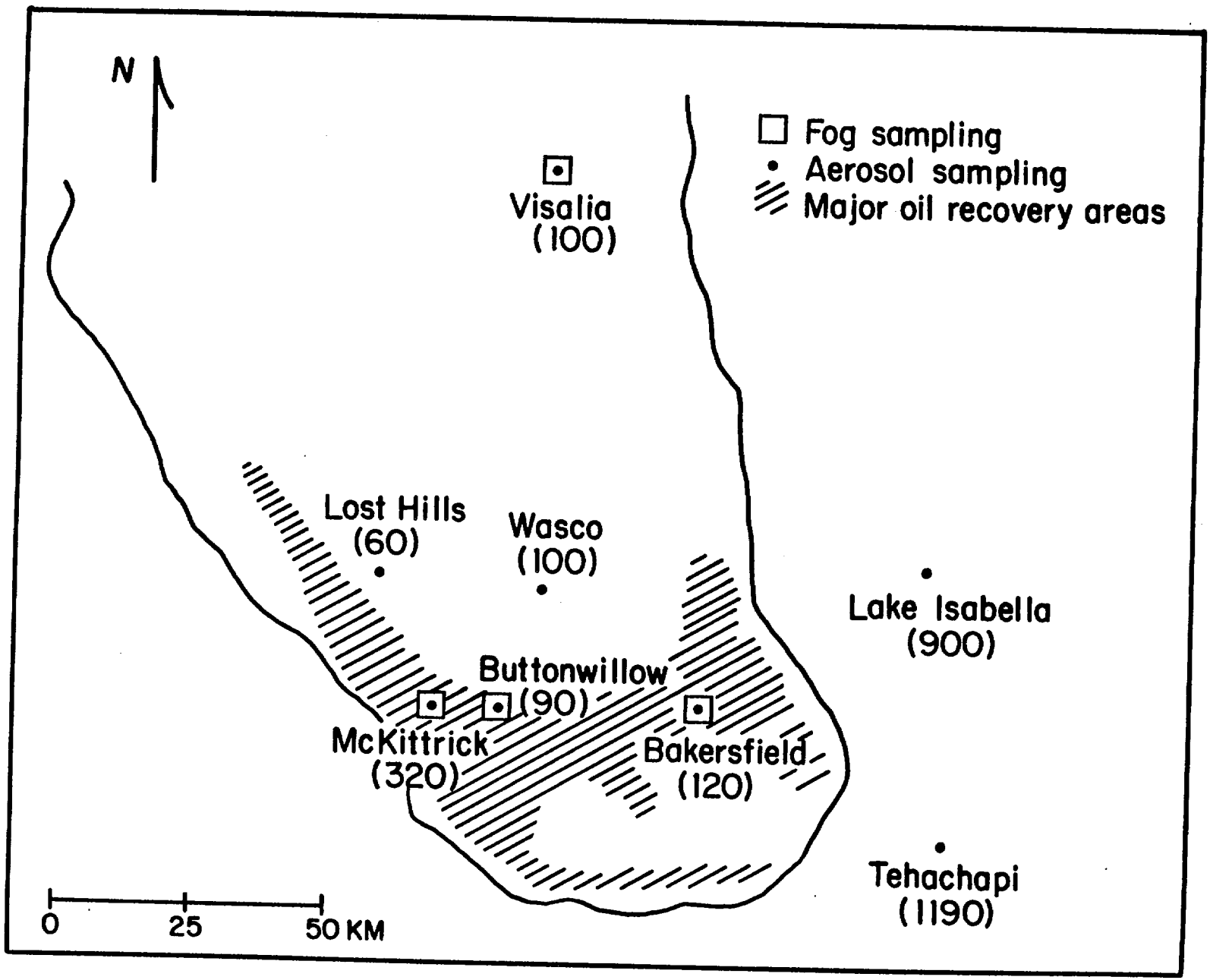
N
Fog sampling
Aerosol sampling
Major oil recovery areas
Visalia
(100)
Lost Hills
(60)
Wasco
(100)
Lake Isabella
(900)
Buttonwillow
(90)
McKittrick
(320)
Bakersfield
(120)
Tehachapi
(1190)
0
25
50 KM

Figure 4.

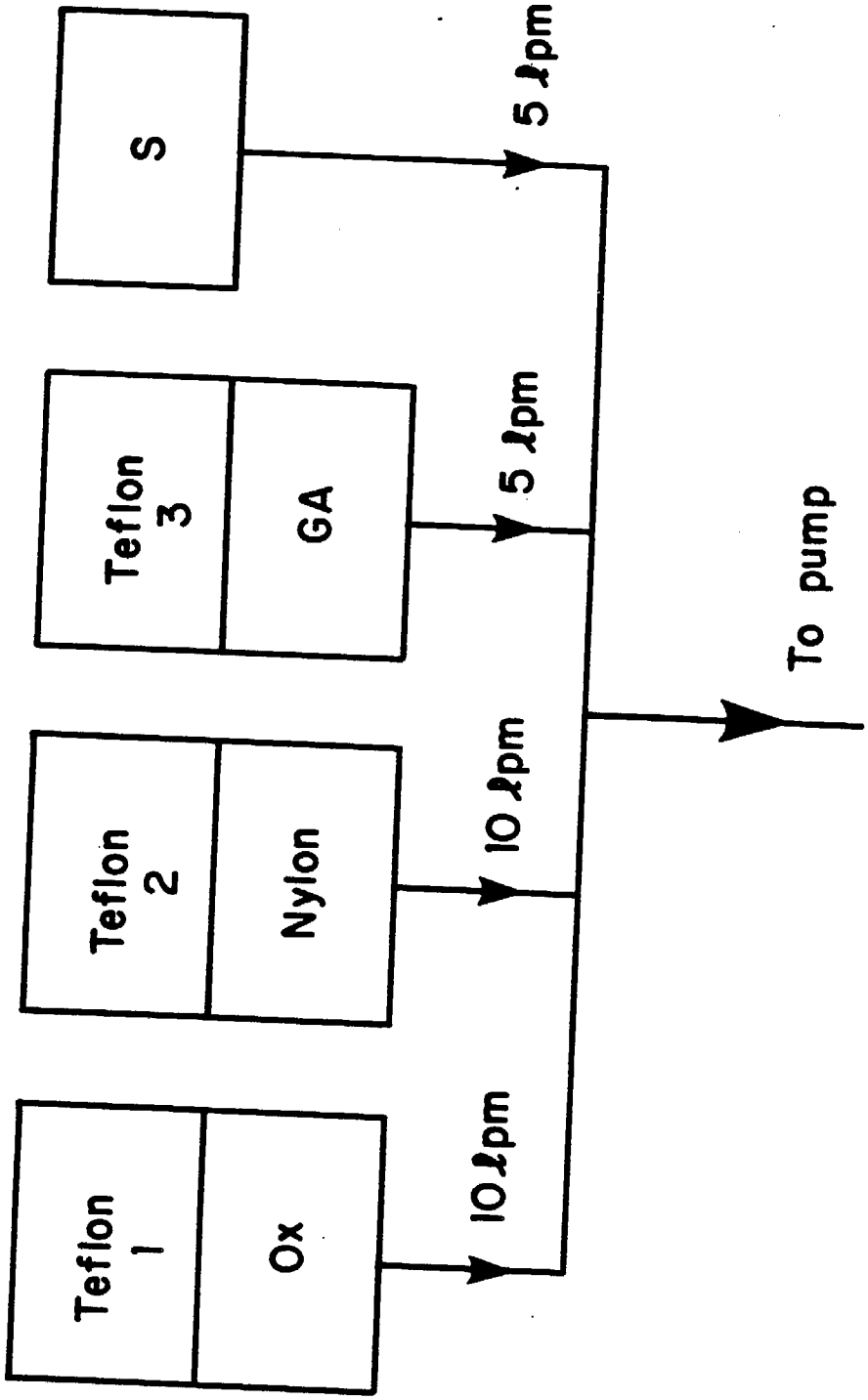
S
5 lpm
Teflon 3
GA
5 lpm
To pump
Teflon 2
Nylon
10 lpm
Teflon 1
Ox
10 lpm

Figure 5.

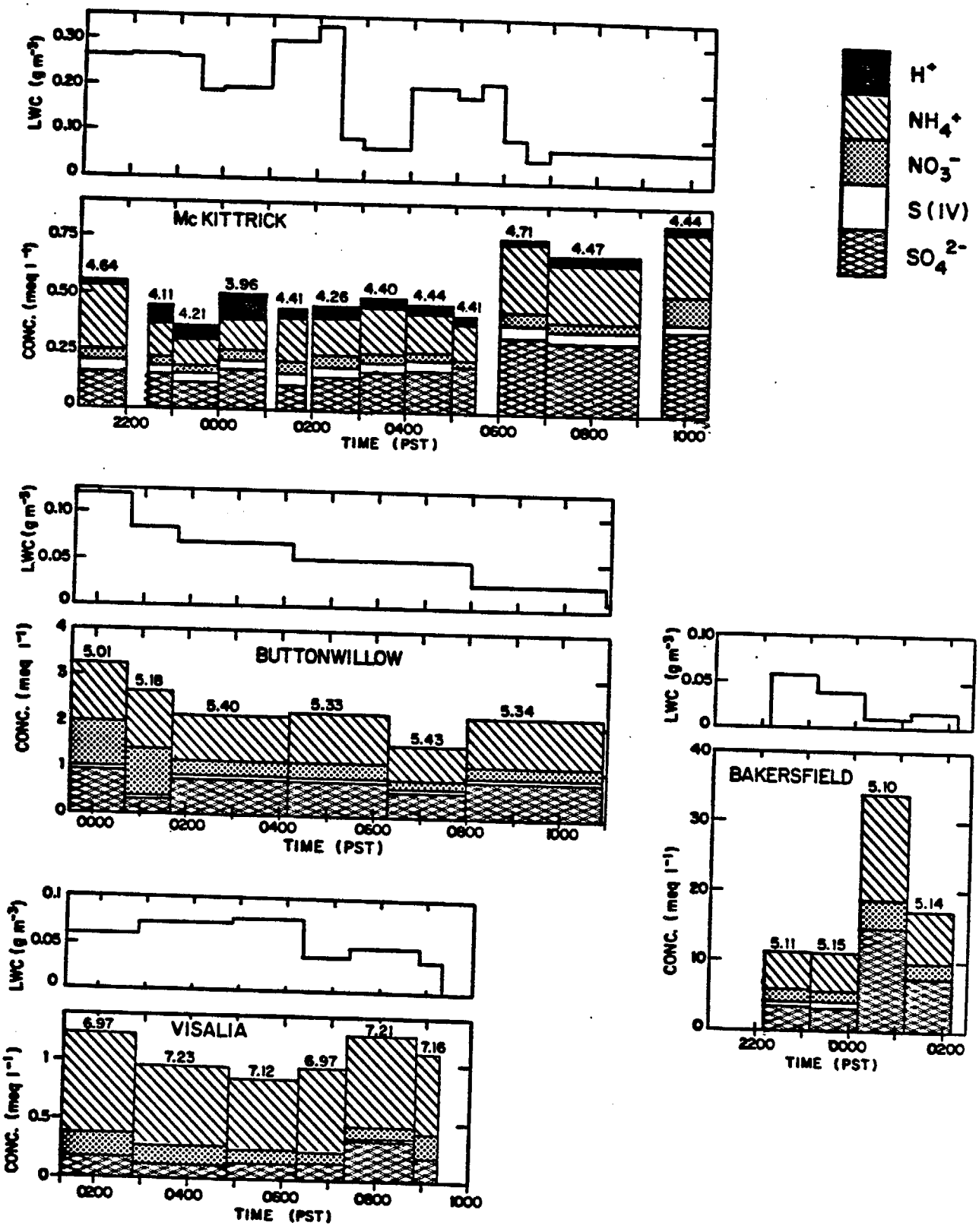
LWC (g m⁻³)
0.30
0.20
0.10
0
Mc KITTRICK
CONC. (meq l⁻¹)
0.75
0.50
0.25
0
4.64
4.11
4.21
3.96
4.41
4.26
4.40
4.44
4.41
4.71
4.47
4.44
2200
0000
0200
0400
0600
0800
1000
TIME (PST)
H⁺
NH₄⁺
NO₃⁻
S(IV)
SO₄²⁻
LWC (g m⁻³)
0.10
0.05
0
BUTTONWILLOW
CONC. (meq l⁻¹)
4
3
2
1
0
5.01
5.18
5.40
5.33
5.43
5.34
0000
0200
0400
0600
0800
1000
TIME (PST)
LWC (g m⁻³)
0.1
0.05
0
VISALIA
CONC. (meq l⁻¹)
1
0.5
0
6.97
7.23
7.12
6.97
7.21
7.16
0200
0400
0600
0800
1000
TIME (PST)
LWC (g m⁻³)
0.10
0.05
0
BAKERSFIELD
CONC. (meq l⁻¹)
40
30
20
10
0
5.11
5.15
5.10
5.14
2200
0000
0200
TIME (PST)

Figure 6.

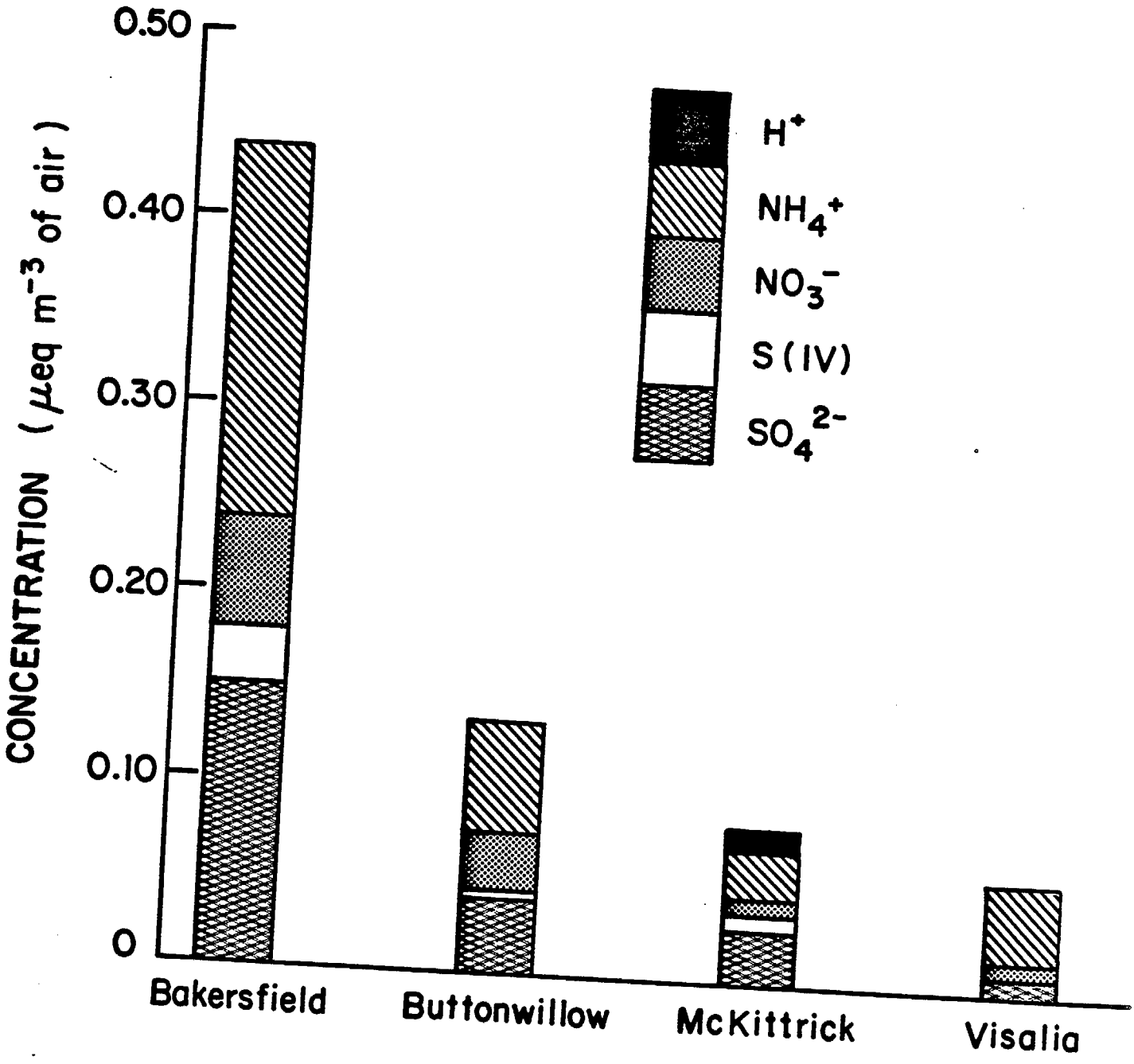
0.50
0.40
0.30
0.20
0.10
0
CONCENTRATION (μeq m⁻³ of air)
H⁺
NH₄⁺
NO₃⁻
S(IV)
SO₄²⁻
Bakersfield
Buttonwillow
McKittrick
Visalia

Figure 7.

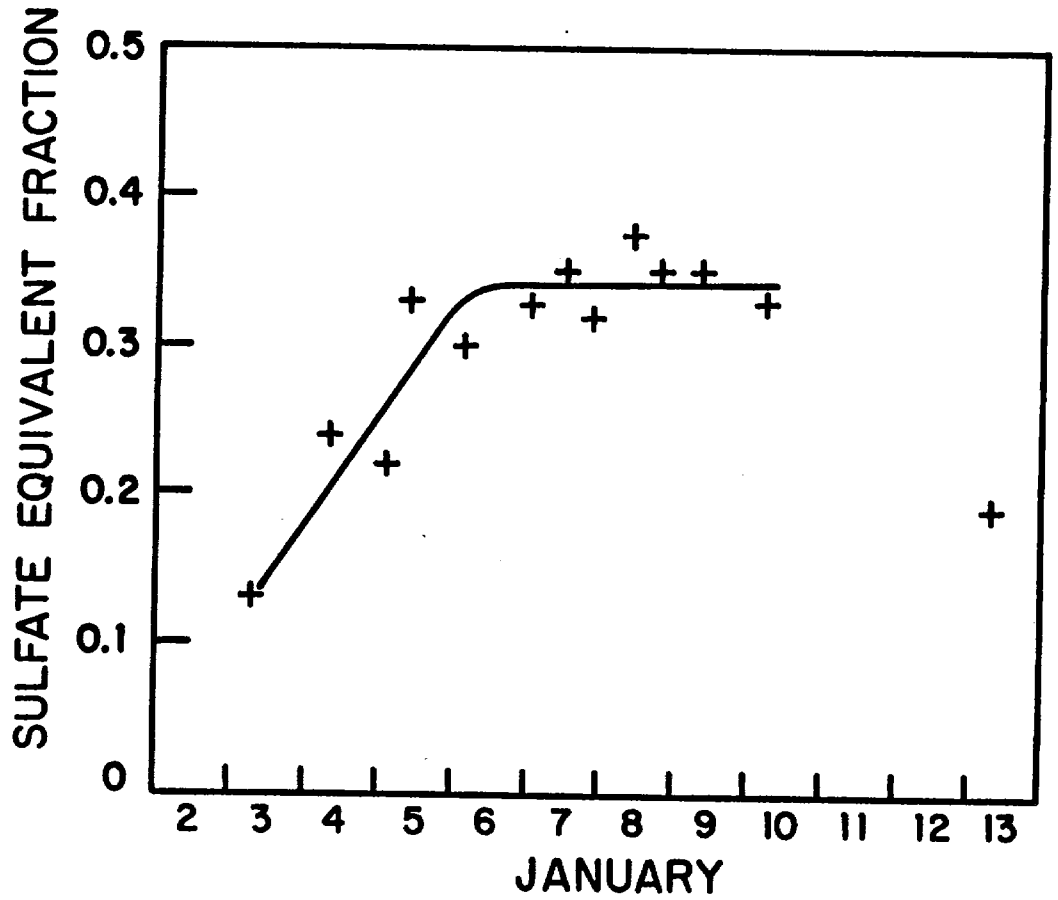
SULFATE EQUIVALENT FRACTION
0.5
0.4
0.3
0.2
0.1
0
2
3
4
5
6
7
8
9
10
11
12
13
JANUARY

Figure 8.

APPENDIX VIII

The Occurrence of Bisulfite-Aldehyde Addition Products in Fog- and Cloudwater

J. W. MUNGER, D. J. JACOB and M. R. HOFFMANN*
Environmental Engineering Science, Mail Code 138–78, California Institute of Technology, Pasadena, CA 91125, U.S.A.

(Received: 24 October 1983; in revised form: 7 February 1984)

Abstract. Elevated concentrations of S(IV) and formaldehyde were observed in fog- and cloudwater at sites in California. The highest concentrations (up to 3 m*M* S(IV) and 0.7 m*M* CH_2O) were measured at Bakersfield, during a prolonged period of repeated fog. In Bakersfield [S(IV)] generally exceeded [CH_2O], while in the Los Angeles area the reverse was observed. The lowest concentrations of both species were observed at marine and high altitude sites away from local emissions. Equilibrium computations indicate that high concentrations of S(IV) cannot be achieved without the formation of S(IV)–RCHO adducts.

Key words. Formaldehyde, sulfur (IV), sulfonic acids, sulfur oxidation, air pollution, fogwater chemistry.

1. Introduction

Formaldehyde and other aldehydes are ubiquitous in the atmosphere, especially in urban areas. Formaldehyde concentrations in three phases at sites ranging from remote to polluted are listed in Table I. In Los Angeles, Grosjean (1982) found other aldehydes at concentrations comparable to formaldehyde. Aerosol-phase concentrations are less than 1% of the gas-phase concentrations at all sites listed in Table I. Rainwater concentrations convert to air concentrations of 0.017 to 0.174 $\mu g\, m^{-3}$ in clouds with liquid water content ranging from 0.1 to 1.0 $g\, m^{-3}$. Again this value is much less than typical gas-phase concentrations.

Aldehydes are emitted directly from combustion sources, while photochemical oxidation of hydrocarbons is a source of secondary aldehydes (Table II). Oxidation of naturally-occurring CH_4 by $HO^{\cdot}$ leads to a background CH_2O level of 0.5–2 ppb (0.6–2.5 $\mu g\, m^{-3}$) (NRC, 1981). In urban areas, photochemical oxidation of alkanes and alkenes produce a variety of aldehydes. Because emissions of reactive hydrocarbons generally exceed direct aldehyde emissions, secondary pathways are the dominant sources of aldehydes in most urban atmospheres. Cleveland *et al.* (1977) report that diurnal patterns of CH_2O concentrations in New Jersey follow O_3 more closely than CO, suggesting a photochemical source for much of the formaldehyde.

Destruction of aldehydes occurs via photolysis and reaction with oxidants (Table III).

* To whom correspondence should be addressed.

Table I. Atmospheric formaldehyde concentrations at selected sites

Site	n	Range ($\mu g\ m^{-3}$)	Mean ($\mu g\ m^{-3}$)	Reference
Gas phase				
Los Angeles, CA, 1980	36	2.4–48	25	Grosjean, 1982
Claremont, CA, 1980	65	3.6–58	30	Grosjean, 1982
New Jersey, summer 1974[a]	4	4.6–7.9	–	Cleveland *et al.*, 1977
Deuselbach, West Germany, 1975–76	–	4–27	12.7	Klippel and Warneck, 1980
Enewetak, South Pacific, 1979	–	–	0.5	Zafirou *et al.*, 1980
Aerosol				
Claremont, 1980	14	0–0.26	0.081	Grosjean, 1982
Mainz, West Germany, 1976	8	–	0.063	Klippel and Warneck, 1980
Deuselbach, 1975–76		–	0.04	Klippel and Warneck, 1980
Ireland, 1975–77 (clean air)	16		0.005	Klippel and Warneck, 1980
Rainwater				
		$\mu g L^{-1}$	$\mu g L^{-1}$	
Mainz, 1976	38	–	174	Klippel and Warneck, 1980
Deuselbach, 1974–76	19	–	141	Klippel and Warneck, 1980
Ireland, 1975–76	16	–	142	Klippel and Warneck, 1980
Enewetak, 1979	6	6–11	7.9	Zafirou *et al.*, 1980
Ireland, 1977 (clean air)	5	–	111	Klippel and Warneck, 1978

[a] Medians of 25-hour averages at 4 sites.

Table II. Summary of reactions involved in the formation of aldehydes from hydrocarbon precursors[a]

No.	Reaction	Reference
(1)	$HO^{\cdot} + CH_4 \rightarrow H_2O + CH_3^{\cdot}$	NRC, 1981
(2)	$CH_3^{\cdot} + O_2 (+ N_2 \text{ or } O_2) \rightarrow CH_3O_2^{\cdot} (+ N_2 \text{ or } O_2)$	NRC, 1981
(3)	$CH_3O_2^{\cdot} + NO \rightarrow CH_3O^{\cdot} + NO_2$	NRC, 1981
(4a)	$2CH_3O_2^{\cdot} \rightarrow 2CH_3O^{\cdot} + O_2$	NRC, 1981
(4b)	$2CH_3O_2^{\cdot} \rightarrow CH_3OH + CH_2O + O_2$	NRC, 1981
(5)	$CH_3O^{\cdot} + O_2 \rightarrow CH_2O + HO_2^{\cdot}$	NRC, 1981
(6a)	$RCH_2CH_3 + HO^{\cdot} \rightarrow RCH_2\dot{C}H_2 + H_2O$	Demerjian *et al.*, 1974
(6b)	$RCH_2CH_3 + HO^{\cdot} \rightarrow R\dot{C}HCH_3 + H_2O$	Demerjian *et al.*, 1974
(7)	$RCH_2\dot{C}H_2$ *or* $R\dot{C}HCH_3$ + (NO, O_2, $h\nu$, or $HO^{\cdot}$) $\rightarrow$ CH_2O, CH_3CHO, RCHO, etc.	Demerjian *et al.*, 1974
(8)	$RCH=CHR' + HO^{\cdot} + (NO, O_2) \rightarrow RCHO + R'CHO + (NO_2)$	Niki *et al.*, 1978
(9)	$2RCH=CH_2 + 2O_3 \rightarrow RCHO + RCHO_2 + CH_2O + CH_2O_2$	NRC, 1981
(10)	$RCHO_2$ *or* CH_2O_2 + (NO or SO_2) $\rightarrow$ RCHO *or* CH_2O + (NO_2 or SO_3)	NRC, 1981

[a] Only major products are shown.

Table III. Summary of reactions involved in aldehyde destruction[a]

No.	Reaction	Reference
(11a)	$RCHO + h\nu \rightarrow R^{\cdot} + HCO^{\cdot}$	Calvert and Pitts, 1966
(11b)	$\rightarrow RH + CO$	
(12)	$R^{\cdot} + O_2 + M \rightarrow RO_2^{\cdot} + M$	Calvert and Pitts, 1966
(13)	$HCO^{\cdot} + O_2 \rightarrow HO_2^{\cdot} + CO$	Calvert and Pitts, 1966
(14)	$HO^{\cdot} + CH_2O \rightarrow H_2O + HCO^{\cdot}$	Smith, 1978
(15)	$HO^{\cdot} + HCO^{\cdot} \rightarrow H_2O + CO$	Smith, 1978
(16)	$NO_3^{\cdot} + CH_2O \rightarrow HNO_3 + HCO^{\cdot}$	NRC, 1981
(17)	$HO_2^{\cdot} + CH_2O \rightleftharpoons {}^{\cdot}O_2CH_2OH$	Su *et al.*, 1979
(18)	${}^{\cdot}O_2CH_2OH + HO_2^{\cdot} \rightarrow HO_2CH_2OH + O_2$	Su *et al.*, 1979
(19)	$HO_2CH_2OH + h\nu \rightarrow HCOOH + H_2O$	Su *et al.*, 1979
(20)	$2\ {}^{\cdot}O_2CH_2OH \rightarrow 2\ OCH_2OH + O_2$	NRC, 1981
(21)	$OCH_2OH + O_2 \rightarrow HCOOH + HO_2^{\cdot}$	NRC, 1981

[a] Only major products are shown.

Photolysis of CH_2O initially forms CO and H_2, and is a source for $HO_2^{\cdot}$ (Calvert, 1980). The most important oxidants for aldehydes are $HO^{\cdot}$, $HO_2^{\cdot}$, and, at night, $NO_3^{\cdot}$. Primary products are CO, HCOOH, and additional $HO_2^{\cdot}$. Nitric acid can be formed by $NO_3^{\cdot}$ attack on aldehydes. The concentration of aldehydes in the atmosphere is thus determined by a dynamic balance between production and destruction.

In the aqueous phase, aldehydes hydrolyze via reactions (22) and (23) to form gem-diols

$$RCHO_{(g)} \overset{H_A}{\rightleftharpoons} RCHO_{(aq)}\ , \tag{22}$$

$$RCHO_{(aq)} + H_2O \overset{K_H}{\rightleftharpoons} RCH(OH)_2\ : \tag{23}$$

The combined Henry's law and hydrolysis constant, H_A, is 6.3×10^3 for CH_2O (Ledbury and Blair, 1925). The hydrolysis constant alone, K_H, is 2530, 1.2, and 1.2 for CH_2O, CH_3CHO, and C_2H_5CHO, respectively (Buschmann *et al.*, 1980). In the hydrated form, aldehydes are less sensitive to photodecomposition (NRC, 1981). Because of glycol formation and limited insolation, fog and clouds may provide ideal environments for the accumulation of aldehydes.

Aldehydes also form hydroxyalkylsulfonic acids in aqueous solutiun by addition of S(IV) to aldehyde (Bell and Evans, 1966; Boyce and Hoffmann, 1984):

$$SO_{2(g)} \overset{H_S}{\rightleftharpoons} SO_{2(aq)} \tag{24}$$

$$SO_{2(aq)} \overset{K_{a_1}}{\rightleftharpoons} H^+ + HSO_3^- \tag{25}$$

$$HSO_3^- \overset{K_{a_2}}{\rightleftharpoons} H^+ + SO_3^{2-} \tag{26}$$

$$HSO_3^- + RCHO_{(aq)} \underset{k_{-1}}{\overset{k_1}{\rightleftharpoons}} RCHOHSO_3^- \tag{27}$$

$$SO_3^{2-} + RCHO_{(aq)} \underset{k_{-2}}{\overset{k_2}{\rightleftharpoons}} {}^-O_3SRCHO^- \quad (28)$$

The addition product with formaldehyde, hydroxymethanesulfonate (HMSA) undergoes acid base equilibria shown in reactions (29) and (30):

$$HO_3SCH_2OH \overset{K_1}{\rightleftharpoons} HO_3SCH_2O^- + H^+ \quad (29)$$

$$HO_3SCH_2O^- \overset{K_2}{\rightleftharpoons} {}^-O_3SCH_2O^- + H^+ \quad (30)$$

HO_3SCH_2OH is a strong acid (Roberts *et al.*, 1971); pK_2 is 10.2 (Sørensen and Andersen 1970). At pH values found in fogs and clouds, HMSA will be in the monovalent form. Reactions (24)–(28) are an additional source of acidity in the droplet because they lead to a supersaturation with respect to S(IV) and a concomitant increase in H^+ from reactions (25) and (26). Oxidation of S(IV) to S(VI) in the presence of strong oxidants or metal catalysts via reaction (31) is a competing sink for S(IV) and an alternate pathway for the production of acidity:

$$HSO_3^- \xrightarrow{\text{oxidants}} H^+ + SO_4^{2-} \quad (31)$$

In a well-buffered, open system, reactions (27), (28), and (31) are independent of one another. If the system is not open with respect to $SO_{2(g)}$, however, (27), (28), and (31) will be in direct competition for a limited amount of S(IV).

Formation of HMSA has been suggested as a possible explanation for excess CH_2O concentrations in aerosol (Klippel and Warneck, 1980; Grosjean, 1982), and the apparent stability of S(IV) in aerosol (Izatt *et al.*, 1978). Richards *et al.* (1983) suggest that HMSA formation inhibits S(IV) oxidation by H_2O_2, but Jacob and Hoffmann (1983) predict that both reactions should proceed in parallel. Because the sources of aledehydes and their precursors are so widespread, the formation of bisulfite-aldehyde adducts could be an important reaction in atmospheric water droplets wherever SO_2 is present. In this paper we present findings of elevated CH_2O and S(IV) concentrations in fog- and cloud-water and discuss these results in light of thermodynamic and kinetic considerations.

2. Methods

As part of a study of fogwater chemistry in Southern California (Waldman *et al.*, 1982; Munger *et al.*, 1983), S(IV) and CH_2O concentrations were routinely measured. Aliquots were removed from the samples immediately after collection and preserved. Formaldehyde was preserved as 3,5-diacetyl-1,4-dihydrolutidine (DDL) (Nash, 1953; Reitz, 1980). The absorbance of the DDL was measured at 412 nm on a Beckman Acta III spectrometer. Beginning in December 1982, I_2 was added to oxidize S(IV) in the samples and eliminate its interference (Smith and Erhardt, 1975). Only for samples with an appreciable excess of S(IV) over CH_2O would this interference be a problem. Standards were made using both CH_2O and $NaCH_2OHSO_3$; with added I_2, both CH_2O sources gave an equivalent response.

Sulfur(IV) in the fog samples was preserved as the formaldehyde adduct by addition of excess CH_2O (Dasgupta *et al.*, 1980; Fortune and Dellinger, 1982) and measured by a colorimetric method using 5,5′,dithio-bis(2-nitrobenzoic acid) (DTNB) under mildly alkaline conditions (Humphrey *et al.*, 1970). The samples collected at Henninger Flats during May and June 1983 were preserved by addition of EDTA and phosphate buffer at pH 7; the two methods were equally efficacious. Absorbance of the colored product was measured at 412 nm on Beckman Acta III spectrophotometer. The standard curve for both Na_2SO_3 and $NaCH_2OHSO_3$ was linear up to 250 μM; the response to $NaCH_2OHSO_3$ was 90 to 100% of the response to Na_2SO_3. The coexistence of CH_2O and S(IV) in samples complicates their analysis. Any analytical procedure used must dissociate the adduct to ensure complete recovery of both species.

Fogwater was collected at several sites in the Los Angeles Basin (Pasadena, Lennox, and Upland), at points along the California coast (Pt Reyes, San Nicholas Island, and Del Mar), and at Bakersfield (Kern County) in the San Joaquin Valley. Stratus clouds were sampled above Pasadena at Henninger Flats (elev. 800 m) and Mt Wilson (elev. 1800 m). Stratus clouds intercept Henninger Flats when the marine layer is moderately deep; clouds at Mt Wilson are associated with an even deeper mixed layer. Stratus clouds were sampled from an airplane over the Los Angeles basin in May 1982 (see Richards *et al.* for details). These samples included plume-impacted clouds and clouds over the ocean.

Bakersfield is heavily impacted by emissions from tertiary oil recovery and refining operations (Table IV, Kern County). In addition, agricultural activity in the San Joaquin valley is a source of particulate matter (CARB, 1982) and ammonia. During the sampling period SO_2 levels up to 80 ppb were observed in Bakersfield (CARB, unpublished data). In Los Angeles (Table IV, South Coast Air Basin), SO_2 emissions from petroleum refining, power production, and other industrial fuel combustion processes are comparable to those in Kern County, but emissions of hydrocarbons are greater due to the high density of mobile sources. As a result, the hydrocarbon to SO_2 mass emission ratio is much greater in the South Coast Air Basin than in Kern County. The South Coast Air Basin also has significantly higher NO_x emissions than Kern County, and O_3 levels are higher.

3. Results

The median and range of S(IV) and CH_2O liquid concentrations are presented in Table V. The highest concentrations of S(IV) were observed at the Bakersfield site during an

Table IV. Emissions of SO_2, NO_x, and reactive hydrocarbons in airsheds surrounding the sampling sites

Airshed	SO_2 (10^3 kg day^{-1})	NO_x (10^3 kg day^{-1})	RHC (10^3 kg day^{-1})	Area (km^2)
South Coast Basin	240	1123	1375	16,930
Kern County	170	171	427	14,460

Source: CARB (1982).

Table V. Concentrations of S(IV) and CH_2O in fog- and cloudwater samples collected in California

Samples series	S(IV) (μM)			CH_2O (μM)		
	Range	Median	*n*	Range	Median	*n*
Urban fog						
Los Angeles, 1981–82	15–196	90	13	93–322[a]	189	15
Southern California Coast, 1983	8–279	48	10	53–256	73	13
Bakersfield, 1983	45–2980	517	88	53–709	170	83
Marine fog						
Point Reyes	3.5–10	5	23	0.57–18[a]	3.1	22
San Nicholas Island, 1982	9–18	12	5	6.6–24	17	5
Stratus clouds						
Henninger Flats, 1982	7–60	13	35	34–132[a]	65	35
Henninger Flats, 1983	1–94	8	64	12–173	50	65
Mt Wilson	2–16	3	9	1.8–14[a]	2.4	9
Los Angeles Basin, 1982	5–365	29	11	11–142[a]	70	11

[a] I_2 was not added to prevent interference by S(IV). Some CH_2O values may be underestimated if [S(IV)] was high relative to $[CH_2O]$.

extended stagnation episode in which fog formed almost every night for three weeks. Sulfur(IV) generally exceeded formaldehyde in these samples, especially when concentrations were highest. At sites in Los Angeles, CH_2O levels were comparable to those in Bakersfield, but S(IV) levels were lower. At coastal sites and at higher elevations (Mt Wilson), concentrations of both CH_2O and S(IV) were low and roughly equimolar. At San Nicholas Island, elevated acidity, nitrate, sulfate, and trace metal concentrations suggest that this site was influenced by anthropogenic emissions; concentrations of S(IV) and CH_2O were higher there than at Pt Reyes. Point Conception and the Santa Barbara Channel, major offshore oil exploration and production areas, were directly upwind of San Nicholas Island during the sampling period. Concentrations in the low-level clouds overlapped those found in ground-level fog in Los Angeles, but were still much higher than at Mt Wilson. The highest cloudwater concentrations were found near emission sources.

The concentrations of S(IV) and CH_2O per unit volume of air (Table VI) were calculated from the measured concentrations in the liquid phase and the liquid water content (LWC). The LWC was measured as mass on an open-faced paper filter or calculated from the collected sample volume. A sampling rate of 5 m^3 min^{-1} and a collection efficiency of 60% (Jacob *et al.*, 1984) were assumed to convert volume collected to LWC. Although the aqueous concentrations of CH_2O per volume of air are less than the gas-phase concentrations typical of urban atmospheres, they generally exceed those previously reported for aerosol (see Table I). This confirms previous findings that the gas phase is the major pool of aldehyde (Klippel and Warneck, 1980; Grosjean, 1982).

Table VI. Concentrations of S(IV) and CH_2O on an air volume basis in fog- and cloudwater samples collected in California

Sample series	S(IV) (ng m^{-3})			CH_2O (ng m^{-3})		
	Range	Average	*n*	Range	Average	*n*
Urban fog						
Southern California coast, 1983	42–725	283	9	195–1140	459	12
Bakersfield, 1983	160–9000	1980	82	45–3800	650	78
Marine fog						
Point Reyes, 1982	11–46	29	24	0.2–26	13	24
San Nicholas Island, 1982	13–26	18	4	29–40	27	4
Stratus clouds						
Henninger Flats, 1982	42–1630	144	38	142–4800	504	37
Henninger Flats, 1983	2–170	84	64	20–476	151	65
Mt Wilson, 1982	10–53	14	9	8–42	13	9
Los Angeles Basin, May 1982	75–3500	–	11	133–1440	–	11

4. Discussion

The S(IV) and CH_2O equilibria are described by the expressions given in Table VII. Other carbonyl compounds that form bisulfite adducts, such as acetaldehyde, propanal, *n*-butanal, *n*-pentanal, benzaldehyde, and acrolein (Bordwell, 1963; Grosjean, 1982) and some transition metals that may form complexes with S(IV) (Eatough and Hansen, 1983) are undoubtedly present in fog- and cloudwater. The presence of these adducts and

Table VII. Equilibria and thermodynamic data

No.	Equilibrium expression	$K_{eq\,298}$ (M atm^{-1} or M^{-1})	ΔH_{298} (kcal mol^{-1})	Reference
(32)	$[SO_2 \cdot H_2O] = H_S P_{SO_2(g)}$	1.245	−6.247	Sillén and Martell, 1964
(33)	$[HSO_3^-] = K_{a1} \dfrac{[SO_2 \cdot H_2O]}{[H^+]}$	1.29×10^{-2}	−4.161	Sillén and Martell, 1964
(34)	$SO_3^{2-} = K_{a2} \dfrac{[HSO_3^-]}{[H^+]}$	6.014×10^{-8}	−2.23	Sillén and Martell, 1964
(35)[b]	$[CH_2O_l] = H_F^* P_{CH_2O(g)}$	6.3×10^3	−12.85	Ledbury and Blair, 1925
(36)	$[CH_2O_{aq}] = \dfrac{[CH_2(OH)_2]}{K_H}$	2.53×10^3	−8.0	Buschmann *et al.*, 1980; Bell, 1966
(37)	$[CH_2OHSO_3^-] = K_F[HSO_3^-]\,[CH_2O_{(l)}]$	10^5	−12.3[a]	Dasgupta *et al.*, 1981

[a] No data for HMSA are available; the ΔH for formation of benzaldehyde-bisulfite adduct (Stewart and Donnally, 1932) is used here.

[b] $CH_2O_l = CH_2O_{aq} + CH_2(OH)_2$.

complexes would contribute to the total S(IV) concentration. Sulfur(IV) concentrations in excess of that predicted from the formaldehyde-bisulfite equilibrium would suggest the presence of other adduct-forming species. We found that trace-metal concentrations were generally insufficient to contribute substantially to the total S(IV), but Grosjean and Wright (1983) report the presence of higher aldehydes in Los Angeles cloud- and fogwater at concentrations comparable to formaldehyde. Because higher aldehydes were not measured in this study, discussion will be limited to the formation of the S(IV)–CH_2O adduct, HMSA.

The appropriate mass balance relationships for the S(IV)–CH_2O equilibria are given below:

$$[S(IV)]_T = [SO_2 \cdot H_2O] + [HSO_3^-] + [SO_3^{2-}] + [CH_2OHSO_3^-] \quad (38)$$

$$[CH_2O]_T = [CH_2O_{(l)}] + [CH_2OHSO_3^-] \quad (39)$$

Substituting the equilibrium expressions of Table VII into the mass balance equations, (38) and (39), followed by rearrangement yields:

$$[S(IV)]_T = H_S P_{SO_2} \left\{1 + \frac{K_{a1}}{[H^+]} \left(1 + K_F H_F^* P_{CH_2O} + \frac{K_{a2}}{[H^+]}\right)\right\} \quad (40)$$

$$[CH_2O]_T = H_F^* P_{CH_2O} \left(1 + K_F H_S \frac{K_{a1}}{[H^+]} P_{SO_2}\right) \quad (41)$$

Equations (40) and (41) show that the concentration of S(IV) and CH_2O vary inversely with pH. Because the enthalpies of reactions (32), (33), (34), (35), and (36) are negative, adduct formation will be enhanced at lower temperature. Equations (40) and (41) (Figures 1 and 2) indicate that high concentrations of S(IV) and CH_2O can exist in solution via adduct formation. Concentrations would be much lower if no adduct was formed.

Because other reactions may compete for the reactants, formation of bisulfite-aldehyde adducts is kinetically controlled. Boyce and Hoffmann (1984) report the following rate expression for the formation of HMSA via reactions (22)–(30).

$$\frac{d[HMSA]}{dt} = H_S H_F^* P_{SO_2} P_{CH_2O} \frac{1}{(1 + K_H)} \left(\frac{k_1 K_{a1}}{H^+} + \frac{k_2 K_{a1} K_{a2}}{[H^+]^2}\right) \quad (42)$$

where $k_1 = 7.9 \times 10^2\ M^{-1}\ s^{-1}$ and $k_2 = 2.48 \times 10^7\ M^{-1}\ s^{-1}$. The activation energies for k_1 and k_2 are 5.9 and 4.8 kcal $mole^{-1}$, respectively. The negative temperature dependence for the acid-base and Henry's law equilibria dominate the positive temperature dependence of the kinetic constants; consequently the reaction rate increases with decreasing temperature. At CH_2O partial pressure of 5 ppb and SO_2 partial pressure of 20 ppb the formation rates at pH 3 are 0.20 at 0°C and 0.09 $\mu M\ h^{-1}$ at 10°C. The rates increase to 1530 and 680 $\mu M\ h^{-1}$ at pH for 0°C and 10°C, respectively. The dissociation reaction is

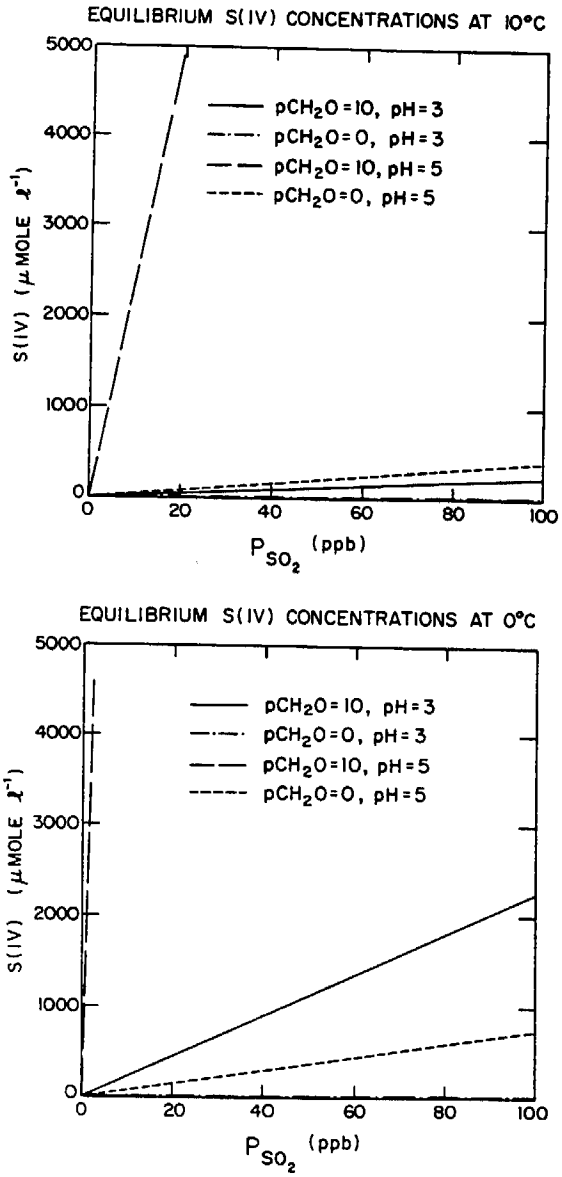

Fig. 1. Equilibrium concentrations of S(IV) with and without CH_2O present for two temperatures and two pH values. 10°C (A) is typical of Los Angeles area fog- and cloudwater; 0°C (B) is typical of Bakersfield fog. 10 ppb is an upper limit for 24-hour average CH_2O concentrations (NRC, 1982).

slower than the formation reaction by a factor of 10^5, so HMSA will not readily break down. Because the time scale for changes in ambient gas concentrations and fog formation and dissipation is much shorter than the reaction time for HMSA formation and

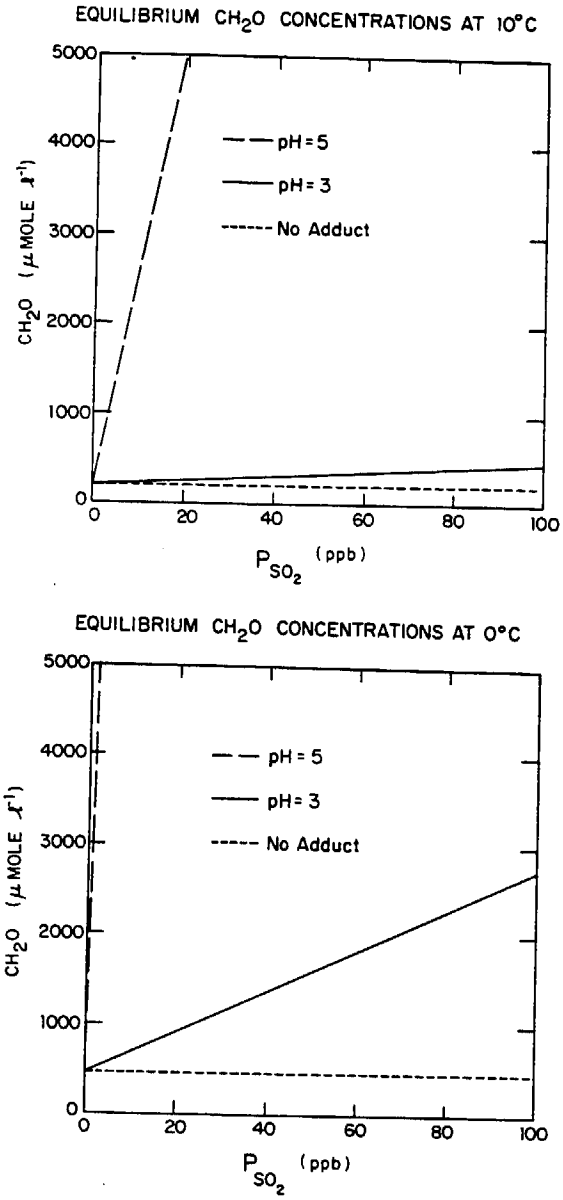

Fig. 2. Concentrations of CH_2O in equilibrium with 10 ppb CH_2O in the gas phase with and without adduct formation for two temperatures and two pH values. 10°C (A) is typical of Los Angeles area fog- and cloudwater; 0°C (B) is typical of Bakersfield fog. 10 ppb is an upper limit for 24-hour average CH_2O concentrations (NRC, 1982).

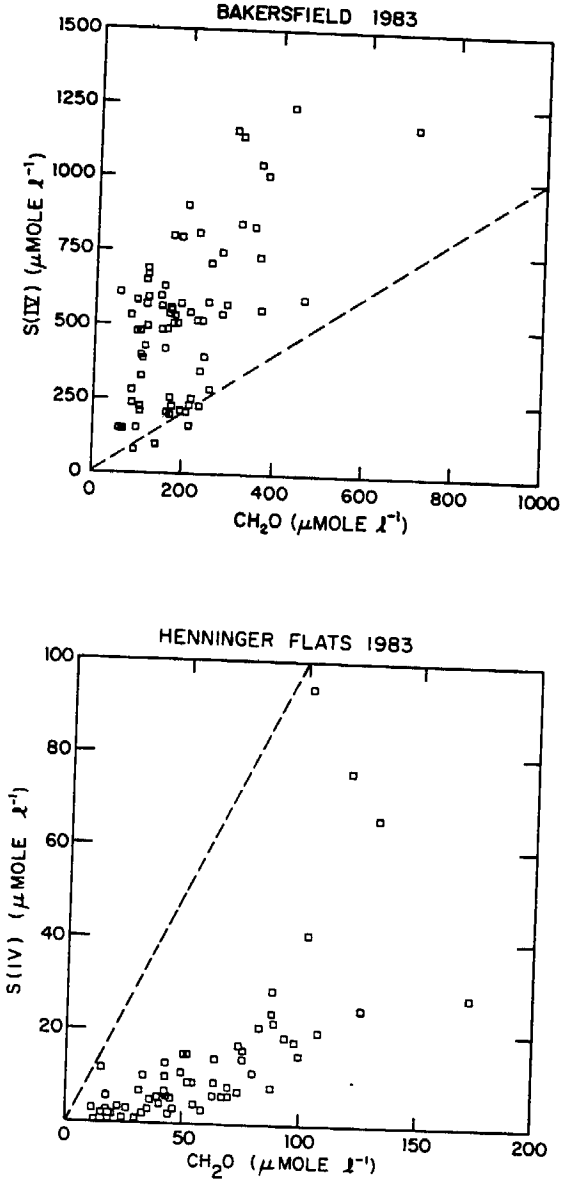

Fig. 3. S(IV) *vs.* CH_2O in fog- and cloudwater. Bakersfield (A), Los Angeles area stratus clouds (B). The line indicates equal concentrations of S(IV) and CH_2O.

dissociation at low pH, S(IV) and aldehyde concentrations may be out of equilibrium. Furthermore, S(IV) oxidation reactions, which are more rapid (McArdle and Hoffmann, 1983; Hoffmann and Boyce, 1983), may diminish the amount of substrate available for adduct formation. Once formed, however, bisulfite-aldehyde adducts would be stable towards oxidants, explaining the coexistence of S(IV) and H_2O_2 reported by Richards *et al.* (1983).

The presence of high concentrations of S(IV) and CH_2O at the onset of fog suggests that HMSA must be present in the condensation nuclei. Adducts present upon fog or cloud dissipation would likely remain as aquated aerosol and provide condensation nuclei for subsequent fogs. In addition, adducts could form in haze aerosol and in fresh plumes containing high concentrations of SO_2 and primary aldehyde. Appreciable concentrations of S(IV) and CH_2O could build up during prolonged cycles of fog and haze such as occur in many parts of Southern California.

The most favorable conditions for S(IV)–aldehyde adduct formation were found at Bakersfield, where temperatures were near 0°C, SO_2 concentrations were high, and fogwater pH was in the range 3–6 (Jacob *et al.*, 1984). Furthermore, the near-stagnant air mass associated with wintertime fog episodes in the San Joaquin Valley (Reible *et al.*, 1983) could lead to a sufficiently long residence time for the formation of appreciable adduct concentrations. In fogs and clouds investigated in the Los Angeles area, temperatures were higher (near 10°C) and pH values were mostly in the range 2–4 (Munger *et al.*, 1983; Hering and Blumenthal, 1983; Richards *et al.*, 1983). Partial pressures of SO_2 were generally lower than in Bakersfield (South Coast Air Quality Management District, unpublished data; Richards *et al.*, 1983), but gas-phase formaldehyde was probably greater because of the higher oxidant levels and abundant hydrocarbon emissions. Sulfur(IV) concentrations were lower in Los Angeles than in Bakersfield; CH_2O concentrations were comparable in the ground-level fog and slightly lower in the stratus samples. Sites more distant from local emissions had the lowest concentrations of all, but both species were measurable. The presence of nearly equimolar concentrations of S(IV) and CH_2O at Point Reyes, San Nicholas Island, and Mt Wilson suggests that S(IV) stabilization by adduct formation during long-distance transport may be an important consideration.

Sulfur(IV) and CH_2O concentrations in Bakersfield fogwater and in Los Angeles area cloudwater are compared in Figure 3. Sulfur(IV) exceeded CH_2O at Bakersfield. The individual concentrations of each S(IV) species in (38) can be calculated from pH, temperature, partial pressures, and the equilibria in Table VII. Excess S(IV) is calculated as the difference between measured S(IV) and the calculated free S(IV) (the first three terms on the right of (38)). This difference consists of HMSA and other adducts, and accounts for most of the measured S(IV) (Figure 4). The excess S(IV) increased with CH_2O concentration. Because S(IV) concentrations were higher than the corresponding CH_2O concentrations and free S(IV) was negligible, adducts with higher aldehydes were probably present as well. The presence of acetic and higher carboxylic acids, which are the products of gas-phase aldehyde destruction (Table III), in fogwater samples (J. W. Munger, unpublished results) suggests that higher aldehydes were present in the Bakersfield fogwater as well. In the stratus cloudwater samples from Los Angeles, only those collected

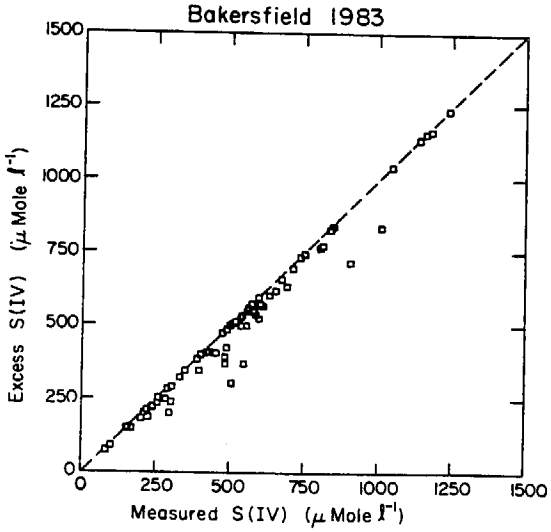

Fig. 4. "Excess" S(IV) *vs.* measured S(IV) in Bakersfield fogwater samples. "Excess" S(IV) is the difference between measured S(IV) and "free" S(IV) (see text). The dashed line indicates equal values for excess and measured S(IV) (i.e., no free S(IV)).

in plumes with high SO_2 concentrations had S(IV) higher than CH_2O. The remainder of the samples had more CH_2O than S(IV). The latter situation would arise if SO_2 concentrations were insufficient to saturate all the available aldehyde, or if adduct formation were very slow.

The stability of the S(IV) and CH_2O in fogwater is indicated by results illustrated in Figure 5. After a month of storage at 4°C without preservatives, appreciable concentrations of both species remain in samples from Bakersfield, often at concentrations near their original value. However, it is apparent that S(IV) undergoes the greatest depletion. In the aged samples S(IV) is nearly equal to or slightly less than CH_2O. Aldehydes, S(IV), and hydroxyalkylsulfonic acids in fog and cloud droplets may oxidize more rapidly when exposed to the atmosphere. Chameides and Davis (1983) report that CH_2O is oxidized to formic acid by $OH^{\cdot}$ in solution. We observe HCOOH in our fogwater samples, but we have no evidence to determine whether it is formed by gas- or liquid-phase reactions. Preliminary work in this laboratory suggests that HMSA is oxidized by aqueous-phase $OH^{\cdot}$. The addition of H_2O_2 and Fe(II), which form $OH^{\cdot}_{(aq)}$ via reaction (42), rapidly destroys HMSA.

$$Fe(II) + H_2O_2 \longrightarrow Fe(III) + {}^{\cdot}OH + {}^{-}OH \qquad (42)$$

5. Summary and Conclusion

The finding of appreciable levels of S(IV) and CH_2O in nearly all fogwater samples

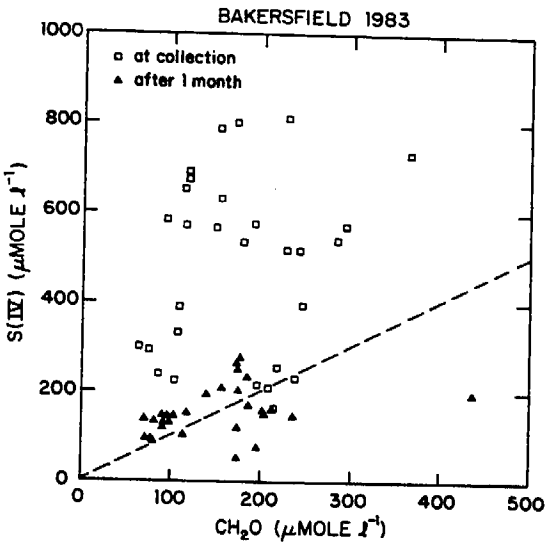

Fig. 5. S(IV) *vs.* CH_2O in Bakersfield samples at the time of collection and after one month of storage at 4°C without preservatives. The line indicates equal concentrations of S(IV) and CH_2O.

examined suggests that the formation of S(IV) aldehyde adducts is an important reaction in atmospheric water droplets. The presence of CH_2O and other aldehydes could lead to the uptake of relatively high concentrations of S(IV) into cloud and fog droplets and aquated aerosol by stabilizing reduced sulfur species. Acidity is produced via adduct formation. Because the formation and dissociation of S(IV) aldehyde adducts are slow at low pH, competition with S(IV) oxidation for substrate may limit adduct formation. The extreme slowness of the adduct dissociation rate is likely to preclude equilibrium in aged air masses (i.e., adduct concentration may exceed that supported by ambient concentrations of SO_2 and CH_2O). These data indicate that aldehyde–S(IV) adduct formation is important in S(IV) chemistry. Bisulfite-aldehyde adducts are likely to form whenever irradiated mixtures of SO_2 and hydrocarbons contact liquid water. The equilibria and kinetics of S(IV)–aldehyde adduct formation should be applied to models of sulfur uptake, transport, and transformation.

Acknowledgements

This research was supported by the California Air Resources Board (Contract A2-048-32). We thank the CARB, the South Coast Air Quality Management District, the Los Angeles County Fire Department Forestry Division, the United States Navy, the National Park Service, and the Mt. Wilson Observatories for logistical support and the use of field facilities. We also thank J. Waldman and S. Boyce for their contributions to the success of this project.

References

Bell, R. P., 1966, The reversible hydration of carbonyl compounds, in V. Gold (ed.), *Advances in Physical Organic Chemistry*, vol. 4, Academic Press, London, pp. 1–29.

Bell, R. P., Evans, F. R. S., and Evans, P. G., 1966, Kinetics of the dehydration of methylene glycol in aqueous solution, *Proc. Roy. Soc. A.* **291**, 297–323.

Bordwell, F. G., 1963, *Organic Chemistry*, Macmillan, New York.

Boyce, S. D. and Hoffmann, M. R., 1984. Kinetics and mechanism of the formation of hydroxymethanesulfonic acid at low pH, *J. Phys. Chem.*, in press.

Buschmann, H. J., Fulderner, H. H., and Knoche, W., 1980, The reversible hydration of carbonyl compounds in aqueous solution. Part I, the ketol gem-diol equilibrium, *Ber. Bunsenges Phys. Chem.* **84**, 41–44.

California Air Resources Board (CARB), 1982, *Emissions Inventory*, California Air Resources Board, Sacramento, California.

Calvert, J. G. and Pitts, J. N., Jr., 1966, *Photochemistry*, John Wiley, New York.

Calvert, J. G., 1980, The homogeneous chemistry of formaldehyde generation and destruction within the atmosphere, in *Proceedings of the NATO Advanced Study Institute on Atmospheric Ozone: Its Variation and Human Influences*, Federal Aviation Administration, Washington, D.C., pp. 153–190.

Chameides, W. L. and Davis, D. D., 1983, Aqueous-phase source of formic acid in clouds, *Nature* **304**, 427–429.

Cleveland, W. S., Graedel, T. E., and Kleiner, B., 1977, Urban formaldehyde: Observed correlation with source emissions and photochemistry, *Atmos. Environ.* **11**, 357–360.

Dasgupta, P. K., DeCesare, K., and Ullrey, J. C., 1980, Determination of atmospheric sulfur dioxide without tetrachlormercurate(II) and the mechanism of the Schiff Reactions, *Anal. Chem.* **52**, 1912–1922.

Demerjian, K. L., Kerr, J. A., and Calvert, J. G., 1974, The mechanism of photochemical smog formation, *Adv. Environ. Sci. Technol.* **4**, 1–262.

Eatough, D. J. and Hansen, L. D., 1983, Organic and inorganic S(IV) compounds in airborne particulate matter, *Adv. Environ. Sci. Technol.* **12**, 221–268.

Fortune, C. R. and Dellinger, B., 1982, Stabilization and analysis of S(IV) aerosols in environmental samples, *Environ. Sci. Tech.* **16**, 62–66.

Grosjean, D., 1982, Formaldehyde and other carbonyls in Los Angeles ambient air, *Environ. Sci. Technol.* **16**, 254–262.

Grosjean, D. and Wright, B., 1983, Carbonyls in urban fog, ice fog, cloudwater and rainwater, *Atmos. Environ.* **17**, 2093–2096.

Hering, S. V. and Blumenthal, D. L., 1983, Field comparison of fog/cloud water collectors: Preliminary results, *Proc. APCA Specialty Conference on the Meteorology of Acid Deposition*, Hartford, Connecticut, October, 1983.

Hoffmann, M. R. and Boyce, S. D., 1983, Catalytic autoxidation of aqueous sulfur dioxide in relationship to atmospheric systems, *Adv. Environ. Sci. Technol.* **12**, 149–189.

Humphrey, R. E., Ward, M. H., and Hinze, W., 1970, Spectrophotometric determination of sulfite with 4,4-Dithiopyridine and 5,5'-Dithiobis(2-Nitrobenzoic acid), *Anal. Chem.* **42**, 698–702.

Izatt, R. M., Eatough, D. J., Lee, M. L., Major, T., Richter, B. E., Hansen, L. D., Meisenheimer, R. G., and Fischer, J. W., 1978, The formation of inorganic and organic S(IV) species in aerosols, *Proc. 4th Joint Conf. on Sensing Environ. Pollutants*, Amer. Chem. Soc., Washington, D.C., pp. 821–824.

Jacob, D. J. and Hoffmann, M. R., 1983, A dynamic model for the production of H^+, NO_3^-, and SO_4^{2-} in urban fog, *J. Geophys. Res.* **88C**, 6611–6621.

Jacob, D. J., Wang, R-F. T., and Flagan, R. C., 1984, Fogwater collector design and characterization, *Environ. Sci. Technol.*, in press.

Jacob, D. J., Waldman, J. M., Munger, J. W., and Hoffmann, M. R., 1984, A field investigation of physical and chemical mechanisms affecting pollutant concentrations in fog droplets, *Tellus*, in press.

Klippel, W. and Warneck, P., 1978, Formaldehyde in rain water and on the atmospheric aerosol, *Geophys. Res. Lett.* **5**, 177–179.

Klippel, W. and Warneck, 1980, The formaldehyde content of the atmospheric aerosol, *Atmos. Environ.* **14**, 809–818.

Ledbury, W. and Blair, E. W., 1925, The partial formaldehyde vapour pressure of aqueous solutions of formaldehyde. Part II. *J. Am. Chem. Soc.* **127**, 2832–2839.

McArdle, J. V. and Hoffmann, M. R., 1983, Kinetics and mechanism of the oxidation of aquated sulfur dioxide by hydrogen peroxide at low pH, *J. Phys. Chem.* **87**, 5425–5429.

Munger, J. W., Jacob, D. J., Waldman, J. M., and Hoffmann, M. R., 1983, Fogwater chemistry in an urban atmosphere, *J. Geophys. Res.* **88**, 5109–5121.

Nash, T., 1953, The colorimetric estimation of formaldehyde by means of the Hantzsch Reaction, *Biochem. J.* **55**, 416–421.

National Research Council (NRC), 1981, *Formaldehyde and Other Aldehydes*, National Academy Press, Washington, D.C.

Niki, H., Maker, P. D., Savage, C. M., and Breitenbach, L. P., 1978, Mechanism for hydroxyl radical initiated oxidation of olefin-nitric oxide mixtures in parts per million concentrations, *J. Phys. Chem.* **82**, 135–137.

Reible, D. D., Shair, F. H., Smith, T. B., Lehrman, D. E., 1983, The origin and fates of air pollutants in California's San Joaquin Valley I. Winter. *Atmos. Environ.*, in press.

Reitz, E. B., 1980, The stabilization of small concentrations of formaldehyde in aqueous solutions, *Anal. Lett.* **13**, 1073–1084.

Richards, L. W., Anderson, J. A., Blumenthal, D. L., McDonald, J. A., Kok, G. L., and Lazrus, A. L., 1983, Hydrogen peroxide and sulfur(IV) in Los Angeles cloudwater, *Atmos. Environ.* **17**, 911–914.

Roberts, J. D., Stewart, R., and Caserio, M. C., 1971, *Organic Chemistry*, W.A. Benjamin, Menlo Park, CA.

Sillén, G. L. and Martell, A. E., 1964, *Stability Constants of Metal-ion Complexes*, special publication No. 17, Chemical Society, London.

Smith, R. H., 1978, Rate constant and activation energy for the gaseous reaction between hydroxyl and formaldehyde, *Int. J. Chem. Kinet.* **10**, 519–528.

Smith, R. V. and Erhardt, P. W., 1975, Nash determination for formaldehyde in the presence of bisulfite, *Anal. Chem.* **47**, 2462–2454.

Sørensen, P. E. and Andersen, V. S., 1970, The formaldehyde-hydrogen sulphite system in alkaline aqueous solution. Kinetics, mechanisms, and equilibria, *Acta Chem. Scand.* **24**, 1301–1306.

Su, F., Calvert, J. G., and Shaw, J. H., 1979, Mechanism of the photooxidation of gaseous formaldehyde, *J. Phys. Chem.* **83**, 3185–3191.

Stewart, T. D. and Donnally, L. H., 1932, The aldehyde bisulfite compounds II. The effect of varying hydrogen ion and of varying temperature upon the equilibrium between benzaldehyde and bisulfite ion, *J. Am. Chem. Soc.* **54**, 3555–3558.

Waldman, J. M., Munger, J. W., Jacob, D. J., Flagan, R. C., Morgan, J. J., and Hoffmann, M. R., 1982, Chemical composition of acid fog., *Science* **218**, 677–680.

Zafiriou, O. C., Alford, J., Herrera, M., Peltzer, E. T., and Gagosian, R. B., 1980, Formaldehyde in remote marine air and rain: Flux measurements and estimates, *Geophys. Res. Lett.* **5**, 341–344.

APPENDIX IX

CHEMICAL CHARACTERIZATION OF STRATUS CLOUDWATER AND ITS ROLE AS A VECTOR FOR POLLUTANT DEPOSITION IN A LOS ANGELES PINE FOREST

by

J. M. Waldman, J. W. Munger, D. J. Jacob, and M. R. Hoffmann
Department of Environmental Engineering Science
W. M. Keck Engineering Laboratories (138-78)
California Institute of Technology
Pasadena, CA 91125

Submitted to: Water Air Soil Pollution

ABSTRACT

Highly concentrated, acidic stratus cloudwater was monitored as it intercepted a Los Angeles pine forest. Observed pH values ranged from 2.06 to 3.87 for over 100 samples collected on 1982 and 1983 with a median value below pH 3. The ratio of nitrate/sulfate in cloudwater samples was nearly 2; rainwater at the same site had a ratio of approximately 1. The solute mass loading in the cloudwater was of the same magnitude as for aerosol samples collected before, during and after fog episodes. The nitrate/sulfate ratio of the dry aerosol was lower than in the cloudwater; the additional nitrate is believed to be derived from dissolution of gaseous nitric acid.

Wet deposition of pollutant solutes at Henninger Flats in 1982-83 was comparable to the value for Pasadena in 1978-79, even though the water flux was more than twice as great. The solute deposition with several light, spring rains (summing to $\sim$1% of annual rainfall) was a disproportionate fraction of the annual total: H^+, NO_3^- and SO_4^{2-} were $\sim$20% or more. Based on a reasonable estimate of fog precipitation, deposition of sulfate, nitrate and free acidity due to intercepting stratus clouds may be of comparable magnitude as that due to the incident rainfall at Henninger Flats.

Cloudwater which had deposited on local pine needles was collected and found to be as or more concentrated and with acidity comparable to suspended cloudwater. Injury to sensitive plant tissue has been observed when prolonged exposure to this severe kind of micro-environment has been imposed.

CHEMICAL CHARACTERIZATION OF STRATUS CLOUDWATER AND ITS ROLE AS A VECTOR FOR POLLUTANT DEPOSITION IN A LOS ANGELES PINE FOREST

INTRODUCTION

In addition to the orographic enhancement of precipitation at mountain sites, wind-driven cloud droplet capture can lead to greater pollutant deposition relative to the surrounding lowlands. Fog (sometimes called "occult") precipitation has been determined to be an important hydrological input (e.g. Kerfoot, 1968) to some ecosystems. Also, measurements of cloudwater composition have shown it to have higher aqueous-phase concentrations compared to precipitation at the same locale (Mrose, 1966; Okita, 1968; Munger et al., 1983a). These two factors combine to suggest the potential for significant pollutant deposition in mountain forests impacted by frequent cloud interception. Often omitted from mass-balance calculations or regional monitoring, this pathway may represent an important component of the total deposition, especially in urban-impacted environments.

Enhanced precipitation in coastal and mountain forests has been reported for collectors located beneath trees exposed to fog-laden wind. In an early study of fog interception in Japan (Hori, 1953), an average fogwater deposition rate of 0.5 mm hr^{-1} was reported for a coastal forest. Oberlander (1956) measured between 45 and 1500 mm of fog-derived precipitation in less than 6 weeks on the San Francisco pennisula with collectors beneath 5 trees. A number of investigators have employed artificial foliar collectors (Schlesinger and Reiners, 1974) or screen "fog-catchers" (Nagel, 1956; Ekern, 1964; Vogelmann et al., 1968; Vogelmann, 1973; Azevedo and Morgan, 1974) to measure the enhancement of water catchment by horizontal interception. The fog-derived catchment in these studies represented a significant fraction of the total precipitation - up to several times the measured incident rainfall. Because of their relatively small interception cross-sections, it is likely that these collectors underestimated the flux of fog precipitation induced by the actual forest canopy.

Fog and cloudwater have been investigated previously for several purposes: a) to characterize the aqueous composition of the droplets and to ascertain the source of its constituents (Houghton, 1955; Lazrus et al., 1970;

Munger et al., 1983b); b) to calculate rates of aqueous oxidation processes in cloud and fog systems (Hegg and Hobbs, 1981, 1982; Daum et al., 1983; Jacob et al., 1984a); and, c) to quantify the flux of intercepted cloudwater solute to deposition surfaces (Dollard et al., 1983; Lovett, 1984). The highest concentrations of pollutant species in fog and cloudwater have been reported for urban atmospheres (Mrose, 1966; Waldman et al., 1982; Brewer et al., 1983). Our objectives were to characterize the chemical composition of stratus cloudwater and to address the potential that droplet capture may play as a vector for pollutant deposition in an urban-impacted forest.

Cloud droplet capture, precipitation and dry mechanisms represent parallel pathways by which ambient pollutants are deposited (see Figure 1). Following the incorporation of aerosol and gaseous species into cloud and fog droplets, the chief mechanisms for deposition are impaction and sedimentation -- both strongly enhanced by increased particle inertia. Damage to sensitive plant tissue and other elements of the biota caused by direct exposure to aqueous acids has been the subject of field and laboratory research (e.g. Tukey, 1970; Evans, 1982). Cases of specific injury and growth retardation have been reported for several plant and tree species in exposure studies (Wood and Bormann, 1974; Haines et al., 1980; Scherbatskoy and Klein, 1983) with threshold for effects generally noted in the range of pH = 2 to 3.

In this paper, we report the composition of rainwater, cloudwater, aerosol and bulk deposition samples collected in a Los Angeles pine forest. These are used to compare the relative contributions by these various deposition pathways. Interception of stratus clouds on the mountain slope is evaluated for its role in enhancing pollutant deposition. Our findings are presented as a measure of regional pollution not generally monitored. We also report the composition of deposited cloudwater collected from pine needles. These data are discussed in terms of chemical interactions occurring at the vegetative surfaces.

EXPERIMENTAL

During the spring and early summer, stratus clouds are common along coastal California, caused by an inversion-capped marine layer (DeMarrais et al., 1965). The inversion base forms the top of the stratus deck; on 80% of summer mornings, the inversion base measured at Los Angeles International Airport is between 100 and 1000 m (Keith, 1980). When drawn inland by an onshore pressure gradient, these low-lying clouds can intercept coastal mountain slopes, leading to frequent, dense fog at elevated sites from late evening through morning hours.

Our monitoring site was located at Henninger Flats, a campground and tree nursery located at approximately 780 m MSL on the southern slope of Mount Wilson, 25 km northeast of Los Angeles. The site is shown in elevation and plan views in Figure 2. During the past 14 years, May and June have had an average of 12 days of dense fog observed at 8 a.m. (L.A. County Fire Department Forestry Division Meteorological Records). Both 1982 and 1983 were above this average, with 31 and 18 morning observations of fog during each May/June period, respectively. Cloudwater was collected on 8 dates in June 1982 and 15 times in May and June 1983. On two of the sampling dates in May 1983, the cloud top was below Henninger Flats, and cloudwater was collected 100-200 m downslope. On most dates sampling proceeded from the time cloud had intercepted the site to the time the fog had dissipated. When fog occurred at the site, it was usually preceded by a relatively strong onshore breeze. The local, nighttime drainage flows inherent to the topography also affected the fog characteristics. Note: we refer to the phenomenon as fog at the site; however on the regional scale, the mountain slope was intercepted by stratus clouds. Hence, we refer to our samples as cloud-, rather than fogwater.

The Caltech rotating arm collector (RAC) was used to collect cloudwater (Jacob et al., 1984b). The axis of the rotating arm was 1.4 m above ground level. The collector was situated approximately 100 m back from the ridge in an open area which sloped gently up from the ridge. Model-scale calibration of the collector design using solid particles has indicated the size-cut to be approximately 20 micron (Jacob et al., 1984b). Little research has been conducted to determine size-composition relationships of the cloud droplet spectrum experimentally. During June 1983, we participated in an intercalibration of fogwater collectors at Henninger Flats (Hering and

Blumenthal, 1984). For four collectors, each with different designs, size cutoffs and sampling rates, the chemical composition for samples collected simultaneously were statistically undistinguishable. On several occasions, a second RAC was operated at the site. Good agreement was found for the composition of samples taken side-by-side as well as at opposite corners of the nursery (Hering and Blumenthal, 1984).

Sampling intervals generally ranged from 30 to 60 minutes; sample volumes were usually 10-30 mL, although some as small as 1 mL were analyzed. Immediately after each sample was collected, pH was measured using a Radiometer PHM 82 meter and combination electrode; standard calibration of the electrode was performed at pH 7, 4 and 1.68. Within 30 minutes, aliquots were preserved from each sample for analysis of major ions, formaldehyde, S(IV) and trace metals. For major ion determinations, aliquots were necessarily diluted from 5 to 50:1. Further details of fogwater sample handling and analytical protocols are presented elsewhere (Munger et al., 1983b).

In addition to cloudwater collection as in 1982, supplementary measurements were made during the spring of 1983. Aerosol loadings were determined using 47 mm Teflon (Zefluor - 1 μm pore size) filters. Samples were collected in parallel open-face and cyclone separator precut (3 μm) configurations. The concentrations of water soluble ions were determined following aqueous extraction with a reciprocating shaker for 1 hour. Subsequent extractions of the filters produced satisfactory blanks.

Liquid water contents of the fog were determined during the 1983 events using four different methods: a) calculation from RAC collection rates; b) mass-difference using paper filters on hi-vol samplers; c) attenuation of infrared (9.4 μm) light using a CO_2 laser transmissometer (CO_2LT) and, d) integration of droplet size spectra for d_p = 2 to 47 μm (Particle Measuring Systems, Inc., Model CSASP-100-HV). The results of these methods are compared in a subsequent section.

Rainwater was monitored at the nursery from November 1982 to June 1983 using a wet-only collector (Liljestrand, 1980). Bulk deposition samples were collected between May and July 1983 in open, plastic buckets. On several occasions droplets which had accumulated on pine needles by cloud droplet capture were collected. This was done by manual, drop-by-drop removal. Select trees were routinely sampled. Further details of these deposition measurements are given in separate sections.

RESULTS AND DISCUSSION

The objective of this field study was to determine the relative contributions of various pathways to the overall pollutant deposition. For clarity, a summary of cloudwater data is first presented and discussed. Several specific fog episodes are described. A brief comparison of liquid water content measurements is given to highlight their uncertainty and temporal variability. Wet and bulk deposition data sets are then presented. This is followed by calculations of the magnitude of fog-derived precipitation and the associated pollutant deposition based on the cloudwater composition reported. With these, a comparison of the pollutant fluxes associated with precipitation (incident and occult) and dry deposition pathways is given. Finally, the composition of intercepted cloudwater is presented with a discussion of its potential interactions with foliar surfaces.

Cloudwater Composition

Summaries of 1982 and 1983 results for cloudwater and rainwater chemical analyses are presented in Table 1. For comparison, values are also given for the 1978-79 volume-weighted mean rainwater concentrations at Pasadena and Mount Wilson (225 and 1800 m MSL, respectively). For most species, the median values for Henninger Flats cloudwater concentrations are 20 or more times those for local rainwater. The ionic balances for cloudwater data are presented in Figure 3. In general, the results for both years are satisfactory with 1983 data giving very consistent balance. Ionic balance was calculated as a check on both the analytical precision and the completeness of the ion determinations. We are confident that all the major ionic species have been measured. There were a few cases in the 1982 data set which gave poor ionic balance, these for samples with the highest concentration (and the smallest sample volumes). For the highest sample concentrations, the worse imbalances are equivalent to no worse than a tenth of a pH unit: e.g. at pH = 2.2, d(pH)= $\pm$0.1 gives d[H] of $\pm$1500 μeq l^{-1}. The better agreement for 1983 data was in part due to our experience working with ambient samples of such high concentrations. The protocol for the latter year included a single, quantitative dilution of each sample (5 to 50:1) rather than separate ones for the individual ion determinations, as for the 1982 samples.

Hydrogen, ammonium, nitrate and sulfate dominate the ionic composition in most samples; this is consistent with previous observations for Los Angeles aerosol (Hidy et al., 1980). For most samples, non-seasalt sulfate was greater that 90% of measured sulfate, even assuming sodium was solely of marine origin. The nitrate-to-sulfate equivalent ratio for these samples was nearly two (Figure 4). This ratio is similar to fogwater samples collected in the Los Angeles basin (cf. Munger et al., 1983b) but markedly different from local rainwater with ratios less than one (Table 1) . The basinwide nitrate-to-sulfate equivalent ratio for emissions has been reported between 2 and 3 (California Air Resources Board, 1979; 1982).

The pH in fog at Henninger Flats was consistently lower, compared to Bakersfield, a site with similar ionic concentations of acidic anions but greater ammonium emissions (cf. Jacob et al., 1984a). The low pH values (Figure 5) in the cloudwater occur in a rather narrow range: pH = 2 to 4. The degree that ambient acids have been neutralized in the atmosphere following their formation is indicated by the equivalent ratio of $[H^+]$ versus $[NO_3^-]$ plus $[SO_4^{2-}]$. The ratio for Los Angeles stratus cloudwater was 0.5 or below (Figure 6). That is, in the cloudwater up to half of the acidic anions were associated with free acidity and not neutralized.

Even for the cases with low aqueous concentrations, sufficient ambient bases were either not available or scavenged to fully neutralize the acid. Gaseous ammonia and ammonium salts are readily scavenged by cloud droplets (Jacob and Hoffmann, 1983). Basinwide, ammonia emissions are one-third of the SO_2 and NO_x sum on an equivalent basis; however, major source areas are located in San Bernadino and eastern Los Angeles counties (Russell et al., 1983). For some of the highly concentrated cloudwater samples, $[Ca^{2+}]$ and $[Mg^{2+}]$ were 10-50% lower for filtered (0.2 μm pore size) compared to non-filtered aliquots. Na^+, K^+ and NH_4^+ showed little difference between aliquots. This suggests that some of these ions in the condensation nuclei do not rapidly or completely dissolve. That is, there may be a kinetic or thermodynamic limitation to the neutralization of cloudwater by the dissolution of an alkaline fraction.

Ambient aerosol was sampled prior, during and following fog episodes in 1983 (Table 2). Solute loadings in the aerosol phase were comparable to cloudwater solute loading (Figure 7). Values for aerosol $[H^+]$ loading were calculated from the ionic charge deficiency. Acidity titrations would have

been preferable, however these were not performed. Several points are suggested from the results of this calculation. First, aquation of the particulate solute to a liquid water content of 0.1 g m^{-3} resulted in predicted pH values that are strikingly similar to the measured cloudwater pH. These results argue qualitatively that the aerosol were of comparable acidity (moles m^{-3} of air) as found in the cloudwater. In contrast, Daum et al. (1983) found precursor aerosol to contain much less acidity than the cloudwater in the eastern United States for samples collected aloft. Second, the nitrate-to-sulfate ratios of the afternoon and late evening (non-fog) intervals were usually less than 0.5, while the concentrations of nitrate generally showed a large increase immediately following the onset of fog, wherein the ratio increased to between 1 and 2. Shown in Figure 7, the aerosol nitrate increased (6/11) while all the other measured species remained unchanged.

We believe that the additional nitrate was due, in large part at least, to the scavenging of nitric acid vapor by the droplets. Nitric acid ranging from 0.03 to 0.59 μeq m^{-3} has been reported for the Los Angeles atmosphere (Spicer et al., 1982), so the measured increase was within the expected, ambient range. For nighttime conditions at Henninger Flats (T = 10^{o}C and R.H.$\geq$ 90%), the equilibrium dissociation constant for NH_4NO_3 is below 1.5×10^{-4} (μeq m^{-3})^2 (Russell et al., 1983). In the aerosol and cloudwater samples, NH_4^+/SO_4^{2-} ratios were always less than one, plus alkaline loading was also relatively low. In these cases all the ammonia would be scavenged by acidic sulfate aerosol, and nitric acid would remain unneutralized and in the gas phase. Aerosol nitrate measured in the pre-fog samples would necessarily be due to the volatilization of Cl_2(g) from NaCl and $CaCl_2$ salts. Upon the activation of haze aerosol into droplets with LWC $\geq 10^{-2}$ g m^{-3}, gaseous nitric acid would be scavenged with nearly 100% efficiency because of its high Henry's law constant.

The lower, pre-fog concentrations measured could have also been caused by nitrate loss due to nitric acid volatization from the Teflon filter medium (Appel et al., 1979). As the sample intervals were short and the temperatures were decreasing, we believe this would not be a significant artifact. A third possiblity exists by which the noted increase in nitrate concentrations were due to its advection to the site. However, there was no increase of measured gaseous pollutants (SO_2, NO_x and O_3) at the onset of the

fog (Southern California Edison, Rosemead, CA, unpublished data).

Prior to the fog, most of the particulate mass, especially sulfate, was measured in the fine (<3 μm) size class. In the late evening, aerosol solute was virtually all in the fine class since the coarser particles settle rapidly when daytime wind speeds and turbulence subside. In the fog, very little of the particulate solute remained in the fine size class. A larger portion of the sulfate than nitrate was found in the fine-size fraction of the aerosol samples. This is noted even for in-fog aerosol samples. As both nitrate and sulfate salts are highly hygroscopic, the difference in the portion which was activated into droplets would be a function of particle size. These data support previous findings that nitrate is associated with larger-sized aerosol (Appel et al., 1978).

The concentration of S(IV) in cloudwater samples ranged between 1 and 100 μmol l^{-1}, with the two season median value of 10. Formaldehyde was measured at concentrations 4 to 10 times greater than for sulfite (median value = 56 μmol l^{-1}). $SO_2(g)$ levels were measured to be generally 0.01 ppm or below (Southern California Edison, Rosemead, CA, unpublished data, 1983). The formation of sulfite-aldehyde adducts in solution can lead to total aqueous S(IV) concentrations which exceed the Henry's law solubility for $SO_2(g)$ at low pH (Munger et al., 1984). However, the low ambient loading of aqueous and gaseous S(IV) indicate that aqueous sulfate production was not an important process affecting droplet acidities.

The median values of trace metals (Fe, Pb, Mn, Ni and Cu) aqueous concentrations for approximately 100 cloudwater samples collected both years were 520, 260, 46, 36, and 20 ppb, respectively. For iron and lead, the values range from ∿100 ppb to several ppm. While iron may be derived in part from soil dust, source apportionment calculations based on Friedlander (1973) indicated approximately 40% of Fe was from fly ash. Similarly, the lead content in cloudwater was virtually all from vehicular exhaust. As a whole, the trace metal concentrations and loadings in the cloud samples reflect the transport of industrial pollutants to elevated sites relatively far downwind from their sources.

Examples of Specific Events

Cloudwater samples during intervals preceded by rainfall had somewhat

lower solute mass loading. The chemical compositions of sequential samples from 6/12,13 & 17/82 are shown in Figure 8a. Sampling on the latter date (6/17/82) occurred during an interval of dense fog between periods of measurable drizzle. Dilution - note the higher liquid water content (LWC) - was partially responsible for the lower concentrations (Figure 8b). The amount of solute per volume of air (Figure 8c) was down by a factor of 2 to 5 from previous days' samples. The LWC indicated in these figures were calculated from the RAC collection rate. As described in the next section, this calculation is subject to a bias which is a function of the size spectrum. It is also possible that, along with the drizzle, marine layer deepening led to some dilution of the regional air mass. Not withstanding these effects, precipitation scavenging was likely responsible for the depleting of airborne pollutants. As shown in a subsequent section, the deposition of pollutants accompanying spring drizzle can be disproportionate to the water flux, sufficient to cause this depletion.

The nitrate-to-sulfate ratios for post-rain cloudwater samples were the lowest of the data set. This would be caused by mechanisms which remove nitrate more effectively than sulfate: e.g. sulfate aerosol are less preferentially scavenged by activation (based on size considerations). Also, nitric acid dissolution in droplets is virtually complete, while SO_2 remains largely in the gas-phase, despite sulfite-aldehyde adduct formation.

Concentration, LWC, and solute mass loading profiles for cloudwater samples from 6/11 & 12/83 are shown in Figure 9. During the first several hours of sampling, as the marine air permeated the forest, the fog was patchy, and the LWC fluctuated dramatically with several brief periods of local clearing at the site. For these first few intervals, the RAC-derived value (estimated from the entire sampling period) would underestimate LWC for the fog actually collected. In addition, during periods of complete dissipation at the onset of this fog episode, deactivation of cloud droplets would remove cloudwater solute mass to the haze size range. Thus, a representative indication of the solute loading is difficult to get for locally patchy fogs.

After 7:00, fog became more stable, and the solute mass per volume air is seen to have remained fairly constant for the next 4-5 hours. Following 13:00, a drop in solute loading occurred, coincident with the onset of measurable drizzle. The total solute deposited in the drizzle (see subsequent section) was of similar order as pollutant loading up to the cloud

tops (i.e. several meq m^{-2}). In addition, the mass median diameter for the cloud droplets was lower ($\sim$20 versus $\sim$25 μm) following the onset of precipitation. Hudson and Rogers (1984) has shown that the larger droplets are produced from larger nuclei. The depletion of larger droplets, taken with the magnitude of solute deposition measured in the drizzle, lends further support to the interpretation that the drop in cloudwater solute loading was caused by its depletion by precipitation scavenging.

The fog continued through that day, with drizzle ceasing in the afternoon. In the evening samples (6/12/83), the solute loading was elevated to the pre-drizzle (6/11/83) level. Nighttime lowering of the inversion probably contributed to some of this increase. The fog continued with fairly uniform density; sampling was interrupted by the operator. The solute loading remained steady at this level during the interval; note that fluctuations in concentration mirrored LWC (Figure 9). The samples became progressively less acidic, and equimolar Na^+ and Cl^- increases occurred. This latter point suggests air of greater marine character was advected to the site. The roles of vertical mixing and ventilation of stratus/fog are major uncertainities. Until we can better quantify the transport conponent of cloud/fog dynamics at a given sampling site, our explanations remain speculative. The drop in cloudwater solute loading for the final sample probably reflects mass removed from the fog-size range by deactivation as it was clearing.

Liquid Water Content Measurements at Henninger Flats

Four separate methods were used to make liquid water content (LWC) determinations in the spring 1983. LWC is not a parameter reliably determined, but it is a crucial one in the interpretation of droplet chemistry. Our experiences at Henninger Flats emphasized the difficulty in ascertaining absolute values (cf. Hering and Blumenthal, 1984). Each of the four methods has biases inherent to it. Given below are brief descriptions of the methods and some possible causes of the disparity between their results.

The RAC collects droplets by inertial impaction. Jacob et al. (1984b) indicated the size cut for this collector to be $\sim$20 micron diameter. This is in the range of the mass median diameter (MMD) of the fog droplets as given in the literature (Garland, 1971) and indicated by droplet spectra measured at the site. Since the cut-off size and MMD are of similar

magnitude, the fraction of collected mass may change significantly if the size spectrum shifts greatly. Also, the conversion of RAC collection rate to LWC is based on a theoretical air sampling rate (5 m^3 min^{-1}), which has not been experimently verified. Jacob et al. (1984b) reported that the theoretical RAC collection rate gave LWC which were approximately 60% the value determined by total filter measurements made in radiation fog. RAC-derived LWC data presented in this paper include this empirical correction factor:
e.g.

$$LWC = \frac{\text{sample volume}}{\text{Sample interval x theoretical air volume sampling rate x } 0.6}$$

Total filter devices have been used to give sensitive and reproducible results in stable fogs (Arvin/Calspan Corp., Buffalo, NY, private communication). A known volume of fog-laden air was sampled by a hi-vol collector using paper towels, and LWC was determined by mass-difference. However, there were situations with patchy fog when the relative humidity fluctuated around 100%. During even a short sample interval, appreciable evaporation can occur when the collected moisture is subjected to subsaturated air flowing through the filter. Also, measurements made during periods of drizzle gave erroneously high values, until rain shields were installed.

The CO_2 Laser Transmissometer (CO_2LT) uses the measure of infrared light attenuation to calculate total mass of fog-sized droplets. LWC has been found to be directly proportionate to attentuation over a wide range (Gertler and Steele, 1980). The conversion factor (i.e. Beta $_{(scat@9.4\ \mu m)}$ to LWC) was based on Mie theory and has not been calibrated against an absolute measure. There is a theoretical limitation (Chylek, 1978): for droplets greater than a certain size (d_p > 25 micron for IR wavelength = 9.4 micron), the method underestimates water mass. The CO_2LT was operated at 1.4 m above ground level across a 20 m, folded length (i.e., a parabolic mirror was located 10 m away).

An optical particle counter (OPC) was used to measure droplet size spectra (Particle Measuring Systems - Model CSASP-100-HV) . LWC were estimated by integrating the spectrum which provided particle number concentrations in 15 size classes between 2 and 47 micron. Because the number concentrations are weighted by d_p^3, small errors in size can be amplified to significant discrepancies in integrated mass. Thus, LWC from OPC's are known to vary instument to instrument (Atmospheric Sciences Research Center, SUNY Albany, private communication). The instrument used at Henninger Flats was

calibrated by the manufacturer, but this calibration is not always accurate (Cerni, 1983). While the MMD calculated from the spectra are in reasonable accord with accepted values (Garland, 1971), the LWC calcuated were consistently unrealistic -- several times too high. This factor, compared to the CO_2LT, was between approximately four. When these OPC data were compared to fog condensation nuclei data taken at the same time (Hudson and Rogers, 1984), it appeared that erroneous number concentrations rather than particle sizing were the cause of the high bias. Note: the scalings of CO_2LT, OPC, and RAC-derived Data were, in fact, ad hoc and intend only to give relative and approximate LWC values. We are in the process of calibrating the OPC used at Henninger Flats; until this is done, these LWC are not intended as absolute values.

The CO_2LT and OPC gave finely time-resolved data which disclosed rapid fluctuations of LWC, observed routinely to vary over an order of magnitude within several minutes. Results for three methods are presented in Figure 10. During the intervals of stable fog, the relative results compared fairly well. For patchy fog and drizzle, there was a greater spread, especially for the total filter method (not shown). When the LWC changed so rapidly, time-averaged value showed less accord. We used fitted RAC-derived LWC for calculation of solute loading. This is because it is representative of the exact sampling location and, hence, available for comparison with RAC data at other locations. As shown, it can give consistent agreement with the CO_2LT and OPC (scaled by 1/4) values for most cases.

In June 1982, the only method employed at the site to give a measure of LWC was the RAC collection rate. On three occasions, measurements of height-integrated cloudwater were made from directly below the cloud base near Henninger Flats using Microwave Atmospheric Remote Sensor - MARS (Gary, 1982). These measurements indicated that rapid or significant changes in the total cloud liquid and vapor water did not occur except during cloud burnoff. From the stability aloft indicated by the MARS data, it appears that the rapid fluctuations of LWC at the ground level were the product of mixing and thermal exchange in the vicinity of complex terrain. CCN measured in 1983 showed that the dry character of the cloud air mass sampled at Henninger Flats changed very little during a given fog episode (Hudson and Rogers, 1984). The downslope drainage flows apparently led to mixing of air with lower relative humidity but the same particulate signature. The droplet spectra at Henninger

Flats revealed time evolutions consistent with the physics of droplet activation, growth and deactivation. As shown in Figure 10, during periods of rapid increase (or decrease) in local LWC, number concentration commensurately increased (or decreased) while MMD decreased (or increased). The smaller droplets grow faster; in a period of rapid water accretion, the added mass would chiefly accompany newly activated rather than larger, growing droplets, hence the MMD initially decreases.

Deposition: Measurements and Calculations

i) Storm and Stratus Rain

Rainfall at Henninger Flats was collected and analyzed from November 1982 to June 1983. Monthly averages for the wet deposition are presented in Table 3; the deposition is split between storm (A) and several spring "drizzle" or light rainfall (B) events. The 1982-83 season was above average rainfall -- the wettest on record at Henninger Flats: 1660 mm compared to an average of 670 mm. Pasadena and Mt. Wilson deposition (from 1978-79 data) are presented for comparison. Considering the storm events alone, solute deposition at Henninger Flats was very close to the total for Pasadena, even though total rainfall was over twice as great. Because of the high frequency and water flux per event, the volume-weighted mean concentrations were lower than for Pasadena or Mt. Wilson in the earlier year.

Presented separately in Table 3 are several precipitation events, referred to as "stratus events". These were light rain and drizzle which occurred within a developed marine layer, similar to that which led to stratus cloudiness and fog on mountain slopes, but with more intense deepening. The ionic concentrations of these light and nearly trace rains were dramatically higher than for the storm events, but in a range somewhat less concentrated and acidic than the cloudwater samples. Morgan and Liljestrand (1980) noted similarly higher concentrations in sparser rains they measured in Pasadena. Brewer et al. (1983) reported a similar relationship between fog and "mist" samples at several Los Angeles locations.

The fog -> drizzle -> rain hierarchy of solute concentration reflect, in part, the relationship between droplet size and dilution. The growth of cloud drops to a size with appreciable sedimentation velocity occurs first by

condensation of water vapor for sizes under 50 μm diameter and subsequently by coalescence to mist (> 100 μm) and raindrop (> 300 μm) sizes (Pruppacher and Klett, 1980). The meteorology is a second important factor to consider. Most wintertime storms are associated with weather systems which advect moist, unstable oceanic air with fairly intense convective activity (Keith, 1980). Alternatively, drizzle and fog events usually occur within a developed marine layer constrained by a strong temperature inversion aloft. This limits vertical mixing; thus, stratus cloud droplets form and can have longer residence times (Reible et al., 1983) in a polluted atmosphere. The mean pH values for stratus and storm rainwater are compared to cloudwater samples in Figure 5.

The stratus events led to solute deposition which was disproportionate to the water flux. While accounting for 1.1% of measured rainfall, nearly 20% or more of H^+, NO_3^- and SO_4^{2-} were deposited in less than 16 mm precipitation. Na^+ and Cl^- were not as much enhanced in stratus rainfall. Storms which form over the eastern Pacific Ocean have a relatively stronger sea salt source plus the greater convective activity to transport these coarse particles further inland. The enhancement of H^+ and NO_3^- was greatest and, for NH_4^+ and SO_4^{2-}, it was somewhat less. This suggests that the scavenging of HNO_3 and NH_4HSO_4 are more important components of the acidification of the stratus rainfall, rather than the differences caused by droplet dilution. Finally, the nitrate/sulfate ratio for stratus (1.4) versus storm (0.8) events is a further indication of the meteorological and seasonal variation in NO_x oxidation.

ii) Bulk Deposition

Surrogate surfaces such as flat plates and open containers have been employed in attempts to quantify the ongoing dry depositional flux. These methods remain controversial due to the variability of their results and the uncertainty in extrapolation of specific results to a regional value. However, dry deposition has been acknowledged to contribute a significant, though uncertain, fraction of total pollutant deposition in southern California (Liljestrand, 1980) . Surrogate surface flux at the very least provides a useful qualitative measurement for ambient conditions.

We used bucket containers for several reasons. From intercomparison of surrogate surfaces (Dolske and Gatz,1984; Dasch, 1983), buckets were shown to

give flux values which were sensitive to ambient aerosol sulfate concentrations and as consistent as the other available surrogate surface collectors. Bucket-measured flux were consistently 2 and 5 times greater than for petri dishes and flat plates, respectively (Dolske and Gatz, 1984). Buckets probably have a bias for collecting and retaining the large particles. However, Davidson and Friedlander (1978) have calculated that >70% of sulfate deposition they measured with flat plate surfaces in Los Angeles came from the 10% of aerosol in the largest size fraction, chiefly from sedimentation and turbulent diffusion. Particle impaction would be negligible due to the bucket geometry. Dry deposition of SO_2 and NO_x has been reported to be inconsequential for the plastic buckets (Dasch, 1983).

For our program, bucket collectors provided a relatively large area, minimized resuspension (relative to flat surfaces) and were convenient to use and rinse. Standard 4-gallon, polyethylene buckets (open area = 566 cm^2) were situated at four locations in the vicinity of the nursery site. The containers were placed with the rim at least 1 meter above the ground; three were situated in the open and one was positioned beneath a dense stand of pine trees. The containers were extracted with 100 to 500 mL of H_2O, depending on the exposure duration.

Overall, bulk deposition for intervals with precipitation was significantly greater than for intervals with none (Table 4). The dry-only deposition (i.e. with the measured wet-only values subtracted) was also greater for the intervals which included precipitation. During dry periods, the below-canopy sample had generally lower pollutant deposition. This reduction may be due to the interception of material to the canopy alone, or the suppression of turbulent transport below the canopy as well. It also appeared that some of this material eventually was deposited as throughfall. However, some of the additional cations had likely leached from the pine needles.

iii) Calculation of Fog Precipitation

Fog droplet capture by the forest canopy has been recognized as an important hydrologic input. Hori (1953) conducted extensive research on the mechanisms and efficiency of droplet capture. Lovett (1984) modeled the transfer of water and solute to the forest canopy in fog-laden winds. Compared to the deposition of dry aerosol (Sehmel, 1974), the capture of fog

droplets is quite efficient. The parameters which control the rate of deposition are the wind speed and turbulence, canopy and leaf geometries, and LWC and droplet spectrum of the fog. Lovett calculated water deposition rates varying linearly from 0.2 to 1.2 mm $hour^{-1}$ for canopy-top wind speeds of 2 to 10 m s^{-1}, chiefly by impaction to the upper 3 m of the canopy. Yosida and Kuroiwa (in Hori, 1953) determined an overall average rate of 0.5 mm $hour^{-1}$ for fogwater capture by the forest canopy.

Measurement of this depositional flux was not made during this study. Instead, we assumed a water deposition rate of 0.2 mm hr^{-1} to make the following calculation and provide approximate values of fog-induced fluxes. For cloudwater with a median free acidity of 1150 μeq $liter^{-1}$. This gave an average rate equal to 230 μeq $m^{-2}hr^{-1}$. Also using the median values for 1982 and 1983 data, nitrate and sulfate deposition rates were calculated to be 300 and 170 μeq $m^{-2}hr^{-1}$, respectively. Henninger Flats has a relatively dense, tall canopy. Canopy-top data were not measured, so a conservative rate was used. Fog-induced water flux deposition can vary greatly. It can exceed 0.2 mm hr^{-1} to specific trees (e.g. Oberlander, 1956). The concentration of solutes was greater at time than the values used above, so locally higher acid deposition rates are quite possible. Conversely, for sparsely forested areas and chaparral, the average would be expected to be lower. Dollard et al. (1983) estimated a mean cloud drop flux of 0.07 mm hr^{-1} to shortgrass in Cumbria, U.K., based on micrometeorological techniques in fog.

iv) Comparison of Pollutant Wet Deposition Pathways

It is difficult to generalize about the frequency and duration of cloud interception within the Los Angeles basin. It is subject to spatial and temporal variability as well as year-to-year fluctuation. The presence of marine layer clouds and fog are persistent spring and summer phenomena in coastal southern California (Keith, 1980). From a daily record made by rangers at Henninger Flats from 1971 to 1983 (LA County Fire Department Forestry Bureau, unpublished data), the median number of times fog was observed at 8 a.m. was approximately 30 per year (Range = 8 to 55), with the greatest number during the spring months. During our two years of monitoring, over 120 fog-hours were observed on the 23 days of sampling. Assuming deposition rates as calculated in a previous section plus 150 hours of cloud

interception per year (i.e. 30 events times 5 hours per event), the product gave an annual total of 35 meq H^+ m^{-2}. Similar calculations for NH_4^+, NO_3^-, and SO_4^{2-} yield 17, 45, and 24 meq m^{-2}, respectively; for lead, 8 mg m^{-2} deposition annually is calculated. Though the preceding calculations are based on limited data and rough estimates, they are intended to demonstrate the order of magnitude that cloud droplet processes may contribute to the acidic deposition in this urban-impacted mountain environment. Comparing these with measured precipitation (Table 3), cloud interception could deliver up to half the total wet deposition.

CLOUDWATER INTERACTIONS WITH FOLIAR SURFACES

Part of our motivation to sample cloudwater at Henninger Flats was the observation in the spring 1982 of an unseasonably high number of pine trees which exhibited necrotic needles on 2nd and 3rd year growth (Gubrud, 1982). Normally, needle necrosis is observed in the late summer and early autumn, due to the high gas-phase pollutant levels (particularly ozone) in the Los Angeles basin (Miller et al., 1977).

To better understand the nature of its interaction with plant tissue, during several fog events cloudwater was removed from pine needles where it had naturally deposited. These samples characterize the aqueous micro-environment to which the pine needles were subjected. The chemical composition of these samples --"tree drops" --is presented in Table 5. They were found to be as acidic though often more concentrated than the suspended cloudwater. The higher concentrations may be attributed to one or more of the following mechanisms: a) lower relative humidities below the canopy caused evaporation of deposited cloudwater; b) accumulated dry deposition was dissolved by cloudwater which collects on the plant surfaces; c) cloudwater solution promoted leaching from internal plant tissue; d) a concentrated residue was left by evaporation of prior tree drops. This residue is only removed by rainfall or copious fog "drip".

This accumulation of soil dust and pollutant constituents appears to have caused the highest concentrations for pre-rain and early fog samples (e.g. 6/12/82, 5/31/83, and 6/9/83). Nitrate was 3 to 5 times greater than sulfate for these samples. Futhermore, the sum of nitrate and sulfate were in excess of the sum of H^+ and NH_4^+, with the difference due to neutralization by

the alkaline soil dust. Samples for intervals following rainfall or a long duration of fog had ionic concentrations which were significantly reduced compared to the earlier samples.

The fraction of K^+ in the fog drops was much higher than in any of the fogwater samples. The proportion of Na^+-, Ca^{2+}- and Mg^{2+}-to-NH_4^+ was also higher. This could be explained by the leaching of internal leaf tissue cations by aqueous proton (Tukey et al., 1965). Leaching of K^+, Ca^{2+} and amino acids was reported for birch and spruce foliage exposed to acidic (pH = 4.3 and 2.8) mists (Scherbatskoy and Klein, 1983). They also suggested that the increase in leachate pH compared to the applied mists involved cation exchange process. Hoffman et al. (1980) indicate that proton exchange with cations was negligible as rain penetrated chestnut canopies, for the total acidity of rainwater was conserved during throughfall, with weak acids exchanging for strong acids. This may be the case for moderate acidity, but at higher $[H^+]$ specific leaf injury could occur accompanied or, more likely, caused by proton exchange.

Miller (1982) has proposed that the observed damage at Henninger Flats was due to a possible synergism of the previous summer season's ozone injury and the frequent exposure to acidic solutions deposited in the spring. The interaction of ozone and acidic deposition on vegetation has not been thoroughly studied. Shriner(1978) reported significant reduction in plant dry weight for greenhouse-grown red kidney bean exposed to simulated acid (pH = 4) rain and multiple O_3 exposures. The attack of ozone on cell membranes in leaf tissue could leave sensitive trees more vulerable to the penetration of acidic material into, and the leaching of minerals from, the pine needles by the deposited cloudwater.

Without further research, it is not possible to confirm a direct relationship between the acidic cloudwater deposition and the needle symptoms observed at Henninger Flats. However, similar damage to leave surfaces have been reported in exposure studies (Thomas et al., 1952; Wood and Bormann, 1974; Haines et al., 1980). In simulated acid rain experiments, Haines et al. (1980) found a threshold for leaf damage for most species tested in a pH range 2.5 to 2.0 and for Pinus strobus needles in a pH range 1.0 to 0.5. Wood and Bormann (1974) observed foliar tissue damage at pH 3 for misting of yellow birch seedlings; significant growth decreases occurred when acidic exposure (pH 2.3) was initiated during the germination stage. Thomas et al. (1952)

reported cases in which plant injury was not initially caused by pure H_2SO_4 aerosol--apparently due to its high surface tension--but followed surface wetting by fog.

Cloudwater capture may represent a more severe threat to plant tissue than deposition accompanying rainfall or by dry pathways alone, because it subjects plant surfaces to much higher aqueous concentrations and acidities. Leaf surface wetting may be a critical component of the interaction between foliar membranes and deposited pollutants. For example, surface wetting greatly reduces particle rebound (Chamberlain, 1967). Finally, intercepted cloudwater may provide a propitious environment for S(IV) dissolution and oxidation, leading to the production of acidity directly in contact with vegetative surfaces.

SUMMARY

Highly concentrated, acidic stratus cloudwater was monitored as it intercepted a Los Angeles pine forest. Observed pH values ranged from 2.06 to 3.87 for samples collected on 8 days in June 1982 and 15 days in May/June 1983. The median value was below pH 3 for both seasons' data. The ratio of nitrate/sulfate in cloudwater samples was nearly 2; rainwater at the same site had a ratio of approximately 1. The solute mass loading in the cloudwater was of the same magnitude as for aerosol samples collected before, during and after fog episodes. The nitrate/sulfate ratio of the dry aerosol was lower than in the cloudwater; the additional nitrate is believed to be derived from dissolution of gaseous nitric acid. In addition, a higher fraction of nitrate than sulfate aerosol appears to be scavenged by activation of the cloud droplets.

Wet deposition at Henninger Flats in 1982-83 was comparable to the value for Pasadena in 1978-79, even though the water flux was more than twice as great. The greater frequency and rainfall amount per storm in the recent year is believed to have led to the lower volume-weighted mean concentrations in the Henninger Flats precipitation. The solute deposition with several light, spring rains (summing to approximately 1% of annual rainfall) was a disproportionate fraction of the annual total: H^+, NO_3^- and SO_4^{2-} were 20% or more.

Based on a reasonable estimate of fog precipitation, deposition of

sulfate, nitrate and free acidity due to intercepted stratus clouds may be of comparable magnitude as that due to the incident rainfall at Henninger Flats. Occult precipitation (fog and mist), though not previously considered on the regional scale, appears to be a seasonally important sink for pollutant emissions in the Los Angeles basin.

Cloudwater which had deposited on local pine needles was collected and found to be as or more concentrated and with acidity comparable to suspended cloudwater. Injury to sensitive plant tissue has been observed when prolonged exposure to this severe kind of micro-environment has been imposed.

REFERENCES

Appel, B. R., Kothny, E. L., Hoffer, E. M., Hidy, G. M., and Wesolowski, J. J. (1978) Sulfate and nitrate data from the California Aerosol Characterization Experiment (ACHEX), Environ. Sci. Tech. 12, 418-425.

Appel, B. R., Wall, S. M., Tokiwa, Y., and Haik, M. (1979) Interference effects in sampling particulate nitrate in ambient air, Atmos. Environ. 13, 319-325.

Azevedo, J. and Morgan, D. L. (1974) Fog precipitation in coastal California forests, Ecology 55, 1135-1141.

Brewer, R. L., Ellis, E. C., Gordon, R. J., and Shepard, L. S. (1983) Chemistry of mist and fog from the Los Angeles urban area, Atmos. Environ. 17, 2267-2271.

California Air Resources Board (1982) Emission Inventory: 1979, Emission Inventory Branch,Sacramento, California.

California Air Resources Board (1979) Emission Inventory: 1974, Emission Inventory Branch, Sacramento, CA.

Cerni, T. A. (1983) Determination of the size and concentration of clouds with an FSSP, J. Clim. Appl. Meteor. 22, 1346-1355.

Chamberlain, A. C. (1967) Transport of Lycopodium spores and other small particles to rough surfaces, Proc. R. Soc.A 296, 45-70.

Chylek, K. P. (1978) Extinction and liquid water content of fogs and clouds, J. Atmos. Sci. 35, 296-300.

Dasch, J. M. (1983) A comparison of surrogate surfaces for dry deposition collection, Precipitation Scavenging, Dry Deposition, and Resuspension, Pruppacher, H. R., et al. (ed), Elsevier Science, Amsterdam, pp 883-902.

Daum, P. H., Schwartz, S. E., Newman, L. (1983) Studies of the gas- and aerosol-phase composition is stratiform clouds, Precipitation Scavenging, Dry Deposition, and Resuspension, Pruppacher, H. R., et al. (ed), Elsevier Science, Amsterdam, pp 31-52.

Davidson, C. I. and Friedlander, S. K. (1978) A filtration model for aerosol dry deposition: application to trace metal deposition from the atmosphere, J. Geopys. Res. 83, 2343-2352.

DeMarrais, G. A., Holzworth, G. C., and Hosler, C. R. (1965) Meteorological Summaries Pertinent to Atmospheric Transport and Dispersion over Southern California, U.S. Weather Bureau Tech. Paper No. 54, Washington, DC.

Dollard, G. J., Unsworth, M. H., and Harve, M. J. (1983) Pollutant transfer in upland regions by occult precipitation, Nature 302, 241-243.

Dolske, D. A. and Gatz, D. F. (1984) A field intercomparison of sulfate dry deposition monitoring and measurement methods, in Acid Precipitation, Hicks, B. B.(ed), Buttonword Publisher, Boston.

Ekern, P. C. (1964) Direct interception of cloud water on Lanaihale, Hawaii, Soil Sci. Soc. Am. Proc. 28, 419-421.

Evans, L. S. (1982) Biological effects of acidity in precipitation on vegetation: a review, Environ. Exp. Bot. 22, 155-169.

Friedlander, S. K. (1973) Chemical element balances and identification of air pollution sources, Environ. Sci. Tech. 7, 235-240.

Garland, J. A. (1971) Some fog droplet size distributions obtained by an impactor method, Quart. J. Roy. Meteor. Soc. 97, 483-494.

Gary, B. (1982) Jet Propulsion Lab., Pasadena, CA , private communication.

Gertler, A. W. and Steele, R. L. (1980) Experimental verification of the linear relationship between IR extinction and liquid water content of clouds, J. Appl. Meteor. 19, 1314-1317.

Gubrud, M. (1982) Senior Deputy Ranger, Los Angeles County Fire Department Forestry Division, private communication.

Haines, B., Stefani, M., and Hendrix, F. (1980) Acid rain: threshold of leaf damage in eight plant species from a southern Appalachian forest succession, Water, Air and Soil Pollut. 14, 403-407.

Hegg, D. A. and Hobbs, P. V. (1981) Cloudwater chemistry and the production of sulfates in clouds, Atmos. Environ. 15, 1597-1604.

Hegg, D. A. and Hobbs, P. V. (1982) Measurements of sulfate production in natural clouds, Atmos. Environ. 16, 2663-2668.

Hering, S. V. and Blumenthal, D. L. (1984) Sampler Intercomparison Study, Final Report (Draft) to Coordinating Research Council, Atlanta, GA, March.

Hidy, G. M., Mueller, P. K., Grosjean, D., Appel, B. R., and Wesolowski, J. J. (ed.) (1980) The Character and Origins of Smog Aerosol (ACHEX), John Wiley & Sons, New York.

Hoffman, Jr., W. A., Lindberg, S. E., and Turner, R. R. (1980) Precipitation acidity: the role of forest canopy in acid exchange, J. Environ. Qual. 9, 95-100.

Hori, T., (ed) (1953) Studies on Fog in Relation to Fog-Preventing Forest, Tanne Trading Co., Japan, 399 pp.

Houghton, H. G. (1955) On the chemical composition of fog and cloud water, J. Meteorol. 12, 355-357.

Hudson, J. G. and Rogers, C. F. (1984) Interstitial CCN measurements related to mixing in clouds, pres. at 9th Internat. Cloud Physics Conf. August 21-28, Tallinn, USSR.

Jacob, D. J. and Hoffmann, M. R. (1983) A dynamic model for the production of H^+, NO_3^-, and SO_4^{2-} in urban fog, J. Geophys. Res. 88C, 6611-6621.

Jacob, D. J., Waldman, J. M., Munger, J. W. and Hoffmann, M. R. (1984a) A field investigation of physical and chemical mechanisms affecting pollutant concentrations in fog droplets, Tellus (in press).

Jacob, D. J., Wang, R-F. T., and Flagan, R. C. (1984b) Fogwater collector design and characterization, Environ. Sci. & Technol. (in press).

Keith, R. W. (1980) A Climatological/Air Quality Profile: California South Coast Air Basin, South Coast Air Quality Management District , El Monte, CA, November.

Kerfoot, O. (1968) Mist precipitation on vegetation, For. Abst. 29, 8-20.

Lazrus, A. L., Baynton, H. W., and Lodge, J. P. (1970) Trace constituents in oceanic cloud water and their origin, Tellus 22, 106-113.

Liljestrand, H. M. (1980) Atmospheric Transport of Acidity in Southern California by Wet and Dry Mechanisms, Ph.D. Thesis, California Institute of Technology, Pasadena, CA.

Liljestrand, H. M. and Morgan, J. J. (1981) Spatial variations of acid precipitation in Southern California, Environ. Sci. & Technol. 15, 333-338.

Lovett, G. M. (1984) Rates and mechanisms of cloud water deposition to a subalpine balsam fir forest, Atmos. Environ. 18, 361-371.

Miller, P. (1982) Soil Scientist, Univ. Calif. Riverside, private communication.

Morgan, J. J. and Liljestrand, H. M. (1980) , Measurement and Interpretation of Acid Rainfall in the Los Angeles Basin, W. M. Keck Laboratory of Hydraulics & Water Resources, California Institute of Technology, Pasadena, CA, Report AC-2-80.

Mrose, H. (1966) Measurements of pH, and chemical analyses of rain-, snow-, and fog-water, Tellus 18, 266-270.

Munger, J. W., Jacob, D J. Waldman, J. M., and Hoffmann, M. R. (1983b) Fogwater chemistry in an urban atmosphere, J. Geophys Res. 88C, 5109-5121.

Munger, J. W., Jacob, D. J., and Hoffmann, M. R. (1984) The occurrence of bisulfite-aldehyde addition products in fog- and cloudwater, J. Atmos. Chem. (in press).

Munger, J. W., Waldman, J. M., Jacob, D. J., Hoffmann, M. R. (1983a) Vertical variability and short-term temporal trends in precipitation chemistry, Precipitation Scavenging, Dry Deposition, and Resuspension, Pruppacher, H. R., et al. (ed), Elsevier Science, Amsterdam, pp 275-282.

Nagel, J. F. (1956) Fog precipitation on Table Mountain, Quart. J. Roy. Meteor. Soc. 82, 452-460.

Oberlander, G. T. (1956) Summer fog precipitation on the San Francisco penninsula, Ecology 37, 851-852.

Okita, T. (1968) Concentration of sulfate and other inorganic materials in fog and cloud water and in aerosol, J. Met. Soc. Japan 46, 120-126.

Pruppacher, H. R. and Klett, J. D. (1978) Microphysics of Clouds and Precipitation, Reidel, Amsterdam 714 pp.

Reible, D. D., Shair, F. H., and Aris, R. (1983) A two-layer model of the atmosphere indicating the effects of mixing between the surface layer and the air aloft, Atmos. Environ. 17, 25-33.

Russell, A. G., McRae, G. J. and Cass, G. R. (1983) Mathematical modeling of the formation and transport of ammonium nitrate aerosol, Atmos. Environ. 17, 949-964.

Scherbatskoy, T. and Klein, R. M. (1983) Response of spruce and birch foliage to leaching by acidic mists, J. Environ. Quality 12, 189-195.

Schlesinger, W. H. and Reiners, W. A. (1974) Deposition of water and cations on artificial foliar collectors in fir krummholz of New England mountains, Ecology 55, 378-386.

Schwartz, S. E., Newman, L., Hegg, D. A. and Hobbs, P. V. (1983) Measurements of sulfate production in natural clouds (discussion), Atmos. Environ. 17, 2629-2633.

Sehmel, G. A. (1980) Particle and gas dry deposition: a review, Atmos. Environ. 14, 983-1011.

Shriner, D. S. (1978) Interactions between acidic precipitation and SO_2 or O_3 on plant response, Phytopath News 12, 153.

Spicer, C. W., Howes, J. E., Bishop, T. A., and Arnold, L. H. (1982) Nitric acid measurement methods: an intercomparison, Atmos. Environ. 16, 1487-1500.

Thomas, M. D., Hendricks, R. H., and Hill, G. R. (1952) Some impurities in the air and their effects on plants, in Air Pollution: Proc. of US Tech. Conf., McCabe, L.(ed), Washington, D.C., McGraw-Hill, New York, pp 41-47.

Tukey,Jr., H. B. (1970) The leaching of substances from plants, Ann. Rev. Plant Physiol. 71, 305-324.

Tukey, H. B., Mecklenburg, R. A., and Morgan, J. V. (1965) , Radiation and Isotopes in Soil-Plant Nutrition Studies , Intern. Atom. Energy Agency, Vienna.

Vogelmann, H. W. (1973) Fog precipitation in the cloud forests of eastern Mexico, Bioscience 23, 96-100.

Vogelmann, H. W., Siccama, T., Leedy, D., and Ovitt, D. C. (1968) Precipitation from fog moisture in the Green Mountains of Vermont, Ecology 49, 1205-1207.

Waldman, J. M., Munger, J. W., Jacob, D. J., Flagan, R. C. Morgan, J. J., and Hoffmann, M. R. (1982) Chemical composition of acid fog, Science 218, 677-680.

Wood, T. and Bormann, F. H. (1974) The effects of an artificial acid mist upon the growth of Betula alleghaniensis Britt., Environ. Pollut. 7, 259-267.

FIGURE CAPTIONS

Figure 1. Schematic showing main processes affecting pollutant deposition in a Los Angeles pine forest. Wet deposition is routinely measured; dry mechanisms are more difficult to quantify. Cloud droplet capture has been rarely considered but may be important in mountain and coastal regions.

Figure 2. Profile of southwestern Mount Wilson slope showing location of sampling site. Los Angeles Civic Center is located at 24 km from Pacific Ocean along same profile.

Figure 3. Ionic balances for cloudwater samples of 1982 and 1983; solid line shows 1:1 balance.

Figure 4. Concentrations of nitrate versus sulfate measured in cloudwater samples of 1982 and 1983. Ratios for local rainwater were below one.

Figure 5. Histograph of pH frequency of cloudwater samples (both seasons); volume-weighted average $[H^+]$ for rainfalls are also shown.

Figure 6. Free acidity (i.e. $[H^+]$) versus sum of nitrate and sulfate concentrations measured in cloudwater samples of 1982 and 1983.

Figure 7. Ambient aerosol compositions for June 10-11, 1983 (cf. Table 2). Total and fine ($d_p < 3$ μm) particulate concentrations given are for same sample intervals. Values of "pH" were calculated for $[H^+]$ assuming ionic balance with major ions and LWC = 0.1 g m^{-3}. The latter two sample sets taken after onset of fog at site. The increase in nitrate relative to other constituents is believed to be due to nitric acid scavenging by cloud droplets. Time-weighted cloudwater loading for the same period is also shown.

Figure 8. (a) Concentration, (b) LWC, and (c) solute loading for sequential cloudwater samples on June 12, 13, and 17, 1982. Measurable drizzle occurred prior to sampling on June 17; note the drop in solute loading and the change in scale (a).

FIGURE CAPTIONS (cont.)

Figure 9. Same as Figure 8 for samples on June 11 and 12, 1983. Drizzle started at 12:00 of June 11. Fog continued until 11:00 of June 12 with samples taken intermittently. After drizzle ceased, solute loading in the cloud increased to the level of the former morning and remained steady: fluctuations in concentrations - note the change in scale (a) - were complimentary to those in LWC.

Figure 10. LWC measurement data for June 11, 1983 for three methods: (a) OPC size spectra, (b) CO_2 laser transmissometer, and (c) RAC collection rate. The OPC data has been scaled by a factor of 1/4; the RAC-derived LWC was calculated from a theoretical sampling volume and an empirical correction factor (see discussion).

TABLE 1.

MEDIAN AND RANGE OF CONCENTRATIONS FOR CLOUDWATER SAMPLES
HENNINGER FLATS: 1982 AND 1983

		Cloudwater		Rainwater		
		1982[a]	1983[b]	Site[c]	Pasadena[d]	Mt.Wilson[d]
pH		2.86 2.06-3.65	2.96 2.07-3.87	4.6	4.4	5.0
H^+	μeq l^{-1}	1365 224-8710	1100 135-8510	24	39	10
Na^+		146 5-2465	285 3-6320	14	24	26
K^+		18 1-161	22 3-197	0.9	1.7	1.7
NH_4^+		576 128-3130	582 62-7420	9.2	21	36
Ca^{2+}		132 5-975	142 3-3020	4.1	6.7	9.3
Mg^{2+}		54 2-762	106 1-1735	5.2	7.2	6.6
Cl^-		125 21-1965	220 15-9650	18	28	28
NO_3^-		1435 191-9500	1510 161-16300	17	31	23
SO_4^{2-}		617 128-7310	971 133-9300	19	39	40
S(IV)	μmol l^{-1}	15 7-85	7 0.4-94	na	na	na
CH_2O		66 34-920	50 12-173	na	na	na
Fe	μg l^{-1}	1055 200-6880	455 20-4800	na	223	28
Pb		346 80-2780	212 38-2500	na	na	na

a. Median and range for 42 samples on 8 days.
b. Median and range for 85 samples on 15 days.
c. Volume-weighted mean values for 1982-83 (see Table 3).
d. Volume-weighted mean values for 1978-79 (Liljestrand and Morgan, 1981).
na = not analyzed.

TABLE 2.

CHEMICAL LOADING IN AEROSOL SAMPLES
HENNINGER FLATS: 1983

Date & Time	size[a]	fog[b]	NH_4^+	NO_3^-	SO_4^{2-}	H^+[c]	"pH"[c]	cloudwater[d] pH	cloudwater[d] NO_3^-/SO_4^{2-}
			μeq m^{-3}						
June 8									
00:00-	T	post	0.196	0.067	0.312	0.154	"2.81"		
06:00	F		0.189	0.018	0.273			2.71	1.11
	(C)		(0.007)	(0.049)	(0.039)	(0.068)	"3.17"		
21:45-	T	fog	0.101	0.294	0.213	0.362	"2.44"		
02:15	F		0.009	0.042	0.086			3.00	1.68
	(C)		(0.092)	(0.252)	(0.127)	(0.270)	"2.56"		
June 10									
12:00-	T	pre	0.154	0.070	0.284	0.113	"2.95"		
18:00	F		0.159	0.012	0.265				
	(C)		(-.005)	(0.058)	(0.019)	(0.021)	"3.69"		
22:30-	T	pre	0.136	0.073	0.195	0.082	"3.09"		
02:30	F		0.188	0.044	0.190				
	(C)		(-.052)	(0.029)	(0.005)	(0.061)	"3.21"		
June 11									
06:30-	T	fog	0.154	0.265	0.185	0.271	"2.57"		
10:30	F		0.050	0.010	0.069			3.01	1.89
	(C)		(0.104)	(0.255)	(0.116)	(0.240)	"2.62"		
10:40-	T	fog	0.057	0.105	0.109	0.122	"2.92"		
14:30	F		0.034	0.004	0.045			2.94	1.42
	(C)		(0.023)	(0.101)	(0.064)	(0.107)	"2.97"		
June 12									
08:00-	T	fog/	0.200	0.201	0.197	0.080	"3.10"		
12:00	F	post	0.041	0.044	0.082			3.57	1.43
	(C)		(0.159)	(0.151)	(0.115)	(0.030)	"3.52"		
June 19									
00:45-	T	patchy	0.027	0.068	0.100	0.094	"3.03"	2.87	1.65
06:00		fog							
June 21									
08:35-	T	patchy	0.257	0.269	0.480	0.225	"2.65"		
10:45	F	fog	0.242	0.057	0.267			2.67	na
	(C)		(0.015)	(0.212)	(0.213)	(0.179)	"2.75"		
June 22									
04:30-	T	fog/	0.243	0.141	0.262	0.069	"3.16"		
08:30	F	post	0.213	0.098	0.229			3.09	2.50
	(C)		(0.030)	(0.043)	(0.033)	(0.006)	"4.22"		
June 25									
06:30-	T	fog	0.211	0.105	0.342	0.170	"2.77"		
10:00								2.65	1.85
02:00-	F	pre/fog	0.210	0.042	0.261				
10:00									

a. T - total particulate (open-face filter); F - fine particulate (d_p < 3μm); (C)- coarse: T minus F.
b. Conditions during sampling relative to fog episode.
c. H^+ concentrations calculated by charge balance of major ions; "pH" calculated assuming LWC = 0.1 g m^{-3}.
d. LWC and time-weighted average values for cloudwater samples relative to b.

TABLE 3.

WET DEPOSITION - HENNINGER FLATS
OCTOBER 1982 TO JULY 1983

Month	#	mm	H^+	Na^+	K^+	NH_4^+	Ca^{2+}	Mg^{2+}	Cl^-	NO_3^-	SO_4^{2-}
			meq m^{-2}								
A. STORMS											
Oct[a]	2	19	0.39	0.29	0.02	0.16	0.06	0.09	0.33	0.24	0.31
Nov[a]	3	196	3.92	2.31	0.13	0.96	0.46	0.67	2.53	1.74	2.57
Dec	3	84	2.11	0.86	0.02	1.12	0.42	0.36	1.71	0.94	2.52
Jan	4	240	3.80	1.22	0.14	1.67	0.91	1.07	2.61	3.48	3.35
Feb	5	198	4.28	1.68	0.15	1.24	0.51	0.61	1.80	2.46	3.03
Mar	9	472	5.76	7.69	0.28	4.12	1.27	2.33	8.92	4.12	5.53
Apr-May 2	7	264	7.32	6.57	0.48	2.83	1.15	2.95	7.19	5.23	6.01
June 2	1	7.5	0.21	0.01	0.01	0.04	0.11	0.09	0.11	0.14	0.08
SUM		1481	27.8	20.6	1.2	12.1	4.9	7.2	25.2	18.4	23.4
(mean[b])			(18.8)	(13.9)	(0.8)	(8.2)	(3.3)	(4.8)	(17.0)	(12.4)	(15.8)
B. STRATUS											
May 31-Jun 1		7.5	3.62	0.55	0.08	0.85	0.63	0.33	0.63	3.46	2.72
Jun 11-12		5.8	3.38	0.18	0.02	0.56	0.41	0.21	0.46	2.76	1.85
Misc[c]	4	2.5	1.34	0.14	0.02	0.27	0.20	0.10	0.21	1.19	0.87
SUM		15.8	8.33	0.87	0.13	1.68	1.24	0.64	1.30	7.40	5.45
(mean[b])			(526)	(55)	(8)	(106)	(78)	(41)	(82)	(467)	(344)
$\frac{B}{A+B} * 100$		1.1	23.1	4.1	9.7	12.2	20.2	8.2	4.9	28.7	18.9
1978/1979[d]											
Pasadena		610	23.8	14.6	1.0	12.8	4.1	4.4	17.1	18.9	23.8
(mean[b])			(39)	(24)	(1.7)	(21)	(6.7)	(7.3)	(28)	(31)	(39)
Mt. Wilson		1270	12.7	33.0	2.2	45.7	11.8	8.4	35.6	29.2	50.8
(mean[b])			(10)	(26)	(1.7)	(36)	(9.3)	(6.6)	(28)	(23)	(40)

Table 3. Footnotes

a. Oct. and first Nov. events occurred before collector was installed; deposition was calculated from mean storm concentration x rain gage volume.

b. Volume-weighted mean concentration ($\mu eq\ l^{-1}$).

c. These Jun. & Jul. events were not collected; deposition was calculated from mean stratus concentration x rain gage volume.

d. Liljestrand and Morgan (1981).

TABLE 4.

BULK DEPOSITION - HENNINGER FLATS
MAY-JULY 1983

Interval/ Bucket	"H^+"[a] meq m^{-2}	(μeq m^{-2} hr^{-1})	Na^+ meq m^{-2}	(μeq m^{-2} hr^{-1})	NH_4^+ meq m^{-2}	(μeq m^{-2} hr^{-1})	$Ca^{2+}+Mg^{2+}$ meq m^{-2}	(μeq m^{-2} hr^{-1})	Cl^- meq m^{-2}	(μeq m^{-2} hr^{-1})	NO_3^- meq m^{-2}	(μeq m^{-2} hr^{-1})	SO_4^{2-} meq m^{-2}	(μeq m^{-2} hr^{-1})
May 12-19														
A	0.0	(0.0)	0.53	(3.14)	0.76	(4.55)	0.99	(5.87)	0.16	(0.96)	0.78	(4.66)	0.83	(4.96)
B	0.0	(0.0)	0.60	(3.56)	0.39	(2.32)	0.80	(4.77)	0.23	(1.34)	0.88	(5.22)	0.63	(3.72)
C	0.0	(0.0)	0.44	(2.61)	0.02	(0.11)	0.50	(2.95)	0.08	(0.48)	0.69	(4.08)	0.31	(1.82)
D	0.0	(0.0)	0.16	(0.97)	0.07	(0.40)	0.31	(1.87)	0.14	(0.81)	0.43	(2.55)	0.17	(0.99)
May 19-26														
A	0.02	(0.14)	0.05	(0.31)	0.36	(2.25)	0.20	(1.24)	0.17	(0.72)	0.52	(3.20)	0.12	(0.76)
B	0.17	(1.00)	0.04	(0.26)	0.04	(0.22)	0.23	(1.40)	0.03	(0.21)	0.41	(2.56)	0.08	(0.52)
D	0.18	(1.13)	0.05	(0.33)	0.05	(0.33)	0.21	(1.29)	0.04	(0.24)	0.45	(2.79)	0.17	(1.06)
May 26-June 3														
A	3.69	(19.3)	2.33	(12.2)	3.04	(15.9)	2.04	(10.7)	1.85	(9.7)	5.54	(29.0)	4.81	(25.2)
B	5.10	(26.7)	1.87	(9.8)	2.10	(11.0)	1.63	(8.53)	1.91	(10.0)	5.42	(28.4)	4.13	(21.6)
C	5.29	(27.7)	1.93	(10.1)	1.70	(8.9)	1.50	(7.9)	1.84	(9.6)	5.52	(28.9)	4.32	(22.6)
D	4.41	(23.1)	3.71	(19.4)	3.48	(18.2)	8.29	(43.4)	2.96	(15.5)	14.5	(76.0)	5.50	(28.8)
Wet only 15 mm	3.83		0.56		0.89		1.16		0.63		3.60		2.80	
June 3-9														
A	0.32	(2.03)	0.27	(1.75)	0.32	(2.02)	0.98	(6.31)	0.16	(1.04)	0.84	(5.38)	0.78	(4.98)
B	0.10	(0.65)	0.25	(1.62)	0.01	(0.09)	1.45	(7.36)	0.22	(1.41)	0.80	(5.11)	0.37	(2.36)
C	1.24	(7.92)	0.31	(1.98)	0.29	(1.86)	0.87	(5.58)	0.22	(1.42)	1.52	(9.77)	1.04	(6.66)
D	0.47	(3.04)	0.16	(1.02)	0.24	(1.53)	0.49	(3.17)	0.10	(0.65)	0.80	(5.15)	0.37	(2.36)
Wet only[b] 0.5 mm	0.26		0.03		0.05		0.06		0.04		0.23		0.17	
June 9-13														
A	2.87	(30.5)	0.42	(4.51)	1.35	(14.4)	0.83	(8.85)	0.24	(2.59)	3.86	(41.1)	2.45	(26.1)
B	4.06	(43.2)	0.56	(6.02)	1.44	(15.3)	1.10	(11.7)	0.51	(5.38)	5.15	(54.8)	3.27	(34.8)
C	3.08	(32.8)	0.26	(2.75)	1.04	(11.1)	0.47	(4.98)	0.23	(2.40)	3.21	(34.2)	2.19	(23.3)
D	4.59	(48.8)	1.34	(14.3)	1.59	(16.9)	3.50	(37.2)	0.90	(9.55)	8.55	(91.0)	4.04	(43.0)
Wet only 5.8 mm	3.38		0.18		0.56		0.62		0.46		2.76		1.85	
June 13-19														
A	0.0	(0.0)	0.09	(0.65)	0.08	(0.58)	0.35	(2.62)	0.12	(0.91)	0.22	(1.62)	0.11	(0.85)
B	---------- missing ----------													
June 19-July 11														
A	0.09	(0.16)	1.08	(2.03)	0.79	(1.48)	1.28	(2.41)	0.11	(0.21)	1.65	(3.11)	1.64	(3.09)
B	0.20	(0.38)	1.07	(2.01)	0.82	(1.55)	1.45	(2.74)	0.11	(0.21)	1.49	(2.80)	1.46	(2.75)
Wet only[b] 2 mm	1.05		0.11		0.21		0.24		0.16		0.93		0.69	
July 11-25														
A	0.04	(0.11)	0.26	(0.77)	0.08	(0.22)	0.94	(2.76)	0.02	(0.05)	0.69	(2.03)	0.13	(0.54)
B	0.06	(0.17)	0.26	(0.76)	0.23	(0.66)	0.21	(0.60)	0.24	(0.71)	0.62	(1.80)	0.24	(0.69)

a. "H^+" deposition from pH of bucket extraction or precipitation sample.
b. Deposition calculated from measured trace rainfall x mean stratus (B) concentration (see Table 3).

TABLE 5.

CHEMICAL COMPOSITION OF CLOUDWATER REMOVED FROM PINE NEEDLES
HENNINGER FLATS: 1982 AND 1983

Sample[a]		---------- μeq l^{-1} ----------								
Date-Time	pH	H^+	Na^+	K^+	NH_4^+	Ca^{2+}	Mg^{2+}	Cl^-	NO_3^-	SO_4^{2-}
1982										
6/12	3.12	760	14500	1625	5650	11700	6170	2000	19900	5910
6/22	2.90	1260	950	750	2400	1300	425	960	1260	880
1983										
5/16 03:00	3.11[b]	780	4500	590	2260	2660	1970	1390	9610	1260
5/31 06:30	2.91[b]	1240	18050	1110	2530	7840	3200	1890	20690	4200
13:00	2.92	1200	2580	1000	1510	5050	1670	1260	11710	1730
6/09 02:00	2.64[b]	2280	6660	1300	5640	10500	3480	2340	21630	8100
6/11 08:00	2.47[c]	3390	3730	645	2250	5000	1500	600	11070	4850
6/12 08:30[d]	2.96	1100	810	1180	340	1270	680	640	3750	1660
	2.88	1320	1090	770	540	2220	620	500	3870	1440
11:00[d]	2.87	1350	900	660	700	1980	560	650	4430	1650
	3.03	930	1310	1500	520	1690	910	910	3940	2000
	2.98	1050	1850	670	1410	1070	590	1580	3080	2060

a. 1982: anion aliquot filtered; cation aliquot unfiltered.
1983: both aliquots filtered.

b. pH calculated from diluted aliquot measurement.

c. pH calculated from ion-balance.

d. Individual samples from different trees.

PATHWAYS FOR POLLUTANT DEPOSITION IN A LOS ANGELES PINE FOREST

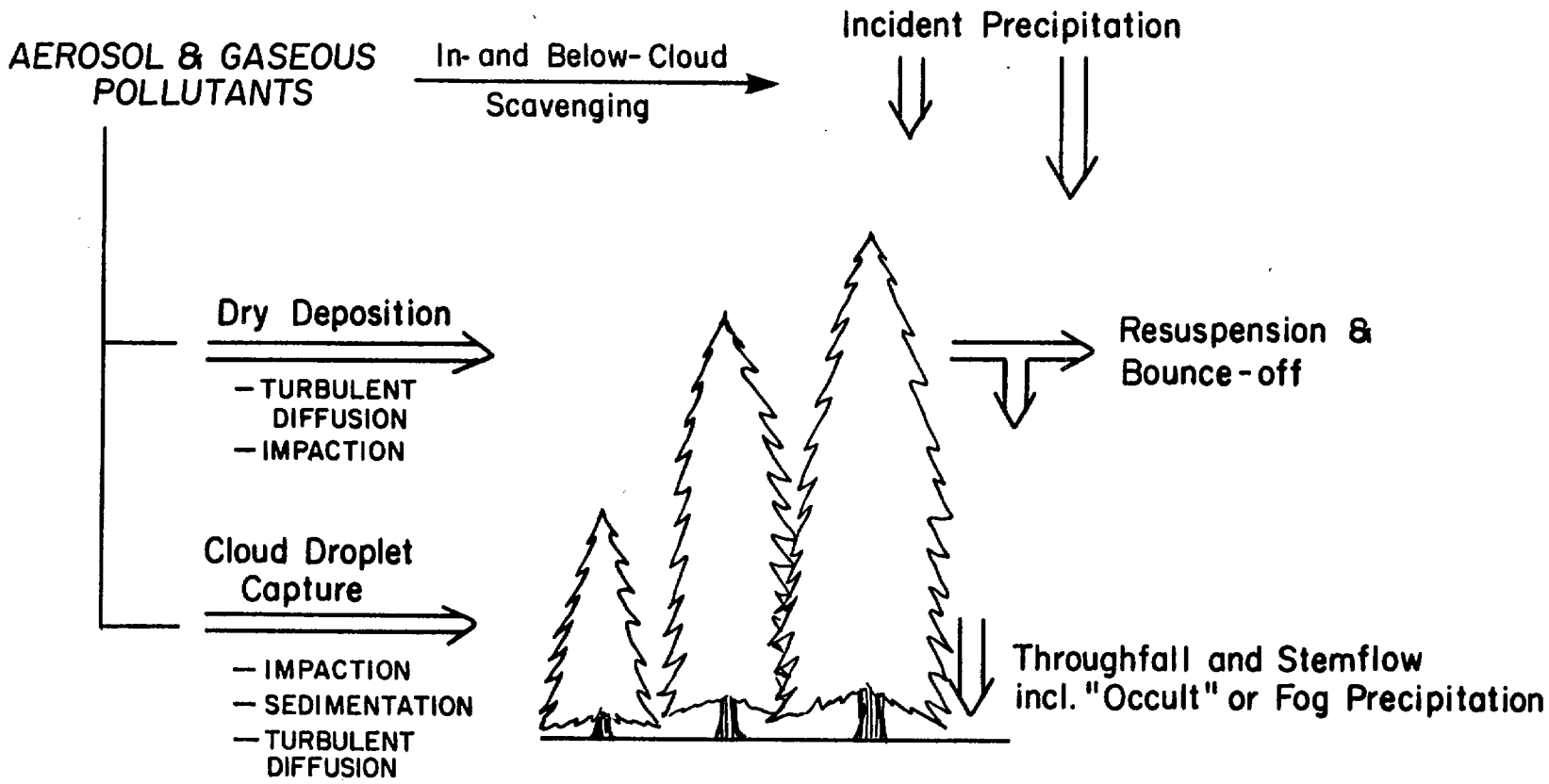

Figure 1.

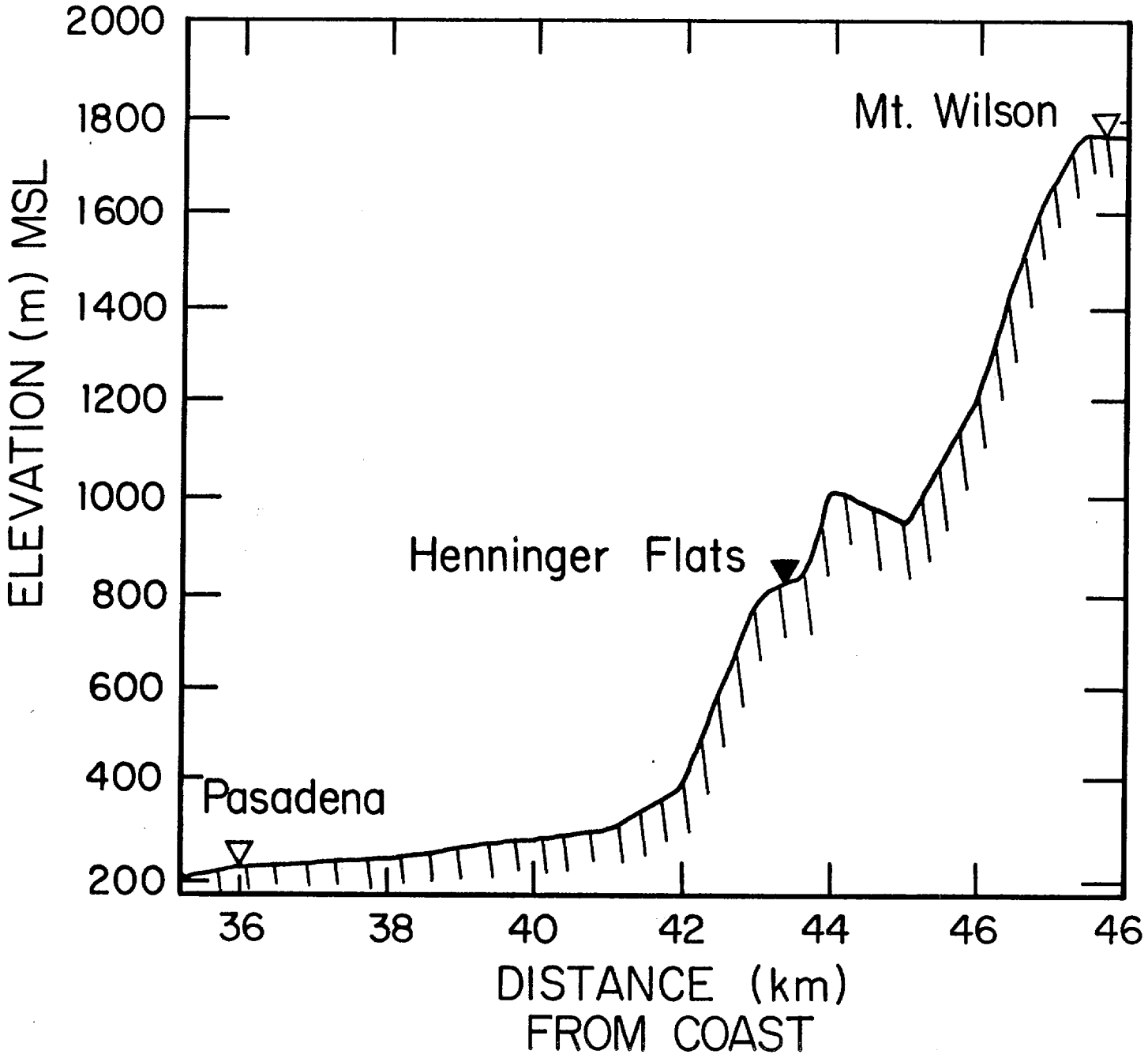
2000
1800
1600
1400
1200
1000
800
600
400
200
ELEVATION (m) MSL
Mt. Wilson
Henninger Flats
Pasadena
36
38
40
42
44
46
46
DISTANCE (km)
FROM COAST

Figure 2.

ION BALANCE

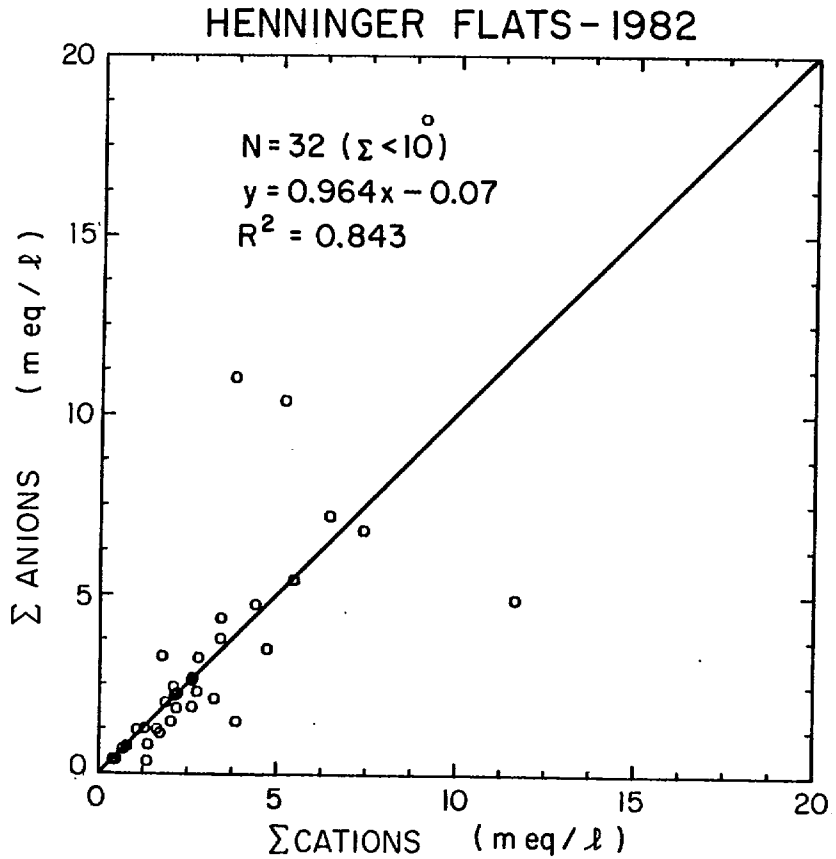

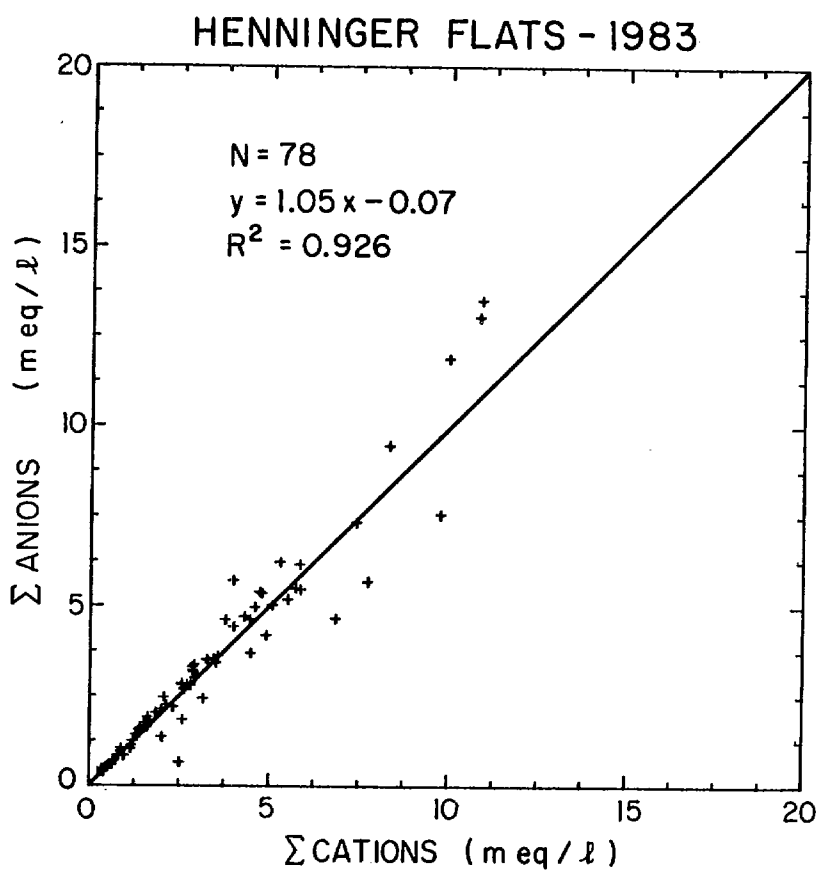

Figure 3.

NO_3^- VS. SO_4^{2-}

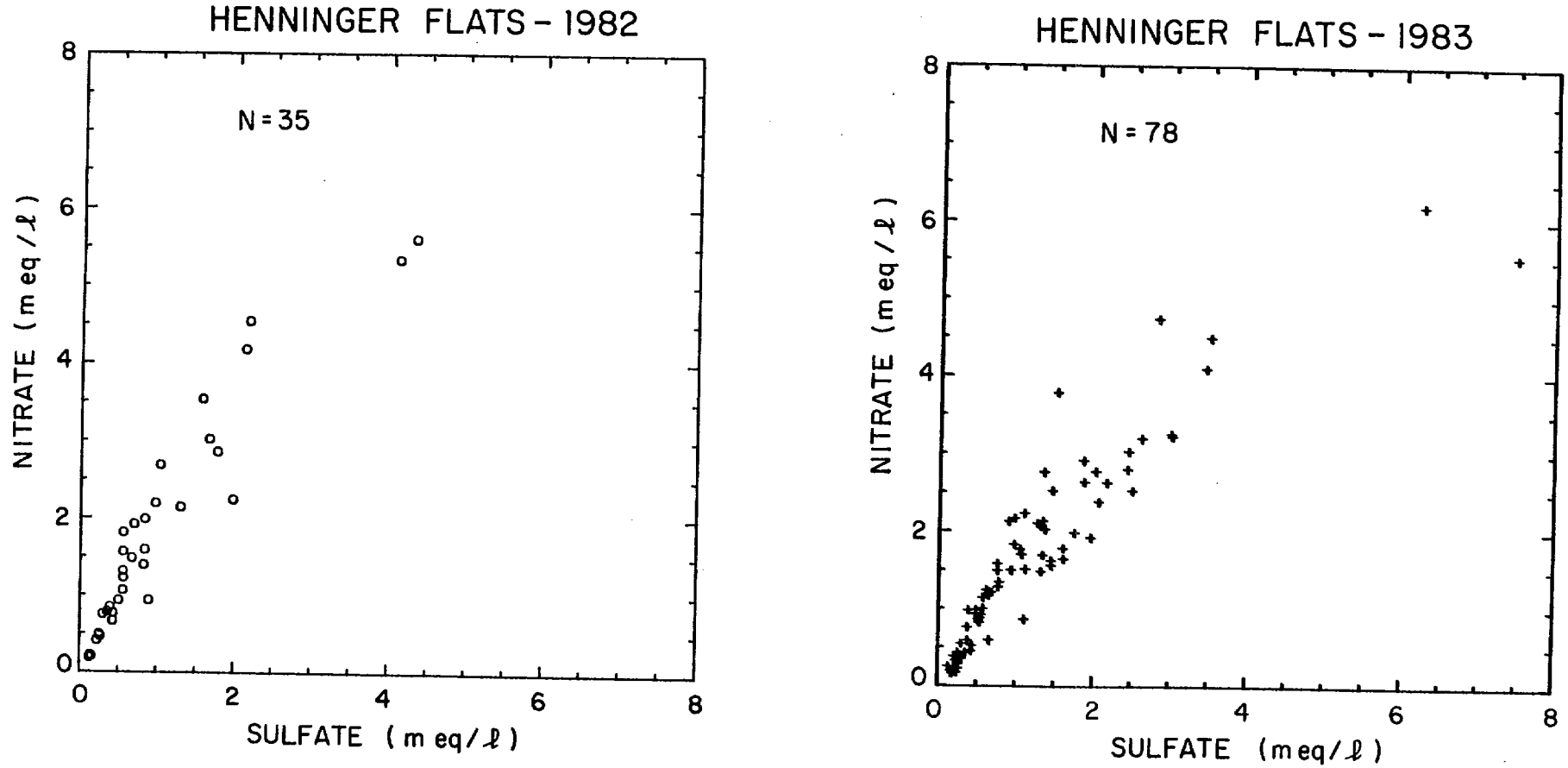

Figure 4.

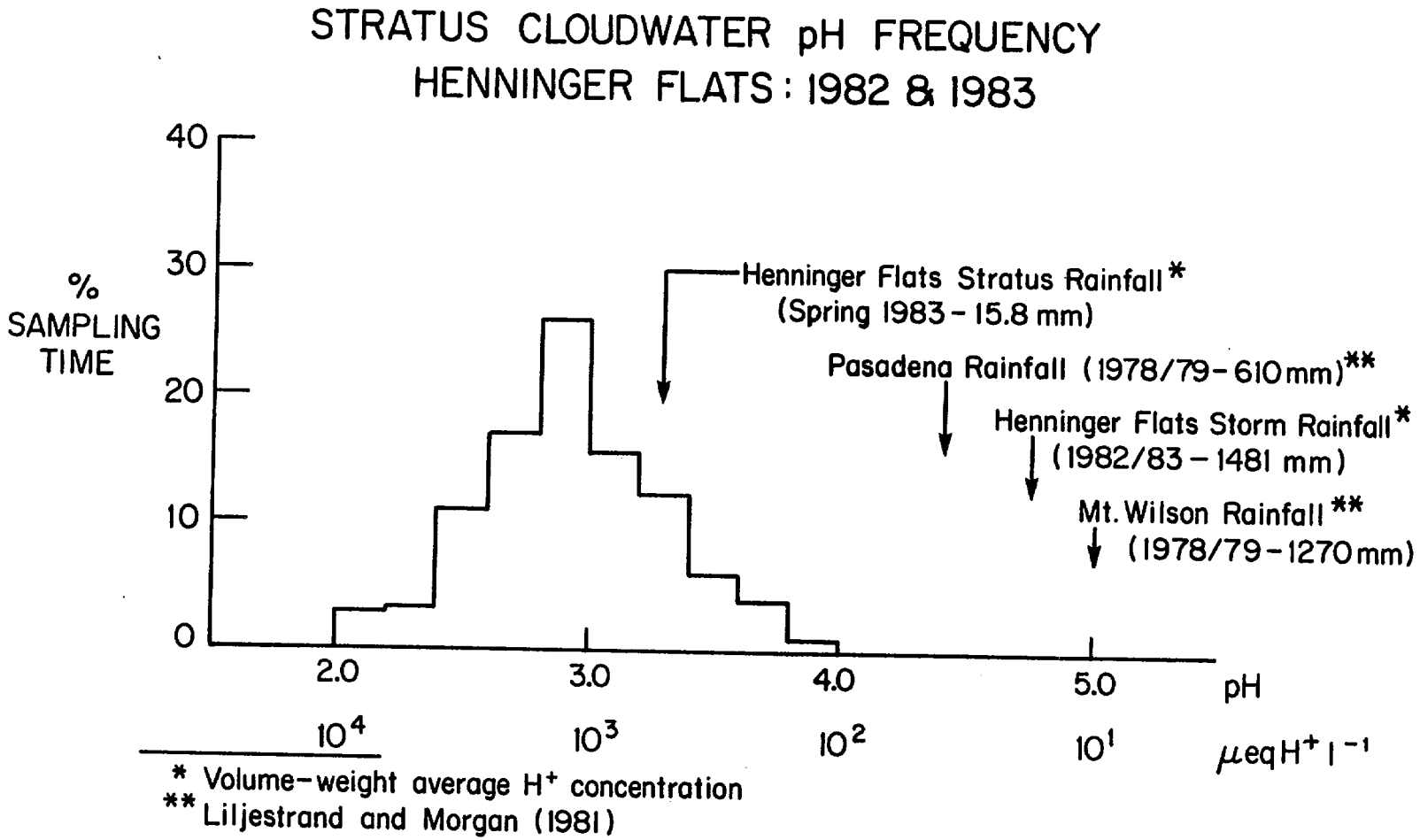
STRATUS CLOUDWATER pH FREQUENCY
HENNINGER FLATS: 1982 & 1983
%
SAMPLING
TIME
40
30
20
10
0
Henninger Flats Stratus Rainfall*
(Spring 1983 - 15.8 mm)
Pasadena Rainfall (1978/79 - 610 mm)**
Henninger Flats Storm Rainfall*
(1982/83 - 1481 mm)
Mt. Wilson Rainfall**
(1978/79 - 1270 mm)
2.0
3.0
4.0
5.0
pH
10^4
10^3
10^2
10^1
$\mu eq H^+ l^{-1}$
* Volume-weight average H^+ concentration
** Liljestrand and Morgan (1981)

Figure 5.

FREE ACIDITY VS. NO_3^- AND SO_4^{2-}

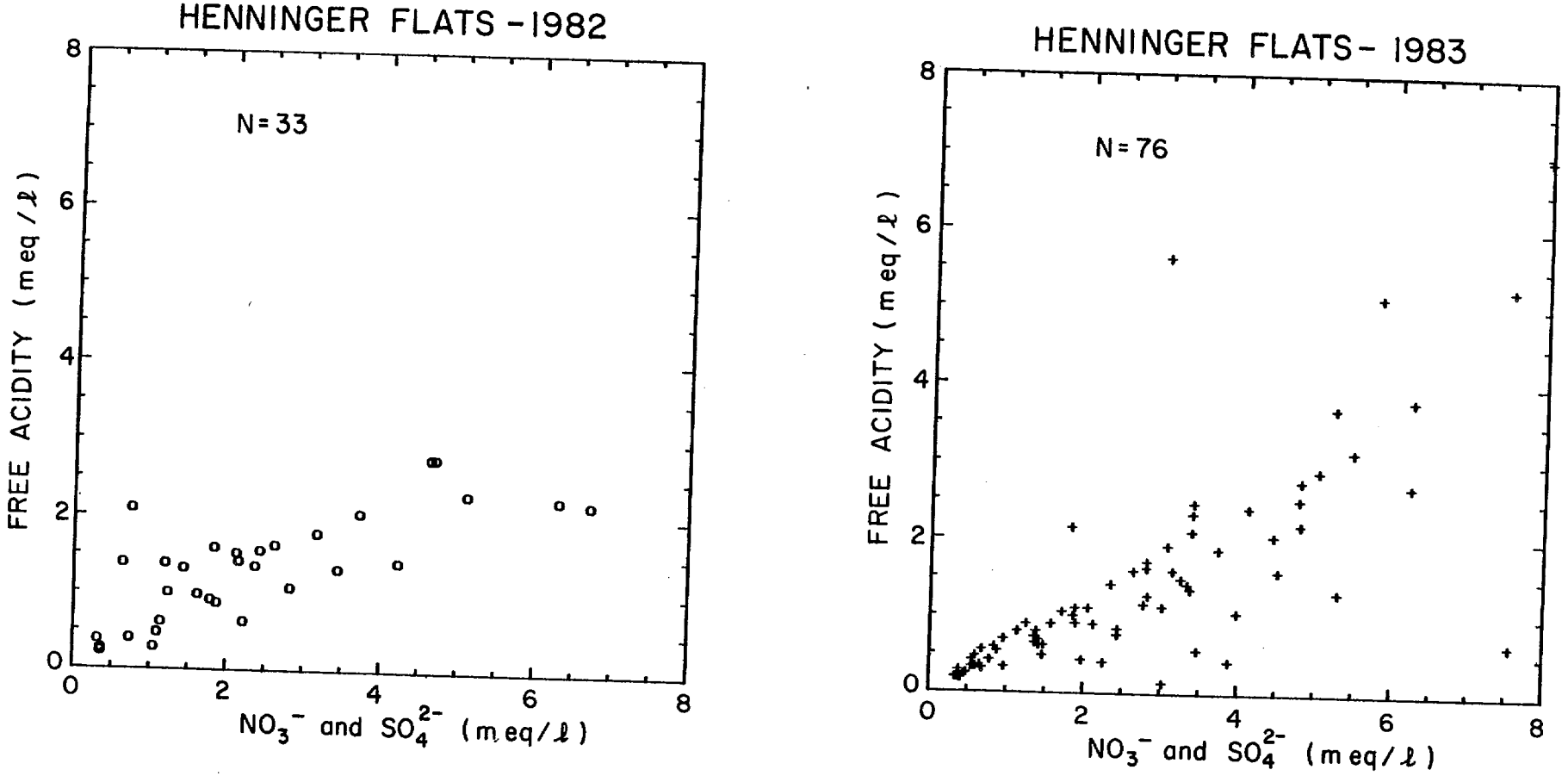

Figure 6.

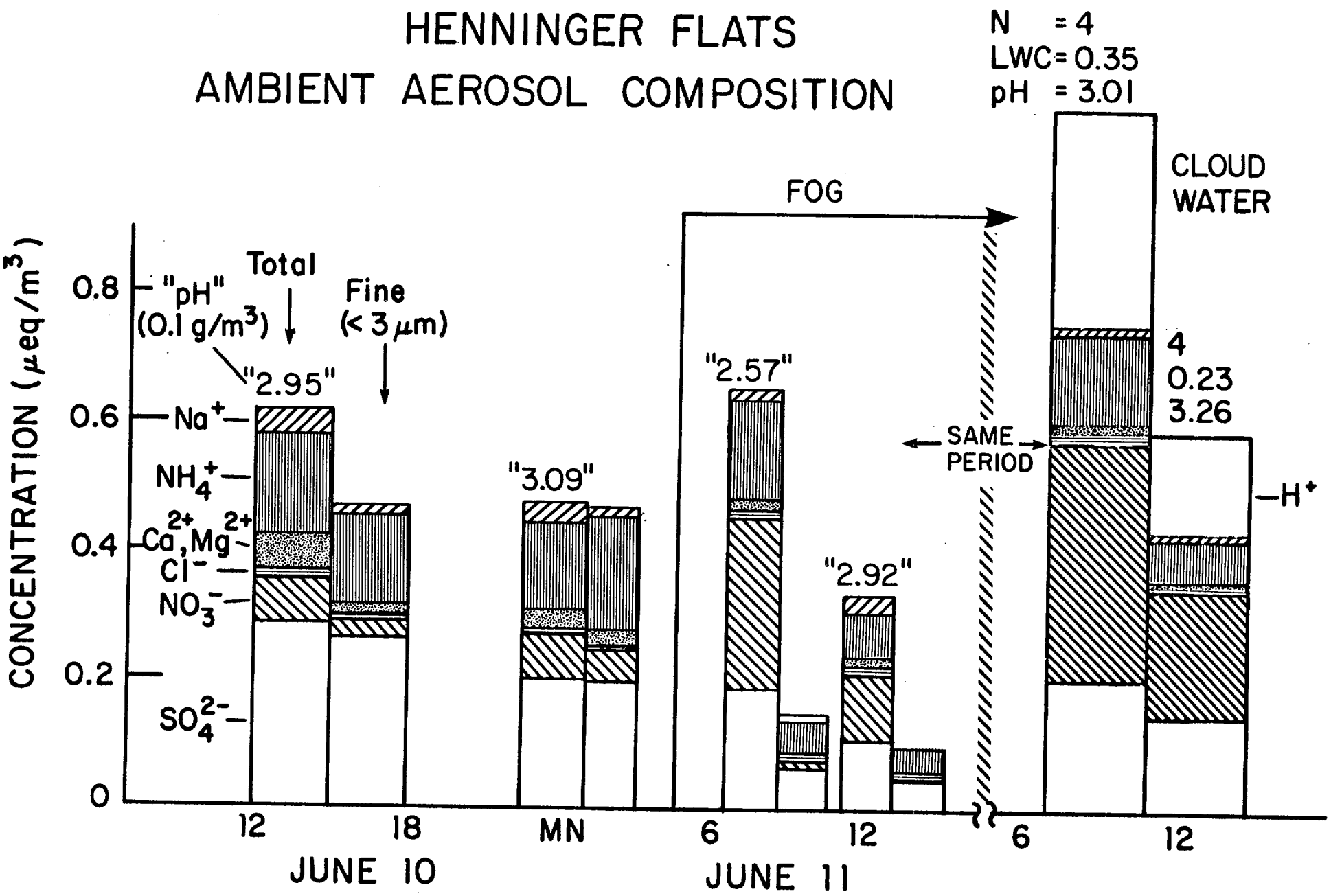
HENNINGER FLATS
AMBIENT AEROSOL COMPOSITION
N = 4
LWC = 0.35
pH = 3.01
CLOUD WATER
FOG
Total
Fine (< 3 μm)
"pH" (0.1 g/m³)
"2.95"
"3.09"
"2.57"
"2.92"
SAME PERIOD
4
0.23
3.26
CONCENTRATION (μeq/m³)
0.8
0.6
0.4
0.2
0
Na⁺
NH₄⁺
Ca²⁺, Mg²⁺
Cl⁻
NO₃⁻
SO₄²⁻
H⁺
12
18
MN
6
12
6
12
JUNE 10
JUNE 11

Figure 7.

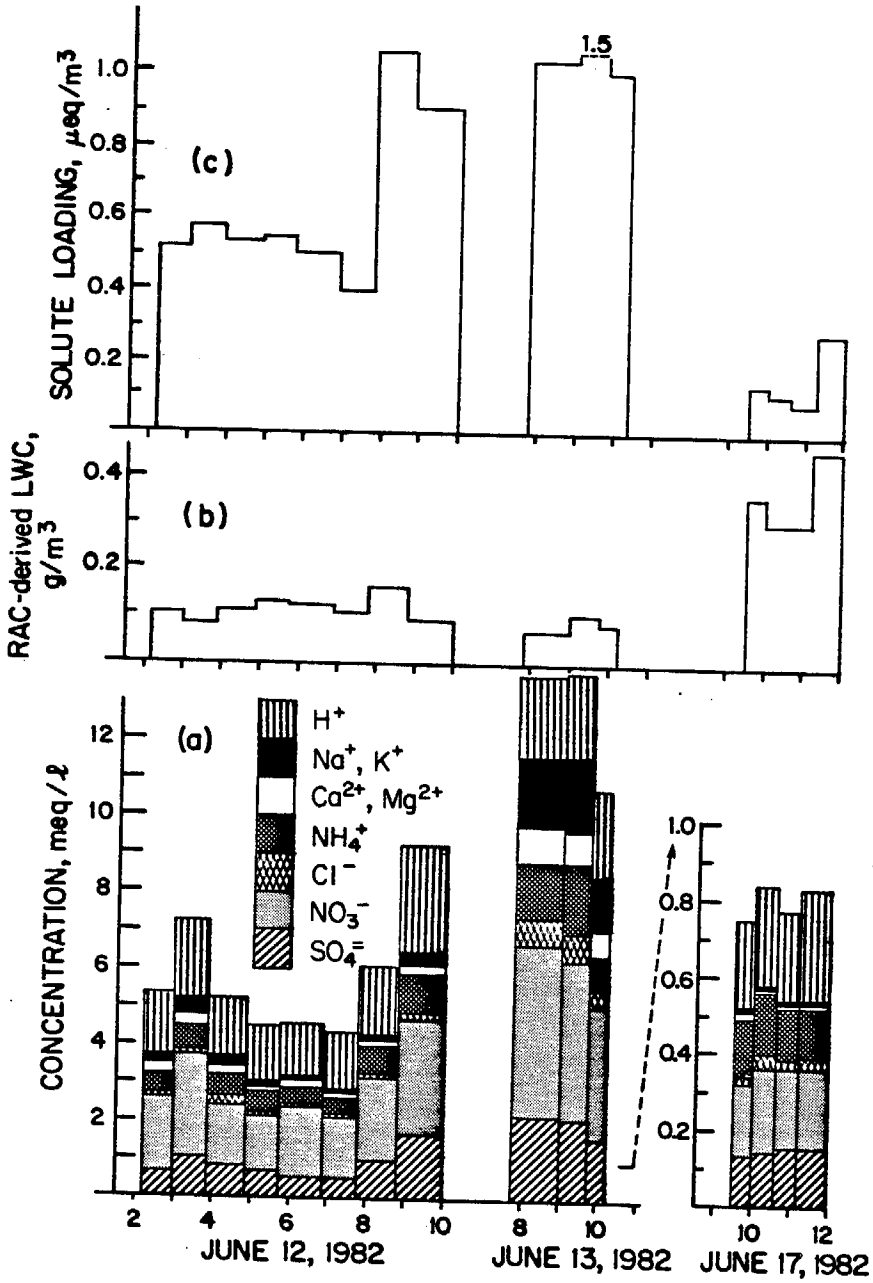
SOLUTE LOADING, μeq/m³
1.0
0.8
0.6
0.4
0.2
(c)
1.5
RAC-derived LWC, g/m³
0.4
0.2
(b)
CONCENTRATION, meq/ℓ
12
10
8
6
4
2
(a)
H⁺
Na⁺, K⁺
Ca²⁺, Mg²⁺
NH₄⁺
Cl⁻
NO₃⁻
SO₄⁼
1.0
0.8
0.6
0.4
0.2
2
4
6
8
10
8
10
10
12
JUNE 12, 1982
JUNE 13, 1982
JUNE 17, 1982

Figure 8.

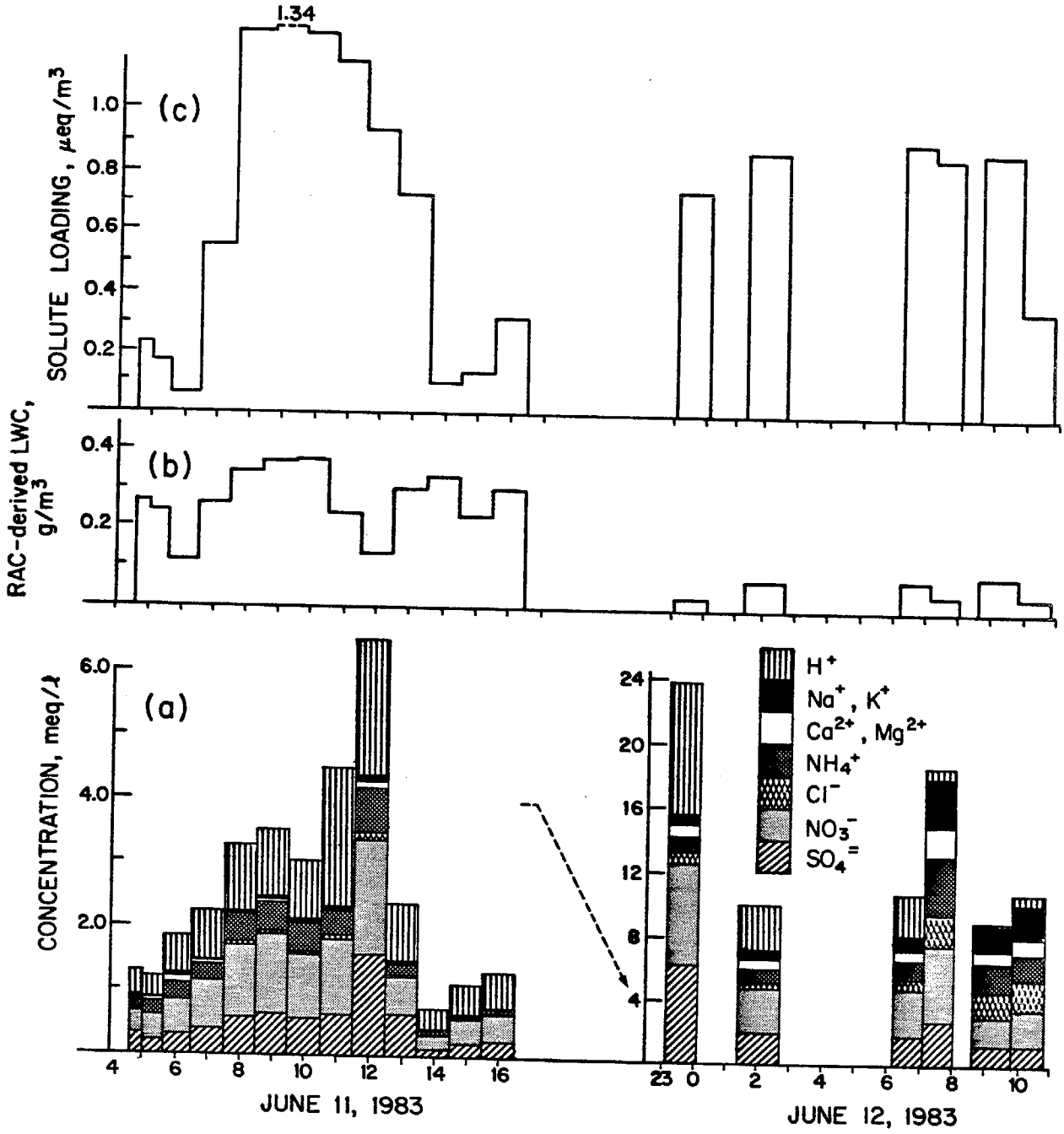
1.34
(c)
SOLUTE LOADING, μeq/m³
1.0
0.8
0.6
0.4
0.2
(b)
RAC-derived LWC, g/m³
0.4
0.2
(a)
CONCENTRATION, meq/ℓ
6.0
4.0
2.0
4
6
8
10
12
14
16
JUNE 11, 1983
24
20
16
12
8
4
23
0
2
4
6
8
10
JUNE 12, 1983
H⁺
Na⁺, K⁺
Ca²⁺, Mg²⁺
NH₄⁺
Cl⁻
NO₃⁻
SO₄⁼

Figure 9.

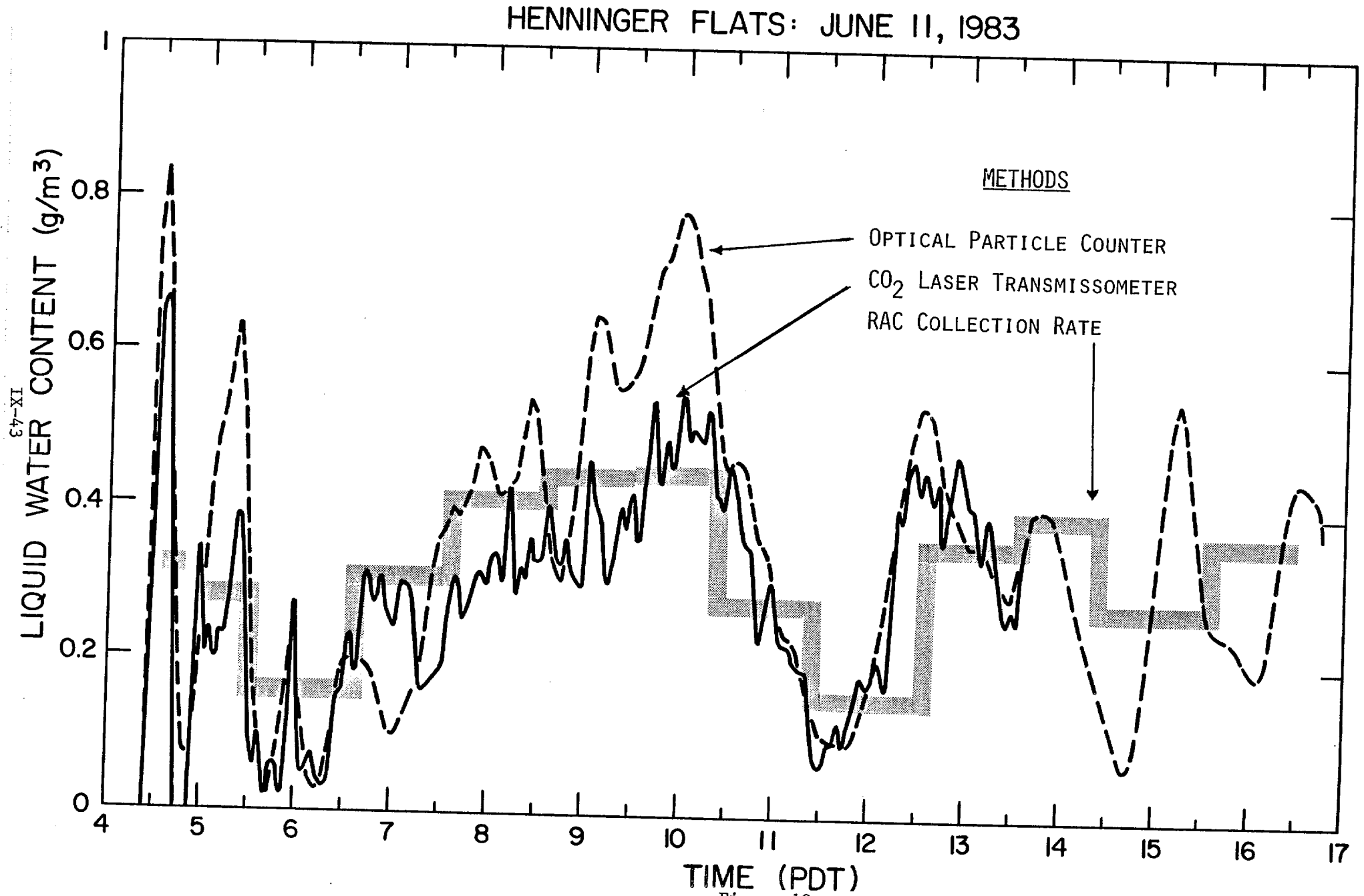
HENNINGER FLATS: JUNE 11, 1983
METHODS
OPTICAL PARTICLE COUNTER
CO_2 LASER TRANSMISSOMETER
RAC COLLECTION RATE
LIQUID WATER CONTENT (g/m³)
0
0.2
0.4
0.6
0.8
1
4
5
6
7
8
9
10
11
12
13
14
15
16
17
TIME (PDT)

Figure 10.

APPENDIX X

Fogwater Collector Design and Characterization

Daniel J. Jacob, Rueen-Fang T. Wang, and Richard C. Flagan*

Environmental Engineering Science, Keck Engineering Laboratories, California Institute of Technology, Pasadena, California 91125

■ The detailed characterization of a rotating arm collector to sample ambient fog droplets for chemical analysis is presented. Because of the large volume of sample required, and because fog droplets are of supermicron size and are sensitive to local thermodynamic disturbances, conventional methods for atmospheric aerosol sampling are not suitable for fogwater sampling. Design criteria for fogwater samplers are outlined. Devices used in previous investigations are evaluated in light of these criteria. The design of a rotating arm collector is discussed, and it is shown that this instrument performs adequately in preserving the physical and chemical integrity of the sample at all stages of collection. Limitations in the design due to mechanical constraints are discussed. Results of an in situ calibration experiment using a chemically tagged monodisperse aerosol indicate a size cut of 20-μm diameter.

Introduction

Supermicron particles contribute significantly to the total mass of a dry aerosol (*1*). This contribution increases considerably when the aerosol is wetted, especially under supersaturated conditions in which activated condensation nuclei grow rapidly to form cloud or fog droplets. Whereas the mass loading of an urban aerosol under nonsaturated conditions is of the order of 10^{-4} g m^{-3}, the liquid water content in a cloud or fog ranges from 0.01 to 1 g m^{-3}, with supermicron droplets constituting the bulk of the aerosol mass. In urban environments fogwater has been found to contain extremely high pollutant concentrations, often associated with high acidities (*2*, *3*).

Supermicron particles are difficult to collect efficiently because their inertia may prevent them from following the air streamlines converging toward the inlet of the sampler (*4*). Furthermore, water droplets in the atmosphere are in a fragile thermodynamic balance with the ambient humidity which is very sensitive to perturbations by a sampling device. Conventional methods for collecting samples of total particulate matter may, therefore, lead to sampling biases due to anisokinetic sampling conditions or changes in temperature or pressure. Fog sampling is further complicated by the relatively large sample volume required for the study of the detailed aquatic chemistry. At least 10 mL of sample is needed for the standard inorganic analysis routinely carried out in our fog program (*3*). If the variation in chemical composition throughout the fog event is to be studied, sampling intervals should be short. For a typical liquid water content of 0.1 g m^{-3}, a sampling rate of over 1.7 m^3 min^{-1} is required to collect 10 mL for analysis in an hour. Larger sampling rates are required for the study of light fogs.

A rotating arm collector based on the principle of inertial impaction has been developed and used in our intensive fog sampling program. Major advances in the understanding of fog chemistry and the role of fogs in acid deposition have been made by using this device (*3*, *5*). In a recent field intercomparison study of fogwater collectors (*6*), samples were collected simultaneously with instruments from five different research groups and analyzed for major ions. Ionic concentrations in samples collected by the rotating arm collector and a jet impactor (*7*) agreed within 5%; other collectors gave systematically either higher or lower concentrations. The rotating arm collector was found to collect water efficiently in both light and heavy fogs.

To date, the sampling characteristics of the rotating arm collector have only been qualitatively explored by measuring the change in the droplet size distribution in a cloud chamber which results from its operation. These measurements indicated that the minimum size of particles collected was at least 8 μm but did not provide sufficient resolution to determine the size-dependent collection efficiency (*8*). In this paper we first elaborate on the design criteria relevant to fogwater collection and then present a detailed examination of the design and operation of our rotating arm collector. Constraints on the design due to power requirements and possible sample biases due to aerodynamic heating are explored. Measurements of the collection efficiency as a function of particle size are presented.

Design Criteria for Fogwater Collectors

Size Cut. Fog droplets form by activation of atmospheric particles (condensation nuclei) under supersaturated conditions. At the levels of supersaturation found in the atmosphere, the lower size limit for particles to be activated is of the order of 0.1 μm (*9*). Figure 1 shows how fog formation can shift the size distribution of an urban aerosol; particles in the first mode (below 0.1 μm) are rather unaffected by the condensation process, but most particles in the two higher modes grow by condensation to much larger sizes. Therefore, two types of particles coexist in a fog: (1) supermicron fog droplets and (2) nonactivated, primarily submicron, particles. Being dilute aqueous solutions, fog droplets do not interact with their environment in the same way as the solid or concentrated submicron particles (*10*, *11*). It is, therefore, important that a fogwater sampler differentiate between the two types of particles.

Fog droplets range in size from 1 to 100 μm, with a mass median diameter usually in the range 10–40 μm (*12–15*). The dependence of the fog droplet chemical composition on droplet size has not been rigorously investigated to date; general predictions from droplet growth theory (*16*) are difficult to make because humidities in fogs fluctuate rapidly in a manner that is still poorly understood (*17*, *18*). Large droplets are not necessarily more dilute than smaller droplets because they generally result from condensation on larger nuclei. If the total pollutant burden associated with fogs is to be determined, droplets of all sizes should be collected with the same efficiency. Nonactivated submicron particles represent a very small fraction of the total aerosol mass but they could, if collected, contribute a sizable amount of solutes to the sample and result in a serious bias. A sharp lower size cut in the range 1–10-μm diameter is, therefore, desired. Furthermore, since most of the fog mass is associated with large droplets, droplets up to about 100-μm diameter must be collected without bias.

Three methods are available to collect the large particles while excluding the smaller particles: sedimentation, inertial separation, and removal of smaller particles by

Table I. Fogwater Collectors Reported in the Literature

reference	type	impaction velocity, cm s^{-1}	sampling rate, m^3 min^{-1}	characteristic width[a] inlet, cm	characteristic width[a] impaction surface, cm	lower size cut, μm	inlet Stokes no. for 100-μm droplets
passive							
Mrose (*20*)	cloth surface	ambient wind	variable		?[f]	variable	
Okita (*21*)	grid	ambient wind	variable		0.01	variable	
Lazrus et al. (*22*)	screen	ambient wind	variable		?	variable	
Sadasivan (*23*)	screen	ambient wind	variable		?	variable	
Falconer and Falconer (*24*)	grid	ambient wind	variable		0.02	variable	
active							
Houghton and Radford (*12*)	screen	600	102	30	0.01	3[c]	0.6
May (*25*)	grid	450	11	10	0.05	7[c]	1.4
May (*25*)	jet impactor	1700	0.05	0.85	0.4	?	13
Okita (*21*)	screen	94	1	7.5	?	?	0.3
Mack and Pilie (*26*)	rotating arm	1500–5000	7		0.45	?	
Katz (*7*)	jet impactor	2000	1.2	?	0.2	5[d]	?
Brewer et al. (*27*)	screen	320	1.5	5	0.02[e]	5[c]	2.0
this paper	rotating arm	3800–5600	5		0.48	20	

[a] Characteristic width of inlet: radius of circular inlet (*12, 21, 25b, 27*), half-width of square inlet (*25a*). Characteristic width of impaction surfaces: radius of wires (*12, 21, 24, 25a, 27*), half-width of jet (*7, 25b*), radius of rod (*26*, this paper). [b] Diameter of droplets collected with 50% efficiency. [c] Calculated from impaction theory for cylinders (*19*). [d] Calculated by Katz from theory and confirmed by experiment. [e] Obtained by personal communication from R. L. Brewer. [f] ? = not reported, or cannot be computed from available data.

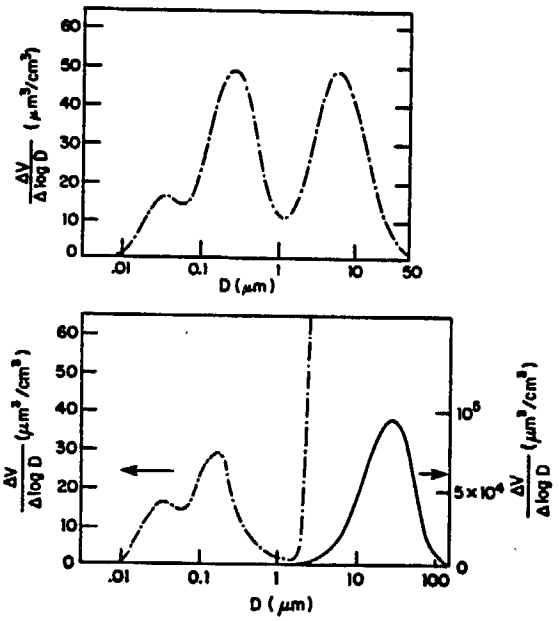

Figure 1. (Top) Typical urban aerosol size distribution profile (*1*). (Bottom) Expected shift in the size distribution profile as a result of fog formation.

diffusion. Of these, inertial separation, particularly impaction, most readily achieves sharp size cuts of a few microns and has been the method favored by past investigators. The efficiency of collection by impaction is a function of the Stokes number St (*19*):

$$\mathrm{St} = \frac{\rho_D D^2 U}{18 \mu a} \qquad (1)$$

where ρ_D is the droplet density, D is the droplet diameter, U is the velocity of approach, μ is the viscosity of air, and a is a characteristic width of the impaction surface. The size cut of a sampler is defined as the diameter D_{50} of droplets collected with 50% efficiency, and the cutoff Stokes number St_{50} is the corresponding Stokes number. Fogwater samplers used in past investigations (Table I) can be divided into two general groups: (1) passive collectors, where droplets impact on the collecting surface with the velocity of the ambient wind, and (2) active collectors, where droplets are accelerated to a certain velocity as they approach the collection surface. Passive collectors have the obvious drawback that the impaction velocity is not well-defined but instead fluctuates with the ambient wind. As a result the size cut varies with time, and the sample is not necessarily representative of the actual fogwater. Furthermore, at low wind speeds the minimum size of particles which will impact becomes large enough that the rate of sample collection becomes unacceptable, thereby precluding the use of these collectors in many locations. In active collectors, the size-dependent collection efficiency can be characterized for a given geometry of the impaction surface. However, modification of the ambient velocity of the droplets introduces two potentially important problems: perturbation of the ambient thermodynamic equilibrium and anisokinetic sampling.

Perturbation of the Ambient Thermodynamic Equilibrium. Modification of the flow field in active collectors may produce significant evaporation or condensation of the droplets as they approach the impaction surface. The total loss of water droplets has been reported past the first two stages of a cascade impactor (*25*). The extent to which droplet sizes are modified during approach can be estimated by simple mass transfer calculations, as shown in the next section. Unfortunately, no such calculations have been reported in the references of Table I.

Evaporation may also occur following collection if the droplets are not sheltered immediately from the flow of air past the impaction surface, because the air mass in a fog is thermodynamically inhomogeneous (*29*) and contains pockets of unsaturated air. Aside from evaporation, contact of the collected droplets with changing air masses may alter their compositions. It is therefore important that collected droplets be removed rapidly from the air flow. In the jet impactor designed by Katz (*7*), this is achieved with a rotating impaction surface; in the rotating arm collector, centrifugal force rapidly drives the impacted droplets into collection bottles where the air is stagnant. The screen collectors of Table I rely on gravity to draw the impacted droplets into storage bottles at the bottom of the

screen, but this is a slow process (especially in light fogs).

Anisokinetic Sampling. Recent studies of anisokinetic sampling biases (*30*, *31*) have indicated that a sampler oriented into the wind can lose over 30% of particles with inlet Stokes' numbers larger than 0.5. In a crosswind, losses are considerably greater. Losses are found to be maximum for sampling velocities 2–5 times the ambient wind velocity. In addition, deposition of most particles to the walls within a few inlet diameters from the inlet has been reported for Re > 5000 (*31*).

Although moderate sampling velocities have been used in the ducted devices listed in Table I, inlet Stokes' numbers are still high in most cases. In screen and grid collectors, the moderate sampling velocities used introduce the additional problem that very thin wires are required for impaction. Because the larger droplets in the fog are then comparable in size to the radius of the impaction cylinder, interception and aerodynamic interactions between the droplets and the wires become important. The impaction characteristics are then quite different from those of the point particles considered in most theoretical treatments of impaction on cylinders. The apparent geometry of a very thin wire also changes significantly as fog droplets collect on it, introducing uncertainty in the size cut.

Proper scaling of the inlet could allow the use of high impaction velocities with little anisokinetic sampling bias. However, droplets tend to fly off collection strings at velocities higher than about 8 m s^{-1} (*12*).

The anisokineticity effect can be suppressed by eliminating the inlet and, instead, generating an apparent velocity by moving the impaction surface at high speed through the ambient air. Such devices have been used in airborne sampling of clouds (*32*, *33*), where the speed of the aircraft constituted the apparent velocity. In ground-based collectors, high velocities can be generated by using a rotating system.

Design of a Rotating Arm Collector

Rotating arm collectors have been used for many years to collect biological particles on adhesive coated surfaces (*34–36*). Recently, a rotating arm virtual impactor has been developed to sample isokinetically giant atmospheric particles (*37*). In another device, the solid arms have been modified to collect fogwater by introducing a slot in the leading edges of a hollow arm (*26*). For the purpose of our field programs, we have developed an improved version of the latter collector.

Principle. The design of the rotating arm collector used in the Caltech fog sampling program is shown in Figure 2. A motor drives at high speed (1700 rpm) a type 304-L stainless steel solid rod of length $2L$ = 63 cm. Each end of the rod has a slot milled into its leading edge. Standard 30-mL VWR narrow mouth bottles are mounted at the ends of the arm to collect the water which impacts in the slots and flows outward by centrifugal force. Threaded Teflon tubes screwed onto the end of the arm and extending inside the collection bottles prevent the collected fogwater from running out after the instrument is stopped. Deflectors prevent water which impacts on the solid part of the arm from entering the slot since the collection of this water would bias the sample toward large droplet sizes. Small fins are welded to the back of the arm for extra strength. The entire arm is Teflon coated. In the absence of previous calibration data, the design was based on a cutoff Stokes number of unity. The cutoff size is weakly dependent on St_{50}; i.e., $D_{50} \propto St_{50}^{1/2}$, so even though the actual St_{50} may differ substantially from unity, the effect on D_{50} was not expected to be too large.

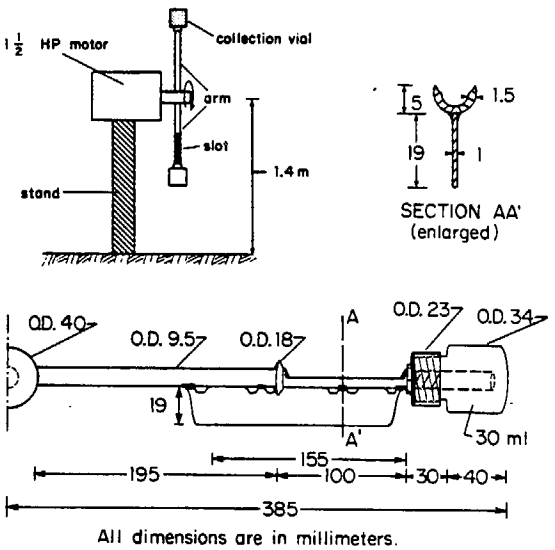

Figure 2. Caltech rotating arm collector. Full welds attaching the fin to the rod are shown in dark.

Mechanical Constraints. The size cut is determined by the choice of $(U/w)^{1/2}$, where w is the width of the slotted portion of the arm. Because reducing w leads to a proportional reduction in the sampling rate achieved with the instrument, a preferable way to obtain an acceptably low D_{50} is to operate at a high approach velocity. However, the resulting aerodynamic drag force F limits the extent to which U can be increased.

The arm consists of cylindrical sections and a half-cylinder cup. The drag coefficients C_d of these shapes at Reynolds numbers in the range 10^4–10^5 are approximately 1 and 2, respectively (*38*). The power P required to rotate the arm at a rotating speed ω (rps) is given by

$$P = 2\int_0^L \frac{dF}{dl}\, U(l)\, dl \qquad (2)$$

This may be separated into the components for the solid rod ($l < L_1$), the slot ($L_1 < l < L_2$), the bottle cap ($L_2 < l < L_3$), and the bottle ($L_3 < l < L$). Noting that the drag force is given by

$$F = C_d A \rho_a (U^2/2) \qquad (3)$$

where A is the projected area of the shape and ρ_a is the density of air, we find

$$P = 2\rho_a \omega^3 \pi^3 \sum_{i=1}^{4} C_{di} w_i (L_i^4 - L_{i-1}^4) \qquad (4)$$

where the w_i's are the widths of the corresponding portions of the arm, $L_0 = 0$, and $L_4 = L$. The power required to drive the arm is a strong function of the dimensions of the arm and the rotation frequency. To facilitate operation of the arm using readily available electrical circuits, the size and speed must be limited. Our rotating arm was designed to achieve an acceptable sampling rate and size cut, while not requiring more than a 110-V, 15-A circuit to drive the sampler. The power required when the collector is rotating at 1700 rpm is calculated from eq 4 to be 900 W. A 1.5-hp (1120-W) motor is sufficient to drive the collector, and this is still compatible with electrical circuits likely to be available in the field. The 30-mL cylindrical collection bottles are major contributors to the drag (450 W) because of their size, shape, and velocity. Collection vials are very small in the instrument described by Mack and Pilie (*26*), but the resulting samples are then too small for chemical determination, and the sampler is

inconvenient because of rapid overloading of the vials. Streamlined bottles or bottle casings could be adapted to the present design to minimize the drag while keeping the sample volume large enough to make the instrument practical.

Specifications. The slot velocities range from 38 to 56 m s^{-1}, and the Reynolds numbers at the slots range from 24 000 to 35 000. Laboratory tests under zero wind conditions indicate that air is drawn through both faces of the collector at a velocity of 1.5 m s^{-1} roughly uniform across the plane of collection (measured 25 cm away from the plane of collection). The sampled air is expelled radially (velocity of 4 m s^{-1} measured 25 cm away from the tip). This induced flow ensures that the sampled air is entirely renewed at every half-rotation of the arm, so that the sampling rate is 5 m^3 of air/min. Assuming 100% efficiency, a collection rate of 0.5 mL min^{-1} would be achieved in a fog of 0.1 g m^{-3} liquid water content. Collection rates of up to 2 mL min^{-1} have been obtained in the field.

Droplet Evaporation. Droplet evaporation may occur at the three stages of collection: (1) as the droplet approaches the impaction surface, (2) in the collection slots, and (3) in the collection bottles.

Evaporation during approach is most likely to occur as the droplet approaches the slot at high apparent velocity. Let us consider, as a worst case, the stagnation streamline; as air approaches the slot its velocity decreases from U_∞ in the free stream to 0 at the stagnation point. This deceleration leads to aerodynamic heating. We write the appropriate equations for mass transfer (*16*) and droplet trajectory: because we are concerned only with activated supermicron droplets, we neglect the effect of solutes on the physical properties of the droplets.

$$r\frac{dr}{dt} = \frac{s - y(T)}{\dfrac{\rho_W R T}{e_{sat}(T) D M_r} + \dfrac{\Delta H \rho_W}{kT}\left(\dfrac{\Delta H M_r}{RT} - 1\right)} \tag{5}$$

$$y(T) = \frac{2\sigma M_r}{RT\rho_W r}$$

$$\frac{dz}{dt} = -U_D \tag{6}$$

$$\frac{dU_D}{dt} = -\frac{3}{8}\left(\frac{\rho_a}{\rho_W}\right)C_d\frac{(U_D - U)^2}{r} \tag{7}$$

r is the droplet radius; $s = (e/e_{sat}(T)) - 1$ is the ambient supersaturation, where e is the water vapor pressure over the droplet and $e_{sat}(T)$ is the saturation water vapor pressure over a plane water surface at temperature T; σ is the surface tension of water against air; R is the universal gas constant; ρ_W and ρ_a are the densities of water and air, respectively; D is the diffusivity of water vapor in air; ΔH is the latent heat of vaporization of water; k is thermal heat conductivity of air; M_r is the molecular weight of water; z is the distance of the droplet to the collector; U is the velocity of the air flow; U_D is the velocity of the approaching droplet. The local Reynolds number Re_1 of the droplet is

$$Re_1 = \frac{2|U_D - U|r}{\nu} \tag{8}$$

where ν is the kinematic viscosity of air. The drag coefficient C_d can be approximated for $Re_1 < 10^3$ by (*39*)

$$C_d = \frac{24}{Re_1}(1 + 0.158Re_1^{2/3}) \tag{9}$$

Under the assumption that the compression proceeds isentropically, the temperature and pressure fields for the approaching droplet are given by

$$T = T_\infty + \frac{U_\infty^2 - U^2}{2c_p} \tag{10}$$

$$P = P_\infty\left(\frac{T}{T_\infty}\right)^{\gamma/(\gamma-1)} \tag{11}$$

where c_p is the specific heat of air at constant pressure and γ is the ratio of specific heats. The water vapor pressure is calculated by assuming that the mixing ratio of water vapor remains constant as the air approaches the collector and that droplets in the free stream are at equilibrium with water vapor:

$$e(T) = \frac{P}{P_\infty}e_{sat}(T_\infty)[1 + y(T_\infty)] \tag{12}$$

For a given $U(z)$ along the stagnation streamline, the coupled eq 5–7 can readily be solved numerically. Unfortunately, the complicated potential flow around a cup has not yet been characterized to the authors' knowledge. It is assumed here that the flow (at least to within some distance of the impaction surface) should be comparable to that around a cylinder of diameter w, for which the potential flow solution along the stagnation streamline yields

$$U = U_\infty\left[1 - \left(\frac{w}{2z}\right)^2\right] \tag{13}$$

The system of eq 5–7 is then integrated with a fourth-order Runge–Kutta routine. Under the conditions U_∞ = 56 m s^{-1}, T_∞ = 283 K, and P_∞ = 1 atm, the percentage of loss in droplet mass by the time the droplet reaches the stagnation point (actually the time at which $(2z - w)/w < 0.001$) is less than 0.1% for activated supermicron droplets. Increasing U_∞ to 100 m s^{-1} does not significantly increase this loss; therefore, evaporation during approach to the slots is not a constraint in choosing higher approach velocities.

A similar mass transfer calculation was conducted to evaluate the effect of thermodynamic modifications as air is drawn through the sampler with a velocity U = 1.5 m s^{-1}. It was found that no significant change in droplet size occurs for supermicron droplets during that stage of approach.

Evaporation in the slot could also occur after impaction from the thin film of water in the slot to the unsaturated air above. Because the flow patterns in the slot originate mostly from turbulent eddies, an accurate description of the transfer phenomena would be very complicated. By using an oversimplified model of tangential flow of unsaturated air over a flat plate, we estimated that under the worst conditions the evaporation rate could be no more than 0.01 g min^{-1}. Even in this case, evaporation is still very small at typical collection rates (0.1–1 g min^{-1}).

Finally, evaporation in the collection bottles must be considered. As a test, the bottles were filled halfway with water (15 mL in each), mounted on the collector, and spun for 30 min in a dry atmosphere. This did not affect the volume of water in the bottles, which shows that evaporation in the bottles is negligible.

Safety. Safety is a primordial concern for a large diameter device rotating in the open. The collector must be carefully balanced to prevent vibrations and securely mounted to a rigid stand. The mechanisms for mounting the bottles must be able to withstand the loads due to high acceleration (1200g). Stainless steel caps with close tol-

erance threads were found to be satisfactory in laboratory tests. The operating site must be carefully selected and supervised to minimize the hazard.

The arm must be inspected to detect any mechanical flaws or stress concentration points which could lead to failure by fatigue. In the original design of the collector (*8*), the back fin was attached to a 304 steel rod with tack welds. This method of attachment produced a sharp angle with the rod, which served as an incipient crack. Stress concentration at that point led to one occasion of failure by fatigue. To prevent this from reoccurring we have modified the design of the fins; the points of contact with the rod are now smooth and fully welded. We have switched to 304-L steel, which is less prone to weakening at the weld points. Also, the instrument is now stress-relieved after welding to further reduce the risk of failure.

Calibration

Mack and Pilie (*26*) used theoretical results for impaction on cylinders to predict the collection efficiency of their rotating arm collector. However, they presented no justification for doing so. Because of the complicated flow inside the cavity, impaction in the slot may differ from impaction on a cylinder. Experimental calibration is necessary.

Scaling Considerations. At high flow Reynolds numbers and low interception numbers, the collection efficiency, η, of an impaction surface can be satisfactorily reduced to a function of the three dimensionless groups St, Re_D, and Mach number (*19*). Re_D is the droplet Reynolds number based on the droplet diameter and the free-stream velocity. When the Mach number based on the local sonic speed is smaller than 0.4, it has a negligible effect on the collection efficiency (*40*). As a good approximation

$$\eta = f(\mathrm{St}, \mathrm{Re_D}) \tag{14}$$

In the range $10^0 < Re_D < 10^3$, which is the range at which the droplets are collected in the slots, η is a strong function of both St and Re_D (*19*). To reduce the dependence of η to one dimensionless group, Israel and Rosner (*28*) have proposed a generalized Stokes number which accounts for the variation in the droplet drag coefficient at higher particle Reynolds numbers:

$$\mathrm{St}' = \frac{4}{3}\left(\frac{\rho_D}{\rho_a}\right)\left(\frac{D}{a}\right)\int_0^{\mathrm{Re_D}} \frac{d\mathrm{Re}'}{C_d(\mathrm{Re}')\mathrm{Re}'} \tag{15}$$

The generalized Stokes number reduces to the Stokes number for $Re_D \ll 1$. For higher particle Reynolds numbers St′ is related to St by

$$\mathrm{St}' = \mathrm{St}\psi(\mathrm{Re_D}) \tag{16}$$

where

$$\psi(\mathrm{Re_D}) = \frac{24}{\mathrm{Re_D}}\int_0^{\mathrm{Re_D}} \frac{d\mathrm{Re}'}{C_d(\mathrm{Re}')\mathrm{Re}'} \tag{17}$$

By substitution of St′ for St, the dependence of η on Re_D is reduced (*28*), so that the collection efficiency is a function of St′ alone, i.e.

$$\eta \simeq f(\mathrm{St}') \tag{18}$$

Calibration Method. Calibration of an aerosol sampling device involves dispersal of a calibration aerosol in a large volume of air under well-controlled conditions and would generally be conducted in a wind tunnel. Since a wind tunnel suitable for the rotating arm collector, or even a scaled-down version of the instrument, was not available, an alternate approach was taken. This method, which has recently been used to test sampler inlets (*41*), allows evaluation of the performance of the instrument under ambient conditions.

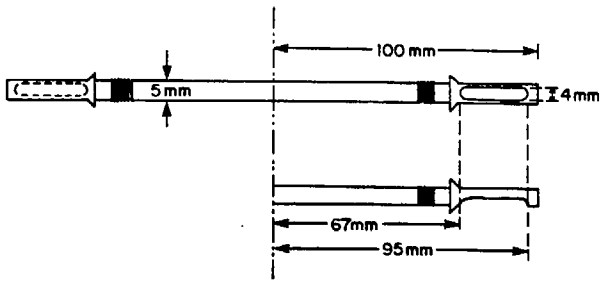

Figure 3. Model rotating arm collector used in calibration experiment.

A tracer gas is used to follow an aerosol plume as it is advected in the atmosphere from an aerosol generator to the collector to be tested. A chemically tagged monodisperse aerosol is released at a constant rate together with a tracer gas. The collection device is set one meter downwind of the point of release and samples the diluted aerosol plume. Prior to testing, the concentration of aerosol at the release point is measured. During testing, tracer gas samples are taken at the release point and next to the impaction surface of the sampler. Automatic continuous gas samplers give integrated measurements of tracer gas concentrations at both locations throughout the testing interval. If sedimentation of the particles is insignificant over the distance from the release point to the sampler, the trajectories of the particles and the gas are nearly identical over that distance. The average concentration C of aerosol crossing the collector path is then given by

$$C = C_0\left(\frac{C^*}{C^*_0}\right) \tag{19}$$

where the subscript 0 refers to the release point and the asterisk refers to the tracer gas. If a mass m of aerosol is collected by the sampler over a time interval Δt with a sampling rate Q, the collection efficiency is

$$\eta = \frac{m}{CQ\Delta t} \tag{20}$$

By running several tests over a range of St′ values, one obtains the dependency of η on St′.

In our tests a monodisperse sodium fluorescein solid aerosol was generated with a Berglund–Liu Model 3050 vibrating orifice generator. Sulfur hexafluoride (SF_6) was used as a tracer gas and connected to the upstream of the dilution air system of the aerosol generator (for which the flow rate was about 40 L min^{-1}) to ensure complete mixing. The aerosol production rate ranged from 10^{-9} to 10^{-7} g min^{-1}, and the flow rate of SF_6 ranged from 0.43 to 0.68 cm^3 min^{-1}. Due to the slow rate of aerosol release, the prototype collector had to be scaled down so that sufficient amounts of aerosol could be conveniently collected for analysis. The model collector (Figure 3) consists of two slotted ends screwed onto a solid rod. It was spun with a variable speed 0.5-hp 10000 rpm motor. Similarity of the Reynolds numbers was maintained, and the aspect ratio was kept as close as possible to that of the prototype. For structural reasons the width/length ratio for the slots is 0.15 in the model, whereas it is 0.095 in the prototype.

The experimental setup is shown in Figure 4. A fan generating a wind speed of about 5 m s^{-1} was used to advect the aerosol toward the collector. The experiments were conducted under conditions of low ambient winds. Dilution of the plume from the point of release to the

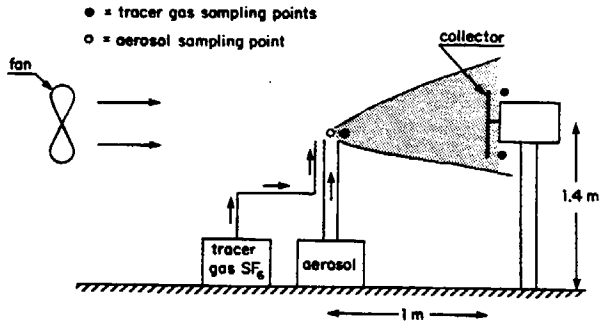

Figure 4. Calibration experiment setup.

sampling point, as measured by C^*/C^*_0, ranged from a factor of 30 to 1000 depending on the meteorological conditions. Particles ranging in diameter from 3 to 20 μm were generated to cover a wide range of Stokes numbers. The settling velocity of 20 μm particles is less than 1 cm s^{-1}, so that sedimentation is negligible over the distances of concern. Tests were run over 30-min intervals, which allowed collection of a sufficient amount of aerosol for accurate determination of the collected mass.

Two automatic continuous gas samplers, sampling over 5-min intervals, and one syringe pump, sampling over 30-min intervals, were used to obtain SF_6 samples. Comparison of the 5- and 30-min integrated measurements provided a check on the SF_6 levels and raised attention to any major changes in the ambient wind speed or turbulence over the course of testing. Analysis was done by gas chromatography using an electron capture detector (*42*). Samples were diluted to reach the optimal SF_6 detection range (100–300 ppt (parts per trillion)). The aerosol concentration at the release point was measured prior to testing by running a known volume of air through a glass-fiber filter. To restrict the aerosol loading on the model arm to the collecting slots, all other parts of the collector were covered with tape, which was removed prior to analysis. A coat of Vaseline grease was applied on one of the two slots to test against possible particle bounce-off. After testing, the sodium fluorescein was extracted in an ultrasonic bath for 30 min with a 0.1 N NH_4OH solution. For the greased slots extraction was first carried out with toluene for 30 min and then with the 0.1 N NH_4OH solution for another 30 min. The aqueous phase was then separated by centrifugation. The sodium fluorescein was analyzed by spectrofluorometry.

Results and Discussion. Figure 5 shows the observed dependence of the collection efficiency on St′ for the scaled-down model. The scale below the abscissa gives the droplet diameter as a function of St′ for a droplet impacting at the middle of the slot in the full-scale arm. Although there is some scatter in the data around $\eta = 50\%$, St'_{50} (based on the data from the greased slots) is about 5, which corresponds to $D_{50} = 20$ μm. Ungreased surfaces collect particles with lower efficiency, which indicates that some particle bounce-off occurs.

Each collection efficiency measurement corresponds to a range of Stokes numbers because velocities of approach vary from one end of the slot to the other. The spread in the Stokes numbers in the scaled-down model is 17% in each direction off the middle of the slot. In the prototype this spread is 19%, which leads to a 10% uncertainty on the size cut of the instrument. A way to eliminate this uncertainty would be to use a tapered slot, i.e., narrow close to the shaft and widening toward the tip, to maintain St′ constant over the whole length of the slot.

In ref 28, it is claimed that the use of St′ in interpreting inertial impaction on a surface greatly reduces the dependence of η on the geometry of that surface. Comparison of our calibration data to the curve obtained in ref 28 from previous calculations for cylinders and spheres shows similarity in shape, but our results are shifted toward the higher Stokes numbers (Figure 5). Because the largest discrepancies occur at low St′ values, this is not likely due to particle bounce. Recent studies of virtual impactors (*43*) have suggested an explanation for the larger St'_{50} in the rotating arm collector. In order to be collected, the particles must not only pass the virtual surface through which there is no mean air flow but also penetrate through the air in the cavity to reach the wall of the collector. Those particles which do not impact on the walls have a significant probability of being reentrained, particularly in the rotating arm collector where there is an induced flow along the length of the collector slot. This may explain the large Stokes numbers required for efficient collection.

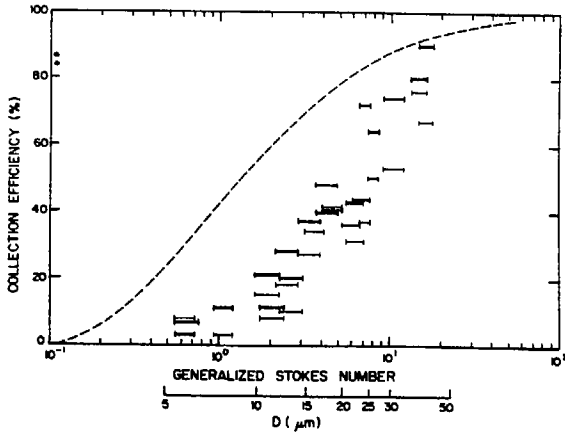

Figure 5. Collection efficiency of model collector vs. the generalized Stokes number, for greased (in bold) and ungreased impaction surfaces. The scale below the abscissa converts the generalized Stokes number to the diameter of droplets impacting in the middle of the slots of the prototype collector. The dashed curve represents theoretical collection efficiencies for cylinders and spheres (*28*).

Comparison with Field Results. Some liquid water content data were obtained at Bakersfield, CA, in Jan 1983 by drawing air with an open-faced Hi-Vol sampler through a paper filter. By measuring the difference in weight of the filters after a certain volume of air has been drawn through the Hi-Vol, one obtains an estimate of the liquid water content. At another location (Albany, NY, Oct 1982) the liquid water content was determined by infrared scattering using a laser transmissometer (*44*). It must be noted that uncertainties as large as 50% are commonly associated with these two liquid water content measurement methods. Figure 6 compares the amount of water collected per cubic meter of air sampled (assuming a sampling rate of 5 m^3 min^{-1}) to the actual liquid water content measured independently. A best fit to the data indicates an overall collection efficiency of 60%. The apparent decrease in collection efficiency when the liquid water content is high may be due to overloading of the bottles before the collector was stopped. To prevent premature overloading due to air lock in the bottles, we have since then added a small hole (0.36-mm diameter) on the upper part of the Teflon tube extending inside the bottle. This allows exchange of air in and out of the bottle during sampling and has been found to improve the collection characteristics in dense fog.

Conclusion

The performance of instruments to collect fogwater for chemical analysis can be assessed in the light of the fol-

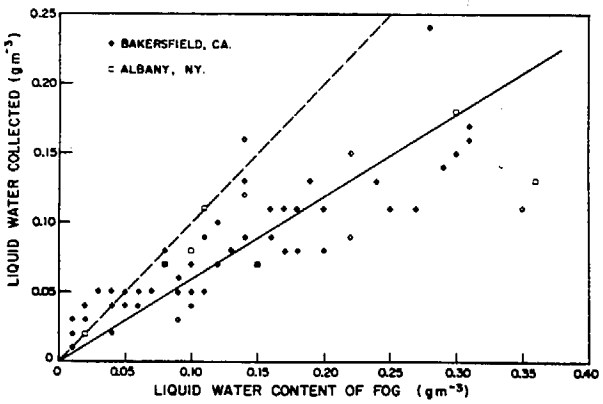

Figure 6. Collected water per cubic meter of air sampled vs. liquid water content. Liquid water content was measured with an open-faced Hi-Vol sampler (Bakersfield, CA) or with an infrared laser transmissometer (Albany, NY). (—) Linear best fit to the data. (---) 100% collection efficiency line.

lowing design criteria: (a) high collection efficiency for droplets in the size window 1–100 μm, (b) collection rate high enough to supply the sample volume required for chemical analysis, (c) conservation of droplet size during approach to the collection surface, and (d) rapid removal of the collected droplets away from the air flow into a quiescent environment.

We discussed in depth the design and characteristics of the rotating arm collector used in our ongoing fogwater chemistry field program and concluded that it performs well in preserving the chemical integrity of the collected droplets while providing large sample volumes. These results have been confirmed in the field (*6*). An in situ calibration indicated a size cut of 20 μm diameter, which is significantly higher than that desired. Because our sampler and the jet impactor designed by Katz (*7*) give consistent determinations of ionic concentrations in fogwater, there appears to be no obvious dependence of the chemical composition on the size of droplets collected. The rotating arm seems to collect samples representative of the fogwater chemistry in spite of its high lower size cut.

Our laboratory is currently investigating several promising designs of fogwater samplers that will collect efficiently droplets in the 1–10-μm size range while minimizing potential sample contamination. The objective is to build a reliable, fully automated instrument suitable for routine monitoring under a wide variety of field conditions. Results will be presented in a future report.

Acknowledgments

E. F. Daly and J. J. Fontana constructed the collectors and provided many valuable practical suggestions. Comments from D. S. Wood, J. M. Waldman, J. W. Munger, and M. R. Hoffmann are gratefully acknowledged.

Literature Cited

(1) Whitby, K. T. *Atmos. Environ.* **1978**, *12*, 135–159.
(2) Waldman, J. M.; Munger, J. W.; Jacob, D. J.; Flagan, R. C.; Morgan, J. J.; Hoffmann, M. R. *Science (Washington, D.C.)* **1982**, *218*, 677–680.
(3) Munger, J. W.; Jacob, D. J.; Waldman, J. M.; Hoffmann, M. R. *J. Geophys. Res.* **1983**, *88*, 5109–5123.
(4) Watson, H. H. *Am. Ind. Hyg. Assoc., Q.* **1954**, *15*, 21–25.
(5) Jacob, D. J.; Waldman, J. M.; Munger, J. W.; Hoffmann, M. R. *Tellus*, in press.
(6) Hering, S. V.; Blumenthal, D. L. "Fog Sampler Intercomparison Study: Final Report". Prepared for Coordinating Research Council, Atlanta, GA, 1984, Project STI 11 90063.
(7) Katz, U. "Communications de la 8eme Conference sur la Physique des Nuages". Clermont-Ferrand, France, July 15–19, 1980.
(8) Jacob, D. J.; Flagan, R. C.; Waldman, J. M.; Hoffmann, M. R. *Proc. Int. Conf. Precipitation Scavenging, Dry Deposition, Resuspension, 4th* **1983**, 125–136.
(9) Junge, C.; McLaren, E. *J. Atmos. Sci.* **1971**, *28*, 382–390.
(10) Jacob, D. J.; Hoffmann, M. R. *J. Geophys. Res.* **1983**, *88*, 6611–6621.
(11) Bassett, M.; Seinfeld, J. H. *Atmos. Environ.* **1983**, *17*, 2237–2253.
(12) Houghton, J. G.; Radford, W. H. *Pap. Phys. Ocean. Met. Mass. Inst. Technol. Woods Hole Ocean. Inst.* **1938**, *6* (4).
(13) Garland, J. A. *Q. J. R. Meteorol. Soc.* **1971**, *97*, 483–494.
(14) Mallow, J. V. *J. Atmos. Sci.* **1975**, *32*, 440–443.
(15) Goodman, J. *J. Appl. Meteorol.* **1977**, *16*, 1056–1067.
(16) Pruppacher, H. R.; Klett, J. D. "Microphysics of Clouds and Precipitation"; Reidel: Dordrecht, Netherlands, 1978; pp 141–142, 418–421.
(17) Roach, W. T. *Q. J. R. Meteorol. Soc.* **1976**, *102*, 355–359.
(18) Gerber, H. E. *J. Atmos. Sci.* **1981**, *38*, 454–458.
(19) Friedlander, S. K. "Smoke, Dust and Haze"; Wiley: New York, 1977; pp 95–109.
(20) Mrose, H. *Tellus* **1966**, *18*, 266–270.
(21) Okita, T. *J. Meteorol. Soc. Jpn.* **1968**, *46*, 120–126.
(22) Lazrus, A. L.; Baynton, H. W.; Lodge, J. P. *Tellus* **1970**, *22*, 106–114.
(23) Sadasivan, S. *Atmos. Environ.* **1980**, *14*, 33–38.
(24) Falconer, R. E.; Falconer, P. D. *J. Geophys. Res.* **1980**, *85*, 7465–7470.
(25) May, K. R. *Q. J. R. Meteorol. Soc.* **1961**, *87*, 535–548.
(26) Mack, E.; Pilie, R. U.S. Patent 3 889 532, 1975.
(27) Brewer, R. L.; Ellis, E. C.; Gordon, R. J.; Shephard, L. S. *Atmos. Environ.* **1983**, *17*, 2267–2271.
(28) Israel, R.; Rosner, D. E. *Aerosol Sci. Technol.* **1983**, *2*, 45–51.
(29) Roach, W. T.; Brown, R.; Caughey, S. J.; Garland, J. A.; Readings, C. J. *Q. J. R. Meteorol. Soc.* **1976**, *102*, 313–333.
(30) Durham, M. D.; Lundgren, D. A. *J. Aerosol Sci.* **1980**, *11*, 179–188.
(31) Davies, C. N.; Subari, M. *J. Aerosol Sci.* **1982**, *13*, 59–71.
(32) Petrenchuk, O. P.; Aleksandrov, N. N. *Glavnoi Geofiz. Obs., Leningr. Tr.* **1966**, *185*, 126–132.
(33) Mohnen, V. A. *Atmos. Technol.* **1980**, *12*, 20–25.
(34) Durham, O. C. *J. Allergy* **1947**, *18*, 231–238.
(35) Perkins, W. A. Stanford University, Palo Alto, CA, 1957, second semiannual report.
(36) Asai, G. N. *Phytopathology* **1960**, *50*, 535–541.
(37) Hameed, R.; McMurry, P. H.; Whitby, K. T. *Aerosol Sci. Technol.* **1983**, *2*, 69–78.
(38) Hoerner, S. "Fluid-Dynamic Drag"; Hoerner Fluid Dynamics: Brick Town, NJ, 1965; pp 3/9, 3/17.
(39) Serafini, J. S. 1954, NACA Report 1159.
(40) Biswas, P.; Flagan, R. C. *Environ. Sci. Technol.* **1984**, *18*, 611–616.
(41) Hofschreuder, P.; Vrins, E.; van Boxel, J. *J. Aerosol Sci.* **1983**, *14*, 65–68.
(42) Drivas, P. J.; Shair, F. H. *Atmos. Environ.* **1974**, *8*, 1155–1163.
(43) Biswas, P., California Institute of Technology, Pasadena, CA, personal communication, 1983.
(44) Jiusto, J. E.; Lala, G. G. State University of New York at Albany, Albany, NY, 1983, ASRC-SUNY Publication 869.

Received for review August 8, 1983. Accepted May 15, 1984. This research was funded by the California Air Resources Board (A2-048-32) and the President's Fund of the California Institute of Technology.

APPENDIX XI

Reprinted from The Journal of Physical Chemistry, 1983, *87*, 5425.
Copyright © 1983 by the American Chemical Society and reprinted by permission of the copyright owner.

Kinetics and Mechanism of the Oxidation of Aquated Sulfur Dioxide by Hydrogen Peroxide at Low pH

James V. McArdle[†] and Michael R. Hoffmann*

W. M. Keck Laboratories, Environmental Engineering Science, California Institute of Technology, Pasadena, California 91125
(Received: January 21, 1983)

A stopped-flow kinetic study of the oxidation of sulfur dioxide by hydrogen peroxide was performed over the pH range 0.0–4.5. A rate expression of the following form was verified experimentally: $d[S(VI)]/dt = k_1K_{a1}[H_2O_2][S(IV)](k_2[H^+] + k_3[HA])/\{(k_{-1} + k_2[H^+] + k_3[HA])(K_{a1} + [H^+])\}$. The following kinetic parameters at 15 °C were determined: $k_1 = (2.6 \pm 0.5) \times 10^6\ M^{-1}\ s^{-1}$, $k_2/k_{-1} = 16 \pm 4\ M^{-1}$, $k_2/k_3 = (5 \pm 1) \times 10^2$ (HA = acetic acid), $\Delta H^{\ddagger}_1 = 37 \pm 2\ kJ\ mol^{-1}$, and $\Delta S^{\ddagger}_1 = 4 \pm 4\ J\ K^{-1}\ mol^{-1}$. The reaction proceeds via a nucleophilic displacement of HSO_3^- by H_2O_2 to form a peroxymonosulfurous acid intermediate which undergoes acid-catalyzed rearrangement to form product: $SO_2{\cdot}H_2O \rightleftharpoons HSO_3^- + H^+$ (K_{a1}), $H_2O_2 + HSO_3^- \rightleftharpoons HOOSO_2^-$ (k_1, k_{-1}), $HOOSO_2^- + H^+ \rightarrow H^+ + HSO_4^-$ (k_2), $HOOSO_2^- + HA \rightarrow HA + HSO_4^-$ (k_3). Application of the above rate expression to reactions occurring in hydrometeors is discussed.

The oxidation of sulfur dioxide by oxygen, ozone, nitrogen dioxide, or hydrogen peroxide in aqueous microdroplets or hydrometeors has been suggested as a non-photolytic pathway for the production of sulfuric acid in humid atmospheres.[1,2] Oxidation by H_2O_2 may be the

[†]Current address: Smithkline Beckman Corp., Philadelphia, PA 19101.

(1) Hoffmann, M. R.; Boyce, S. D. "Advances in Environmental Science and Technology"; Schwartz, S. E., Ed.; Wiley: New York, 1983; Vol. 12, pp 147–89.

preferred pathway due to favorable kinetics and thermodynamics at low pH. (The Henry's law equilibrium constant, represented by $H_{H_2O_2}$, for $H_2O_2(g) \rightleftharpoons H_2O_2(l)$ is 1.65×10^5 M atm^{-1}.) Hydrogen peroxide is generated in the gas phase by the recombination of hydroperoxyl radicals[3] and at air–water interfaces due to photoinduced redox processes.[4] Kok and co-workers[5] have reported hydrometeor concentrations of H_2O_2 as high as 50 μM.

The kinetics of this reaction have been studied previously by Mader,[6] Hoffmann and Edwards,[7] Penkett et al.,[8] and Martin and Damschen.[9] Mader[6] determined that S(IV) oxidation was characterized by a multiterm rate expression over the pH range 8–13. Evidence for specific and general acid catalysis by phosphate, carbonate, and arsenate was presented.[6] Hoffmann and Edwards reported a two-term rate law for the pH range 4–8 and proposed that the reaction occurs via a nucleophilic substitution by H_2O_2 on HSO_3^- to form a peroxymonosulfurous acid intermediate, which undergoes rearrangement assisted by H^+ or HA, to form HSO_4^-, where HA is a suitable weak acid such as phosphoric, citric, pivalic, acetic, or phthalic acid. Penkett et al.[8] confirmed the two-term rate law reported by Hoffmann and Edwards,[7] but they reported a hydrogen ion reaction order of 0.7 over the pH range 4–6 as opposed to an order of 1 in the aforementioned study. Results reported by Martin and Damschen[9] support the mechanism postulated by Hoffmann and Edwards. They found a single-term rate expression with a direct dependence on [H^+] from pH 1–3 and a reciprocal dependence on [H^+] below pH 1. It was our intention in undertaking this study to define carefully the dependence of rate on pH. Dasgupta[10] asserts that the data collected over the pH range of 0–13 by the above investigators[6-9] cannot be interpreted solely in terms of the Hoffmann and Edwards mechanism. He argues in favor of a radical pathway as a partial explanation for a variable pH dependency through the neutral domain.

With renewed interest in the reaction of H_2O_2 and S(IV) due to its potential importance to the production of atmospheric acidity,[11] we have decided to extend our earlier study to a pH domain (0–4) encountered in atmospheric water droplets and aquated urban aerosols. Of particular interest are the exact pH dependency, the role of general acid catalysis at low pH, and the contribution of free-radical pathways.

A. Methods

All kinetic measurements were made on a Durrum-Dionex Model D-110 stopped-flow spectrophotometer. Absorbance output was digitized with a Gould Biomation Model 2805 wave form analyzer equipped with a variable input sensitivity and variable sampling interval. One hundred data points were collected for each kinetic determination. At least six kinetic determinations were made for each value of k_{obsd}. Above pH 1.8, an average of 12 determinations was made for each value of k_{obsd}. Data were reduced by a DEC MINC-23 computer and were permanently stored on magnetic disks. Constant temperature was maintained at 15 °C with a Haake FK2 constant-temperature water bath. Water was circulated to the optical cuvette and reactant syringes by a $^1/_3$ hp Oberdorfer pump. A Beckman Altex Φ71 pH meter was used to determine [H^+] in buffered solutions. In unbuffered solutions, hydrogen ion concentrations were calculated by dilution of standardized HCl solution. Water used to prepare reagent solutions was obtained from a Milli-Q water purification system (Millipore) and had a resistivity of 18 MΩ-cm. Ionic strength (μ = 1.0 M) was maintained with sodium chloride, and all reagents were analytical grade. EDTA was used (10 μM) to inhibit trace-metal catalysis. The extent of reaction was monitored at 280 nm (the absorbance maximum for $SO_2(aq)$) for reactions at pH ≤1.8 (the pK_{a1} of $SO_2(aq)$) and at 220 nm for unbuffered reactions at pH >1.8. Loss of H_2O_2 and S(IV) contributes to the decrease in absorbance at 220 nm. The reaction at pH 0.5 was followed at both 220 and 280 nm to determine if k_{obsd} values are dependent upon the wavelength of observation. The concentration of S(IV) was determined directly by weight of Na_2SO_3 dissolved in a volumetric flask. The concentration of H_2O_2 in approximately 30% stock solution was determined periodically according to the method given by Wilson and Wilson.[12] In unbuffered solution, the total S(IV) concentration was 6×10^{-5} M except at pH 3.4 where it was 5×10^{-5} M in order to maintain an eightfold excess of hydrogen ion concentration, and the hydrogen peroxide concentration was at least 7 times the S(IV) concentration. In acetate-buffered solution, S(IV) was maintained in at least 10-fold excess over H_2O_2. The H_2O_2 concentration was 1×10^{-3} M, and the reaction was followed at 260 nm. In formate buffers, H_2O_2 was maintained in at least sevenfold excess over S(IV). Sulfur(IV) concentration was 2.4×10^{-4} M, and the reaction was followed at 220 nm. In solutions buffered by either trichloroacetic acid or bisulfate, the S(IV) concentration was 6×10^{-5} M, the H_2O_2 concentration was 4.24×10^{-4} M, and the reaction was followed at 280 nm.

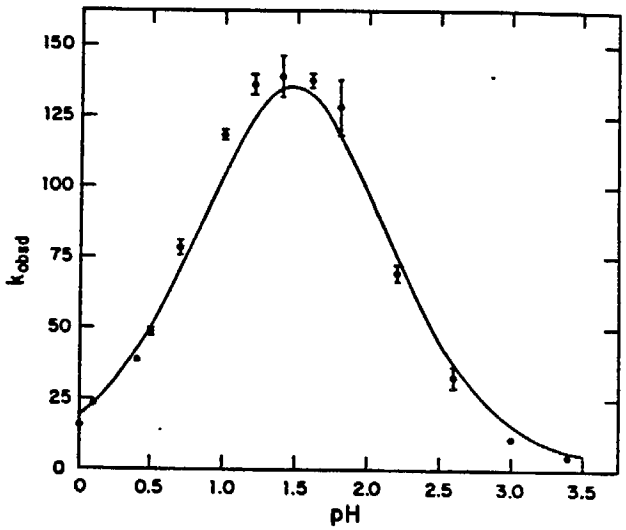

Figure 1. Dependence of k_{obsd} on pH for the oxidation of S(IV) by hydrogen peroxide at 15 °C. The solid line represents the least-squares fit to the data.

(2) Jacob, D. J.; Hoffmann, M. E. *J. Geophys. Res.* **1983**, *88*, 6611–21.
(3) Chaimedes, W. L.; Davis, D. D. *J. Geophys. Res.* **1982**, *87*, 4863–77.
(4) Zika, R. G.; Saltzman, E.; Chaimedes, W. L.; Davis, D. D. *J. Geophys. Res.* **1982**, *87*, 5015–7.
(5) (a) Kok, G. L.; Darnall, K. R.; Winer, A. M.; Pitts, J. N., Jr.; Gay, B. W. *Environ. Sci. Technol.* **1978**, *12*, 1077–80. (b) Kok, G. L. *Atmos. Environ.* **1980**, *14*, 653–6. (c) Richards, L. W.; Anderson, J. A.; Blumenthal, D. L.; McDonald, J. A. *Ibid.* **1983**, *17*, 911–14.
(6) Mader, P. M. *J. Am. Chem. Soc.* **1958**, *80*, 2634–9.
(7) Hoffmann, M. R.; Edwards, J. O. *J. Phys. Chem.* **1975**, *79*, 2096–8.
(8) Penkett, S. A.; Jones, B. M. R.; Brice, K. A.; Eggleton, A. E. J. *Atmos. Environ.* **1979**, *13*, 123–37.
(9) Martin, L. R.; Damschen, D. E. *Atmos. Environ.* **1981**, *15*, 1615–21.
(10) Dasgupta, P. K. *Atmos. Environ.* **1980**, *14*, 620–1.
(11) Waldman, J. M.; Munger, J. W.; Jacob, D. J.; Flagan, R. C.; Morgan, J. J.; Hoffmann, M. R. *Science* **1982**, *218*, 677–9.
(12) Wilson, C. L.; Wilson, D. W., Eds. "Comprehensive Analytical Chemistry"; Elsevier: New York, 1960; Vol. 1B, p 278.

TABLE I: Kinetic Data for the Oxidation of S(IV) by Hydrogen Peroxide in the Absence of Buffer at 15 °C[a]

pH	k_{obsd}, s^{-1}	k_{calcd}, s^{-1}
0.00	15.6 ± 0.3	18.6
0.10	23.8 ± 0.4	22.9
0.40	39.6 ± 0.6	41.6
0.50	48.8 ± 1.3	50.0
0.70	78.1 ± 2.6	70.0
1.00	119.6 ± 1.0	104.2
1.20	137.0 ± 4.0	123.6
1.40	139.4 ± 7.7	134.1
1.60	137.4 ± 2.8	132.2
1.80	128.0 ± 10.0	118.5
2.20	69.4 ± 2.9	74.6
2.60	32.7 ± 3.4	37.2
3.00	10.4 ± 0.4	16.4
3.40	5.2 ± 0.4	6.8

[a] $[H_2O_2] = 4.24 \times 10^{-4}$ M. [S(IV)] = 6×10^{-6} M except at pH 3.40 [S(IV)] = 5×10^{-5} M.

B. **Results**

For oxidation of S(IV) by H_2O_2 under pseudo-first-order conditions with hydrogen peroxide in excess, plots of ln $(A_t - A_\infty)$ vs. t were linear ($r^2 \geq 0.99$) for between 50% and 90% of the reaction. The linearity of the assumed first-order relationships establishes the fact that the rate of reaction is first order in S(IV). A study of the dependence of rate on the concentration of hydrogen peroxide was done at pH 0.4. A plot of k_{obsd} vs. hydrogen peroxide concentration up to 1.70 mM yields a straight line ($r^2 = 0.99$) with a slope of $(9.43 \pm 0.20) \times 10^4$ M^{-1} s^{-1} and an intercept of -0.1 ± 1.2 s^{-1}. Thus, the rate of reaction is also first order in hydrogen peroxide. The dependence of k_{obsd} on pH in the absence of a buffer is shown by the experimental points in Figure 1 and is listed in Table I. The pH dependence at low pH may be investigated further by plotting k_{obsd} vs. the reciprocal of the proton concentration. Such a plot for the pH range 0.0–0.7 yields a straight line ($r^2 = 0.96$) with a slope of 15.4 ± 0.3 M s^{-1} and an intercept of 1.5 ± 0.5 s^{-1}. The data from pH 2.6 to 3.4 also yield a reasonable straight line ($r^2 = 0.96$) when k_{obsd} is plotted against the proton concentration (slope = $(10.0 \pm 0.8) \times 10^3$ M^{-1} s^{-1} and intercept = 0.7 ± 0.7). Thus, the rate becomes inversely first-order dependent on hydrogen ion at low pH, and it becomes directly first-order dependent on hydrogen ion at higher pH. Data for pH 0.5 were collected at two wavelengths. At 280 nm with $[H_2O_2] = 4.24 \times 10^{-4}$ M and [S(IV)] = 6×10^{-6} M, k_{obsd} was found to be 48.7 ± 1.2 s^{-1}, and at 220 nm with the same reagent concentrations k_{obsd} was found to be 49.0 ± 1.6 s^{-1}.

Earlier investigations showed that the oxidation of S(IV) by hydrogen peroxide is sensitive to general acid catalysis.[6-8] In acetate buffer of pH 4.45 with S(IV) present in excess, plots of ln $(A_t - A_\infty)$ vs. t were linear for about 90% of the reaction and established that the rate of reaction is first order in hydrogen peroxide. A plot of k_{obsd} vs. the concentration of S(IV) up to 49.5 mM with the acetic acid concentration equal to 30.0 mM is linear ($r^2 = 0.99$) with a slope of $(1.51 \pm 0.09) \times 10^3$ M^{-1} s^{-1} and an intercept of -0.2 ± 1.2. This plot establishes a first-order dependence on S(IV). Figure 2 demonstrates that two pathways are operating in the oxidation of S(IV) by hydrogen peroxide in the presence of acetic acid. One pathway has a first-order dependence on acetic acid, and the rate of the other pathway is independent of acetic acid. The data in Figure 2 at 15 °C yield a slope of $(2.98 \pm 0.18) \times 10^4$ M^{-2} s^{-1} and an intercept of $(6.0 \pm 0.9) \times 10^2$ M^{-1} s^{-1} with $r^2 = 0.99$.

The dependence of k_{obsd} on formic acid at pH 3.40 is listed in Table II. A linear dependence of k_{obsd} on formic acid was not observed. The dependence of k_{obsd} on either

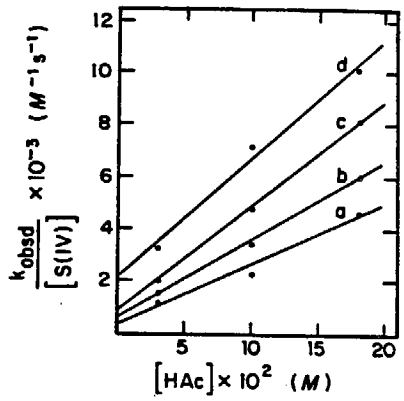

Figure 2. Dependence of $k_{obsd}/[S(IV)]$ on the concentration of acetic acid for the oxidation of S(IV) by H_2O_2 at pH 4.45; [S(IV)] = 10.0 and 20.0 mM for each point: (a) 6, (b) 15, (c) 21, (d) 30 °C.

TABLE II: Kinetic Data for the Oxidation of S(IV) by Hydrogen Peroxide in the Presence of Buffers at 15 °C

pH	HA[a]	[HA], M	k^b
3.40	formic	1.0×10^{-2}	20.2 ± 1.6
3.40	formic	5.0×10^{-2}	41.7 ± 3.4
3.40	formic	1.5×10^{-1}	73.2 ± 8.5
0.71	Cl_3AcOH	2.0×10^{-3}	14.9 ± 0.3
0.72	Cl_3AcOH	5.0×10^{-3}	14.5 ± 0.2
0.64	Cl_3AcOH	5.0×10^{-2}	17.3 ± 0.6
0.62	Cl_3AcOH	1.0×10^{-1}	16.0 ± 0.8
0.65	HSO_4^-	5.0×10^{-4}	16.2 ± 0.7
0.69	HSO_4^-	5.0×10^{-3}	16.9 ± 0.7
0.69	HSO_4^-	5.0×10^{-2}	17.9 ± 0.4
0.65	HSO_4^-	1.0×10^{-1}	18.7 ± 0.8
0.64	HSO_4^-	2.0×10^{-1}	18.1 ± 0.7

[a] Cl_3AcOH = trichloroacetic acid. [b] Quantities reported are k_{obsd} (s^{-1}) for formic acid and $k_{obsd}[H^+]$ (M s^{-1}) for Cl_3AcOH and HSO_4^-. The quantity $k_{obsd}[H^+]$ is reported in the latter two cases to compensate for the slightly varying values of pH according to eq 10.

trichloroacetic acid or bisulfate at pH ~0.7 also is listed in Table II. The pH of individual solutions varied slightly so a correction is made by comparing $k_{obsd}[H^+]$ to [HA]. Inspection of the data in Table II shows the $k_{obsd}[H^+]$ varies by a factor of 1.3 for a general acid concentration that varies by a factor of 400 in the case of bisulfate. Therefore, k_{obsd} appears to be independent of either trichloroacetic acid or bisulfate at pH ~0.7.

The above kinetic information is consistent with the following mechanism:

$$SO_2(aq) \overset{\text{fast}}{\rightleftharpoons} H^+ + HSO_3^- \qquad (K_{a1}) \qquad (1)$$

$$HSO_3^- + H_2O_2 \underset{k_{-1}}{\overset{k_1}{\rightleftharpoons}} \text{peroxomonosulfate} + H_2O \qquad (K) \qquad (2)$$

$$\text{peroxomonosulfate} + H^+ \xrightarrow{k_2} H_2SO_4 \qquad (3)$$

$$\text{peroxomonosulfate} + HA \xrightarrow{k_3} H_2SO_4 + A^- \qquad (4)$$

This mechanism is similar to the mechanism originally postulated by Hoffmann and Edwards[7] and is consistent with the absence of dithionate as a product.[7] According to this mechanism the rate of appearance of product is given by

$$v = d[H_2SO_4]/dt = k_2[H^+][O_2SOOH^-] + k_3[HA][O_2SOOH^-] \qquad (5)$$

From steady-state considerations the concentration of the

peroxymonosulfurous acid intermediate, $HOOSO_2^-$, may be obtained.

$$[HOOSO_2^-] = k_1[H_2O_2][HSO_3^-]/\{k_{-1} + k_2[H^+] + k_3[HA]\} \quad (6)$$

The concentration of HSO_3^- may be expressed as a function of total S(IV).

$$[HSO_3^-] = [S(IV)]K_{a1}/\{K_{a1} + [H^+]\} \quad (7)$$

Substitution of eq 7 into eq 6 and then eq 6 into eq 5 yields

$$r = \frac{k_1K_{a1}[H_2O_2][S(IV)]}{(k_{-1} + k_2[H^+] + k_3[HA])(K_{a1} + [H^+])}(k_2[H^+] + k_3[HA]) \quad (8)$$

This rate law applies to the entire pH range in this study. In the absence of buffer and with hydrogen peroxide in excess, k_{obsd} is given by

$$k_{obsd} = k_1k_2K_{a1}[H^+][H_2O_2]/\{(k_{-1} + k_2[H^+])(K_{a1} + [H^+])\} \quad (9)$$

Equation 9 also applies to the entire pH range studied. Estimates of the various parameters in eq 9 may be obtained by considering behavior at the extremes of pH. At low pH, $[H^+] \gg K_{a1}$. (The value of K_{a1} at 15 °C is 1.82×10^{-2} M.[13] See discussion below.) The observed inverse first-order dependence on hydrogen ion at low pH requires that $k_2[H^+] \gg k_{-1}$. Equation 9 reduces to

$$k_{obsd} = k_1K_{a1}[H_2O_2]/[H^+] \quad (10)$$

from pH 0.0 to ~0.7 with $k_1 = (2.06 \pm 0.05) \times 10^6$ M^{-1} s^{-1}. A temperature-dependence study at pH 0.40 gave $\Delta H^{\ddagger}_1 = 37 \pm 2$ kJ mol^{-1} and $\Delta S^{\ddagger}_1 = 4 \pm 4$ J K^{-1} mol^{-1} (or 8.8 kcal mol^{-1} and 1.0 cal K^{-1} mol^{-1}, respectively) for the forward reaction of eq 2. The temperature dependence of K_{a1} is given by Deveze and Rumpf.[13] At higher pH, the first-order dependence on hydrogen ion requires that $k_{-1} \gg k_2[H^+]$. At pH 2.6, $K_{a1} = 7.25[H^+]$. Thus, at pH values above 2.6, eq 9 reduces to

$$k_{obsd} \simeq (k_1k_2/k_{-1})[H^+][H_2O_2] \quad (11)$$

$$k_{obsd} \simeq k_2K[H^+][H_2O_2] \quad (12)$$

with $k_2K \simeq 2.4 \times 10^7$ M^{-2} s^{-1} and $k_2/k_{-1} \simeq 12$ M^{-1}. At pH 4.45 in the presence of acetic acid and with S(IV) present in excess, the rate expression is

$$k_{obsd} = k_1[S(IV)](k_2[H^+] + k_3[HA])/(k_{-1} + k_3[HA]) \quad (13)$$

The linear dependence of rate on acetic acid shown in Figure 2 indicates that $k_{-1} \gg k_3[HA]$ for concentrations of acetic acid up to 0.18 M. A pseudo-second-order constant may be calculated by dividing eq 13 by the S(IV) concentration.

$$k_{obsd}/[S(IV)] = k_1k_2[H^+]/k_{-1} + k_1k_3[HA]/k_{-1} \quad (14)$$

At 15 °C, $k_3K = (3.0 \pm 0.2) \times 10^4$ M^{-2} s^{-1}, $k_2K = (1.7 \pm 0.3) \times 10^7$ M^{-2} s^{-1}, $k_2/k_3 = (5 \pm 1) \times 10^2$, and $k_{-1}/k_3 \simeq 44$ M.

The parameters obtained in the absence of buffer were further refined by using nonlinear least-squares analysis in which the function minimized is Φ.

$$\Phi = \sum_{i=1}^{n} [(k_{obsd} - k_{calcd})wts(i)]^2 \quad (15)$$

where

$$wts(i) = \sigma(i)^{-2} \quad (16)$$

The values of k_{obsd} were calculated according to eq 9 and the trial parameters were those found in the high- and low-pH regions as described above. Values of the parameters obtained after least-squares refinement are $k_1 = (2.6 \pm 0.5) \times 10^6$ M^{-1} s^{-1} and $k_2/k_{-1} = 16 \pm 4$ M^{-1}. The solid line in Figure 1 is a plot of k_{obsd} using these values for the parameters. Calculated values of pseudo-first-order rate constants (k_{calcd}) are compared to the experimental values in Table I.

C. Discussion

The mechanism presented herein is essentially the same as previously postulated for the pH range 4–8.[7] However, the present mechanism assumes that the formation of HSO_3^- from SO_2(aq) is fast compared to other steps in the mechanism. Unfortunately, there is no agreement in the literature on the rate of formation of HSO_3^-. Reported rate constants vary by 10 orders of magnitude from 2.18×10^{-2} (20 °C)[14] to 1.06×10^8 (20 °C) s^{-1}.[15] The absence of first-order rate-limiting behavior in this study means that, according to our mechanism, the rate of formation of HSO_3^- must be greater than 160 s^{-1} (the largest k_{obsd} measured). This value is consistent with some reports in the literature[15-17] but inconsistent with others.[14] However, the rate reported by Wang and Himmelblau[14] has been criticized for being too low.[18] A more recent study by Roberts[16] establishes a lower specific rate of 320 s^{-1}. Thus, it is likely that the formation of HSO_3^- is fast compared to other steps in the mechanism.

There is a similar disagreement over values for K_{a1}, but the values have a smaller range. Huss and Eckert[19] critically reviewed reported values of K_{a1} and reevaluated K_{a1} at 25 °C by independent conductometric and spectrophotometric methods. The value determined by either method agrees well with the earlier temperature-dependent study of Deveze and Rumpf.[13] Because the temperature-dependent data are needed in this work, the values of Deveze and Rumpf[13] have been used. The thermodynamic acid-dissociation constant was given for dilute solutions. However, the present data were collected at an ionic strength of 1.0 M. Clarke[20] has discussed the importance of ionic strength effects in the kinetics of aqueous sulfur dioxide. To account for ionic strength effects, a correction of the acid-dissociation constant reported by Deveze and Rumpf[13] was made according to the Davies approximation:

$$\log \gamma = -Az^2\left(\frac{\mu^{1/2}}{1 + \mu^{1/2}} - 0.2\mu\right) \quad (17)$$

where $A = (1.82 \times 10^6)(\epsilon T)^{-3/2}$ (ϵ = dielectric constant). Application of eq 17 yields values of $k_1 = 1.3 \times 10^6$ M^{-1} s^{-1}, $\Delta H^{\ddagger}_1 = 8.8 \pm 0.5$ kcal mol^{-1}, and $\Delta S^{\ddagger} = -1 \pm 1$ cal K^{-1} mol^{-1}. By comparison to these parameters reported in the Results section, it is seen that corrections for ionic strength effects are not large.

A near-zero activation entropy is expected for a reaction between a singly charged ion and a neutral molecule[21] as

(13) Deveze, D.; Rumpf, P. *C. R. Hebd. Seances Acad. Sci.* **1964**, *258*, 6135–8.

(14) Wang, J. C.; Himmelblau, D. M. *AIChE J.* **1964**, *10*, 574–80.
(15) Betts, R. H.; Voss, R. H. *Can. J. Chem.* **1970**, *48*, 2035–41.
(16) (a) Roberts, D. L. Ph.D. Thesis, California Institute of Technology, 1979, Pasadena, CA, pp 26, 162. (b) Roberts, D. L.; Friedlander, S. K. *AIChE J.* **1980**, *26*, 593–610.
(17) Eigen, M.; Kustin, K.; Maass, G. *Z. Phys. Chem.* **1961**, *30*, 130–6.
(18) Beilke, S.; Lamb, D. *AIChE J.* **1975**, *21*, 402–4.
(19) Huss, A., Jr.; Eckert, C. A. *J. Phys. Chem.* **1977**, *81*, 2268–70.
(20) Clarke, A. G. *Atmos. Environ.* **1981**, *15*, 1591–5.

in the forward reaction of eq 2. A possible structure for the transition-state complex is the following:

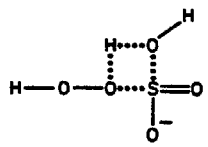

The activated complex retains the same charge as the sum of the charges of the reactants; therefore, the degree of solvent ordering, which is largely responsible for the entropy of a system, is not expected to change. If the transition state does resemble the structure suggested above, then it is easy to see that HSO_3^- should be a much more reactive species than SO_3^{2-} because water is a more effective leaving group than hydroxide. The structure of $SO_2(aq)$ is not known with certainty, but the existence of H_2SO_3 in solution has never been demonstrated. Hydrated but uncombined SO_2 is the principal if not exclusive form of sulfur dioxide in solution,[16] and the transition-state complex pictured above would be difficult to attain from $SO_2(aq)$ in acidic solution. Very negative values of ΔS^* for reactions between an ion and a neutral molecule have been attributed to bond formation between substrate and nucelophile *before* departure of the leaving group.[21] Since ΔS^* is near zero, a mechanism of the latter type is unlikely in the present case. Activation parameters reported by Penkett et al.[8] for this reaction have little meaning because they simply reflect the temperature dependence of k_{obsd}. Other arguments supporting the peroxymonosulfurous acid intermediate have been presented previously.[7]

Further support for the postulated mechanism of eq 1–4 comes from agreement of the value of k_2K in unbuffered solution at pH 2.6–3.4 (2.4×10^7 M^{-2} s^{-1}) and the value of the same parameter from the intercept of the data in Figure 2 (1.7×10^7 M^{-2} s^{-1}).

The absence of a contribution by a free-radical pathway to the mechanism was ascertained at pH 0.50 by making kinetic determinations in the presence of the free-radical scavenger mannitol, present in 4×10^{-5} M concentration. The average value of k_{obsd} obtained in the presence of mannitol is 48.4 ± 1.0 s^{-1} with $[H_2O_2] = 4.24 \times 10^{-4}$ M and $[S(IV)] = 6 \times 10^{-5}$ M. In the absence of mannitol, k_{obsd} was determined to be 48.8 ± 1.3 s^{-1} with the same reagent concentrations. Mannitol has been used as a free-radical scavenger in the autooxidation of SO_3^{2-}.[22]

The dependence of rate on acetic acid was noted earlier by Penkett.[8] The value of k_2/k_3 reported herein is about one-sixth that of the earlier value, however, and no obvious reason exists to explain this discrepancy. A similar analysis of the data of Hoffmann and Edwards[7] yields $k_2/k_3 = 2.5 \times 10^5$ for the reaction carried out in the presence of $H_2PO_4^-$. For at least these two acids, therefore, k_3 varies qualitatively with K_{HA} as predicted by the Bronsted equation (eq 18):[23]

$$k_3 = G_A K_{HA}^{\alpha} \tag{18}$$

where G_A and α are constants.

The absence of a linear dependence of rate on the concentration of formic acid may be due to the failure of the inequality $k_{-1} \gg k_3[HA]$. If, at higher concentrations of HA, $k_{-1} \simeq k_3[HA]$, then the behavior predicted is first-order linear dependence of rate on HA at very low concentrations of HA and no dependence of rate on HA at very high concentrations of HA. The independence of the observed rate on HA at pH 0.7 simply reflects the fact that at high proton concentration $k_2[H^+] \gg k_3[HA]$.

The rate of aqueous-phase oxidation of S(IV) from pH 1 to 5 in an open atmosphere can be calculated by substituting eq 19 and 20 into eq 8. The symbol P represents

$$[H_2O_2] = P_{H_2O_2} H_{H_2O_2} \tag{19}$$

$$[S(IV)] = P_{SO_2} H_{SO_2}([H^+] + K_{a1})/[H^+] \tag{20}$$

partial pressure. Assuming the absence of any appreciable concentration of a general acid and evaluating the rate constants yields

$$r = \frac{(7.6 \times 10^5\ M^{-1}\ s^{-1}) P_{H_2O_2} H_{H_2O_2} P_{SO_2} H_{SO_2}}{1.0 + 16\ M^{-1}[H^+]} \tag{21}$$

The rate law given here agrees with that of Martin and Damschen[9] and the predictions of atmospheric reactivity rate also agree well. At 15 °C, $H_{H_2O_2} = 1.65 \times 10^5$ M atm^{-1} (ref 9), $H_{SO_2} = 1.67$ M atm^{-1} (ref 24), and assuming pH 3.0, $P_{H_2O_2} = P_{SO_2} = 1$ ppb, the rate of appearance of S(VI) is 7.4×10^{-4} M h^{-1}. As is obvious from eq 21 there is little dependence of rate on pH from 2 to 5. According to the treatment of Schwartz[25] and Schwartz and Freiberg,[26] the aqueous-phase reaction is not limited by mass transport until the atmospheric concentration of either reagent reaches about 100 ppb. This conclusion is independent of pH. The rate-limiting concentration of either reagent is far above estimates for typical atmospheric conditions, and thus it appears that under all but the most extreme conditions eq 21 will correctly predict the aqueous-phase rate of oxidation of SO_2 by H_2O_2. The absence of mass-transport limitation in the present reaction directly contradicts an earlier conclusion.[9]

In preliminary investigations, the presence of either iron(II) or formaldehyde in the reaction mixtures described above has been found to alter markedly the reaction kinetics. These effects are now being studied in detail and will be the subject of forthcoming reports.

Acknowledgment. We are grateful to the U.S. Environmental Protection Agency (R808086-1) for providing financial support for this research and to the Sloan Foundation Fund administered by Caltech which provided the necessary instrumentation.

Registry No. SO_2, 7446-09-5; H_2O_2, 7722-84-1; H_2SO_4, 7664-93-9; HSO_4^-, 14996-02-2; $HOOSO_2^-$, 87712-70-7; sulfate, 14808-79-8.

(21) Moore, J. W.; Pearson, R. G. "Kinetics and Mechanism", 3rd ed.; Wiley: New York, 1981, pp 260–72.
(22) Bäckström, H. L. J. *J. Am. Chem. Soc.* **1927**, *49*, 1460–72.
(23) Edwards, J. O. "Inorganic Reaction Mechanisms"; Benjamin: New York, 1964; p 18.
(24) Rabe, A. E.; Harris, J. F. *J. Chem. Eng. Data* **1963**, *8*, 333–6.
(25) Schwartz, S. E. In "Acid Precipitation: SO_2, NO, NO_2 Oxidation Mechanisms"; Calvert, J. G., Ed.; Ann Arbor Science: Ann Arbor, MI, in press.
(26) Schwartz, S. E.; Freiberg, J. E. *Atmos. Environ.* **1981**, *15*, 1129–44.

J. Phys. Chem. 1984, *88*, 4740–4746

Kinetics and Mechanism of the Formation of Hydroxymethanesulfonic Acid at Low pH

Scott D. Boyce[†] and Michael R. Hoffmann*

Environmental Engineering Science, W. M. Keck Laboratories, California Institute of Technology, Pasadena, California 91125 (Received: September 20, 1983)

A spectrophotometric kinetic study of the reaction of sulfur dioxide with formaldehyde to form hydroxymethanesulfonic acid in aqueous solution was performed over the pH range 0.0 to 3.5. A kinetic expression of the following form was verified experimentally: $-d[S(IV)]/dt = \{(k_1\alpha_1 + k_2\alpha_2)K_d/(K_d + 1)\}[S(IV)][CH_2O]_t$ where $[CH_2O]_t = [CH_2(OH)_2] + [CH_2O]$, $K_d = k_d/k_{-d} = [CH_2O]/[CH_2(OH)_2]$, $[S(IV)] = [SO_2{\cdot}H_2O] + [HSO_3^-] + [SO_3^{2-}]$, $\alpha_1 = [HSO_3^-]/[S(IV)] = K_{a1}[H^+]/([H^+]^2 + K_{a1}[H^+] + K_{a1}K_{a2})$, $\alpha_2 = [SO_3^{2-}]/[S(IV)] = K_{a1}K_{a2}/([H^+]^2 + K_{a1}[H^+] + K_{a1}K_{a2})$, $K_{a1} = [H^+][HSO_3^-]/[SO_2{\cdot}H_2O]$, and $K_{a2} = [H^+][SO_3^{2-}]/[HSO_3^-]$. The following kinetic parameters were determined at 25 °C and $\mu = 1.0$ M: $k_1 = (7.90 \pm 0.32) \times 10^2$ M^{-1} s^{-1}, $k_2 = (2.48 \pm 0.05) \times 10^7$ M^{-1} s^{-1}, $\Delta H_1^* = (24.9 \pm 0.8)$ kJ mol^{-1}, $\Delta S_1^* = (-108.0 \pm 2.6)$ J mol^{-1} K^{-1}, $\Delta H_2^* = (20.4 \pm 0.5)$ kJ mol^{-1}, and $\Delta S_2^* = (-31.7 \pm 1.6)$ J mol^{-1} K^{-1} for values of $K_d = 5.50 \times 10^{-4}$, $K_{a1} = 1.45 \times 10^{-2}$ M, and $K_{a2} = 6.31 \times 10^{-8}$ M. Application of the Davies approximation ($\log \gamma = -Az^2\{\mu^{1/2}/(1 + \mu^{1/2}) - 0.2\mu\}$) to correct for ionic strength effects yielded ${}^c k_1 = (4.51 \pm 0.15) \times 10^2$ M^{-1} s^{-1} and ${}^c k_2 = (5.42 \pm 0.07) \times 10^6$ M^{-1} s^{-1} for concentration-dependent equilibrium constants ${}^c K_{a1} = K_{a1}\gamma_{SO_2{\cdot}H_2O}/\gamma_{H^+}\gamma_{HSO_3^-} = 2.92 \times 10^{-2}$ M and ${}^c K_{a2} = K_{a2}\gamma_{HSO_3^-}/\gamma_{H^+}\gamma_{SO_3^{2-}} = 2.58 \times 10^{-7}$ M. The reaction proceeds via each of two parallel pathways involving the nucleophilic addition of HSO_3^- and SO_3^{2-} to the carbonyl C-atom of formaldehyde as follows: $CH_2(OH)_2 \underset{k_{-d}}{\overset{k_d}{\rightleftharpoons}} CH_2O + H_2O$ (fast); $SO_2{\cdot}H_2O \overset{K_{a1}}{\rightleftharpoons} H^+ + HSO_3^-$ (fast); $HSO_3^- \overset{K_{a2}}{\rightleftharpoons} H^+ + SO_3^{2-}$ (fast); $HSO_3^- + CH_2O \overset{k_1}{\rightarrow} CH_2(OH)SO_3^-$ (slow); $SO_3^{2-} + CH_2O \overset{k_2}{\rightarrow} CH_2(O^-)SO_3^-$ (slow); $CH_2(O^-)SO_3^- + H^+ \overset{K_{a2}^{(HMSA)}}{\rightleftharpoons} CH_2(OH)SO_3^-$ (fast). Previous investigations of this reaction have demonstrated that the dehydration of methylene glycol, $CH_2(OH)_2$, to form CH_2O becomes rate limiting under neutral pH conditions. The experimental data obtained in the present study indicate that rate of CH_2O production from $CH_2(OH)_2$ is strongly influenced by specific acid catalysis. Application of the aforementioned results to liquid-phase reaction processes occurring in atmospheric microdroplets is discussed.

A Introduction

The reaction of formaldehyde with sulfur dioxide to form hydroxymethanesulfonate has been suggested as a viable pathway for the stabilization of SO_2 with respect to oxidation by hydrogen peroxide dissolved in atmospheric microdroplets.[1] At low pH, the oxidation of S(IV) by H_2O_2 proceeds rapidly to yield sulfuric acid. However, a recent investigation by McArdle and Hoffmann[2] has shown that the presence of formaldehyde in aqueous solution dramatically alters the kinetics of sulfate production. Formaldehyde is generated naturally in the gas phase at low concentration (P_{CH_2O} = 2–6 ppb) by the reaction of methane with hydroxyl radical.[3] The reaction of CH_2O and SO_2 may occur readily in the condensed phase due to the favorable thermodynamics for the dissolution of formaldehyde ($H_{CH_2O} = 6.30 \times 10^3$ M atm^{-1})[4] and sulfur dioxide (1.26 M atm^{-1})[5] in water. Klippel and Warneck[6] have detected formaldehyde in rainwater at concentrations in excess of 5.8 μM and Munger and co-workers[1a] and Richards et al.[1b] have reported the coexistence of CH_2O, S(IV), and H_2O_2 in fogwater and cloudwater samples collected from a polluted atmosphere.

The kinetics of hydroxymethanesulfonate formation have been studied previously by Wagner,[7] Jones and Oldham,[8] Skrabal and Skrabal,[9] Sorensen and Andersen,[10] and Bell and Evans.[11] Wagner[7] determined that the kinetics of reaction under neutral and alkaline pH conditions conformed to a two-term rate law in which the rate of S(IV) consumption exhibited first-order dependecies on the concentrations of formaldehyde, bisulfite, and/or sulfite. A subsequent analysis of Wagner's data by Jones and Oldham[8] indicated that HSO_3^- was the only reactant to undergo reaction with CH_2O. Conversely, Skrabal and Skrabal[9] obtained evidence that showed that the reactivity of SO_3^{2-} was much greater than bisulfite ion. These findings were later confirmed by Sorensen and Andersen[10] for reactions conducted in strongly alkaline solution (pH 9–12). Bell and Evans[11] proposed that production of hydroxymethanesulfonate occured by the rapid nucleophilic addition of sulfite to formaldehyde following rate-limiting dehydration of methylene glycol, which is the principal species of formaldehyde in aqueous solution.

From the preceeding discussion, it is apparent that considerable ambiguity exists as to the detailed mechanism of reaction between S(IV) and formaldehyde. The primary objective of the current investigation is to evaluate the kinetics of this reaction in dilute aqueous solution for a pH domain (0.0–3.5) characteristic of water droplets and aqueous aerosols encountered in a polluted urban atmosphere. Particular emphasis is directed toward an assessment of the reaction rate dependency on pH and the relative reactivity of $SO_2{\cdot}H_2O$, HSO_3^-, and SO_3^{2-}.

B. Experimental Procedure

Materials. Reagent grade chloroacetic acid (MCB), dichloroacetic acid (MCB), formaldehyde (37% solution, Mallinckrodt), formic acid (Mallinckrodt), hydrochloric acid (Mallinckrodt), phosphoric acid (Spectrum), sodium hydroxide (Mallinckrodt), monobasic sodium phosphate (Mallinckrodt), and sodium sulfite (Mallinckrodt) were utilized without further purification for the preparation of the pH buffers and reagent solutions. Sodium chloride (Mallinckrodt) was employed to maintain constant ionic strength (μ = 1.0 M). The solutions were prepared in a glovebox under a nitrogen atmosphere with deionized water (18 MΩ cm resistivity) obtained from a Milli RO-4/Milli Q (Millipore) water purification system. The water was deoxygenated by purging with N_2 prior to the preparation of the solutions. A Beckman Altex Model Φ71 pH meter was used to

[†] Present address: The PQ Corporation, Research & Development Center, 280 Cedar Grove Rd., Lafayette Hill, PA 19444

(1) (a) Munger, J. W.; Jacob, D. J.; Waldman, J. M.; Hoffmann, M. R. *J. Geophys. Res.* 1983, *88*, 5109–21. (b) Richards, L. W.; Anderson, J. A.; Blumenthal, D. L., McDonald, J. A.; Kok, G. L.; Lazrus, A. L. *Atmos. Environ.* 1983, *17*, 911–4.
(2) McArdle, J. V.; Hoffmann, M. R. *J. Phys. Chem.* 1983, *87*, 5425–9.
(3) "Formaldehyde and Other Aldehydes"; National Research Council, National Academy Press: Washington, DC, 1981; pp 1–340.
(4) Ledbury, W.; Blair, E. W. *J. Chem. Soc.* 1925, 2832–9.
(5) Johnstone, H. F.; Leppla, P. W. *J. Am. Chem. Soc.* 1934, *56*, 2233–8.
(6) Klippel, W.; Warneck, P. *Atmos. Environ.* 1980, *14*, 809–18.
(7) Wagner, C. *Ber. Dtsch. Chem. Ges.* 1929, *62*, 2873–7.
(8) Jones, P.; Oldham, K. B. *J. Chem. Educ.* 1963, *40*, 366–7.
(9) Skrabal, A.; Skrabal, R. *Sitz. Akad. Wirs. Wien.* 1936, *145*, 617–47.
(10) Sorensen, P. E.; Andersen, V. S. *Acta Chem. Scand.* 1970, *24*, 1301–6.
(11) Bell, R. P.; Evans, F. R. S.; Evans, P. G. *Proc. R. Soc. London, Ser. A* 1966, *291*, 297–323.

TABLE I: Kinetic Data for the Reaction of S(IV) and Formaldehyde in Aqueous Solution[a]

pH	10^3[S(IV)], M	$10[CH_2O]_t$, M	$10^4(k_{obsd} \pm \sigma)$,[b] s^{-1}	$10^4 k_{calcd}$,[c] s^{-1}	$10^4 {}^c k_{calcd}$,[d] s^{-1}
0.0	0.25	1.00	7.24 ± 0.08	6.20	7.10
0.3	0.25	1.00	11.90 ± 0.74	12.30	13.90
0.6	0.25	1.00	21.50 ± 0.21	23.90	26.30
1.0	0.25	0.50	23.30 ± 0.82	28.00	29.30
1.3	0.25	0.20	15.60 ± 0.52	20.30	19.70
1.5	0.25	0.20	24.10 ± 0.29	28.80	26.40
1.9	0.50	0.20	42.90 ± 1.84	53.80	44.30
2.2	0.50	0.10	33.90 ± 1.87	39.80	31.60
2.5	1.25	0.10	58.30 ± 0.73	58.00	46.60
2.8	1.25	0.10	81.70 ± 7.62	88.30	74.20
3.1	1.25	0.10	135.00 ± 15.20	143.00	127.00
3.4	1.25	0.10	226.00 ± 23.00	253.00	233.00

[a] [S(IV)] = (0.25–1.25) × 10^{-3} M, [CH_2O] = 0.01–0.1 M, μ = 1.0 M, T = 25 °C. [b] $\sigma = \{(k_{obsd} - \bar{k}_{obsd})^2/N\}^{1/2}$ where $N = 4$. [c] k_{calcd} refers to calculated pseudo-first-order rate constants obtained from the thermodynamic equilibrium constants K_{a1} and K_{a2} in the theoretical rate expression given by eq 14. [d] ${}^c k_{calcd}$ refers to calculated pseudo-first-order rate constants obtained from ${}^c K_{a1}$ and ${}^c K_{a2}$ in the theoretical rate expression given by eq 14.

measure [H^+] in the buffer solutions. In unbuffered systems, the prescribed pH(−log [H^+]) was attained by dilution of a standardized HCl solution.

Methods. Kinetic measurements were performed with a Hewlett-Packard Model 8450A UV/vis spectrophotometer. The extent of reaction was monitored at 280 nm (λ_{max} for $SO_2{\cdot}H_2O$). Absorbance data were analyzed on a Digital Equipment Corporation MINC 23 computer. Observed pseudo-first-order rate constants, k_{obsd}, were determined from the slopes of plots of ln (A_{280}) as a function of time. From 20 to 200 data points were collected for each kinetic analysis and an average of four determinations was calculated for each value of k_{obsd}. Experiments were conducted directly in a water-jacketed quartz cell of 10-cm path length. Constant temperature was maintained at 25 °C (and other desired values) through the use of a Haake Model FK-2 water recirculation bath and temperature controller. Reagent solutions were prepared by dilution of an appropriate volume of either 0.1 or 1.0 M Na_2SO_3 and 37% aqueous formaldehyde with buffer in a volumetric flask. The concentrations of S(IV) and CH_2O in the stock solutions were determined periodically by standard iodometric titration procedures described by Skoog and West[12] and Kolthoff et al.[13] The reactions were initiated by mixing the reagent solutions after they had been allowed to attain thermal equilibrium for 15 min. Sulfur(IV) concentrations ranged from 0.25 to 10 mM and $[CH_2O]_t$ varied from 0.08 to 250 mM.

C. Results

For the reaction of S(IV) with formaldehyde under pseudo-first-order concentration conditions, i.e., $[CH_2O]_t >> [S(IV)]$ and $[S(IV)] >> [CH_2O]_t$, at pH ≤3, plots of ln $\{(A_t - A_\infty)/(A_0 - A_\infty)\}$ vs. time were linear ($R^2 > 0.99$) for greater than 90% of the reaction. At pH >3, the absorbance at λ = 280 nm due to $SO_2{\cdot}H_2O$ became very small. Consequently, the decrease in the signal-to-noise ratio prevented the collection of reproducible absorbance data at reaction times exceeding 1–1.5 half-lives (1 − $1.5t_{1/2}$). The linearity of the relationship between ln $\{(A_t - A_\infty)/(A_0 - A_\infty)\}$ and time for $[CH_2O]_t >> [S(IV)]$ demonstrates that the rate of hydroxymethanesulfonate production is first order with respect to [S(IV)]. Confirmation of this result was obtained by examining the dependence of the observed pseudo-first-order rate constant, k_{obsd}, on [S(IV)] in the presence of formaldehyde as the limiting reagent (i.e., $[S(IV)] >> [CH_2O]_t$). For example, a plot of k_{obsd} as a function of sulfur(IV) concentration (Figure 1) yielded a straight line (R^2 = 0.9937) with a slope of (5.32 ± 0.19) × 10^{-1} M^{-1} s^{-1} and a y intercept of (0.08 ± 1.00) × 10^{-4} s^{-1}. Similar results were obtained throughout the entire pH range under investigation. Experimental data obtained from a study of the variation in reaction rate as a function of formaldehyde concentration for $[CH_2O]_t >> [S(IV)]$ at pH 0.0, 0.3, 0.6, and 1.0 are presented in Figure 2. In each case, k_{obsd} exhibited a linear dependence ($R^2 > 0.99$) on $[CH_2O]_t$ up to a formaldehyde concentration of 250 mM. Consequently, the rate of reaction is also first order with respect to $[CH_2O]_t$.

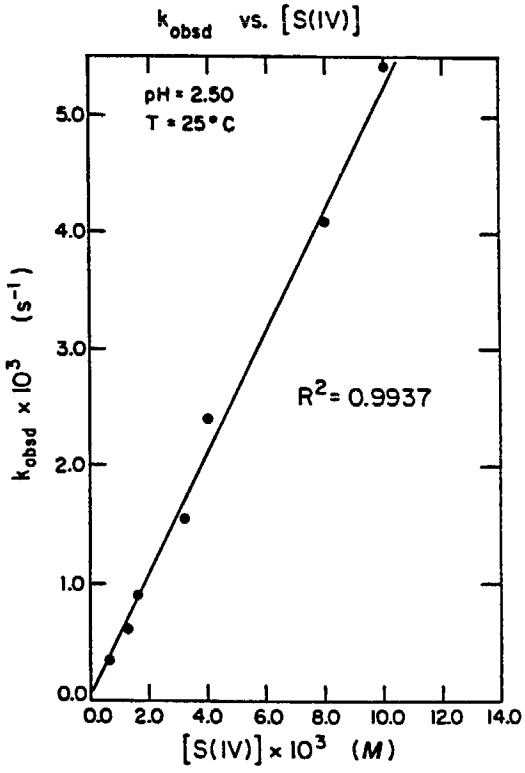

Figure 1. Dependence of the observed pseudo-first-order rate constant, k_{obsd}, on [S(IV)] at pH 2.5. The solid line denotes the linear least-squares fit to the experimental data. Reaction conditions: $[CH_2O]_t$ = 0.08–1.25 mM, [S(IV)] = 0.65–10 mM, μ = 1.0 M, and T = 25 °C.

The depletion of S(IV) proceeds more rapidly at higher pH as shown by the experimental data depicted in Figures 3 and 4 and summarized in Table I. The dependence of the reaction rate on pH may be examined at both low and high pH by plotting the observed pseudo-second-order rate constant, $k_{obsd}/[CH_2O]_t$, as a function of the reciprocal of the hydrogen-ion concentration. A plot of $k_{obsd}/[CH_2O]_t$ vs $[H^+]^{-1}$ (Figure 3) over the pH range 0.0 to 1.0 yields a straight line (R^2 = 0.9991) with a slope of (4.35 ± 0.09) × 10^{-3} s^{-1} and an intercept of (3.30 ± 0.52) × 10^{-3} M^{-1} s^{-1}. Experimental measurements recorded between pH 2.5 and 3.4 (Figure 4) also exhibit linear behavior (R^2 = 0.9990) when $k_{obsd}/[CH_2O]_t$ is plotted vs. $[H^+]^{-1}$ (slope = (7.68 ± 0.18) × 10^{-4} s^{-1} and intercept = (3.48 ± 0.25) × 10^{-1} M^{-1} s^{-1}). Therefore, the

(12) Skoog, D. A.; West, D. M. "Fundamentals of Analytical Chemistry"; Holt, Rinehart, and Winston: New York, 1969; 2nd ed, pp 453–62.
(13) Kolthoff, I. M.; Belcher, R.; Stenger, V. A.; Matsuyama, G. "Volumetric Analysis"; Interscience: New York, 1957; Vol. III, pp 375–6.

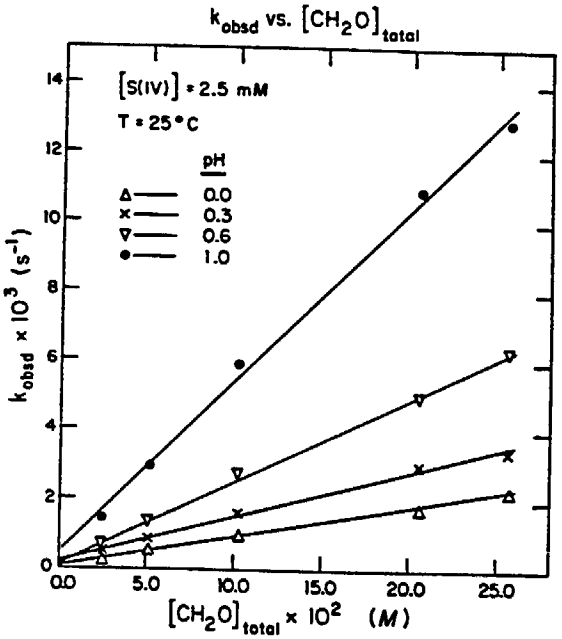

Figure 2. Dependence of the observed pseudo-first-order rate constant, k_{obsd}, on $[CH_2O]_t$ at pH (−log $[H^+]$) 0.0, 0.3, 0.6, and 1.0. The solid line denotes the linear least-squares fit to the experimental data. Reaction conditions: [S(IV)] = 2.5 mM, $[CH_2O]_t$ = 25–250 mM, μ = 1.0 M, and T = 25 °C.

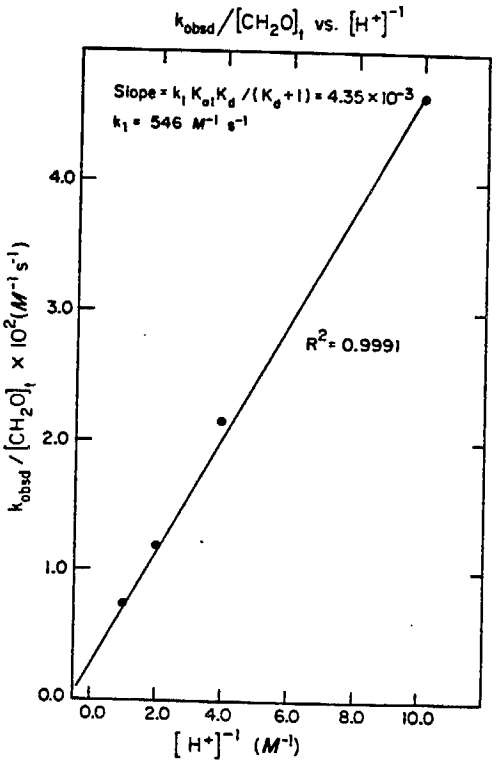

Figure 3. Dependence of the observed pseudo-second-order rate constant, $k_{obsd}/[CH_2O]_t$, on $[H^+]^{-1}$ over the pH (−log $[H^+]$) range 0–1. The solid line denotes the linear least-squares fit to the experimental data. Reaction conditions are listed in Table I.

rate of reaction becomes inversely dependent on proton concentration in both the low and high pH regions under investigation. In the latter case, the nonzero intercept demonstrates that two pathways are operating to produce hydroxymethanesulfonate.

An earlier study by Bell and Evans[11] showed that the reaction of sulfite and formaldehyde under neutral and weakly alkaline pH conditions was sensitive to general base catalysis by a wide

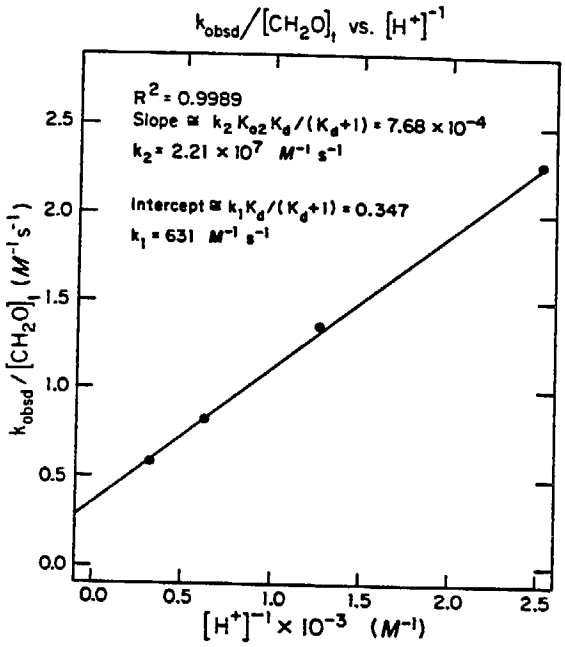

Figure 4. Dependence of the observed pseudo-second-order rate constant, $k_{obsd}/[CH_2O]_t$, on $[H^+]^{-1}$ over the pH (−log $[H^+]$) range 2.5 to 3.4. The solid line denotes the linear least-squares fit to the experimental data. Reaction conditions are listed in Table I.

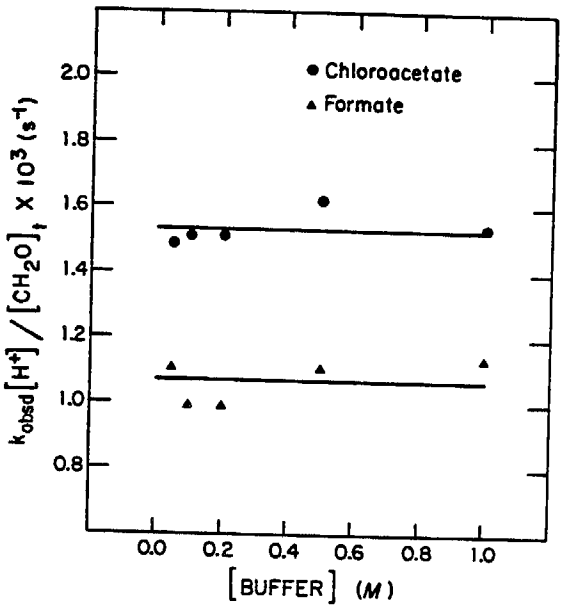

Figure 5. Dependence of $k_{obsd}[H^+]/[CH_2O]_t$ on the concentration of chloroacetate and formate buffers. Reaction conditions: [S(IV)] = 1.25 mM, $[CH_2O]_t$ = 10.0 μM, μ = 1.0 M, and T = 25 °C.

variety of carboxylate anions. The dependence of the reaction rate on buffer concentration at pH 2.5 and 3.4 is depicted in Figure 5. Because the pH of the individual reaction solutions varied slightly, it was necessary to correct the experimental measurements by comparing $k_{obsd}[H^+]/[CH_2O]_t$ to $[A^-]$. Inspection of Figure 5 shows that $k_{obsd}[H^+]/[CH_2O]_t$ remains constant over a tenfold range in $[ClCH_2CO_2^-]$ and $[HCO_2^-]$ at pH 2.5 and 3.4, respectively. Analogous results were obtained upon examination of variations in the rate of reaction as a function of $[Cl_2CHCO_2^-]$ (pH 1.5) and $[H_2PO_4^-]$ (pH 1.9). Thus, the observed reaction rate appears to be independent of the concentration of chloroacetate, dichloroacetate, dihydrogen phosphate, and formate over the pH range 1.5–3.4.

The aforementioned kinetic data are consistent with the following reaction mechanism:

$$CH_2(OH)_2 \underset{k_{-d}}{\overset{k_d}{\rightleftharpoons}} CH_2O + H_2O \quad \text{(fast)} \quad (1)$$

$$SO_2{\cdot}H_2O \overset{K_{a1}}{\rightleftharpoons} H^+ + HSO_3^- \quad \text{(fast)} \quad (2)$$

$$HSO_3^- \overset{K_{a2}}{\rightleftharpoons} H^+ + SO_3^{2-} \quad \text{(fast)} \quad (3)$$

$$HSO_3^- + CH_2O \underset{k_{-1}}{\overset{k_1}{\rightleftharpoons}} CH_2(OH)SO_3^- \quad \text{(slow)} \quad (4)$$

$$SO_3^{2-} + CH_2O \underset{k_{-2}}{\overset{k_2}{\rightleftharpoons}} CH_2(O^-)SO_3^- \quad \text{(slow)} \quad (5)$$

$$CH_2(O^-)SO_3^- + H^+ \overset{K_{a2}^{-1}(HMSA)}{\rightleftharpoons} CH_2(OH)SO_3^- \quad \text{(fast)} \quad (6)$$

This mechanism involves nucleophilic addition of bisulfite and sulfite to the carbonyl C atom of CH_2O. In aqueous solution, formaldehyde exists predominantly as methylene glycol, $CH_2(OH)_2$ ($K_d = k_d/k_{-d} = 5.5 \times 10^{-4}$ at 25 °C).[14] The value of the acid-dissociation constant for the hydroxyl group of hydroxymethanesulfonate, $K_{a2(HMSA)}$, has been estimated by Sorensen and Andersen[10] to be 2.00×10^{-12} M at 25 °C. According to the mechanistic scheme outlined in eq 1–6, the rate of formation of hydroxymethanesulfonate is given by

$$\nu = d[HMSA]/dt = k_1[HSO_3^-][CH_2O] + k_2[SO_3^{2-}][CH_2O] - k_{-1}[CH_2(OH)SO_3^-] - k_{-2}[CH_2(O^-)SO_3^-] \quad (7)$$

Since the equilibrium for the reaction is displaced far to the right ($K_{eq} = [HMSA]_t/[S(IV)][CH_2O]_t = 6.5 \times 10^3$ M^{-1} at pH 2),[15] the terms in eq 7 that describe the decomposition of hydroxymethanesulfonate may be omitted in the derivation of the theoretical kinetic expression. The concentrations of the reactive species, CH_2O, HSO_3^-, and SO_3^{2-}, can be expressed in terms of $[CH_2O]_t$ and [S(IV)] as follows:

$$[CH_2O] = \frac{K_d[CH_2O]_t}{K_d + 1} \quad (8)$$

$$[HSO_3^-] = \alpha_1[S(IV)] \quad (9)$$

$$[SO_3^{2-}] = \alpha_2[S(IV)] \quad (10)$$

where

$$\alpha_1 = \frac{K_{a1}[H^+]}{[H^+]^2 + K_{a1}[H^+] + K_{a1}K_{a2}} \quad (11)$$

$$\alpha_2 = \frac{K_{a1}K_{a2}}{[H^+]^2 + K_{a1}[H^+] + K_{a1}K_{a2}} \quad (12)$$

Substitution of eq 8–10 into eq 7 yields

$$\nu = \left\{\frac{K_d(k_1\alpha_1 + k_2\alpha_2)}{K_d + 1}\right\}[S(IV)][CH_2O]_t \quad (13)$$

where k_{obsd} for reactions carried out under pseudo-first-order conditions in [S(IV)] is given by

$$k_{obsd} = \frac{K_d(k_1\alpha_1 + k_2\alpha_2)[CH_2O]_t}{K_d + 1} \quad (14)$$

Initial estimates of the intrinsic kinetic parameters, k_1 and k_2, may be obtained by considering the rate behavior at the extremes of pH as depicted in Figures 3 and 4. For example, the contribution of SO_3^{2-} to the observed reaction rate in strongly acidic solution (pH ≤ 1.5) can be neglected such that

$$k_{obsd} = \frac{K_d k_1 \alpha_1[CH_2O]_t}{K_d + 1} \quad (15)$$

(14) Bell, R. P. In "Advances in Physical Organic Chemistry", Gold, V., Ed.; Academic Press: London, 1966; Vol. 4, pp 1–29.
(15) Dasgupta, P. K.; DeCesare, K.; Ullrey, J. C. *Anal. Chem.* **1980**, *52*, 1912–22.

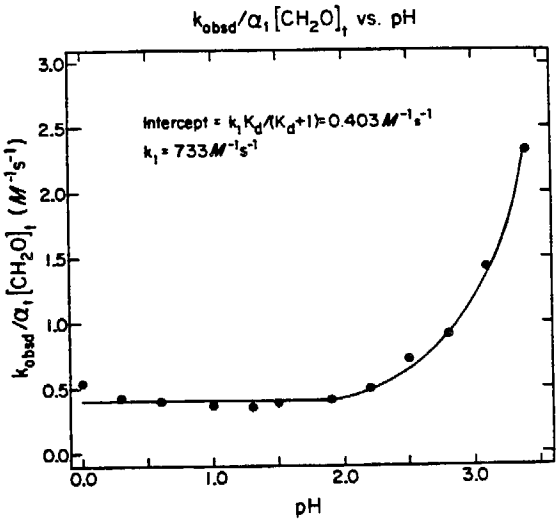

Figure 6. Dependence of $k_{obsd}/\alpha_1[CH_2O]_t$ ($= \nu/[HSO_3^-][CH_2O]_t$) on pH (–log $[H^+]$). Reaction conditions are listed in Table I.

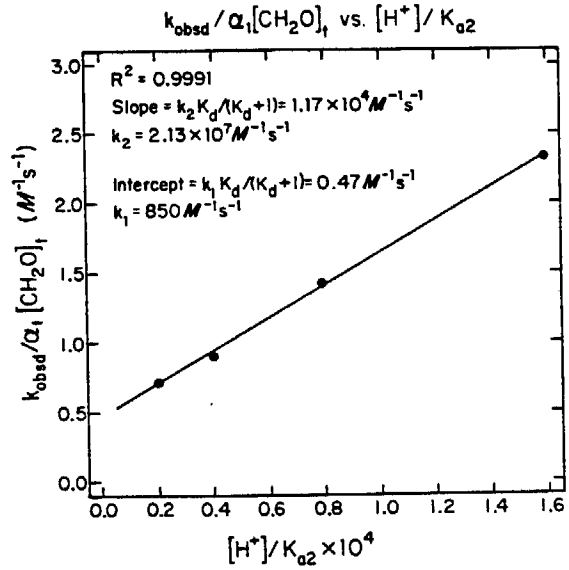

Figure 7. Dependence of $k_{obsd}/\alpha_1[CH_2O]_t$ ($= \nu/[HSO_3^-][CH_2O]_t$) on $K_{a2}/[H^+]$ over the pH (–log $[H^+]$) range 2.5–3.4. The solid lines denotes the linear least-squares fit to the experimental data. Reaction conditions are listed in Table I.

At very low pH, when $[H^+] >> K_{a1}$ and $[H^+]^2 >> K_{a1}[H^+]$ and $K_{a1}K_{a2}$ ($K_{a1} = 1.45 \times 10^{-2}$ M and $K_{a2} = 6.31 \times 10^{-8}$ M at 25 °C),[16,17] $\alpha_1 \simeq K_{a1}/[H^+]$ and eq 15 reduces to

$$k_{obsd} = \frac{K_d k_1 K_{a1}[CH_2O]_t}{(K_d + 1)[H^+]} \quad (16)$$

Equation 16 is consistent with the observed linear dependence of $k_{obsd}/[CH_2O]_t$ on $[H^+]^{-1}$ from pH 0.0 to 1.0 with $k_1 \pm \sigma = (5.46 \pm 0.11) \times 10^2$ M^{-1} s^{-1} at 25 °C. At higher pH, the contribution of sulfite ion to the observed reactivity cannot be neglected. However, simplification of eq 14 is achieved for reaction conditions under which $K_{a1} >> [H^+]$ (pH ≥ 2.5). In this case, the approximation that $K_{a1}[H^+] >> [H^+]^2$ and $K_{a1}K_{a2}$ is valid and the theoretical expression for k_{obsd} becomes

$$k_{obsd} = \left\{\frac{K_d}{K_d + 1}\left(k_1 + \frac{k_2K_{a2}}{[H^+]}\right)\right\}[CH_2O]_t \quad (17)$$

The linear plot of the measured pseudo-second-order rate constant as a function of the inverse of the hydrogen-ion concentration over the pH range 2.5–3.4 (Figure 4) yields values of $k_1 \pm \sigma = (6.31$

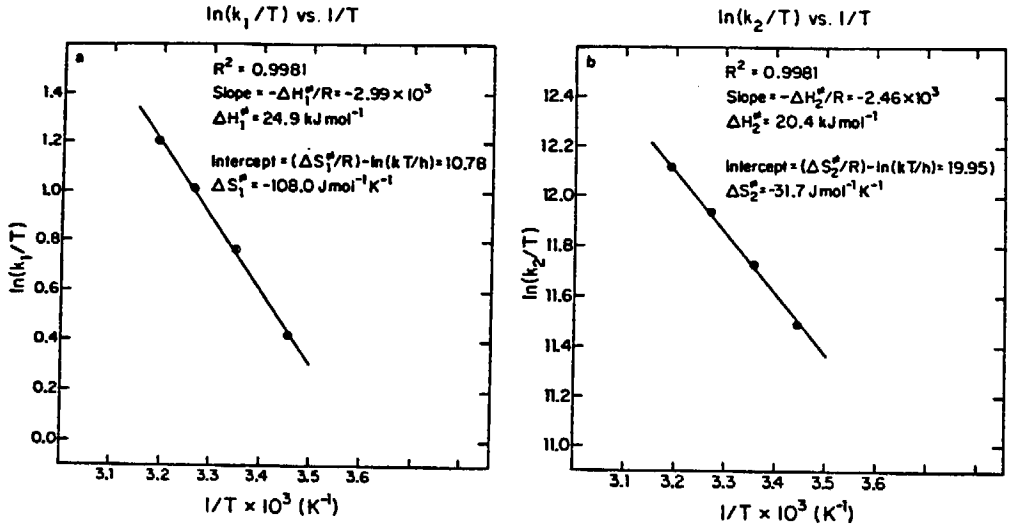

Figure 8. Temperature dependencies of (a) the intrinsic rate constant, k_1, for the nucleophilic addition of bisulfite ion to formaldehyde and (b) the intrinsic rate contant, k_2, for the nucleophilic addition of sulfite ion to formaldehyde. The solid lines denote the linear least-squares fits to the experimental data. Reaction conditions: [S(IV)] = 1.25 mM, $[CH_2O]_t$ = 10.0 mM, pH (-log $[H^+]$) = (a) 1.3 and (b) 2.5 ([chloroacetate]$_t$ = 0.1 M), μ = 1.0 M, and T = 25 °C.

$\pm$ 0.46) $\times 10^2$ M^{-1} s^{-1} and $k_2 \pm \sigma = (2.21 \pm 0.05) \times 10^7$ M^{-1} s^{-1} at 25 °C.

The empirical estimates of k_1 and k_2 were refined by examining in detail the variation in $k_{obsd}/\alpha_1[CH_2O]_t$ ($= \nu/[HSO_3^-][CH_2O]_t$) with pH. This quotient remains virtually constant over the pH range 0.0–2.0 with an average value of $(4.03 \pm 0.52) \times 10^{-1}$ M^{-1} s^{-1} as shown in Figure 6. Analysis of these data in terms of eq 15 confirms that bisulfite ion is the principal reactive S(IV) species in strongly acidic solution with $k_1 \pm \sigma = (7.33 \pm 0.94) \times 10^2$ M^{-1} s^{-1}. At pH > 2, $k_{obsd}/\alpha_1[CH_2O]_t$ increased sharply with increasing pH. The latter observation supports the hypothesis that SO_3^{2-} becomes the predominant reactant species under weakly acidic pH conditions. A plot of $k_{obsd}/\alpha_1[CH_2O]_t$ vs. $K_{a2}/[H^+]$ (Figure 7) was linear (R^2 = 0.9991) with a slope of $(1.17 \pm 0.03) \times 10^4$ M^{-1} s^{-1} and a y intercept of $(4.67 \pm 0.25) \times 10^{-1}$ M^{-1} s^{-1}. Application of eq 14 yields values of $k_1 \pm \sigma = (8.50 \pm 0.46) \times 10^2$ M^{-1} s^{-1} and $k_2 \pm \sigma = (2.13 \pm 0.05) \times 10^7$ M^{-1} s^{-1}. Temperature dependence studies conducted at pH 1.3 (Figure 8a) and 2.5 (Figure 8b) yielded $\Delta H_1^* \pm \sigma$ = (24.9 ± 0.8) kJ mol^{-1}, $\Delta S_1^* \pm \sigma$ = (−108.0 ± 2.6) J mol^{-1} K^{-1}, $\Delta H_2^* \pm \sigma$ = (20.4 ± 0.5) kJ mol^{-1}, and $\Delta S_2^* \pm \sigma$ = (−31.7 ± 1.6) J mol^{-1} K^{-1} for 15 °C $\leq T \leq$ 40 °C. The temperature dependencies of K_d (ΔH° = 33.6 kJ mol^{-1}), K_{a1} (ΔH° = −16.2 kJ mol^{-1}), and K_{a2} (ΔH° = −11.7 kJ mol^{-1}) have been described previously by Bell,[14] by Deveez and Rumpf,[16] and by Hayon and co-workers,[17] respectively.

The kinetic parameters obtained from the preceding analysis were further refined by a nonlinear least-squares regression technique in which the function Φ defined by eq 18

$$\Phi = \sum_{i=1}^{n} \{(k_{obsd} - k_{calcd})\mathrm{wts}(i)\}^2 \qquad (18)$$

where

$$\mathrm{wts}(i) = (\sigma_i^{-1})^2 / \sum_{i=1}^{n} (\sigma_i^{-1})^2 \qquad (19)$$

is minimized with respect to k_1, k_2, K_{a1}, K_{a2}, and K_d. The values of the thermodynamic constants K_d (5.50×10^{-4}),[14] K_{a1} (1.45×10^{-2} M),[16] and K_{a2} (6.31×10^{-8} M)[17] were held constant in order to simplify the regression analysis. The values of k_{obsd} were calculated from eq 14 and the trial values of k_1 and k_2 were those determined from the preceding analysis of the experimental data for the low and high pH regions. Considering the slight degree of uncertainty in the calculated values of k_1 (relative σ = ±19%) and k_2 (~4%), the mean of the aforementioned results were utilized for initial estimates. Values of the intrinsic rate constants obtained following the least-squares analysis are k_1 = (7.90 ± 0.32) $\times 10^2$ M^{-1} s^{-1} and k_2 = (2.48 ± 0.24) $\times 10^7$ M^{-1} s^{-1}. The calculated values for the pseudo-first-order rate constants, k_{calcd}, are compared with the experimental measurements in Table I. The results obtained from the regression analysis were independent of the initial estimates of k_1 and k_2.

There exists some disagreement over the values of the thermodynamic constants K_d, K_{a1}, and K_{a2}. Bell[16] and LeHĕnaff[18] have critically reviewed the documented equilibrium measurements of K_d and recommended values of $K_d = 5.5 \times 10^{-4}$ (25 °C) and ΔH° = 33.6 kJ mol^{-1}. Similarly, Maahs[19] has examined the published thermodynamic data for the speciation of sulfur dioxide in water. The author's recommended values of K_{a1} and K_{a2} agree closely with the constants measured by Deveez and Rumpf[16] and Hayon and co-workers.[17] Because temperature-dependent data were required for the calculations performed in the current study, the results obtained by Deveez and Rumpf[16] and by Hayon et al.[17] were utilized directly. It is important to note that the thermodynamic acid-dissociation constants for $SO_2{\cdot}H_2O$ and HSO_3^- are reported for dilute solutions, whereas, the kinetic data described herein are collected at an ionic strength, μ, of 1.0 M. Clarke[20] has discussed the importance of ionic strength effects on the equilibria and kinetics of reactions of SO_2 in aqueous solution. In order to account for the influence of μ, the values of K_{a1} and K_{a2} were corrected according to the Davies approximation

$$\log \gamma = -Az^2\left(\frac{\mu^{1/2}}{1+\mu^{1/2}} - 0.2\mu\right) \qquad (20)$$

where z is the ionic charge and $A = 1.82 \times 10^6(\epsilon T)^{-3/2}$ (ϵ is the dielectric constant of water). Application of eq 20 to the experimental data yields $^ck_1$ = (4.51 ± 0.15) $\times 10^2$ $M^{-1}s^{-1}$, $^ck_2$ = (5.42 ± 0.07) $\times 10^6$ M^{-1} s^{-1}, $^c\Delta H_1^*$ = (22.1 ± 1.1) kJ mol^{-1}, $^c\Delta S_1^*$ = (−121.3 ± 3.7) J mol^{-1} K^{-1}, $^c\Delta H_2^*$ = (21.0 ± 0.2) kJ mol^{-1}, and $^c\Delta S_2^*$ = (−40.2 ± 0.7) J mol^{-1} K^{-1} for values of $^cK_{a1} = K_{a1}\gamma_{SO_2{\cdot}H_2O}/\gamma_{H^+}\gamma_{HSO_3^-}$ = 2.93 × 10^{-2} M and $^cK_{a2} = K_{a2}\gamma_{HSO_3^-}/\gamma_{H^+}\gamma_{SO_3^{2-}}$ = 2.58 × 10^{-7} M at 25 °C.

The correction to the intrinsic rate parameter, k_1, for ionic strength effects is not large, especially upon consideration of the fact that the experimental conditions employed in the current investigation exceed the upper limit for strict applicability of the

(16) Deveez, D.; Rumpf, P. *C. R. Acad. Sci.* **1964**, *258*, 6135–8.
(17) Hayon, E.; Treinin, A.; Wilf, J. *J. Am. Chem. Soc.* **1972**, *94*, 47–57.
(18) LeHĕnaff, P. *Bull. Soc. Chim. Fr.* **1968**, 4687–700.
(19) Maahs, H. G. In "Heterogeneous Atmospheric Chemistry", Schryer, D. R., Ed.; American Geophysical Union: Washington, DC, 1982; pp 187–95.
(20) Clarke, A. G. *Atmos. Environ.* **1981**, *15*, 1591–5.

Davies equation (μ = 0.5 M).[21] However, the value of k_2 is decreased by approximately a factor of 4 due to the large ionic strength correction for the acid-dissociation constant of HSO_3^-. The calculated values of the pseudo-first-order rate constants, $^c k_{calcd}$, following application of the ionic strength corrections are also presented in Table I.

D. Discussion

The mechanism outlined in eq 1–6 is virtually identical with the scheme suggested previously by Bell and Evans[11] for the reaction of sulfite with formaldehyde under neutral and alkaline pH conditions. However, in the present case we propose that the rate-determining step for the formation of hydroxymethanesulfonate in acidic solution involves nucleophilic addition of HSO_3^- and/or SO_3^{2-} to the carbonyl functionality of CH_2O. Bell and Evans[11] demonstrated unambiguously that the dehydration of methylene glycol (reaction 1) was rate limiting (vide infra) at weakly acidic and neutral pH. However, if the rate-limiting step of the reaction at low pH involves a bimolecular process, then $SO_2{\cdot}H_2O$, HSO_3^-, and SO_3^{2-} should react with CH_2O at different rates. In a previous study, Skrabal and Skrabal[9] observed that the reactivity of S(IV) species with formaldehyde decreased in the following order: $SO_3^{2-} >> HSO_3^- >> SO_2{\cdot}H_2O$. It is well-known that sulfite ion is a much stronger nucleophile than HSO_3^- in reactions with a broad variety of organic and inorganic substrates.[22] Consequently, the relative contributions of bisulfite ion and SO_3^{2-} to the observed reaction rate with formaldehyde will depend on both the relative equilibrium concentrations of HSO_3^- and SO_3^{2-} as determined by pH and the intrinsic nucleophilicity of each species.

In order to permit the application of steady-state considerations, the present mechanism assumes that the formation of HSO_3^- from $SO_2{\cdot}H_2O$, SO_3^{2-} from HSO_3^-, and CH_2O from $CH_2(OH)_2$ occurs rapidly with respect to the other elementary steps leading to the production of hydroxymethanesulfonate. Unfortunately, there is little agreement in the available literature concerning the rates of formation of HSO_3^- and SO_3^{2-}. Betts and Voss[23] reported that the first-order rate constant for the deprotonation of aquated sulfur dioxide was 1.06×10^8 s^{-1} at 20 °C. A more recent study conducted by McArdle and Hoffmann[2] showed that the rate of HSO_3^- production must be greater than 160 s^{-1}. This value is consistent with data reported by Roberts[24] which establishes a lower limit of 320 s^{-1}. Since formation of HSO_3^- and SO_3^{2-} involves simple proton transfer to H_2O, it is likely that the production of these reactants is rapid in comparison to the other steps in the mechanism.

A review of the available literature revealed that there is a more general consensus among earlier studies of the dehydration kinetics of methylene glycol (eq 1). The rate constants reported for the "uncatalyzed" reaction range from 4.4×10^{-3} (22 °C)[25] to 5.7×10^{-3} s^{-1} (25 °C).[26] In addition, several authors have demonstrated that reaction 1 is sensitive to specific acid/base as well as general acid/base catalysis by buffer systems such as chloroacetate and formate. With the values of the catalytic rate constants for H^+, OH^-, $ClCH_2CO_2H$, $ClCH_2CO_2^-$, HCO_2H, and HCO_2^- tabulated by Bell and Evans,[11] the predicted rate constants of methylene glycol dehydration at pH 2.5 and 3.4 would be 1.09×10^{-2} and 1.04×10^{-2} s^{-1}, respectively. However, the absence of first-order rate-limiting behavior in the present study indicates that, according to the mechanism depicted in eq 1–6, the rate constants for CH_2O formation must exceed 7.29×10^{-4} s^{-1}

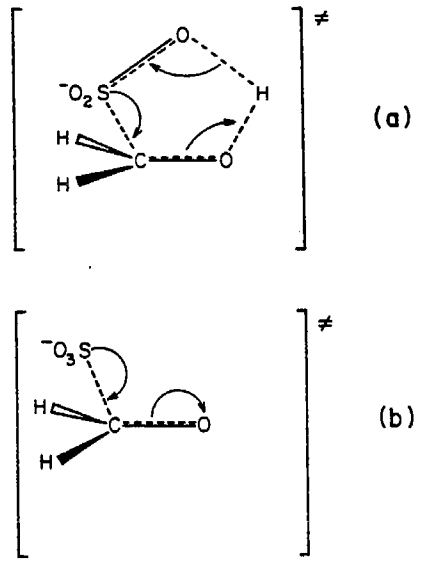

Figure 9. Structures postulated for the activated complexes formed by the nucleophilic addition of (a) bisulfite and (b) sulfite to formaldehyde. Approach of the nucleophiles occurs in the π-electron plane of the carbonyl group.

(k_{obsd}[S(IV)]/[CH_2O]$_t$) at pH 2.5 and 2.83×10^{-3} s^{-1} (k_{obsd}[S(IV)]/[CH_2O]$_t$) at pH 3.4. These results confirm that the dehydration of $CH_2(OH)_2$ ($v = k_d$[$CH_2(OH)_2$] = 1.09×10^{-4} M s^{-1} at pH 2.5 and $v = 1.04 \times 10^{-4}$ M s^{-1} at pH 3.4 for [CH_2O]$_t$ = 0.01 M) occurs rapidly relative to the nucleophilic addition of HSO_3^- ($v = k_1$[HSO_3^-][CH_2O]$_t$ = 4.46×10^{-6} M s^{-1} at pH 2.5 and $v = 5.28 \times 10^{-6}$ M s^{-1} at pH 3.4 for [S(IV)] = 1.25×10^{-3} M and [CH_2O]$_t$ = 0.01 M) and SO_3^{2-} ($v = k_2$[SO_3^{2-}][CH_2O] = 2.79×10^{-6} M s^{-1} at pH 2.5 and $v = 2.63 \times 10^{-5}$ M s^{-1} at pH 3.4 for [S(IV)] = 1.25×10^{-3} M and [CH_2O]$_t$ = 0.01 M) to formaldehyde.

The enhanced reactivity of sulfite, relative to HSO_3^-, toward CH_2O is manifested in the more positive value of ΔS^* for reaction 5. An activation entropy of approximately zero would generally be expected for a reaction between an ion and a neutral molecule, because the activated complex retains a charge equivalent to the sum of the charges of the reactants thereby minimizing the degree of change in solvent ordering.[27] Possible transition-state structures for the nuclophilic addition of HSO_3^- and SO_3^{2-} to formaldehyde are illustrated in Figure 9. The large negative value of ΔS_1^* is consistent with the activated complex in which the intramolecular transfer of the hydrogen ion from bisulfite to the carbonyl oxygen atom of CH_2O occurs readily through a cyclization process as depicted in Figure 9a. Conversely, formation of the activated complex from the addition of SO_3^{2-} to formaldehyde (Figure 9b) is not restricted by the aforementioned structural constraint. This may allow partial desolvation of the transition-state complex that would result in only a small decrease in the entropy of the system.

An alternative reaction mechanism for the production of hydroxymethanesulfonate that is consistent with the observed rate dependence on [S(IV)], [CH_2O]$_t$, and [H^+] involves the nucleophilic displacement of H_2O and OH^- from methylene glycol by HSO_3^- and SO_3^{2-} as follows:

$$CH_2O + H_2O \underset{k_d}{\overset{k_d}{\rightleftharpoons}} CH_2(OH)_2 \quad \text{(fast)} \quad (21)$$

$$SO_2{\cdot}H_2O \overset{K_{a1}}{\rightleftharpoons} H^+ + HSO_3^- \quad \text{(fast)} \quad (22)$$

$$HSO_3^- \overset{K_{a2}}{\rightleftharpoons} H^+ + SO_3^{2-} \quad \text{(fast)} \quad (23)$$

$$HSO_3^- + CH_2(OH)_2 \xrightarrow{k_1'} CH_2(OH)SO_3^- + H_2O \quad \text{(slow)} \quad (24)$$

(21) Stumm, W.; Morgan, J. J. "Aquatic Chemistry"; Wiley-Interscience: New York, 1981; 2nd ed, p 135.
(22) Edwards, J. O. "Inorganic Reaction Mechanisms"; Benjamin: New York, 1965; pp 51–71.
(23) Betts, R. H.; Voss, R. H. *Can. J. Chem.* **1970**, *48*, 2035–41.
(24) (a) Roberts, D. L. Ph.D. Thesis, California Institute of Technology, 1979, pp 26, 162. (b) Roberts, D. L.; Friedlander, S. K. *AIChE J.* **1980**, *26*, 593–610.
(25) Sutton, H. C.; Downes, T. M. *J. Chem. Soc., Chem. Commun.* **1972**, 1–2.
(26) Los, J. M.; Roeleveld, L. F.; Wetsema, B. J. C. *J. Electroanal. Chem.* **1977**, *75*, 819–37.
(27) Moore, J. W.; Pearson, R. G. "Kinetics and Mechanism"; Wiley-Interscience: New York, 1981; 3rd ed, pp 260–72.

$$SO_3^{2-} + CH_2(OH)_2 \xrightarrow{k_2'} CH_2(OH)SO_3^- + OH^- \text{ (slow)} \quad (25)$$

Analysis of the experimental rate data in terms of the corresponding kinetic expression

$$r = (k_1\alpha_1 + k_2\alpha_2)[S(IV)][CH_2O]_t \quad (26)$$

where $[CH_2O]_t \simeq [CH_2(OH)_2]$ ($K_d^{-1} = k_{-d}/k_d = 1.82 \times 10^3$ at 25 °C) yields $k_1' = (4.36 \pm 0.17) \times 10^{-1}$ M^{-1} s^{-1}, $k_2' = (1.36 \pm 0.03) \times 10^5$ M^{-1} s^{-1}, $\Delta H_1'^{\ddagger} = (58.3 \pm 0.7)$ kJ mol^{-1}, $\Delta S_1'^{\ddagger} = (-58.4 \pm 2.4)$ J mol^{-1} K^{-1}, $\Delta H_2'^{\ddagger} = (53.4 \pm 0.4)$ kJ mol^{-1}, $\Delta S_2'^{\ddagger} = (16.7 \pm 1.3)$ J mol^{-1} K^{-1}. Large values of $-\Delta S^{\ddagger}$ are characteristic of substitution reactions in which bond formation between the substrate and nucleophile *precedes* departure of the leaving group.[27] Since $\Delta S_2'^{\ddagger}$ is positive, the operation of a S_N2 mechanism would seem unlikely in the present case. That hydroxide ion is virtually never a leaving group in nulcleophilic displacement reactions at saturated carbon lends further support to the preceding conclusion.[28]

Application to Atmospheric Systems. The rate of formation of hydroxymethanesulfonate in the solution phase at pH 0 to 3.5 in equlibrium with an open atmosphere can be determined by substituting eq 27 and 28 into eq 13.

$$[CH_2O]_t = H_{CH_2O}P_{CH_2O} \quad (27)$$

$$[S(IV)] = H_{SO_2}P_{SO_2}\left(\frac{[H^+]^2 + K_{a1}[H^+] + K_{a1}K_{a2}}{[H^+]^2}\right) \quad (28)$$

This yields

$$r = \left\{\frac{K_d}{K_d + 1}\left(\frac{k_1K_{a1}[H^+] + k_2K_{a1}K_{a2}}{[H^+]^2}\right)\right\}H_{SO_2}P_{SO_2}H_{CH_2O}P_{CH_2O} \quad (29)$$

where the symbols H and P refer to the Henry's law constants and the partial pressures of the reactants. Evaluation of the rate constants yields

$$r = \left(\frac{(6.33 \times 10^{-3}\ s^{-1}\ [H^+] + 1.25 \times 10^{-5}\ M\ s^{-1}}{[H^+]^2}\right) \times H_{SO_2}P_{SO_2}H_{CH_2O}P_{CH_2O} \quad (30)$$

At 25 °C, $H_{SO_2} = 1.26$ M atm^{-1},[5] $H_{CH_2O} = 6.30 \times 10^3$ M atm^{-1},[4] and if the pH is 3.0, $P_{SO_2} = 20$ ppb, and $P_{CH_2O} = 5$ ppb, then the rate of hydroxymethanesulfonate formation is 5.38×10^{-8} M h^{-1}. It is unlikely that the aqueous-phase reaction is limited by mass transport at these atmospheric concentrations of formaldehyde and sulfur dioxide. Consequently, eq 29 will correctly predict the droplet-phase rate of hydroxymethanesulfonate production under conditions typically encountered in a polluted atmosphere.

Preliminary investigations conducted in the authors' laboratory have shown that the presence of formaldehyde in aqueous solution alters dramatically the kinetics of oxidation of sulfur(IV) by hydrogen peroxide. Hydroxymethanesulfonate appears to be resistant to oxidation by H_2O_2 at low pH in the absence of transition-metal catalysts such as iron(II).

Acknowledgment. The authors gratefully acknowledge the United States Environmental Protection Agency (R808086-01) for providing financial support for this research. Also, we thank the reviewers for offering several constructive suggestions concerning the preparation of the paper.

Registry No. SO_2, 7446-09-5; CH_2O, 50-00-0; hydroxymethanesulfonic acid, 75-92-3.

(28) Hendrickson, J. B.; Cram, D. J.; Hammond, G. S. "Organic Chemistry"; McGraw-Hill: New York, 1970; 3rd ed, p 397.